THESE DE DOCTORAT DE

L'UNIVERSITE D'ANGERS
COMUE UNIVERSITE BRETAGNE LOIRE

ECOLE DOCTORALE N° 605
BIOLOGIE SANTE
SPECIALITE : « SCIENCES PHARMACEUTIQUES »

Par
« Amel DJOUDI»

« Development of innovative nanocomposite hydrogels for locoregional treatment of Glioblastoma»

Thèse présentée et soutenue à « Amphithéâtre Germain UFR Pharmacie d'Angers », le «10/11/2022»

Unité de recherche : Université d'Angers, Inserm UMR 1307, CNRS UMR 6075, Nantes Université, CRCI2NA, F-49000 Angers - France

Rapporteurs avant soutenance :

Pr. Maria Marlow
Professeur associée
University of Nottingham

Dr. Virginie Busignies
Directrice de recherche
Université de Bordeaux

Composition du Jury :

Dr. Franck Artzner
Directeur de recherche
Institut de Physique de Rennes, Université de Rennes 1

Pr. Frank Boury, Directeur de thèse
Professeur
Université d'Angers, France

Dr. Emmanuel Garcion, Co-encadrant
Directeur de recherche
Université d'Angers, France

L'auteur du présent document vous autorise à le partager, reproduire, distribuer et communiquer selon les conditions suivantes :



- Vous devez le citer en l'attribuant de la manière indiquée par l'auteur (mais pas d'une manière qui suggérerait qu'il approuve votre utilisation de l'œuvre).
- Vous n'avez pas le droit d'utiliser ce document à des fins commerciales.
- Vous n'avez pas le droit de le modifier, de le transformer ou de l'adapter.

Consulter la licence creative commons complète en français :
http://creativecommons.org/licences/by-nc-nd/2.0/fr/

Ces conditions d'utilisation (attribution, pas d'utilisation commerciale, pas de modification) sont symbolisées par les icônes positionnées en pied de page.



ACKNOWLEDGEMENTS

First of all, I would like to thank Dr. Emmanuel Garcion, director of the research unit 5 GLIAD of the CRCI2NA, for giving me the opportunity to carry out my thesis in the laboratory. I deeply thank Pr. Frank Boury, my thesis director, for having welcomed me in his team. I also thank him for his advice, his patience, his encouragement and for the trust he gave me during my thesis.

I am grateful to the members of the jury, Pr. Maria Marlow, Professor at the University of Nottingham, Dr. Virginie Busignies, Researcher at the University of Bordeaux and Dr. Franck Artzner, Director of Research CNRS at the Institute of Physics of Rennes, for having honored me by participating in this jury and for having agreed to devote time to the evaluation of this thesis as reviewers and examiners.

I am very grateful to the Ligue contre le Cancer for the 3 years of funding that was granted to me. I would like to thank my colleagues Natalia Ferreira and Rodolfo Molina Peña, Ilaria Ottonelli Loris Roncali and Charlotte Roy for helping me with the *in vitro* and *in vivo* experiments, writing and proofreading of the articles. I am also thankful for Polytech Angers team: Fida Khater, Jean-Michel Oger, Sonia Jerjir and Maryline Plaud for helping me in the practical works organization.

I would also like to thank Sylvie Avril for sharing her experience in Western blot and her sense of humor and Laurence Sindji and Lisa Meslier for their support and kindness. I would like to thank all my colleagues Rodolfo Molina Peña, Natalia Ferreira, Loris Roncali, Ilaria Ottonelli, and Arianna Rinaldi for their good mood, their sympathy, their advices, their support and encouragement throughout my thesis and for all the good moments and memories we had together. I would also like to thank the master degree trainees who helped me in the progress of my thesis project and those of my colleagues: Nicolas Hauville, Mickael Aoun, Eugénie Kluzska, Mael Bouillon.

Once again, I would like to express my sincere thanks to the entire GLIAD team, for their hospitality and the good times we shared together. I would like to thank all the platforms and collaborators who have been of great help during my thesis: PACEM (Catherine Guillet and Jérôme Cayon), SCIAM (Romain Mallet), MINT (Olivier Thomas), IPR of Rennes (Dr. Frank Artzner), MOLTECH (Olivier Aleveque, Magali Allain), RMes (François Loll and Thierry Rouillon).

Finally, I thank with all my heart my family and especially my mom for her infinite support and her unconditional love as well as my sister for her patience and her encouragements. Thanks to them, I could live more serenely these 3 years of challenge, full of emotions, but also of happiness.

CONTENTS

Chapter 1 1
General Introduction 1

1. GENERAL INTRODUCTION 2

Chapter 2 24
Thesis aim and objectives 24

2. THESIS AIM AND OBJECTIVES 25

Chapter 3 28
Hyaluronic acid-based systems 28

3. HYALURONIC ACID BASED SYSTEMS: HYALURONIC ACID SCAFFOLDS FOR LOCO-REGIONAL THERAPY IN NERVOUS SYSTEM RELATED DISORDERS: REVIEW: MDPI (2022) (ACCEPTED) 29

SUPPLEMENTARY DATA : 56

Chapter 4 68
Encapsulation of BMP-4 into polymer-based nanoparticles 68

4. ENCAPSULATION OF BMP-4 INTO POLYMER-BASED NANOPARTICLES 69

Chapter 5 95
Development of nanocomposite 95
hydrogels for Glioblastoma application 95

5. DEVELOPMENT OF NANOCOMPOSITE HYDROGELS FOR GB APPLICATION 96

Chapter 6 116
General discussion and 116
perspectives 116

6.GENERAL DISCUSSION AND PERSPECTIVES 117

TABLE OF FIGURES : 125

SUPPLEMENTARY FIGURES 128

Annexes 134

ABBREVIATIONS

ATR-FTIR Attenuated total reflectance-Fourier transform infrared
BBB Blood-brain barrier
bFGF Basic fibroblast growth factor
BMP Bone morphogenetic protein
BMPR BMP receptor
BSA Bovine serum albumin
CDKN2A Cyclin-dependent kinase inhibitor 2A
CHI3L1 Chitinase-3-like protein 1
CNS Central Nervous System
CSCs Cancer stem cells
CT Computed Tomography scan
CXCR4 C-X-C chemokine receptor type 4
DCM Dichloromethane
DLS Dynamic light scattering
DMEM Dulbecco's modified Eagle's medium
DMI Isosorbide dimethyl ether/dimethyl isosorbide
ECM Extracellular matrix
EE Encapsulation efficiency
EGF Epidermal growth factor
EGFR EGF receptor
ELISA Enzyme-linked immunosorbent assay
EMT Epithelial-mesenchymal transition
EZH2 Enhancer of zeste homolog 2
F98 Murine malignant glioblastoma cell line F98
FBS Fetal bovine serum
FDA Food and Drug Administration
FE Electrostatic force
FGF Fibroblast growth factor
GB Glioblastoma
GFAP Glial fibrillary acidic protein
GSC Glioblastoma stem-like cell
HA Hyaluronic acid
HGFR Hepatocyte growth factor receptor
HIF Hypoxia-inducible factor
HPBCD Hydroxypropyl-β-cyclodextrin
ICH International Conference on Harmonization chloride
IDH1 Isocitrate déshydrogenase 1
L929 Fibroblast cell line
MAPK Mitogen-activated protein kinase
MC Methyl cellulose
MDR Multidrug resistance MP Microparticule
MGMT O6-methylguanine–DNA methyltransferase
MRI Magnetic Resonance Imaging
MSC Mesenchymal stem cell
Mw Weight average molecular weight
NaCl Sodium chloride
NaOH Sodium hydroxide
NC Nanocomposite scaffold
NF1 Neurofibromine 1
NGF β-nerve growth factor

NHS N-hydroxysuccinimide
NIH3T3 Fibroblast cell line
NIR Near infrared
NPs Nanoparticles
NSCs Neural Stem Cell
O/W Oil-in-water
P188 Poloxamer 188
PANCMA Poly(acrylonitrile-co-maleic acid)
PBS Phosphate-buffered saline
PD-1 Programmed cell death protein 1
PDGF Platelet-derived growth factor
PDI Polydispersity index
PE Precipitation efficiency
PEG Poly(ethylene glycol)
PEO Poly(ethylene oxide)
pI Isoelectric point
PLGA Poly(lactic-co-glycolic acid)
PLGA-COOH PLGA with uncapped carboxylic acid terminal
PLGA-COOR PLGA with ester capped carboxylic acid terminal
POL Poloxamer 407
PTEN Phosphatase and tensin homolog
SD Standard deviation
SDF-1α Stromal cell-derived factor-1α
SEM Scanning electron microscopy
TEM Transmission electron microscopy
TGF-β Transforming growth factor beta
TGF-β Transforming growth factor-β
THF Tetrahydrofuran
TiO2 Titanium dioxide
TMZ Temozolomide
TMZ Temozolomide
TP53 Tumor protein 53
Tris Tris(hydroxymethyl)aminomethane
TTF Tumor-treating field
U87-MG Human malignant glioblastoma cell line U87-MG
VEGF Vascular endothelial growth factor
W/O Water-in-oil
ZP Zeta-potential

Chapter 1
General Introduction

1. GENERAL INTRODUCTION

1.1. Glioblastoma

1.1.1. Glioblastoma tumor physiopathology

Glioblastoma (GB) is the most severe and highest grade malignant glioma with an annual incidence of 5.26 per 100,000 and accounts for 17,000 new cases each year [1–3]. Unfortunately, these types of tumors reduce patients' quality of life and prognosis, with a median survival time of 15 months after diagnosis [1,2]. In fact, GB is defined as grade IV glioma and is the most deadly and most common malignant primary brain tumor. Unlike other solid tumors, GB is highly invasive to adjacent tissues in the brain and rarely metastasizes to other organs, but it causes an increased rate of recurrence and tumor transformation in healthy cells [1–3]. Current FDA-approved treatments are based on surgical resection of most tumors, followed by systemic chemotherapy and radiation therapy, and adjuvant therapy with temozolomide (TMZ) according to the Stupp protocol [2–5]. Despite the unquestionable benefits associated with this therapeutic approach, recurrence occurs in 90% of cases after initial surgery[4]. This common problem is primarily due to a specific population of cancer stem cells, called tumor-initiating stem cells, that are highly tumorigenic and often remain unaffected after surgery or chemotherapy [6–10]. Therefore, the ability to divide asymmetrically leads to GB recurrence, but few treatment options are available in this case [6–10].

GB is a malignant tumor that seriously affects the central nervous system (CNS). The disease occurs primarily in caucasian men and is more prevalent by age 60 [11–13] ; the etiology of GB is previously unknown and requires further research. However, exposure to intense ionizing radiation has been shown to rise up the risk of developing GB but no studies have shown the involvement of other environmental factors such as cell phones waves, exposure to N-nitroso compounds and pesticides [13–15]. Cases mainly occur sporadically in individuals with no family history, but a few cases are associated with autosomal dominant hereditary syndromes: neurofibromatosis types 1 and 2, turcot syndrome [2]. Patients who develop GB exhibit general and tumor site-specific symptoms such as loss of consciousness, headaches and seizures [16–18]. GB is a deadly cancer with an estimated survival time of 3-4 months due to lack of treatment [19,20]. Its detection is made by imaging techniques such as magnetic resonance imaging MRI or computed tomography (CT) scan [14,21]. Currently, first-line treatment for this condition consists on maximal removal of the tumor to reduce the risk of recurrence. This surgical procedure associate chemotherapy combined with radiotherapy (RT) [1–4,20]. A good tumor management and a concomitant RT and chemotherapy improves life expectancy in patients to 15 months, but GB remains a tumor with a high recurrence rate. As a result, survival at 30 months is low, with less than 5% of patients surviving up to 5 years [13–15]. GB represents 54% of diagnosed gliomas in adults and 16% of primary brain tumors. It is also the tumor with the highest incidence and malignancy among primary astrocyte tumors [20,22,23]. Most often (about 90%) GB occur spontaneously within 6 months and are called "primary" or "*de novo*" GB. Low-grade gliomas can develop over the years and form what is known as "secondary" GB [24]. This tumor originates from astrocyte-shaped cancer cells, but remains highly heterogeneous. In fact, GB is composed of cancer cells that form tumor masses, as well as cancer stem cells (CSCs) and non-neoplastic cells (macrophages, neutrophils, endothelial cells, perinatal period ...). This set of cells forms various niches within the tumor and the hypoxic niche consists of a dense set of cells surrounding the necrotic core.

High cell density and insufficient vascularization of the area results in hypoxia, which activates hypoxia factors HIF-1α and HIF-2α, responsible for promoting CSC. Necrotic cells in the center of the niche release proinflammatory signals that allow recruitment of cells of the innate immune system, resulting in

immunosuppressive and angiogenic effects. Perivascular lymphadenopathy provides a microenvironment favorable for the growth of CSCs because the interactions between neoplastic and non-neoplastic cells promote increased vascular endothelium growth factor (VEGF) activity and release of angiogenic factors such as FGF and PDGF. Thus, the perivascular niche allows neovascularization of the tumor and also recruitment of non-

cancerous cells to maintain the immunosuppressive effect. Finally, the invasive niche includes cancer cells in the periphery of the tumor. Perivascular niches have the ability to penetrate healthy tissue with the brain's white matter. This entry is accomplished by an epithelial-mesenchymal transition (EMT) mechanism, which allows cells to acquire a parent phenotype and by taking over endocrine communications from astrocytes and microglial cells [25,26].

Besides, methylation types play a valuable function in gliomas. They are not quite required for the tumor subclassification however they may be helpful when using novel therapies. Methylation of the O6-methylguanine DNA methyltransferase (MGMT) promoter has emerged as sturdy prognostic element withinside the remedy of GB. It is related to an advanced reaction to chemotherapy with temozolomide and longer average survival. MGMT promoter methylation has implications for the physiopathology of the tumor of patients [27]
It has been shown that the MGMT promoter methylation can change from the primary tumor to relapse in about 24% of glioma patients [27]. Testing MGMT promoter methylation not only in the primary tumor, but also in relapse would be helpful. It is recommended that clinical studies on GB recurrence take into consideration MGMT promoter methylation changes and investigate if these changes should be accounted for the treatment decision [27–29].

Immunotherapy focused on poor regulatory molecules on the immune inhibitory checkpoint axis (programmed cell death protein 1 (PD-1) and its ligand ([PD-L1) have shown breakthroughs in lots of cancers. PD-L1 is broadly expressed in nearly all tumor cells [30]. PD-1 is the receptor of PD-L1 and is expressed on CTLs and immune natural killer (NK) cells [30]. Indeed, the PD-1/PD-L1 axis is the essential pathway that inhibits the activation or proliferation of CTLs and NK cells within the tumor microenvironment [30]. Moreover, PD-L1-mediated immunosuppression in GB is related to M2 macrophage polarization and low survival [30]. The PD-L1 is linked to the PD-L1 blockade, and responses had been substantially better in PD-L1-positive tumors than in PD-L1-negative tumors [30]. Thus, the PD-L1 degree in GB is taken into consideration as a first-line predictive marker of PD-1/PD-L1 antibody response. Precise detection of PD-L1 expression in GB tissues can also forecast PD-1/PD-L1 antibody response [30]. Some studies have shown that PD-L1 is an adverse prognostic marker for GB affected patients; PD-L1-mediated immunosuppression may be also associated to the infiltration and M2-polarization of macrophages, and that PD-L1 may act as a good predictor and an effective GB therapeutic target [31,32].

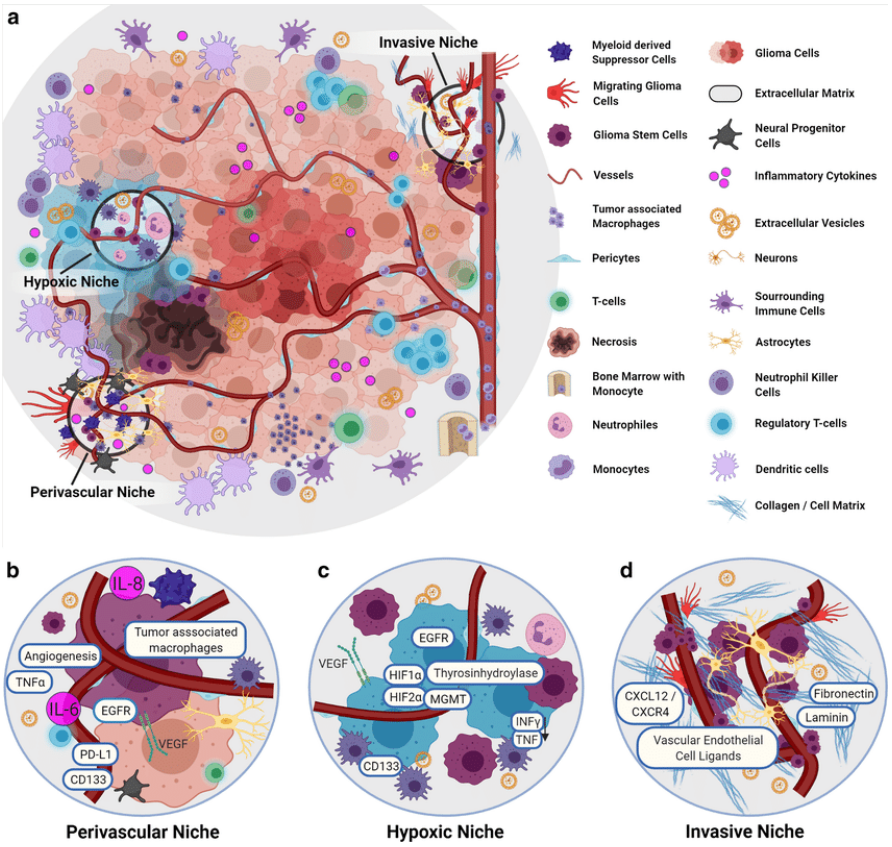


Figure 1: GB different niches and microenvironments elements. Barthel, Lennart et al. "Glioma: molecular signature and crossroads with tumor microenvironment." Cancer metastasis reviews vol. 41,1 (2022): 53-75. doi:10.1007/s10555-021-09997-9 (Authorization in course)

The GB tumor microenvironment with immune agents and three major niches revealed the presence of specific molecular profiles (Figure 1 from Barthel et al 2022).

(i) Vascular niche: this niche is characterized by marked angiogenesis with a corresponding increase in VEGF. This is where tumor macrophages accumulate. Cytokines such as interleukines IL-6 and IL-8 are elevated. Similarly, PTEN increases protein matrix crosslinking and promotes angiogenesis.

(ii) The hypoxic niche contributes to glioma growth and resistance. Elevated PTEN, HIF contribute to the regulation of VEGF and IL-8 and support the presence of stem cells indicated by elevated CD133. Inflammatory cytokines are reduced through tyrosine hydroxylase activity.

(iii) Invasive niche: this niche is characterized by transition to a state of normal blood vessels and normal brain tissue. Vascular-associated stem cells, glioma cells and glioma cells are involved in tumor growth, and endothelial cell-associated glioma stem cells via CXCL12/ CXCR4. The cellular matrix also supports the growth of invasive tumors.

In summary, GB has multiple abilities, including uncontrolled cell proliferation, invasiveness, necrosis tendency, and a high triggering of angiogenesis. Interactions between cells and interactions with the microenvironment are crucial because they affect the phenotype of tumor cells and promote proliferation or infiltration depending on the factors present in the environment. For example, hypoxia, ionizing radiation and chemotherapy cause multiple molecular pathways (Ras, HGFR, STAT3 ...) leading to an invasive phenotype while angiogenesis or anaerobic glycolysis will cause a proliferative phenotype via other pathways (Myc, VEGF, CSPG...) [33]. The ability to proliferate and migrate and high genetic instability grants CSCs resistance

to apoptosis and chemotherapy, often leading to recurrence [6–8]. Despite this ability to invade GB, it localizes only in the CNS and does not form extracranial metastases except in rare cases [34]. This localization appears to be associated with the specificity of the brain tumor microenvironment and systemic immunity that limits the spread of cancer cells in the body [35]. Due to GB heterogeneity, it is classified as a subtype with certain genetic changes. It is called classical, mesenchymal, anterior, and nervous GB. It is associated with high proliferation. It is mutated in the gene encoding EGFR, leading to increased expression. GB has a deletion at the CDKN2A p16INK4a locus and has one chromosome on chromosome 10 pair. Mesenchymal GB is characterized by frequent mutations and deletions of the neurofibromin 1 (NF1) gene, which is involved in the regulation of Ras signaling pathways, and overexpression of genes involved in protein synthesis (NF-κB, CHI3L1, HGFR). Nerve subtypes overexpress many mythological markers, whereas preneuronal GB shows changes in the PDGFRA gene and mutations in the IDH1 and TP53 genes that are involved in tumor progression. These clusters may share common mutations, such as deletions of the PTEN gene, which are involved in the regulation of the cell cycle. Classic and mesenchymal GB are often associated with a poor prognosis, as opposed to the anterior and nerve subtypes of this disease type. In particular, unlike other subtypes, classical and mesenchymal GB primarily affect the aging population [24].

1.1.2. Current treatments and their drawbacks

Surgery progresses

A comprehensive strategy is necessary for the treatment of newly diagnosed GB. The current standard care consists of the most safe surgical resection possible, followed by concomitant radiotherapy with the oral alkylating chemotherapy drug temozolomide (TMZ; Temodar®), and adjuvant treatment with TMZ. Because these tumors are frequently invasive and frequently located in crucial regions of the brain, such as regions that regulate speech, motor function, and the senses, extensive and complete surgical resection of GB is challenging. Radical removal of the original tumor mass is not curative because to the high degree of invasiveness, and infiltrating tumor cells inevitably persist in the surrounding brain, causing the illness to develop or return in the future [36,37].

Numerous studies have shown the value of aggressive surgical resection when feasible, with trends showing better results in individuals who undergo more extensive resection [37–39]. Many studies have found statistically significant relationships between higher resection extent and longer progression-free survival (PFS) and overall survival (OS) [37,40–43]. More extensive resections may now be accomplished while maintaining function and quality of life because to advancements in surgical and preoperative imaging techniques [37,42].

In preoperative planning, the use of functional MRI and diffusion tensor imaging (DTI), as well as ultrasonography, CT scans, and MRI with direct stimulation during surgery, has enabled multimodal neuronavigation and the integration of patient-specific anatomic and functional data. Despite these advancements, distinguishing between normal brain and residual tumor remains a significant issue, and the use of 5-aminolevulinic acid (5-ALA) dye for fluorescence guiding has been shown to be more successful than standard neuronavigation-guided surgery alone [44]. A Cochrane study, on the other hand, discovered only low- to very low-quality evidence that image-guided surgery utilizing 5-ALA, intra-operative MRI, or DTI neuronavigation enhanced the proportion of patients with high-grade glioma who had a complete tumor excision on postoperative MRI [45].

Cost and the requirement for specialized equipment, operators, and surgical suites are two further drawbacks of these new technologies. More research is needed to explain the clinical advantages before they are adopted as the standard of therapy for GB affected patients.

Despite breakthroughs in surgical resection, individuals with GB have a terrible prognosis, with a median survival of 15 months [46]. Aside from the quantity of surgical resection, additional variables have been linked to improved survival. Patient age and Karnofsky Performance Status are well known as prognostic markers, with younger patients and higher performance status having a better chance of survival. Tumors larger than 5-6 cm in diameter and those that cross the midline have been linked to poor outcomes [47]. Supratentorial (cerebrum) and cerebellar tumors have a better prognosis than tumors in the brainstem or diencephalon because they are more susceptible to surgical therapy [48]. A statistically significant improvement in OS following the start of vigorous multimodality therapy [49].

Gliadel® wafer therapeutic strategy

Arbor Pharmaceuticals' Gliadel® wafers (prolifeprospan 20) are biodegradable copolymers loaded with the alkylating chemical carmustine (1,3-bis(2chloroethyl)-1-nitrosurea (BCNU)). At the early 1990s, Gliadel® wafers were created for the treatment of high-grade glioma (HGG) in order to overcome the constraints of blood-brain barrier impermeability to antineoplastic drugs [50]. It consists on a biodegradable matrix system that can provide a targeted and sustained release of BCNU after being implanted into the resection cavity. It has shown to be a relatively safe and adapted treatment for HMG in randomized, double-blinded, placebo-controlled, multicenter human Phase III clinical trials [51–53]

Adjuvant systemic chemotherapy extends primary malignant glioma patients' survival beyond 12-18 months. Gliadel® wafers with carmustine (BCNU) implanted in the resection cavity after surgery are the only interstitial chemotherapy treatments approved for malignant glioma. Westphal and colleagues (n = 240) found a 29% risk decrease (P = 0.03) in the BCNU wafer-treated group throughout the course of a 30-month study [54].
Patients with malignant glioma who received BCNU wafers at the time of first surgery in conjunction with radiotherapy treatment had a survival benefit at 2 and 3 years compared to placebo [54]. Besides, convulsions, disorientation, cerebral edema, infection, hemiparesis, aphasia, and visual field abnormalities were the most commonly reported side effects [54].

The wafer Gliadel® is an alternative for individuals with newly diagnosed malignant glioma who have a near gross complete resection [50,54]. There is no data to compare Gliadel® to systemic therapy, and the choice to combine Gliadel® with systemic therapy should be determined for each patient individually. The patient group that would benefit from Gliadel® (based on age, histology, and performance status) is unknown; more research is needed. Gliadel® is also a possibility for individuals with recurrent malignant glioma that has been surgically resected [50,54].

1.2. Differentiation: an interesting strategy in cancer therapy

1.2.1. Differentiation as a therapeutic strategy for GB cells

Novel therapies in development include monoclonal antibodies against vascular endothelial growth factor (VEGF), tyrosine kinase receptor inhibitors [55–57], and Programmed death-ligand 1 (PD-L1) [23,31,32,58]. Despite recent advancements, only a few people with GB survive 5 years following diagnosis (3-10%, depending on the regimen used) [23].
The following criteria were used to validate the stem cell phenotype of CSCs: their ability to form primary spheres in vitro; their capacity for self-renewal on clonogenic and population analysis; their capacity to differentiate under serum stimulation both into GFAP-positive astrocyte-like cells and into neurofilament expressing neuron-like cells; the generation of tumors upon orthotopic (intracerebral) transplantation in immunodeficient mice; and keeping the chromosomal abnormalities from the parent tumor [59].

Differentiation reduces the tumorigenic and stem cell-like capacity of neurosphere cultures and that targeting the bCSC population is achievable by directly reducing EGFR signaling. Some findings have shown that targeting the bCSC population with differentiation therapy, perhaps in conjunction with anti-EGFR medication, might be a viable therapeutic strategy for patients with GB [60].

Because of its severity, high risk of recurrence, and resistance brought on by CSC, GB is a cancer that is challenging to treat. Numerous markers for this cell type are present in CSCs (CD24, CD34, Nestin, Sox2). Prominin-1, also known as CD133, is one of them and may distinguish CSCs from other cancer cells[62–64]. It is frequently seen in several malignancies, including glioma and GB [61]. GB-CSC modifies the cell fate-determining Nocht, Wnt, NF-B, and BMP signaling pathways in order to preserve the phenotypic of this strain. CSCs can resist apoptosis, maintain the parental phenotype, and lessen receptivity to differentiation cues thanks to these changes [9,62]. With the goal of creating medicines that can eradicate CSCs and prevent the recurrence of illness, several signaling pathways are being researched.

It has been demonstrated that CSCs overexpress Gremlin 1, an endogenous BMP (bone morphogenetic protein) antagonist. CSCs can express this molecule, which preserves their parental phenotype, although cancer cells that do so frequently become undifferentiated [63]. Additionally, GB-CSC activates the Zestehomolog 2 (EZH2) gene's enhancer abnormally, blocking the BMP pathway and producing the same-named polycomb enzyme. In actuality, EZH2 short-circuits cellular impulses and methylates the BMP receptor gene. The BMP signaling pathway's forced expression or inhibition of this methylation restores the differentiation effect and lessens the number of CSCs and their invasiveness [64–66]

While it is obvious that GB stem cells can differentiate, it is less clear if they can commit to sustained differentiation and enter the terminal cell cycle. Clinical translation of BMP-based differentiation therapy may thus be challenging. First, there are distinct differences in responses amongst cell lines, and this is to be expected in patients. Secondly, whereas induction is quick, methylation alterations are gradual and need prolonged exposure. Thirdly, acquired changes are not permanent, and reversion, de-differentiation, or selection of differentiation-resistant clones are all possibilities [67].
Clearly, overcoming these hurdles at the outset will be a significant task in the design of differentiation treatments. Implementing differentiation treatment for GB requires a better knowledge of the processes by which tumor cells avoid differentiation commitment [67].

1.2.2. Bone Morphogenic Proteins as biodrugs

Specifically involved in growth control or differentiation, BMP is a class of proteins that is part of the transforming growth factor-superfamily. BMPs play a role in all stages of organism development, including early and late embryogenesis. 15 BMPs have been discovered to have a pleiotropic effect in mammals. BMP is a proprotein that is present in the cytoplasm [68]. Type I or type II transmembrane receptors (BMPR-I / II) detect its cleavage and phosphorylate the Smad protein, a family of mediator proteins [69,70]. The Smad1/5/8 protein, which binds to the Smad4 cofactor, is phosphorylated by the receptor. The complex is subsequently moved into the nucleus, where it interacts with different coactivators or cosuppressors to change the expression of certain genes (Figure 2) [71].

There are non-standard routes mediated by MAPK (mitogen-activated protein kinase), in addition to the usual Smad pathway [72,73]. The study stresses its capacity to stimulate BMP4 and glioblastoma CSC differentiation based on existing information. This protein can produce neural stem cell (NSC) and CSC-differentiated phenotypes by activating BMP typical pathways. Additionally, it lessens the proliferative, invasive, and tumorigenic capacity of glioblastoma CSCs both *in vitro* and *in vivo*. Additionally, these effects are associated with elevated levels of the cell-differentiation proteins claudin and E-cadherin [74,75]

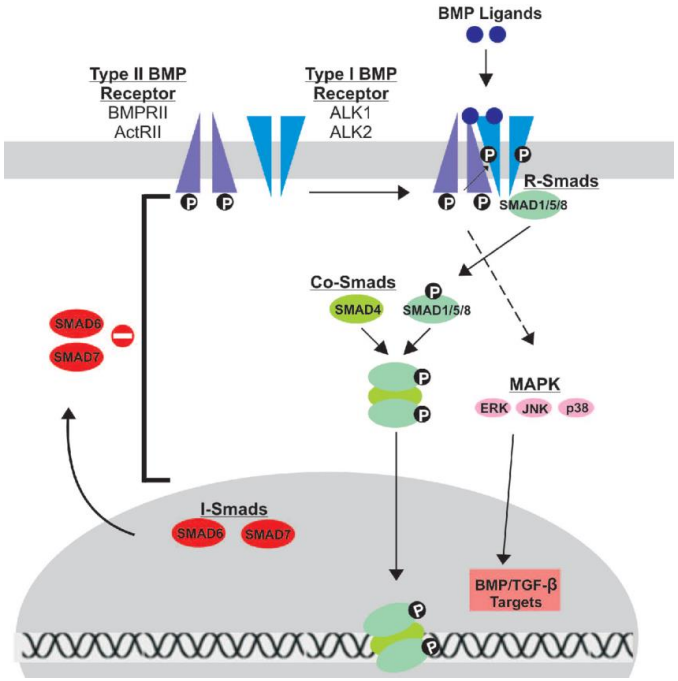


Figure 2: SMAD pathway triggered by BMP-4 Beederman, M. et al. BMP signaling in mesenchymal stem cell differentiation and bone formation. Journal of Biomedical Science and Engineering 6, 32–52 (2013).(Autorisation in course)

Consequently, the use of BMPs, notably BMP4, appears promising in raising knowledge of chemotherapy and radiation therapies among CSCs [73]. Among over 20 BMPs family proteins, BMP-2, BMP-4, BMP-6, and BMP-9 are significantly involved in ossification, of which, the effects of BMP-9 on ossification are the strongest, followed by those of BMP-2 and BMP-7. BMP-2, BMP-6, BMP-7 and BMP-9 that have shown differentiation properties on osteoblasts and bone marrow mesenchymal stem cells [76–82]. BMP-2 is a protein with similar properties as BMP-4 and are both very important for bone formation.
As a secretory, acidic, hydrophobic glycoprotein, BMP-4 is a mature polypeptide has 116 amino acids and a molecular weight of around 30 kDa. BMP-4 and BMP-2 are similar structurally. Between BMP-4 and BMP-2, there is an 83% identity in the amino acid sequence [72,83,84]. Human BMP-4 exists in two different forms, one of which is expressed in the mature placenta tissue and has a protein precursor with 402 amino acid residues, and the other of which is expressed in osteosarcomas and has a protein precursor with 408 amino acid residues. As a member of the BMP family, the core of the BMP-4 monomer is a family-conserved cysteine knot structure[72,83,84]. There is a signal peptide region at the N-terminus of BMP-4. It may contain four N-linked glycosylation sites. Three of these are in the same location [84].
Mature human BMP-2 is an acidic glycoprotein with a molecular weight of approximately 32 kDa. It contains 114 amino acid residues, enriched with glutamate, and is soluble in neutral saline with an isoelectric point of 4.8–5.1. BMP-2 has cross-species homology among bovine, rabbit, mouse, and human. The crystal structure of BMP-2 was assessed at a resolution of 2.7 Å by X-ray diffraction analysis [85]. The structural basis of the BMP-2 monomer is three intrachain disulfide bonds formed by six family-conserved cysteine residues [84]. Human BMP-2 proprotein contains four glycosylation sites. Below this are the glycosylation sites of the polypeptide chain of mature BMP-2 [84].

Despite extensive study on systemic routes, transport and targeting of BMP-4 and other common molecules in the brain remains problematic due to the blood-brain barrier (BBB) and biodistribution. The BBB is a crucial barrier for brain protection. It is made up of endothelial cells, astrocytes, pericytes, neurons, and the brain

basement membrane, and it allows for finely regulated impermeability. Exchanges occur via a variety of mechanisms, including passive diffusion, transcytosis, and transporters [86,87]. This mechanism protects the brain by permitting only tiny lipophilic molecules (400 Da) to pass by diffusion while peptides and proteins are transported via specialized transporters. As a result, the BBB blocks the majority of medicinal compounds [88–91]

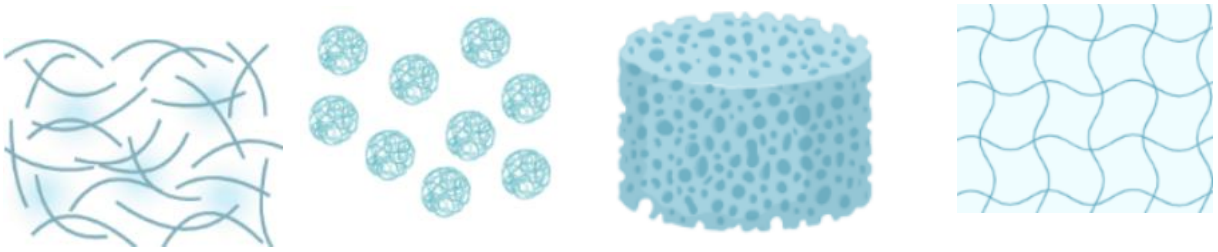
The permeability of this physiologic barrier is a significant research area, and numerous bioengineering strategies, such as the use of viral vectors and micro and nanoparticles (MP, NP) based on their physicochemical features, have been proposed [92].
Many characteristics, including as solubility, stability, distribution, method of administration, and potential adverse effects, must be addressed while developing therapeutic proteins [93,94]. Subtle modifications in this structure cause denaturation and, as a result, inefficiency. As a result, preserving protein integrity is critical. However, these therapeutic proteins are rapidly destroyed by proteases in the circulation and are difficult to precisely target [95–97]

Due of these challenges, researchers have developed local area techniques to minimize degradation and better target therapeutic proteins. Protein delivery systems based on polymer architectures include MPs and NPs, hydrogels, and porous structures loaded with drugs and biodrugs, displaying controlled drug release properties.

1.3. Polymer-based protein delivery systems

1.3.1. Common forms of polymer-based protein delivery systems

Therapeutic proteins have gotten a lot of interest because they play important roles in a variety of biological processes [93,94]. Their distribution to target locations, on the contrary, is difficult because to their inherent sensitivity to varied environmental conditions [93,94]. Polymeric systems can provide not only physical protection from external stimuli, but also tailored protein delivery to specified areas [93,94]. Many applications favor NPs containing charged polymers because they provide moderate protection via electrostatic interactions [93,94]. Furthermore, most organs have a certain pH, and by adjusting the degree of electrostatic interactions and contact length between the target and polymeric NPs, the latter's intracellular absorption and hence long-term therapeutic effectiveness may be improved [98–102].
Others systems such as fibers, scaffolds, sponges and hydrogels have been developed in order to vectorize and administer proteins in a locoregional way (Figure 3) [103–105].



Fibers Micro/Nanoparticles Scaffold Hydrogel

Figure 3: Common types of polymer-based delivery systems

However, these protein carriers have substantial drawbacks, such as limited encapsulation efficiency, physical instability, and intrinsic toxicity to cells or tissues [106,107]. Polymeric NPs, namely polymer aggregates prepared from natural or synthetic polymers using various strategies, have recently got the interest of researchers as protein carrier systems due to their multifunctionality; they can protect loaded drug from extreme conditions, allowing for enhanced bioavailability at target sites by forming complex or in the complex state with proteins [97].

These properties make polymeric NPs ideal for carrying therapeutic, yet non-toxic, quantities of protein to specified areas. For biomedical polymeric nanoparticles (NPs) are non-toxic colloidal particles with sizes ranging from 10 to 1000 nm that can aggregate form spheres, discs, rods, or ellipsoids [101,108,109].
They are frequently made from biodegradable synthetic polymers such as poly(lactide-glycolide) (PLGA) copolymers and poly(caprolactone)s (PCLs), as well as natural polymers such as albumin, gelatin, alginate, collagen, and chitosan [110–117]. Depending on the specifications of the NP design, the polymers might be functional or non-functional. Polymeric NPs inert nature allows them to avoid endosomal internalization, which would otherwise result in clearance and breakdown by lysosomes. Furthermore, charged polymers can be functional, such as being switched to stimuli-responsive drug release such as pH, temperature, radiations [118–120].

1.3.2. Nanoprecipitation of proteins

Proteins are large biological macromolecules made up of one or more chains of amino acids [93,121]. They play a variety of important roles in biological systems. Intracellular proteins that exist naturally provide critical tasks such as enzyme catalysis, signal transmission, gene control, and the maintaining of a delicate balance between cell survival and programmed death [93,121]. Proteins are vulnerable to environmental conditions or neighboring modifications because to their fragile and tertiary structure [97]. Many diseases are connected with damage to their function [93]. Proteins have acquired great appeal in the pharmaceutical sector due to their dynamic ability to execute a wide range of complicated tasks and their lesser propensity to disturb normal biological processes [93,94,122].
Their inherent vulnerability to various environmental stresses found within the human body, such as hydrolysis, oxidation, and proteolysis, limits their clinical use [97].
They are readily destroyed by enzymes in the gastrointestinal tract (GIT) when delivered orally or parenterally, have difficulties penetrating across gastrointestinal mucosa, and are removed during first-pass hepatic clearance [93,94].

Furthermore, protein distribution to the intracellular space (their primary location of action) is hampered by many proteins' intrinsic features, such as their large size, variable surface charges, and fragile tertiary structures [121].
It has therefore been proposed that encapsulating therapeutic proteins within biocompatible matrices can protect them from early denaturation and subsequent loss of efficiency while also decreasing their immunogenicity and systemic toxicity [93,94].
Encapsulating fragile proteins within carrier systems not only allows for targeted delivery to a specific organ or tissue by functionalizing the carrier with targeting moieties, but it also reduces the overall concentration necessary to provide therapeutic effects and, the size of the carrier systems must be in the nm range to allow intracellular absorption [93,94].

Numerous research have been conducted to investigate the influence of protein interactions with polyelectrolytes on protein release from polymeric systems. In one research, lysozyme and chondroitin sulfate were complexed before being encapsulated in PLGA microparticles [98,99,123,124], which improved protein release relative to natural lysozyme. The complex's release profile revealed an initial moderate release followed by a zero-order release with homogenous complex dispersion in the polymeric matrix [125]. In another work, complexing lysozyme with glycolic chitosan reduced early release while increasing total protein release rate [126].

Proteins in the solid state are known to be more stable than those in an aqueous solution. The protein structural mobility is reduced in the solid state, which promotes stability and protects activity. Encapsulation technologies such as solid/oil/water (S/O/W) [127] and solid/oil/oil (S/O/O) [128] emulsions have been developed for this purpose in order to stabilize the proteins and prevent adsorption at the water/oil interface. Nevertheless, protective additives such as cyclodextrins and surfactants are required to keep some proteins active [100,101,129].

Surfactants are amphiphilic compounds that tend to lower the surface tension of the protein solution, preventing adsorption and aggregation on hydrophobic surfaces *via* an often competitive mechanism. Non-ionic surfactants are preferred to ionic surfactants, which can bind to various protein groups and cause denaturation of the proteins. Surfactants with varying hydrophilic-lipophilic balances (HLB) were co-encapsulated in a research of insulin encapsulation via the water/oil/water emulsification technique. Within these surfactants, only polysorbate 20 improved protein stability in PLGA particles [130]. Polysorbate 20 and polysorbate 80 were not successful in stabilizing lysozyme in another study [131].
Poloxamer 407, on the contrary hand, was effectively employed to encapsulate urease in PLGA particles; the gel structure of the hydrophilic poloxamer chains preserved the protein during formation. Furthermore, it was demonstrated that phosphatidyl choline may stabilize interleukin-1- during encapsulation [129]
Poloxamer 188, has been successful to stabilize lysozyme, chymotrypsin, peroxidase, TGFβ3 and TGFβ1 during nanoprecipitation process followed by phase separation encapsulation [100–102,132].

1.3.3. Nanoparticles processes and non-toxic solvents

Indeed, hydrophobic interactions during formulation between the polymer (PLGA) and the protein pose a stability issue since the protein might adsorb onto the polymer and denature. Likewise, the pH, ionic strength, and polarity of the solvent all have an impact on protein adsorption. Because of the protein neutrality, a pH near to the isoelectric point (Pi) promotes this phenomena. Adsorption is increased by increasing the ionic strength and employing more polar solvents [133]. According to one research, because ethyl acetate is less polar than dichloromethane, it less interacts with the polymer, making it a more appealing solvent for formulation procedures in terms of protein stability (Figure 4) [133,134] .
The chapter 4 focuses on the validation of a phase separation-based formulation approach for therapeutic protein encapsulation. Under specific conditions, adding an aqueous solution to a polymer solution causes controlled desolvation of the polymer, permitting particle formation. This procedure was developed without the use of any harmful solvents [100–102,132,135].

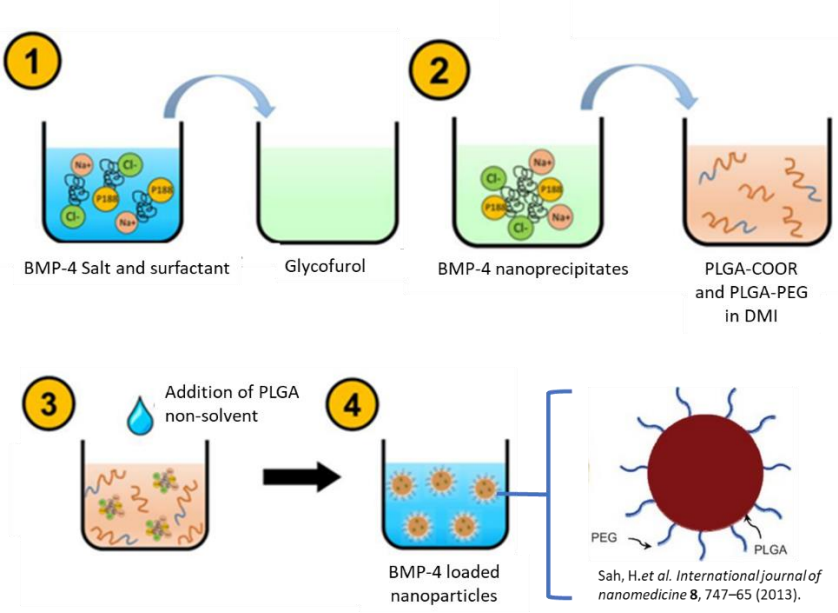


Figure 4 Phase separation process of PLGA NPs. Adapted from Haji Mansor, M. et al. Eur J Pharm Biopharm 125, 38–50 (2018). (Autorisation in course)

Glycofurol (GF) is a colorless, odorless liquid that is transparent. It is a non-volatile organic solvent that is soluble in water and is suitable for intravenous or intramuscular usage up to a concentration of 50% (v/v) [136]. It is employed as a co-solvent in various pharmaceutical formulations [136–138], but it is also used as a vaccines adjuvant [139] and as a vehicle for injectable polymeric implants [140–142]. Co-administration of glycofurol has been demonstrated to increase peptide absorption, including insulin and T-peptide [143]. Furthermore, it has recently been reported as a PLGA solvent in the formation of micro- and nanoparticles [109,144–146]

Dimethyl isosorbide (DMI) is a colorless, transparent liquid that is non-flammable and non-volatile. It is highly soluble in water (1.103 g.L-1 at 25°C). It is utilized as a solvent for various active substances and cosmetic oils [147], as well as a co-solvent to improve the solubility of weakly water-soluble components such steroids [148]. DMI is utilized in cosmetic formulation to promote the penetration of certain cosmetic chemicals since it is not irritating to the skin, eyes, or ears. It is also used in pharmaceutical applications [82] and as a solvent to dissolve embolic biomaterials [149–151]. This solvent, which may be injected intravenously or intraarterially, is employed in formulations with weakly water-soluble components [150].

An overview of glycofurol and dimethylisosorbide's characteristics is provided. According to the bibliographic studies and toxicity data, we believe that DMI and GF are the least harmful organic solvents (Table 1). In this project, we will utilize these solvents to dissolve the polymer (PLGA) in the formulation stages of particulate systems for growth factor Lysozyme and BMP-4 encapsulation.

Table 1: Solvent characteristics tested in in vivo models

Injectable solvents	LD50*(ml/kg)	Hemolytic activity[149]**	Cardiovascular toxicity [150]	Arterial Pressure reduction [150]	Angiotoxicity/ vasospasm duration (min) [151]
GF	3.5(iv./m)	Moderate	Insignificant	None	10.5
DMI	8.54(iv./r)	Low	Insignificant	None	5.9
DMSO	6.9(iv./m) 12.6(ip./m) 15(po./m)	Very high	Moderate	Moderate	19.1
NMP	4.4(ip./m)	Moderate	Significant	Significant	5

*LD50: median lethal dose; iv: intravenous, ip: intraperitoneal, po: oral, m and r: in mice and rats. **The study is performed by the intravenous and intra-arterial routes [149–151] .

1.3.4. Hydrogels

A hydrogel is a network of hydrophilic polymers that may absorb hundreds of times their dry weight in water, or between 10 and 20% (an approximate lower limit). Chemically, hydrogels can either be stable or they can break down and finally dissolve. When the networks are kept together by molecular entanglements and/or secondary forces such as ionic, H-bonding, or hydrophobic interactions, they are referred to be "reversible" or "physical" gels [118]. Physical hydrogels are not homogenous because they may contain molecular entanglements in groups or domains that are hydrophobically or ionically linked. In physical gels, free chain ends or chain loops also signify transient network flaws [152,153].
Systems of interest that are going to be described and characterized in this work, are physical hydrogels. Physical interactions such as hydrogen bonding [118,152,153], hydrophobic, electrostatic, van der Waals, and even - interactions cross-link physical HGs. This physical cross-linking can occur spontaneously or be driven by changes in environmental properties, the most frequent of which is temperature variation. The utilization of thermoresponsive particles that self-assemble following hydrophobic contact via heating has also been described. There are some hydrogels that are formulated using a cold gelation process and where the polymer is dissolved at 4 °C then the hydrogel undergoes structural modifications when the temperature increases and assess a hydrogel network at physiological temperature like poloxamer [154–158]. A change in light intensity is another way to generate physical cross-linking [97,99]. More detailed characteristics of hydrogels and other types of scaffolds will be discussed in Chapter 3.

References:

[1] Adamson C, Kanu OO, Mehta AI, Di C, Lin N, Mattox AK, et al. Glioblastoma multiforme: a review of where we have been and where we are going. Expert Opinion on Investigational Drugs 2009;18:1061–83. https://doi.org/10.1517/13543780903052764.
[2] Alifieris C, Trafalis DT. Glioblastoma multiforme: Pathogenesis and treatment. Pharmacology & Therapeutics 2015;152:63–82. https://doi.org/10.1016/j.pharmthera.2015.05.005.
[3] Stupp R, Brada M. High-grade glioma: ESMO Clinical Practice Guidelines for diagnosis, treatment and follow-up. Annals of Oncology 2014;25:9.
[4] Stupp R, Weller M, Belanger K, Bogdahn U, Ludwin SK, Lacombe D, et al. Radiotherapy plus Concomitant and Adjuvant Temozolomide for Glioblastoma. The New England Journal of Medicine 2005:10.
[5] Bahadur S, Sahu AK, Baghel P, Saha S. Current promising treatment strategy for glioblastoma multiform: A review. Oncol Rev 2019;13. https://doi.org/10.4081/oncol.2019.417.
[6] Alves ALV, Gomes INF, Carloni AC, Rosa MN, da Silva LS, Evangelista AF, et al. Role of glioblastoma stem cells in cancer therapeutic resistance: a perspective on antineoplastic agents from natural sources and chemical derivatives. Stem Cell Research & Therapy 2021;12:206. https://doi.org/10.1186/s13287-021-02231-x.
[7] Bradshaw A, Wickremesekera A, Brasch HD, Chibnall AM, Davis PF, Tan ST, et al. Cancer Stem Cells in Glioblastoma Multiforme. Front Surg 2016;3. https://doi.org/10.3389/fsurg.2016.00048.
[8] Huang Z, Cheng L, Guryanova OA, Wu Q, Bao S. Cancer stem cells in glioblastoma—molecular signaling and therapeutic targeting. Protein Cell 2010;1:638–55. https://doi.org/10.1007/s13238-010-0078-y.
[9] Lathia JD, Mack SC, Mulkearns-Hubert EE, Valentim CLL, Rich JN. Cancer stem cells in glioblastoma n.d.:16.
[10] Altaner C. Glioblastoma and stem cells. Neoplasma 2008;55:369–74.
[11] Gramatzki D, Dehler S, Rushing EJ, Zaugg K, Hofer S, Yonekawa Y, et al. Glioblastoma in the Canton of Zurich, Switzerland revisited: 2005 to 2009. Cancer 2016;122:2206–15. https://doi.org/10.1002/cncr.30023.
[12] Ostrom QT, Rubin JB, Lathia JD, Berens ME, Barnholtz-Sloan JS. Females have the survival advantage in glioblastoma. Neuro Oncol 2018;20:576–7. https://doi.org/10.1093/neuonc/noy002.
[13] Tamimi AF, Juweid M. Epidemiology and Outcome of Glioblastoma. In: De Vleeschouwer S, editor. Glioblastoma, Brisbane (AU): Codon Publications; 2017.
[14] Hanif F, Muzaffar K, Perveen K, Malhi SM, Simjee SU. Glioblastoma Multiforme: A Review of its Epidemiology and Pathogenesis through Clinical Presentation and Treatment. Asian Pac J Cancer Prev 2017;18:3–9. https://doi.org/10.22034/APJCP.2017.18.1.3.
[15] Bondy ML, Scheurer ME, Malmer B, Barnholtz-Sloan JS, Davis FG, Il'yasova D, et al. Brain tumor epidemiology: consensus from the Brain Tumor Epidemiology Consortium. Cancer 2008;113:1953–68. https://doi.org/10.1002/cncr.23741.
[16] Sizoo EM, Braam L, Postma TJ, Pasman HRW, Heimans JJ, Klein M, et al. Symptoms and problems in the end-of-life phase of high-grade glioma patients. Neuro-Oncology 2010;12:1162–6. https://doi.org/10.1093/neuonc/nop045.
[17] IJzerman-Korevaar M, Snijders TJ, de Graeff A, Teunissen SCCM, de Vos FYF. Prevalence of symptoms in glioma patients throughout the disease trajectory: a systematic review. J Neurooncol 2018;140:485–96. https://doi.org/10.1007/s11060-018-03015-9.
[18] Gilard V, Tebani A, Dabaj I, Laquerrière A, Fontanilles M, Derrey S, et al. Diagnosis and Management of Glioblastoma: A Comprehensive Perspective. J Pers Med 2021;11:258. https://doi.org/10.3390/jpm11040258.
[19] Faraz S, Pannullo S, Rosenblum M, Smith A, Wernicke AG. Long-term survival in a patient with glioblastoma on antipsychotic therapy for schizophrenia: a case report and literature review. Ther Adv Med Oncol 2016;8:421–8. https://doi.org/10.1177/1758834016659791.
[20] Omuro A, DeAngelis LM. Glioblastoma and other malignant gliomas: a clinical review. JAMA 2013;310:1842–50. https://doi.org/10.1001/jama.2013.280319.
[21] Bolcaen J, Kleynhans J, Nair S, Verhoeven J, Goethals I, Sathekge M, et al. A perspective on the radiopharmaceutical requirements for imaging and therapy of glioblastoma. Theranostics 2021;11:7911–47. https://doi.org/10.7150/thno.56639.

[22] Dolecek TA, Propp JM, Stroup NE, Kruchko C. CBTRUS statistical report: primary brain and central nervous system tumors diagnosed in the United States in 2005-2009. Neuro Oncol 2012;14 Suppl 5:v1-49. https://doi.org/10.1093/neuonc/nos218.
[23] De Vleeschouwer S, editor. Glioblastoma. Brisbane (AU): Codon Publications; 2017.
[24] Lombardi MY, Assem M. Glioblastoma Genomics: A Very Complicated Story. In: De Vleeschouwer S, editor. Glioblastoma, Brisbane (AU): Codon Publications; 2017.
[25] Hambardzumyan D, Bergers G. Glioblastoma: Defining Tumor Niches. Trends Cancer 2015;1:252–65. https://doi.org/10.1016/j.trecan.2015.10.009.
[26] de Almeida Sassi F, Lunardi Brunetto A, Schwartsmann G, Roesler R, Abujamra AL. Glioma Revisited: From Neurogenesis and Cancer Stem Cells to the Epigenetic Regulation of the Niche. Journal of Oncology 2012;2012:1–20. https://doi.org/10.1155/2012/537861.
[27] Feldheim J, Kessler AF, Monoranu CM, Ernestus R-I, Löhr M, Hagemann C. Changes of O6-Methylguanine DNA Methyltransferase (MGMT) Promoter Methylation in Glioblastoma Relapse—A Meta-Analysis Type Literature Review. Cancers (Basel) 2019;11:1837. https://doi.org/10.3390/cancers11121837.
[28] Butler M, Pongor L, Su Y-T, Xi L, Raffeld M, Quezado M, et al. MGMT Status as a Clinical Biomarker in Glioblastoma. Trends in Cancer 2020;6:380–91. https://doi.org/10.1016/j.trecan.2020.02.010.
[29] Katsigiannis S, Grau S, Krischek B, Er K, Pintea B, Goldbrunner R, et al. MGMT-Positive vs MGMT-Negative Patients With Glioblastoma: Identification of Prognostic Factors and Resection Threshold. Neurosurgery 2021;88:E323–9. https://doi.org/10.1093/neuros/nyaa562.
[30] Lee GA, Lin W-L, Kuo D-P, Li Y-T, Chang Y-W, Chen Y-C, et al. Detection of PD-L1 Expression in Temozolomide-Resistant Glioblastoma by Using PD-L1 Antibodies Conjugated with Lipid‑Coated Superparamagnetic Iron Oxide . IJN 2021;16:5233–46. https://doi.org/10.2147/IJN.S310464.
[31] Hao C, Chen G, Zhao H, Li Y, Chen J, Zhang H, et al. PD-L1 Expression in Glioblastoma, the Clinical and Prognostic Significance: A Systematic Literature Review and Meta-Analysis. Frontiers in Oncology 2020;10.
[32] Zhu Z, Zhang H, Chen B, Liu X, Zhang S, Zong Z, et al. PD-L1-Mediated Immunosuppression in Glioblastoma Is Associated With the Infiltration and M2-Polarization of Tumor-Associated Macrophages. Frontiers in Immunology 2020;11.
[33] Xie Q, Mittal S, Berens ME. Targeting adaptive glioblastoma: an overview of proliferation and invasion. Neuro Oncol 2014;16:1575–84. https://doi.org/10.1093/neuonc/nou147.
[34] Lun M, Lok E, Gautam S, Wu E, Wong ET. The natural history of extracranial metastasis from glioblastoma multiforme. J Neurooncol 2011;105:261–73. https://doi.org/10.1007/s11060-011-0575-8.
[35] Volovitz I, Marmor Y, Azulay M, Machlenkin A, Goldberger O, Mor F, et al. Split Immunity: Immune Inhibition of Rat Gliomas by Subcutaneous Exposure to Unmodified Live Tumor Cells. The Journal of Immunology 2011;187:5452–62. https://doi.org/10.4049/jimmunol.1003946.
[36] Wilson TA, Karajannis MA, Harter DH. Glioblastoma multiforme: State of the art and future therapeutics. Surg Neurol Int 2014;5:64. https://doi.org/10.4103/2152-7806.132138.
[37] Davis ME. Glioblastoma: Overview of Disease and Treatment. Clin J Oncol Nurs 2016;20:S2–8. https://doi.org/10.1188/16.CJON.S1.2-8.
[38] Roder C, Bisdas S, Ebner FH, Honegger J, Naegele T, Ernemann U, et al. Maximizing the extent of resection and survival benefit of patients in glioblastoma surgery: high-field iMRI versus conventional and 5-ALA-assisted surgery. Eur J Surg Oncol 2014;40:297–304. https://doi.org/10.1016/j.ejso.2013.11.022.
[39] Kuhnt D, Becker A, Ganslandt O, Bauer M, Buchfelder M, Nimsky C. Correlation of the extent of tumor volume resection and patient survival in surgery of glioblastoma multiforme with high-field intraoperative MRI guidance. Neuro Oncol 2011;13:1339–48. https://doi.org/10.1093/neuonc/nor133.
[40] Keles GE, Anderson B, Berger MS. The effect of extent of resection on time to tumor progression and survival in patients with glioblastoma multiforme of the cerebral hemisphere. Surg Neurol 1999;52:371–9. https://doi.org/10.1016/s0090-3019(99)00103-2.
[41] Lacroix M, Abi-Said D, Fourney DR, Gokaslan ZL, Shi W, DeMonte F, et al. A multivariate analysis of 416 patients with glioblastoma multiforme: prognosis, extent of resection, and survival. J Neurosurg 2001;95:190–8. https://doi.org/10.3171/jns.2001.95.2.0190.

[42] Mukherjee D, Quinones-Hinojosa A. Impact of Extent of Resection on Outcomes in Patients with High-Grade Gliomas. In: Hayat MA, editor. Tumors of the Central Nervous System, Volume 2: Gliomas: Glioblastoma (Part 2), Dordrecht: Springer Netherlands; 2011, p. 173–9. https://doi.org/10.1007/978-94-007-0618-7_19.
[43] Stummer W, Pichlmeier U, Meinel T, Wiestler OD, Zanella F, Reulen H-J, et al. Fluorescence-guided surgery with 5-aminolevulinic acid for resection of malignant glioma: a randomised controlled multicentre phase III trial. Lancet Oncol 2006;7:392–401. https://doi.org/10.1016/S1470-2045(06)70665-9.
[44] Zhao S, Wu J, Wang C, Liu H, Dong X, Shi C, et al. Intraoperative fluorescence-guided resection of high-grade malignant gliomas using 5-aminolevulinic acid-induced porphyrins: a systematic review and meta-analysis of prospective studies. PLoS One 2013;8:e63682. https://doi.org/10.1371/journal.pone.0063682.
[45] Barone DG, Lawrie TA, Hart MG. Image guided surgery for the resection of brain tumours. Cochrane Database Syst Rev 2014:CD009685. https://doi.org/10.1002/14651858.CD009685.pub2.
[46] Thakkar JP, Dolecek TA, Horbinski C, Ostrom QT, Lightner DD, Barnholtz-Sloan JS, et al. Epidemiologic and molecular prognostic review of glioblastoma. Cancer Epidemiol Biomarkers Prev 2014;23:1985–96. https://doi.org/10.1158/1055-9965.EPI-14-0275.
[47] Ellor SV, Pagano-Young TA, Avgeropoulos NG. Glioblastoma: background, standard treatment paradigms, and supportive care considerations. J Law Med Ethics 2014;42:171–82. https://doi.org/10.1111/jlme.12133.
[48] Walid MS. Prognostic factors for long-term survival after glioblastoma. Perm J 2008;12:45–8. https://doi.org/10.7812/TPP/08-027.
[49] Johnson DR, O'Neill BP. Glioblastoma survival in the United States before and during the temozolomide era. J Neurooncol 2012;107:359–64. https://doi.org/10.1007/s11060-011-0749-4.
[50] Ashby LS, Smith KA, Stea B. Gliadel wafer implantation combined with standard radiotherapy and concurrent followed by adjuvant temozolomide for treatment of newly diagnosed high-grade glioma: a systematic literature review. World J Surg Onc 2016;14:225. https://doi.org/10.1186/s12957-016-0975-5.
[51] Dang W, Daviau T, Brem H. Morphological Characterization of Polyanhydride Biodegradable Implant Gliadel® During in Vitro and in Vivo Erosion Using Scanning Electron Microscopy. Pharm Res 1996;13:683–91. https://doi.org/10.1023/A:1016035229961.
[52] H B, S P, Pc B, M W, R S, Na V, et al. Placebo-controlled trial of safety and efficacy of intraoperative controlled delivery by biodegradable polymers of chemotherapy for recurrent gliomas. The Polymer-brain Tumor Treatment Group. Lancet (London, England) 1995;345. https://doi.org/10.1016/s0140-6736(95)90755-6.
[53] Valtonen S, Timonen U, Toivanen P, Kalimo H, Kivipelto L, Heiskanen O, et al. Interstitial chemotherapy with carmustine-loaded polymers for high-grade gliomas: a randomized double-blind study. Neurosurgery 1997;41:44–8; discussion 48-49. https://doi.org/10.1097/00006123-199707000-00011.
[54] Westphal M, Ram Z, Riddle V, Hilt D, Bortey E, On behalf of the Executive Committee of the Gliadel® Study Group. Gliadel® wafer in initial surgery for malignant glioma: long-term follow-up of a multicenter controlled trial. Acta Neurochir (Wien) 2006;148:269–75. https://doi.org/10.1007/s00701-005-0707-z.
[55] Kim G, Ko YT. Small molecule tyrosine kinase inhibitors in glioblastoma. Arch Pharm Res 2020;43:385–94. https://doi.org/10.1007/s12272-020-01232-3.
[56] Reardon DA, Turner S, Peters KB, Desjardins A, Gururangan S, Sampson JH, et al. A Review of VEGF/VEGFR-Targeted Therapeutics for Recurrent Glioblastoma. J Natl Compr Canc Netw 2011;9:414–27.
[57] Rubenstein JL, Kim J, Ozawa T, Zhang M, Westphal M, Deen DF, et al. Anti-VEGF Antibody Treatment of Glioblastoma Prolongs Survival But Results in Increased Vascular Cooption. Neoplasia 2000;2:306–14.
[58] Filippone A, Lanza M, Mannino D, Raciti G, Colarossi C, Sciacca D, et al. PD1/PD-L1 immune checkpoint as a potential target for preventing brain tumor progression. Cancer Immunol Immunother 2022;71:2067–75. https://doi.org/10.1007/s00262-021-03130-z.
[59] Ricci-Vitiani L, Pallini R, Larocca LM, Lombardi DG, Signore M, Pierconti F, et al. Mesenchymal differentiation of glioblastoma stem cells. Cell Death Differ 2008;15:1491–8. https://doi.org/10.1038/cdd.2008.72.
[60] Stockhausen M-T, Kristoffersen K, Stobbe L, Poulsen HS. Differentiation of glioblastoma multiforme stem-like cells leads to downregulation of EGFR and EGFRvIII and decreased tumorigenic and stem-like cell potential. Cancer Biol Ther 2014;15:216–24. https://doi.org/10.4161/cbt.26736.

[61] Kim Y, Jeon H, Othmer H. The role of the tumor microenvironment in glioblastoma: A mathematical model. IEEE Trans Biomed Eng 2017;64:519–27. https://doi.org/10.1109/TBME.2016.2637828.
[62] Balasubramaniyan V, Vaillant B, Wang S, Gumin J, Butalid ME, Sai K, et al. Aberrant mesenchymal differentiation of glioma stem-like cells: implications for therapeutic targeting. Oncotarget 2015;6:31007–17.
[63] Yan K, Wu Q, Yan DH, Lee CH, Rahim N, Tritschler I, et al. Glioma cancer stem cells secrete Gremlin1 to promote their maintenance within the tumor hierarchy. Genes Dev 2014;28:1085–100. https://doi.org/10.1101/gad.235515.113.
[64] Cheray M, Bessette B, Lacroix A, Mélin C, Jawhari S, Pinet S, et al. KLRC3, a Natural Killer receptor gene, is a key factor involved in glioblastoma tumourigenesis and aggressiveness. J Cell Mol Med 2017;21:244–53. https://doi.org/10.1111/jcmm.12960.
[65] Beederman M, Lamplot JD, Nan G, Wang J, Liu X, Yin L, et al. BMP signaling in mesenchymal stem cell differentiation and bone formation. JBiSE 2013;06:32–52. https://doi.org/10.4236/jbise.2013.68A1004.
[66] Barati D, Shariati SRP, Moeinzadeh S, Melero-Martin JM, Khademhosseini A, Jabbari E. Spatiotemporal release of BMP-2 and VEGF enhances osteogenic and vasculogenic differentiation of human mesenchymal stem cells and endothelial colony-forming cells co-encapsulated in a patterned hydrogel. Journal of Controlled Release 2016;223:126–36. https://doi.org/10.1016/j.jconrel.2015.12.031.
[67] Carén H, Beck S, Pollard SM. Differentiation therapy for glioblastoma – too many obstacles? Mol Cell Oncol 2015;3:e1124174. https://doi.org/10.1080/23723556.2015.1124174.
[68] González-Gómez P, Anselmo NP, Mira H. BMPs as Therapeutic Targets and Biomarkers in Astrocytic Glioma. Biomed Res Int 2014;2014. https://doi.org/10.1155/2014/549742.
[69] Katagiri T, Tsukamoto S. The unique activity of bone morphogenetic proteins in bone: a critical role of the Smad signaling pathway. Biological Chemistry 2013;394:703–14. https://doi.org/10.1515/hsz-2012-0310.
[70] Kokabua S, Katagiria T, Yodab T, Rosenc V. Role of Smad phosphatases in BMP-Smad signaling axis-induced osteoblast differentiation. Journal of Oral Biosciences 2012;54:73–8. https://doi.org/10.1016/j.job.2012.02.003.
[71] Páez-Pereda M, Giacomini D, Refojo D, Nagashima AC, Hopfner U, Grübler Y, et al. Involvement of bone morphogenetic protein 4 (BMP-4) in pituitary prolactinoma pathogenesis through a Smad/estrogen receptor crosstalk. PNAS 2003;100:1034–9. https://doi.org/10.1073/pnas.0237312100.
[72] Wang RN, Green J, Wang Z, Deng Y, Qiao M, Peabody M, et al. Bone Morphogenetic Protein (BMP) signaling in development and human diseases. Genes & Diseases 2014;1:87–105. https://doi.org/10.1016/j.gendis.2014.07.005.
[73] Xi G, Best B, Mania-Farnell B, James CD, Tomita T. Therapeutic Potential for Bone Morphogenetic Protein 4 in Human Malignant Glioma. Neoplasia 2017;19:261–70. https://doi.org/10.1016/j.neo.2017.01.006.
[74] Piccirillo SGM, Reynolds BA, Zanetti N, Lamorte G, Binda E, Broggi G, et al. Bone morphogenetic proteins inhibit the tumorigenic potential of human brain tumour-initiating cells. Nature 2006;444:761–5. https://doi.org/10.1038/nature05349.
[75] Zhang L, Luo Q, Shu Y, Zeng Z, Huang B, Feng Y, et al. Transcriptomic landscape regulated by the 14 types of bone morphogenetic proteins (BMPs) in lineage commitment and differentiation of mesenchymal stem cells (MSCs). Genes & Diseases 2019;6:258–75. https://doi.org/10.1016/j.gendis.2019.03.008.
[76] Bai X, Li G, Zhao C, Duan H, Qu F. BMP7 induces the differentiation of bone marrow-derived mesenchymal cells into chondrocytes. Med Biol Eng Comput 2011;49:687–92. https://doi.org/10.1007/s11517-010-0729-4.
[77] Cai H, Zou J, Wang W, Yang A. BMP2 induces hMSC osteogenesis and matrix remodeling. Molecular Medicine Reports 2021;23:1–1. https://doi.org/10.3892/mmr.2020.11764.
[78] Cui J, Zhang W, Huang E, Wang J, Liao J, Li R, et al. BMP9-induced osteoblastic differentiation requires functional Notch signaling in mesenchymal stem cells. Lab Invest 2019;99:58–71. https://doi.org/10.1038/s41374-018-0087-7.
[79] Zhou N, Li Q, Lin X, Hu N, Liao J-Y, Lin L-B, et al. BMP2 induces chondrogenic differentiation, osteogenic differentiation and endochondral ossification in stem cells. Cell Tissue Res 2016;366:101–11. https://doi.org/10.1007/s00441-016-2403-0.

[80] Zhang H, Zhang W, Bai G, Gao L, Li K. Bone Morphogenetic Protein-7 (BMP-7) Promotes Neuronal Differentiation of Bone Marrow Mesenchymal Stem Cells (BMSCs) In Vitro. BioMed Research International n.d.:9.
[81] Lamplot JD, Qin J, Nan G, Wang J, Liu X, Yin L, et al. BMP9 signaling in stem cell differentiation and osteogenesis. Am J Stem Cells 2013;2:1–21.
[82] Vukicevic S, Grgurevic L. BMP-6 and mesenchymal stem cell differentiation. Cytokine Growth Factor Rev 2009;20:441–8. https://doi.org/10.1016/j.cytogfr.2009.10.020.
[83] Shore EM, Xu M, Shah PB, Janoff HB, Hahn GV, Deardorff MA, et al. The human bone morphogenetic protein 4 (BMP-4) gene: molecular structure and transcriptional regulation. Calcif Tissue Int 1998;63:221–9. https://doi.org/10.1007/s002239900518.
[84] Yang J, Shi P, Tu M, Wang Y, Liu M, Fan F, et al. Bone morphogenetic proteins: Relationship between molecular structure and their osteogenic activity. Food Science and Human Wellness 2014;3:127–35. https://doi.org/10.1016/j.fshw.2014.12.002.
[85] Scheufler C, Sebald W, Hülsmeyer M. Crystal structure of human bone morphogenetic protein-2 at 2.7 A resolution. J Mol Biol 1999;287:103–15. https://doi.org/10.1006/jmbi.1999.2590.
[86] Dardet JP, Serrano N, András IE, Toborek M. Overcoming Blood-Brain Barrier Resistance: Implications for Extracellular Vesicle-Mediated Drug Brain Delivery. Frontiers in Drug Delivery 2022;2.
[87] Dong X. Current Strategies for Brain Drug Delivery. Theranostics 2018;8:1481–93. https://doi.org/10.7150/thno.21254.
[88] Daneman R. The blood-brain barrier in health and disease. Ann Neurol 2012;72:648–72. https://doi.org/10.1002/ana.23648.
[89] Pardridge WM. Blood-brain barrier drug targeting: the future of brain drug development. Mol Interv 2003;3:90–105, 51. https://doi.org/10.1124/mi.3.2.90.
[90] Obermeier B, Daneman R, Ransohoff RM. Development, maintenance and disruption of the blood-brain barrier. Nat Med 2013;19:1584–96. https://doi.org/10.1038/nm.3407.
[91] Abbott NJ, Patabendige AAK, Dolman DEM, Yusof SR, Begley DJ. Structure and function of the blood-brain barrier. Neurobiol Dis 2010;37:13–25. https://doi.org/10.1016/j.nbd.2009.07.030.
[92] Wong A, Ye M, Levy A, Rothstein J, Bergles D, Searson P. The blood-brain barrier: an engineering perspective. Frontiers in Neuroengineering 2013;6.
[93] Dimitrov DS. Therapeutic Proteins. Methods Mol Biol 2012;899:1–26. https://doi.org/10.1007/978-1-61779-921-1_1.
[94] Pisal DS, Kosloski MP, Balu-Iyer SV. DELIVERY OF THERAPEUTIC PROTEINS. J Pharm Sci 2010;99:2557–75. https://doi.org/10.1002/jps.22054.
[95] Zaman R, Islam R, Ibnat N, Othman I, Zain A, Lee C, et al. Current Strategies in Extending Half-lives of Therapeutic Proteins. Journal of Controlled Release 2019. https://doi.org/10.1016/j.jconrel.2019.02.016.
[96] Böttger R, Hoffmann R, Knappe D. Differential stability of therapeutic peptides with different proteolytic cleavage sites in blood, plasma and serum. PLOS ONE 2017;12:e0178943. https://doi.org/10.1371/journal.pone.0178943.
[97] Manning MC, Chou DK, Murphy BM, Payne RW, Katayama DS. Stability of protein pharmaceuticals: an update. Pharm Res 2010;27:544–75. https://doi.org/10.1007/s11095-009-0045-6.
[98] Markwalter CE, Pagels RF, Wilson BK, Ristroph KD, Prud'homme RK. Flash NanoPrecipitation for the Encapsulation of Hydrophobic and Hydrophilic Compounds in Polymeric Nanoparticles. JoVE (Journal of Visualized Experiments) 2019:e58757. https://doi.org/10.3791/58757.
[99] Bilati U, Allémann E, Doelker E. Nanoprecipitation versus emulsion-based techniques for the encapsulation of proteins into biodegradable nanoparticles and process-related stability issues. AAPS PharmSciTech 2005;6:E594–604. https://doi.org/10.1208/pt060474.
[100] Haji Mansor M, Najberg M, Contini A, Alvarez-Lorenzo C, Garcion E, Jérôme C, et al. Development of a non-toxic and non-denaturing formulation process for encapsulation of SDF-1α into PLGA/PEG-PLGA nanoparticles to achieve sustained release. Eur J Pharm Biopharm 2018;125:38–50. https://doi.org/10.1016/j.ejpb.2017.12.020.

[101] Swed A, Cordonnier T, Fleury F, Boury F. Protein Encapsulation into PLGA Nanoparticles by a Novel Phase Separation Method Using Non-Toxic Solvents. Journal of Nanomedicine & Nanotechnology 2014;6. https://doi.org/10.4172/2157-7439.1000241.
[102] Giteau A, Venier-Julienne M-C, Marchal S, Courthaudon J-L, Sergent M, Montero-Menei C, et al. Reversible protein precipitation to ensure stability during encapsulation within PLGA microspheres. Eur J Pharm Biopharm 2008;70:127–36. https://doi.org/10.1016/j.ejpb.2008.03.006.
[103] Wang Y, Tan H, Hui X. Biomaterial Scaffolds in Regenerative Therapy of the Central Nervous System. BioMed Research International 2018;2018:1–19. https://doi.org/10.1155/2018/7848901.
[104] Chan BP, Leong KW. Scaffolding in tissue engineering: general approaches and tissue-specific considerations. Eur Spine J 2008;17:467–79. https://doi.org/10.1007/s00586-008-0745-3.
[105] El-Sherbiny IM, Yacoub MH. Hydrogel scaffolds for tissue engineering: Progress and challenges. Glob Cardiol Sci Pract 2013;2013:316–42. https://doi.org/10.5339/gcsp.2013.38.
[106] Savaser A, Esim O, Kurbanoglu S, Ozkan SA, Ozkan Y. Current perspectives on drug release studies from polymeric nanoparticles. Organic Materials as Smart Nanocarriers for Drug Delivery, Elsevier; 2018, p. 101–45. https://doi.org/10.1016/B978-0-12-813663-8.00003-8.
[107] Mura S, Hillaireau H, Nicolas J, Le Droumaguet B, Gueutin C, Zanna S, et al. Influence of surface charge on the potential toxicity of PLGA nanoparticles towards Calu-3 cells. Int J Nanomedicine 2011;6:2591–605. https://doi.org/10.2147/IJN.S24552.
[108] Lee KY, Yuk SH. Polymeric protein delivery systems. Progress in Polymer Science 2007;32:669–97. https://doi.org/10.1016/j.progpolymsci.2007.04.001.
[109] Viehof A, Javot L, Béduneau A, Pellequer Y, Lamprecht A. Oral insulin delivery in rats by nanoparticles prepared with non-toxic solvents. International Journal of Pharmaceutics 2013;443:169–74. https://doi.org/10.1016/j.ijpharm.2013.01.017.
[110] Xue J, He M, Liu H, Niu Y, Crawford A, Coates PD, et al. Drug loaded homogeneous electrospun PCL/gelatin hybrid nanofiber structures for anti-infective tissue regeneration membranes. Biomaterials 2014;35:9395–405. https://doi.org/10.1016/j.biomaterials.2014.07.060.
[111] Unal S, Arslan S, Yilmaz BK, Oktar FN, Ficai D, Ficai A, et al. Polycaprolactone/Gelatin/Hyaluronic Acid Electrospun Scaffolds to Mimic Glioblastoma Extracellular Matrix. Materials 2020;13:2661. https://doi.org/10.3390/ma13112661.
[112] Draget KI, Skjåk-Bræk G. Chapter 7. Alginates: Existing and Potential Biotechnological and Medical Applications. In: Williams PA, editor. Polymer Chemistry Series, Cambridge: Royal Society of Chemistry; 2011, p. 186–209. https://doi.org/10.1039/9781849733519-00186.
[113] Abdi SIH, Choi JY, Lee JS, Lim HJ, Lee C, Kim J, et al. In Vivo study of a blended hydrogel composed of pluronic F-127-alginate-hyaluronic acid for its cell injection application. Tissue Eng Regen Med 2012;9:1–9. https://doi.org/10.1007/s13770-012-0001-0.
[114] Lin Y-C, Tan F, Marra KG, Jan S-S, Liu D-C. Synthesis and characterization of collagen/hyaluronan/chitosan composite sponges for potential biomedical applications. Acta Biomaterialia 2009;5:2591–600. https://doi.org/10.1016/j.actbio.2009.03.038.
[115] Entekhabi E, Haghbin Nazarpak M, Shafieian M, Mohammadi H, Firouzi M, Hassannejad Z. Fabrication and in vitro evaluation of 3D composite scaffold based on collagen/hyaluronic acid sponge and electrospun polycaprolactone nanofibers for peripheral nerve regeneration. Journal of Biomedical Materials Research Part A 2021;109:300–12. https://doi.org/10.1002/jbm.a.37023.
[116] Kean T, Thanou M. Chapter 10. Chitin and Chitosan: Sources, Production and Medical Applications. In: Williams PA, editor. Polymer Chemistry Series, Cambridge: Royal Society of Chemistry; 2011, p. 292–318. https://doi.org/10.1039/9781849733519-00292.
[117] Chen C-H, Chen S-H, Mao S-H, Tsai M-J, Chou P-Y, Liao C-H, et al. Injectable thermosensitive hydrogel containing hyaluronic acid and chitosan as a barrier for prevention of postoperative peritoneal adhesion. Carbohydrate Polymers 2017;173. https://doi.org/10.1016/j.carbpol.2017.06.019.
[118] Jung Y, Park W, Park H, Lee D-K, Na K. Thermo-sensitive injectable hydrogel based on the physical mixing of hyaluronic acid and Pluronic F-127 for sustained NSAID delivery. Carbohydrate Polymers 2017;156:403–8. https://doi.org/10.1016/j.carbpol.2016.08.068.

[119] Bolla PK, Rodriguez VA, Kalhapure RS, Kolli CS, Andrews S, Renukuntla J. A review on pH and temperature responsive gels and other less explored drug delivery systems. Journal of Drug Delivery Science and Technology 2018;46:416–35. https://doi.org/10.1016/j.jddst.2018.05.037.
[120] Pushpavanam K, Dutta S, Zhang N, Ratcliff T, Bista T, Sokolowski T, et al. Radiation-Responsive Amino Acid Nanosensor Gel (RANG) for Radiotherapy Monitoring and Trauma Care. Bioconjugate Chem 2021;32:1984–98. https://doi.org/10.1021/acs.bioconjchem.1c00262.
[121] Alberts B, Johnson A, Lewis J, Raff M, Roberts K, Walter P. Protein Function. Molecular Biology of the Cell 4th Edition 2002.
[122] Matthews BW. Structural and genetic analysis of protein stability. Annu Rev Biochem 1993;62:139–60. https://doi.org/10.1146/annurev.bi.62.070193.001035.
[123] Morales-Cruz M. Two-step nanoprecipitation for the production of protein-loaded PLGA nanospheres. Results in Pharma Sciences 2012:7.
[124] Tarhini M, Benlyamani I, Hamdani S, Agusti G, Fessi H, Greige-Gerges H, et al. Protein-Based Nanoparticle Preparation via Nanoprecipitation Method. Materials 2018;11:394. https://doi.org/10.3390/ma11030394.
[125] Lee ES, Park K-H, Kang D, Park IS, Min HY, Lee DH, et al. Protein complexed with chondroitin sulfate in poly(lactide-co-glycolide) microspheres. Biomaterials 2007;28:2754–62. https://doi.org/10.1016/j.biomaterials.2007.01.049.
[126] Lee ES, Park K-H, Park IS, Na K. Glycol chitosan as a stabilizer for protein encapsulated into poly(lactide-co-glycolide) microparticle. Int J Pharm 2007;338:310–6. https://doi.org/10.1016/j.ijpharm.2007.02.008.
[127] Wang J, Chua KM, Wang C-H. Stabilization and encapsulation of human immunoglobulin G into biodegradable microspheres. J Colloid Interface Sci 2004;271:92–101. https://doi.org/10.1016/j.jcis.2003.08.072.
[128] Carrasquillo KG, Stanley AM, Aponte-Carro JC, De Jésus P, Costantino HR, Bosques CJ, et al. Non-aqueous encapsulation of excipient-stabilized spray-freeze dried BSA into poly(lactide-co-glycolide) microspheres results in release of native protein. J Control Release 2001;76:199–208. https://doi.org/10.1016/s0168-3659(01)00430-8.
[129] Chen L, Apte RN, Cohen S. Characterization of PLGA microspheres for the controlled delivery of IL-1α for tumor immunotherapy. Journal of Controlled Release 1997;43:261–72. https://doi.org/10.1016/S0168-3659(96)01496-4.
[130] Rosa GD, Iommelli R, La Rotonda MI, Miro A, Quaglia F. Influence of the co-encapsulation of different non-ionic surfactants on the properties of PLGA insulin-loaded microspheres. J Control Release 2000;69:283–95. https://doi.org/10.1016/s0168-3659(00)00315-1.
[131] van de Weert M, Hoechstetter J, Hennink WE, Crommelin DJ. The effect of a water/organic solvent interface on the structural stability of lysozyme. J Control Release 2000;68:351–9. https://doi.org/10.1016/s0168-3659(00)00277-7.
[132] Morille M, Van-Thanh T, Garric X, Cayon J, Coudane J, Noël D, et al. New PLGA–P188–PLGA matrix enhances TGF-β3 release from pharmacologically active microcarriers and promotes chondrogenesis of mesenchymal stem cells. Journal of Controlled Release 2013;170:99–110. https://doi.org/10.1016/j.jconrel.2013.04.017.
[133] Sah H. Protein instability toward organic solvent/water emulsification: implications for protein microencapsulation into microspheres. PDA J Pharm Sci Technol 1999;53:3–10.
[134] Sturesson C, Carlfors J. Incorporation of protein in PLG-microspheres with retention of bioactivity. J Control Release 2000;67:171–8. https://doi.org/10.1016/s0168-3659(00)00205-4.
[135] Paillard-Giteau A, Tran VT, Thomas O, Garric X, Coudane J, Marchal S, et al. Effect of various additives and polymers on lysozyme release from PLGA microspheres prepared by an s/o/w emulsion technique. European Journal of Pharmaceutics and Biopharmaceutics 2010;75:128–36. https://doi.org/10.1016/j.ejpb.2010.03.005.
[136] Rowe RC, Sheskey PJ, Owen SC, American Pharmacists Association, editors. Handbook of pharmaceutical excipients: edited by Raymond C. Rowe, Paul J. Sheskey, Siân C. Owen. 5th ed. London ; Greyslake, IL : Washington, DC: Pharmaceutical Press ; American Pharmacists Association; 2006.

[137] Cho W, Kim M-S, Kim J-S, Park J, Park HJ, Cha K-H, et al. Optimized formulation of solid self-microemulsifying sirolimus delivery systems. Int J Nanomedicine 2013;8:1673–82. https://doi.org/10.2147/IJN.S43299.
[138] Ivaturi VD, Riss JR, Kriel RL, Siegel RA, Cloyd JC. Bioavailability and tolerability of intranasal diazepam in healthy adult volunteers. Epilepsy Res 2009;84:120–6. https://doi.org/10.1016/j.eplepsyres.2009.01.001.
[139] Gizurarson S, Georgsson G, Aggerbeck H, Thorarinsdóttir H, Heron I. Evaluation of local toxicity after repeated intranasal vaccination of guinea-pigs. Toxicology 1996;107:61–8. https://doi.org/10.1016/0300-483x(95)03201-p.
[140] Nasongkla N, Boongird A, Hongeng S, Manaspon C, Larbcharoensub N. Preparation and biocompatibility study of in situ forming polymer implants in rat brains. J Mater Sci Mater Med 2012;23:497–505. https://doi.org/10.1007/s10856-011-4520-3.
[141] Eliaz RE, Wallach D, Kost J. Delivery of soluble tumor necrosis factor receptor from in-situ forming PLGA implants: in-vivo. Pharm Res 2000;17:1546–50. https://doi.org/10.1023/a:1007621512647.
[142] Eliaz RE, Szoka FC. Robust and prolonged gene expression from injectable polymeric implants. Gene Ther 2002;9:1230–7. https://doi.org/10.1038/sj.gt.3301786.
[143] Bagger MA, Nielsen HW, Bechgaard E. Nasal bioavailability of peptide T in rabbits: absorption enhancement by sodium glycocholate and glycofurol. Eur J Pharm Sci 2001;14:69–74. https://doi.org/10.1016/s0928-0987(01)00146-4.
[144] Aubert-Pouëssel A, Venier-Julienne M-C, Saulnier P, Sergent M, Benoît J-P. Preparation of PLGA microparticles by an emulsion-extraction process using glycofurol as polymer solvent. Pharm Res 2004;21:2384–91. https://doi.org/10.1007/s11095-004-7693-3.
[145] Allhenn D, Lamprecht A. Microsphere preparation using the untoxic solvent glycofurol. Pharm Res 2011;28:563–71. https://doi.org/10.1007/s11095-010-0304-6.
[146] Tran M-K, Hassani LN, Calvignac B, Beuvier T, Hindré F, Boury F. Lysozyme encapsulation within PLGA and CaCO3 microparticles using supercritical CO2 medium. The Journal of Supercritical Fluids 2013;79:159–69. https://doi.org/10.1016/j.supflu.2013.02.024.
[147] Durand M, Zhu Y, Molinier V, Féron T, Aubry J-M. Solubilizing and Hydrotropic Properties of Isosorbide Monoalkyl- and Dimethyl-Ethers. Journal of Surfactants and Detergents 2009;12:371–8. https://doi.org/10.1007/s11743-009-1128-4.
[148] Zia H, Ma JK, O'Donnell JP, Luzzi LA. Cosolvency of dimethyl isosorbide for steroid solubility. Pharm Res 1991;8:502–4. https://doi.org/10.1023/a:1015807413141.
[149] Laurent A, Mottu F, Chapot R, Zhang JQ, Jordan O, Rüfenacht DA, et al. Cardiovascular effects of selected water-miscible solvents for pharmaceutical injections and embolization materials: a comparative hemodynamic study using a sheep model. PDA J Pharm Sci Technol 2007;61:64–74.
[150] Mottu F, Stelling MJ, Rüfenacht DA, Doelker E. Comparative hemolytic activity of undiluted organic water-miscible solvents for intravenous and intra-arterial injection. PDA J Pharm Sci Technol 2001;55:16–23.
[151] Dudeck O, Jordan O, Hoffmann KT, Okuducu AF, Tesmer K, Kreuzer-Nagy T, et al. Organic Solvents as Vehicles for Precipitating Liquid Embolics: A Comparative Angiotoxicity Study with Superselective Injections of Swine Rete Mirabile. AJNR Am J Neuroradiol 2006;27:1900–6.
[152] Gong C, Qi T, Wei X, Qu Y, Wu Q, Luo F, et al. Thermosensitive polymeric hydrogels as drug delivery systems. Curr Med Chem 2013;20:79–94.
[153] Fan R, Cheng Y, Wang R, Zhang T, Zhang H, Li J, et al. Thermosensitive Hydrogels and Advances in Their Application in Disease Therapy. Polymers (Basel) 2022;14:2379. https://doi.org/10.3390/polym14122379.
[154] Russo E, Villa C. Poloxamer Hydrogels for Biomedical Applications. Pharmaceutics 2019;11. https://doi.org/10.3390/pharmaceutics11120671.
[155] Dumortier G, Grossiord JL, Agnely F, Chaumeil JC. A Review of Poloxamer 407 Pharmaceutical and Pharmacological Characteristics. Pharm Res 2006;23:2709–28. https://doi.org/10.1007/s11095-006-9104-4.
[156] Zarrintaj P, Ramsey JD, Samadi A, Atoufi Z, Yazdi MK, Ganjali MR, et al. Poloxamer: A versatile tri-block copolymer for biomedical applications. Acta Biomaterialia 2020;110:37–67. https://doi.org/10.1016/j.actbio.2020.04.028.

[157] Mayol L, Quaglia F, Borzacchiello A, Ambrosio L, La Rotonda MI. A novel poloxamers/hyaluronic acid in situ forming hydrogel for drug delivery: rheological, mucoadhesive and in vitro release properties. Eur J Pharm Biopharm 2008;70:199–206. https://doi.org/10.1016/j.ejpb.2008.04.025.
[158] Hsieh H-Y, Lin W-Y, Lee A, Li Y-C, Chen Y-J, Chen K-C, et al. Hyaluronic acid on the urokinase sustained release with a hydrogel system composed of poloxamer 407: HA/P407 hydrogel system for drug delivery. PLOS ONE 2020;15:e0227784. https://doi.org/10.1371/journal.pone.0227784.

Chapter 2
Thesis aim and objectives

2. Thesis aim and objectives

The chemokine BMP-4 has been shown to alter the phenotype of GB cells through differentiation. It is also widely recognized that extensive GB tumor excision is frequently not possible with current surgical methods.

The remaining GB cells in the brain might grow and reform the tumor, worsening the patients' clinical condition and leading to a high risk of death. **Hence, the project aims to create a polymer-based hydrogel capable of releasing BMP-4 on a long-term basis that could be injected into the resection cavity to differentiate residual GB cells, making them more sensitive to radiotherapy and chemotherapy and thus facilitating their selective killing.**

The main specifications that have been highlighted as critical to achieving the aforementioned goal are:

• Encapsulating BMP-4 in polymer-based nanoparticles to produce main carriers of this cytokine

• Incorporating BMP-4-loaded nanoparticles into an injectable hydrogel to offer a secondary barrier to BMP-4 release

The results of these aims are presented and discussed in the next two chapters of this thesis (Chapters 3 and 4).

The third chapter is called Hyaluronic acid-based systems and consists on a review written and accepted in MDPI International Journal of Molecular Sciences. It is titled “Hyaluronic acid scaffolds for loco-regional therapy in nervous system related disorders” and discusses different types of scaffolds developed in the literature whether they are hydrogels, sponges, Electrospun fibers and nanocomposite systems.

The fourth chapter is called “Encapsulation of BMP-4 into polymer-based nanoparticles”. This chapter explains how to make homogenous nanoparticles out of PLGA and a PEG-PLGA co-polymer to load BMP-4. It is also presented as an article intended for submission on MDPI Pharmaceuticals. The careful tuning of the nanoparticle composition to achieve a suitable compromise between BMP-4 encapsulation efficiency and release capacity is one of the chapter's highlights.

The fifth chapter is entitled "Development of nanocomposite hydrogels for Glioblastoma application". This chapter focuses on formulating a nanocomposite hydrogel and its physico-chemical and biological characterization. It is also presented as an article intended for submission on MDPI Gels. This section of the thesis featured detailed discussions on the influence of nanoparticle presence on the physico-chemical properties of the hydrogel as well as the BMP-4 release profile from the nanocomposite hydrogel.

The sixth chapter is a general discussion and a conclusions of the project and its perspectives. Followed by the annexes, that consist on one published article on another therapeutic strategy based on Rapamycin delivery using lipid nanocapsules for Glioblastoma treatment.

Chapter 3
Hyaluronic acid-based systems

3. HYALURONIC ACID BASED SYSTEMS: Hyaluronic acid scaffolds for loco-regional therapy in nervous system related disorders: Review: MDPI (2022) (Accepted)

International Journal of *Molecular Sciences*

MDPI

Review

Hyaluronic acid scaffolds for loco-regional therapy in nervous system related disorders

Amel Djoudi*[1], Rodolfo Molina-Peña[1], Natalia Ferreira[1], Ilaria Ottonelli[2,3], Giovanni Tosi[2], Emmanuel Garcion[1], Frank Boury*[1]

Citation: Djoudi, A.; Molina-Peña, R.; Ferreira, N.. *IJMS* **2022**, *15*, x. https://doi.org/10.3390/xxxxx

Academic Editor: Firstname Lastname

Received: date
Accepted: date
Published: date

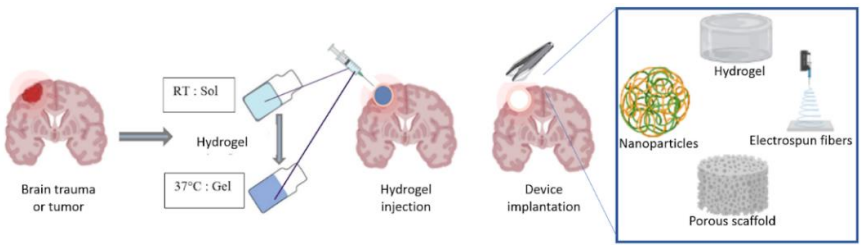
Publisher's Note: MDPI stays neutral with regard to jurisdictional claims in published maps and institutional affiliations.

Copyright: © 2022 by the authors. Submitted for possible open access publication under the terms and conditions of the Creative Commons Attribution (CC BY) license (https://creativecommons.org/licenses/by/4.0/).

[1] Université d'Angers, Inserm UMR 1307, CNRS UMR 6075, Nantes Université, CRCINA, F-49000
Angers - France
[2]Nanotech Lab, Te.Far.T.I., Department Life Sciences, University of Modena and Reggio Emilia,
41125 Modena, Italy
[3]Clinical and Experimental Medicine PhD Program, University of Modena and Reggio Emilia,
41125 Modena, Italy

* Correspondence: djoudi-amel@hotmail.fr, frank.boury@univ-angers.fr

Abstract: Hyaluronic acid is a Glycosaminoglycan made of disaccharide units containing N-acetyl-D-glucosamine and glucuronic acid. Its molecular mass can reach 10 MDa and its physiological properties depend on its polymeric property, polyelectrolyte feature and viscous nature. HA is a ubiquitous compound found in almost all biological tissues and fluids. So far, HA grades are produced by biotechnology processes, while in the human organism it is a major component of extracellular matrix (ECM) in brain tissue, synovial fluid, vitreous humor, cartilage, and skin. Indeed, HA is capable of forming hydrogels, polymer crosslinked networks that are very hygroscopic. Based on these considerations, we propose an overview of HA-based scaffolds developed for brain cancer treatment, Central and Peripheral Nervous Systems, discuss their relevance and identify the most successful developed systems.



Graphical abstract. Various systems developed for CNS injuries treatment with 2 intracerebral administrations ways: injection and implantation

Keywords: Hyaluronic acid, scaffolds, hydrogels, nervous system.

1. Introduction

Hyaluronic acid (HA), also known as hyaluronan, is a linear polysaccharide composed of disaccharide units containing N-acetyl-D-glucosamine and glucuronic acid [1–3]. Its molecular mass varies between 0.2 to 10 MDa and its physiological properties are governed by its polyelectrolyte and polymeric features, as well as by its viscous nature [1–3]. HA is a ubiquitous compound present in almost all biological tissues and fluids [1–3]. In the human organism, it is found in the extracellular matrix (ECM) of the skin, vitreous humor, cartilage, and umbilical cord, CNS, PNS [1,4].

HA has various applications. For instance, in cosmetology, it is used as an anti-ageing agent, in pharmaceutics and regenerative medicine as an excipient and constituent of scaffolds for drug delivery and regeneration, and in biology as a component of *in vitro* models [5–7]. Research and medical grade HA samples are produced by biotechnological processes, mainly from bacteria or isolated from rooster combs [1,4]. HA is FDA-approved and Generally Recognized As Safe (GRAS) for medical applications. Besides, HA can be administered topically, orally or by injection [1–3].

HA is a natural polymer present in the Central Nervous System (CNS) and Peripheral Nervous System (PNS) [7,8]. It is capable of forming a polymeric crosslinked network that exhibits a high water-absorbing ability, called a hydrogel [9]. HA polymers are biodegradable *in vivo* by free radicals and by vertebrates by specific enzymes from type I to type VI hyaluronidases [2,4]. HA biomimetic properties have motivated the development of HA-featuring devices for CNS and PNS disorders, displaying the following characteristics: injectability, biocompatibility, bioadhesion, controlled drug release and biodegradability [1,3,10].

HA-based systems are tunable. They are usually formulated with HA alone or in association with other biopolymers with biological properties such as chitosan, alginate and cellulose; or synthetic ones with thermosensitive and mechanical properties, for example, poloxamers, polyethylene glycol (PEG) and polycaprolactone (PCL) [7,10–14]. Due to their versatility, research on HA-based polymers has increased over the past decade with potential applications for drug delivery and regenerative medicine[9]. The aim of this review is to highlight HA properties, summarize emerging *in vitro* and *in vivo* evidence of HA-based scaffolds developed for brain cancer treatment [15], CNS [16] and PNS [17], and discuss relevant results for the locoregional administration of these scaffolds (Table 2, Table 3, Table 4).

2. Pathologies of the central and peripheral nervous system and current therapeutic approaches

Pathologies of the Nervous System are considered among the most difficult to treat, due to the complexity of the system and its numerous protective barriers that play a critical role in the brain's metabolic activity as well as neuronal function [18,19]. At the same time, the occurrence of brain diseases like cancer, traumatic injuries, and neurodegenerative diseases are currently increasing [20]. Notwithstanding the advances in research regarding novel therapeutic approaches to treat pathologies of the CNS, the majority of these diseases still lack an effective and permanent cure. Here, we introduce the main issues and current therapeutic approaches for three classes of brain pathologies: i) cancer, particularly focusing on the most common and hard-to-treat brain cancer, i.e. Glioblastoma [15]; ii) traumatic brain injuries [16]; and iii) peripheral nerve injuries [17].

2.1 Glioblastoma and gliomas

Grade IV Glioblastoma (GB) and malignant gliomas are the most common form of brain tumors. They have an annual incidence of 5.26 per 100,000 people, accounting for 17,000 new cases each year [21,22]. Unfortunately, these kinds of tumors lead to poor quality of life and prognosis for patients, with a survival median of 15 months after diagnosis [15,21]. In fact, GB is defined as a IV grade glioma, and it is the most lethal and frequent malignant primary brain tumor [21]. On contrary to other solid tumors, GB is highly invasive towards neighboring tissues in the brain, causing high rates of recurrence and tumoral transformation in healthy cells, although rarely metastasize to other organs [15,21,23].

Current FDA-approved therapy is based on surgical resection of the majority of the tumor, followed by systemic chemotherapy and radiotherapy together with adjuvant therapy with temozolomide (TMZ), according to Stupp protocol [24,25]. In spite of the undoubted advantages linked to this therapeutic approach, in 90% of the cases patients experiment recurrence after the first surgery [15,26]. This common issue is mainly due to a specific population of cancer stem cells, called tumor-initiating stem cells, which display a high tumorigenic potential and often remain intact even after surgery and chemotherapy [23,27]. Thus, their ability to proliferate in an asymmetric way leads to the relapse of GB, but few therapeutic options are available in this scenario [15,21,23,28].

To reduce the risk of recurrence, several therapeutic approaches are now under investigation (Table S1). Of particular interest is the possibility to develop peptide- and cell-based vaccines that specifically target GB cells leading to their death by stimulation of the immune system [26]. More recently, CAR-T cells have also gained increasing interest from scientists thanks to their high potential for the treatment of GB [29]. Other approved molecules for the treatment of GB, carmustine, lomustine, and even monoclonal antibodies such as bevacizumab [30]. Another innovative approach is represented by nanomedicines; in fact, the particular tumor microenvironment and surface characteristics of GBM cells allow for specific targeting of drug-loaded nanosystems that can release cytotoxic drugs in tumor cells with low off-target effects [31,32]. Despite the several advantages that these innovative therapies may involve, few of them have reached the market. Besides, one approach is represented by Gliadel® [33–35]. Developed in early 2000, Gliadel® consists of polymeric wafers loaded with carmustine. They are approved to be implanted into the resected cavity after surgery and are able to release the drug for up to 3 weeks, thus reducing the risk of GB setback and promoting a better prognosis for patients [35]. However, this treatment only produces modest effects as the released drug can only penetrate 1-2 mm into the surrounding brain tissues, preventing the complete killing of residual GB cells, which may reside more than one centimetre away from the resection margin. Moreover, the shape of the scaffold does not quite fit the resection cavity border and induces some side effects in many patients according to various clinical trials [36–38].

2.2 Traumatic Brain Injuries

Traumatic brain injuries (TBIs) are on the rise, not only in the elder population, where almost 500 out of 100,000 people over 80 years are estimated to suffer from this pathology each year, but also in children, with an annual incidence of almost 500,000 cases among children aged 0-14 [16]. In particular, TBIs are one of the major causes of impairments in young adults, and for this reason, they represent a huge healthcare burden [39]. After the traumatic event, many phenomena can occur in the brain, both at physical and chemical levels [40,41]. In particular, the first phase after the trauma is generally considered crucial to determine the development of secondary damage, as it can include haemorrhages, disruption of the Blood Brain Barrier (BBB), high levels of inflammation, with consequences such as seizures, hypoxia, ischemic areas, and edema [42]. All these events, if not timely treated, may lead to metabolic failure, eventually leading to critical impairments or even death of the patient [16,40,41].

Therapeutic approaches approved in the case of TBIs are generally linked to the specific case and history of the disease [16]. Considering physical and pharmacological approaches, these may include surgery to reduce edema-induced intracranial pressure, administration of neuroprotective agents, antioxidants to reduce free radical production, and antiinflammatory drugs; also, other therapies can involve hypothermia, regulation of blood flow dysregulation and ischemia, regulation of ion homeostasis and cytoskeleton stabilization [43]. All these pharmacological strategies, though, present a common limitation due to their fast clearance, thus resulting in hampered prolonged release and the need for several therapeutic systems [42]. At the same time, surgery often includes craniotomy and cranioplasty, calling for the need to develop biocompatible materials that can substitute physiological tissues and promote recovery [44,45]. Both these issues have been under investigation in recent years, leading to the design and formulation of biocompatible scaffolds that allow the prolonged release of therapeutics, along with the promotion of tissue curing [46,47]. In fact, many scaffolds have been developed, using different materials and production techniques (Table 3). In particular, hyaluronic acid-based scaffolds will be discussed in part 5.

2.3 Peripheral nerve injuries

Peripheral nerve accidents are not unusual situations, with a vast range of symptoms depending on the severity of the trauma and the nerves involved [17]. Although a lot of information exists on the mechanisms of damage and regeneration, reliable treatments that allow for complete recovery are rare [17,48,49].

Peripheral nerve accidents can imply various challenges to patients, starting from moderate pain to life-long impairment (Table S3). Seddon pioneered nerve accidents classification, by identifying three primary classes based on the degree of demyelination and the amount of damage to the axons and the connective tissues of the nerve [17]. The mildest shape of harm is referred to as neurapraxia, described by focal demyelination in the absence of harm to the axons or the connective tissues [17,50]. Neurapraxia generally happens as consequence to moderate compression or traction of the nerve and results in lower conduction velocity [17,50,51]. Depending on the severity of demyelination, the consequences can change from asynchronous conduction to conduction block, resulting in muscle weakness [17,52]. The subsequent stage is referred to as axonotmesis, which includes direct harm to the axons as well as focal demyelination, but the continuity of the nerve`s connective tissues is preserved [17,51]. The most extreme form of damage is referred to as neurotmesis, involving the complete transection of the axons and total nerve discontinuity [17,51,52].

3. Routes of Administration of active pharmaceutical ingredients (API) into the CNS and challenges

3.1 BBB and limits of drug diffusion

The blood vessels that supply the central nervous system (CNS) have unique properties, known as the blood-brain barrier, that allow them to tightly regulate the movement of ions, molecules, and cells between the blood and the brain. This precise control of CNS homeostasis enables proper neuronal function and also protects neural tissue from toxins, pathogens, and changes in barrier properties. This is an important part of the pathology and progression of various neurological diseases. The physiological barrier is coordinated by a series of physical, transport and metabolic properties possessed by the endothelial cells (ECs) that make up the vascular wall, and these properties are regulated by interactions with various vascular, immune, and nerve cells [53–55].

CNS vessels are continuous, non-windowed vessels, but they also contain many additional properties that allow tight control of the movement of molecules, ions, and cells between blood and CNS [54,56]. This highly restrictive barrier capacity allows the endothelial cells of the BBB to tightly regulate CNS homeostasis, which is essential for proper neuronal function, as well as for CNS protection. protected from toxins, pathogens, inflammation, injury and disease. The limited nature of BBB is a barrier to drug delivery to the CNS and therefore great efforts have been made to create methods to modulate or disrupt the BBB for therapeutic drug

delivery. The main route used to administer drugs is the intravenous route, and the BBB is a limiting factor. Hence, to overcome this hurdle, locoregional direct routes have been used [57,58].

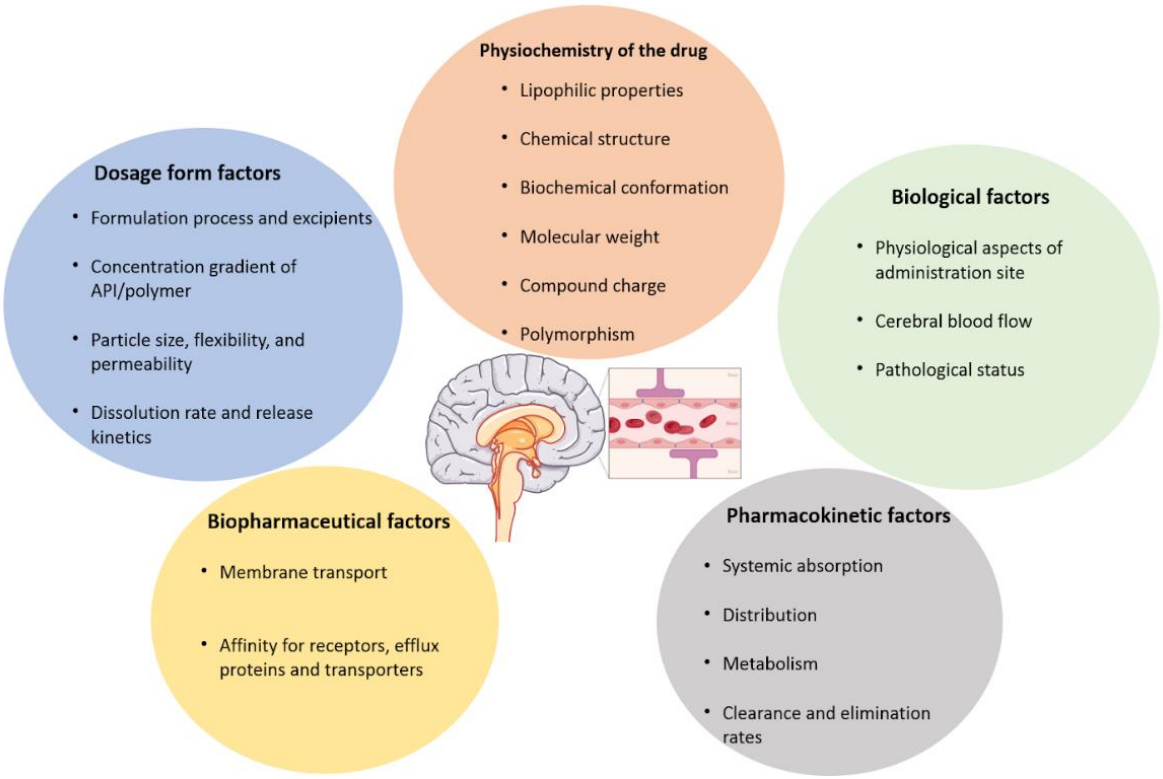


Figure 5: Parameters affecting the ability of drugs to cross the blood brain barrier (BBB)

The Figure 5 shows main drawbacks of the BBB, among them, biological factors such as cerebral blood flow, physicochemical properties of the drug, like the chemical and biochemical structure, the compound charge and molecular mass, dosage form parameters like formulation process used, particle size, release kinetics. Other factors affecting the drug transport through the BBB are pharmacokinetics (ADME and clearance types), and biopharmaceutical factors like the membrane transport and affinity of the drug for cell receptors. Several administration types have been developed in the following parts among them, enhanced systemic administration, intranasal administration, convection- enhanced delivery, intracerebral route (Figure 6)

Enhanced systemic administration

One of the main challenges in the treatment of CNS related diseases is the bioavailability of the API in the damaged tissue. Systemic administration faces the constraint of the BBB, overall biodistribution and clearance from the body [53,57]. To overcome such limits, techniques such as aortic injection and enhanced permeation of the BBB by differential osmotic pressure [19] and cavitation generated by high intensity ultrasound combined with intravenous administration of microbubbles [59–61] have been investigated (Figure 6A). Although these techniques have the potential to increase the diffusion of active compounds, the accumulation into the desired site could be compromised while at the same time the clearance from the CNS tissues and

circulating blood is held. Thus, the therapeutic agent needs to be continuously administered on a planned basis in order to avoid considerable systemic toxicities [19].

Intranasal administration

Intranasal administration consists in the penetration of APIs into the CNS through the nasal barrier. The intranasal pathway can deliver therapeutics directly from the nasal cavity to the brain via the olfactory and trigeminal neurons. The intranasal route is made up of two routes, one intracellular and one extracellular [62]. The intracellular process begins with olfactory sensory cell endocytosis, which is followed by axonal transport to synaptic clefts in the olfactory bulb, where the drug is exocytosed [62]. This transynaptic process is replicated by olfactory neurons, allowing the medication to be distributed to different brain areas [62]. Drugs are carried directly into the cerebral spinal fluid via the extracellular method by first going via the paracellular space over the nasal epithelium, then through the perineural space to the brain's subarachnoid space [62].

One of the limitations of this route is the availability of the compound in contact with the nasal mucous membrane. Hydrogels may function as a reservoir for a prolonged release of APIs in the nasal route towards the CNS [63](Figure 6B-4). In other works, the development of nanobodies have been recently explored for the intranasal delivery of vaccines encapsulated in a nanogel [64], Temozolomide administration for glioblastoma treatment [65], poorly soluble drugs such as Simvastatin [66], and intranasal clozapine-loaded Technetium-99m-labeled mixed micelles for the treatment of Schizophrenia [67]. Overall, although under investigation, this route may offer a non-invasive approach to the delivery of APIs in combination with appropriate encapsulation in nanoparticles including nanogels.

Direct administration into the CNS compartment: the intracerebro-ventricular and parenchymal routes

Since the majority of GB recurrences arise within the margins of the resection cavity, the chance exists that intraoperative loco-regional therapies (e.g. ascribed to differentiation, chemoattraction-trapping, immunostimulation strategies) from this space has received little attention to date and should get special consideration [68]. Invasive techniques that include the physical disruption of the BBB have also been investigated with the aim of reaching the damaged area more directly while reducing the total dose needed. For example, intracerebroventricular and intrathecal injections have the advantage that the drug is administered in the fluid compartment that is already in the CNS, hence the drug can more quickly reach the area of interest [18,69]. (Figure 6B-2&3). Moreover, administration *via* this route can be continuous by depositing a catheter connected to a pumping system [70]. Both routes of administration have the advantage that the main BBB step is bypassed contrary to systemic administration [69,71]. However, the diffusion into a distal site within the CNS can still be reduced due to other biological barriers, and the active compound may affect healthy tissues causing neurotoxicity or off-target effects [71–73].

A more direct approach consists in the injection of the drug directly into the damaged site. This approach, referred to as intracerebral parenchymal injection (Figure 6B-1), is relevant in the case of macroscopic lesions such as visible brain tumors and brain ischemia. The challenge of this strategy is the internal fluid pressure that can cause a reflux of the administered substance if performed in a single shot. Therefore, an additional force is needed to enhance the distribution of the administered substance. This is the principle of the strategy called Convection Enhanced Delivery (CED) in which a differential pressure is applied by means of a pumping system connected to a catheter that delivers the load gradually as the molecule of interest is locally and regionally spread into the interstitial space by convection and diffusion [74,75] (Figure 6B-1.2). CED has various benefits, such as a bulk flow-controlled process, bypassing the BBB, targeted delivery, and achieving reproducible diffusion [76].

These techniques have been used for the administration of soluble drugs or colloidal dispersions of nanoparticles, sometimes delivering radiopharmaceuticals with promising results [63,64]. Nevertheless, although they offer a more loco-regional delivery, the absence of a reservoir that gradually releases the active

compound represents a limitation. CED may function as a reservoir strategy for gradual delivery, however the optimal regime depending on drug formulations needs to be established in order to diminish potential risks in the neurological status of the patient linked to an accumulation of the drug and/or the increase of the intracerebral pressure [77].

Delivery of scaffolds as prolonged releasing platforms

A novel approach consists in the use of implantable devices which can ensure a sustained release of the active compound without the need of repeated injections. These releasing platforms are often formulated as hydrogels, fibers, and porous scaffolds [78–80]. The success of these systems has already been demonstrated, as in the case of Gliadel® wafers: when implanted in the margins of the glioblastoma resection cavity, they allow for a sustained release of carmustine [33–35,38]. However, the main disadvantage is that the wafers do not fit perfectly into the space and the contact with brain margins could be compromised [36].

Hydrogels by contrast offer the possibility of an adequate fitting into cavities and are very attractive as delivery systems. Indeed, they are of special interest in zones where the tissue has been resected such as tumors, brain and spinal cord injuries that undergo surgery (Figure 6B-1.1). The versatility of such systems relies on the feasibility of injection as a consolidated hydrogels or as soluble components that are sensitive to temperature or radiation to become stable hydrogels *in situ* [78]. The selection of either strategy is dependent on the application. For example, to fill a superficial cavity, thermosensitive soluble components would be easier to deposit with subsequent instantaneously reaction upon a change in temperature, whereas endoscopic delivery of thermosensitive compounds may not be suited for long distances that could result in gelation of the solution in the tubing system [81–83].Contrary, injection of a consolidated hydrogel may be limited to the rheological behavior and nature of the components. For instance, changes in structure or properties after injection and degradation due to hydrolysis are variables that could constrain their application [82,84–86].

Delivery of hydrogels by CED

The main advantage of the use of convection for delivery is the control of the time-space distribution of the load. While CED has been investigated since the early '90s on liquid formulations for intracerebral injections, little research has been made with regard to the delivery of hydrogels [78]. For instance, Mukerji R et al. 2015 [87] developed a system of soluble elastin-like polypeptide (ELP) containing periodic cysteine residues and conjugated with chlorin-e6 (Ce6) as a photosensitizer. The soluble peptide was distributed *in vivo* into a solid tumor by CED to allow an even distribution within the whole tumoral mass (Figure 6B-1.2). Upon photon stimulation the produced ROS allowed disulphide crosslinking across the cysteine chains that eventually originated a reticulated network forming a hydrogel embedded in the tumor [87]. This strategy allowed to overcome the rheological constraints that can impose the injection of viscous materials. Additionally to photoradiation, thermal, enzymatic [63] and sonication [88] activation of the gelling of the injectable liquid mix might be explored in combination with CED.

Potential hazards and challenges

The fact that the direct administration of drugs into the CNS is an invasive approach, can cause patient side effects such as edema, infection, and neuron damage [69,89,90]. The safety hazards, drawbacks, and relatively high prices held up their applications as standard therapeutic strategies for those CNS diseases with relatively long disease processes and needing repeated administration[90]. Reducing the invasiveness of the procedure by exploring minimally invasive surgery such as keyhole surgery [44,91] for deposition of catheters or injection of scaffolds (Figure 6B-5), accompanied with image guided surgery might result in benefit to the patient.
Intracerebral drug delivery is a method of passing through the BBB and other mechanisms that limit drug distribution in the brain, allowing high concentrations of drug to enter the central compartment. Factors that affect the efficacy and safety of this route of administration are osmotic pressure, pH, volume, and the presence of preservatives and drug vehicles being administered [90]. Physicians should be aware of the ongoing

pathology process and the patient's neurological status, as well as the physicochemical properties of the associated drug when prescribing for intracerebral administration. High suspicion parameters should be maintained when monitoring patients for adverse drug events after administration [90].

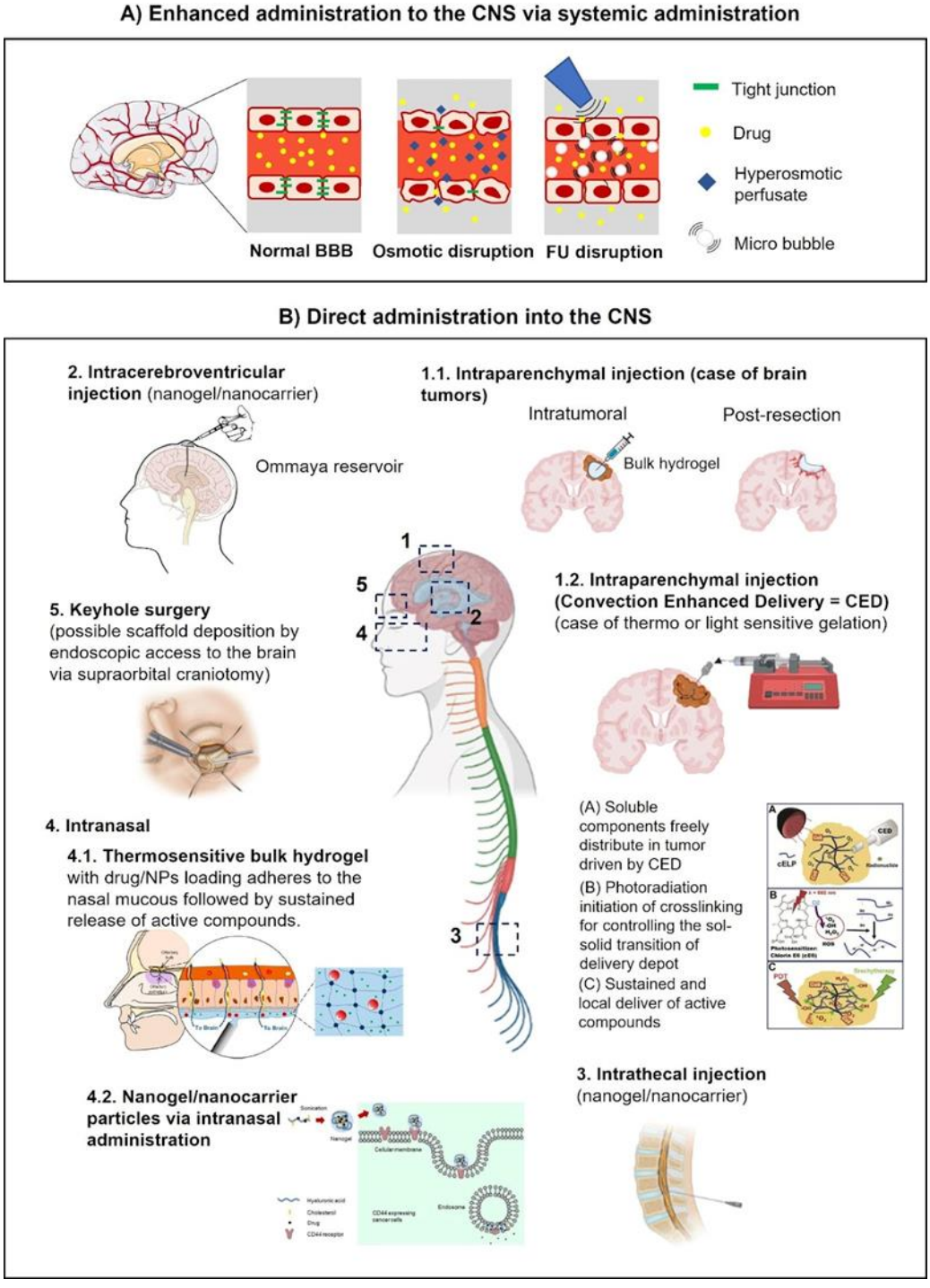


Figure 6: Routes of administration into the CNS. reprinted from Mukerji R et al. Biomaterials 2016 [Ref 83], with permission from Elsevier. Figure 2B-2: artwork by Patrick J. Lynch. Reprinted from the public domain accessat https://en.wikipedia.org/wiki/Ommaya_reservoir#/media/File:Ommaya_01.png. Figure 2B-4.1: reprinted from Kiparissides C et al. Ind Eng Chem Res 2020 [Ref 60], with permission from ACS. Figure 2B-4.2: reprinted from Wei X et al. Bioconjug Chem 2013 [Ref 84], with permission from ACS. Figure 2B-5: reprinted from Core Techniques in Operative Neurosurgery [Add ref], with permission from Elsevier. Further permission related to the material excerpted should be directed to the editors.

A) Enhanced administration of molecules and nanobodies by osmotic or focused ultrasound (FU) disruption of the BBB. B) Direct administration: 1.1. Intraparenchymal injection. A brain tumor case is schematized where hydrogel injection might be performed intratumorally or after resection around the cavity edges. 1.2. Intraparenchymal injection assisted by CED (convection-enhanced delivery). Depicted is the case where soluble compounds are evenly distributed by CED within the tumor before a gelation reaction is induced by photoirradiation. The resulting embedded gel can be used as a platform for the sustained release of active compounds [87]. 2. Intracerebroventricular administration of drugs directly into the cerebrospinal fluid (CSF). The Ommaya reservoir consists of a catheter connected to one lateral ventricle and a reservoir implanted under the scalp [92]. 3. Intrathecal injection. Lumbar puncture showing the direct administration of a drug directly into the CSF. 4. Intranasal delivery. 4.1 Intranasal application of modified HA in the nasal endothelium. Upon in situ polymerization the generated patch might be used as a reservoir for sustained release of compounds [63]. 4.2 After permeation of the nasal barrier, HA nanogels may be used to enhance intracellular trafficking of drugs in CD44 expressing cells [88]. 5. Keyhole surgery [44,91] might be used as an alternative access route to the implantation of hydrogels into the brain. Credits: figures were reused with authorization of the authors and or editors.

4. Therapeutic relevance of HA based scaffolds in the CNS

4.1 Composition, biological properties & mechanical properties of CNS

The extracellular matrix (ECM) plays a diverse role in several physiological and pathological conditions [93]. In the brain, ECM is unique in both composition and function. In addition, almost every cell in the central nervous system contributes to various aspects of this complex structure [94]. ECMs in the brain, rich in proteoglycans and other small proteins, aggregate into distinct structures around neurons and oligodendrocytes [95]. These special structures play important roles in normal brain functions such as learning, memory, and synaptic regulation [93,94].

Chemical modification further diversifies the processing and manufacturing techniques that can be used to create 3D HA scaffolds [96–98]. By easily changing the treatment method, HA hydrogels, granular hydrogels (microgels), electrospinning fibers, and HA-based composites can be formed [78,99–101]. Various types of HA scaffolds have their own characteristics which offer several benefits to CNS regenerative medicine [80].

Murine and human brain ECM stiffness and physico-chemical specification of these composite scaffolds need to be associated. Indeed, brain ECM is mainly composed of HA and gives this tissue a softness property [94]. Moreover, murine brain Young modulus according to the region (hippocampus, cerebellum, cerebral cortex) brain varies from 0.5 to 10kPa are quite close according to the region studied [102]. It can be around 2 kPa for a healthy brain and go up to 20 kPa for tumor affected brain, but in more rigid regions such as the dura mater, it can reach very high young moduli 32 MPa and 62 MPa [102–105]. Thus, formulating scaffolds with Young modulus in this range is possible, especially for systems like hydrogels, sponges and fibers [78,79,106–109]. It also has been shown that in a healthy brain *vs* an injured brain, the stiffness of the tissue can either increase or decrease according to the brain region and the type of injury (neurodegenerative disease, cancer) [110–114]. Various scientific projects on brain tissue mechanics have concluded that the brain is a very soft tissue, non-linearly viscoelastic solid material, with a very low linear viscoelastic strain interval, around 0.1 to 0.3% [106].

Brain tissue is made up of white and grey matter, and different areas of the brain are composed of various proportions [63,115]. White matter mainly consists of myelinated axons from nerve fibers, the grey matter is driven by unmyelinated axons and perikaryons [106,107]. It is necessary to understand the mechanical properties of brain tissue, as the brain is so well isolated from mechanical damage under normal circumstances[110]. Mechanical factors are thought to play a role in many diseases, including brain

development, but brain mechanics has been most often studied to understand stressed conditions, in an indirect or direct way [106,112,113].

4.2 Physico-chemistry of HA based semi-solid dosage forms:

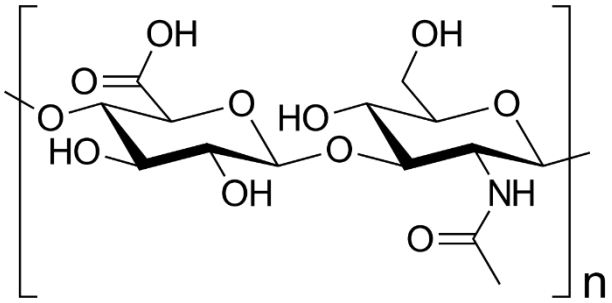


Figure 7: Hyaluronic acid chemical structure

Hyaluronic acid (HA) is negatively charged and non-branched GAG (figure 7). Brain has a HA-enriched ECM, in a healthy one, high molecular weight (> 10^6 Da) HA chains function as the tissue center of ECM and interact with proteins and PGs via a small linker protein called HABP to form a hydrogel-like network[93,94]. HA is upregulated in GB tumors and contributes to many phenotypic changes associated with cancer progression, including early tumor development, cancer cell proliferation, infiltration, drug resistance, and post-treatment recurrence [105,116]. Besides, hyaluronidases, HA synthases, HA receptors, and some HABPs are overexpressed. Co-overexpression of these factors may be implicated in GB invasion and treatment resistance [115,117,118].

For better mechanics, biomimetism, biocompatibility, sustained release and smart properties such as thermosensitivity, poloxamer and HA are well-studied and great candidates for semi-solid dosage forms and more precisely composite hydrogel formulations [78,85].

Hydrogels are 3D water-swelling polymer networks formed by chemical and / or physical interactions. The main advantage of using hydrogels in tissue engineering constructs is that they are not only easy to process and mold, but also have the ability to adjust mechanical and biochemical properties to mimic soft tissues [78,119]. HA is interesting in CNS, brain cancer and peripheral nerve engineering, because of its natural origin, non-immunogenicity, high biodegradability by hyaluronidase and hydrolysis, porosity, biocompatibility, neuronal differentiation and neurite outgrowth capacity [8,80]. Hydrogels have received a great deal of attention due to their unique properties such as excellent biocompatibility, high water content and ability to decompose into safe products, and are widely used in various biomedical applications such as regenerative medicine, aesthetic medicine and drug delivery [9,120].

Poloxamer is a family of synthetic nonionic triblock copolymers in which the central hydrophobic block of polypropylene oxide is sandwiched between two hydrophilic blocks of polyethylene oxide. Polyethylene oxide copolymers [67,94,95] amongst them, Poloxamer 407 (P407) hydrogels exhibit interesting thermal properties and are attractive candidates for formulations, especially in combination with HA. P407 is a temperature-responsive polymer that is cold and liquid [86]. Aqueous polymer solutions gel as the temperature rises. P407 is considered to be one of the safest polymeric materials for the production of thermal hydrogels. It has excellent biocompatibility and injectability and is used in various fields of tissue engineering [121–123]. Hydrophobic domains in the chemical structure of P407 are useful for retaining poorly water-soluble compounds. Various active substance-containing hydrogels based on P407 were developed and characterized as a function of active substance concentration. Since then, hydrogels have been used as a controlled drug delivery system to promote local, sustained, and long-term release of APIs, thereby reducing

dosing frequency, avoiding side effects, and complying with low doses. The most widely studied environment-sensitive systems are temperature-sensitive hydrogels, where physical entanglement, hydrogen bonds, and hydrophobic interactions are key functions that make up the crosslinks. There are two distinct types of thermal hydrogels that gel by cooling below the upper critical gelation temperature (UCGT) such as agarose or by heating above the lower critical gelation temperature (LCGT) such as poloxamer [124,125].

Hydrogels with LCGT behavior and sol-gel transition at 37°C can be loaded under mild conditions (temperature ≤ 37 ° C), making them very popular in the biomedical field as carriers for cells, drugs and biomolecules [120,126]. The solubility of hydrophobic parts decreases when aggregated, to reduce the interaction of PPO blocks with the solvent used. Poloxamer is well-known for its thermal responsiveness, biocompatibility and low toxicity, P407 is widely used in smart drug delivery and in various formulations such as ophthalmic, nasal and other parenteral galenic forms [121–123]. When P407 gel is used alone, it rapidly loses its gelling ability after being diluted in a water-enriched environment. Blending P407 with other polymers such as hyaluronic acid or molecules is a solution to improve drug loading; these composite hydrogels are widely developed in the literature [96,127–129]. For example, P407-based hydrogels are widely used to encapsulate some small molecule drugs, such as ketorolac, metoprolol, and doxycycline, which have a molecular weight (MW) of less than 500 Da. They are also suitable for achieving optimal release of proteins to facilitate transfer of water molecules and release proteins or other compounds with a Mw > 500 Da such as Urokinase and Rutin [127,130].

5. HA-based specific device for various applications

Hydrogels are hydrophilic polymer networks that swell in water or body fluids. Recently, *in situ* gelation systems based on various synthetic and natural polymers have been extensively investigated for biomedical applications due to their ability to efficiently encapsulate cells and bioactive molecules, minimally invasive injection and easy to form in any desired defect shape, in addition to some advantages of typical hydrogels including high water content similar to extracellular matrix (ECM) [78,93,94], controllable physico-chemical properties (rheology, injectability) and biocompatibility [120,126]. When hydrogels are developed by covalent crosslinking, they form chemical or permanent gels. On the other hand, when physical bonding between molecules produces hydrogels, they form physical gels, and they are usually reversible [82,86,131]. Hydrogels are polymeric mesh networks that have the ability to bind a high amount of water [78,119,132]. It is a semi-solid dosage form that is usually used for transdermal, subcutaneous, intra-articular, ophthalmic, nasal, vaginal, rectal administration routes [119,132]. The intracerebral route is the route that will be discussed in the following part; it is of high interest for brain cancer and central nervous system therapeutic strategies [69,89,90].

Unlike scaffolds that have a particular shape before being applied (figure 8), injectable scaffolds are injected into the defect area and then acquire their shape *in situ* [108,133,134] (see Graphical abstract p26). This function allows solidifying precursor scaffolds and cell mixtures to be site-specifically delivered into cavities and defects with irregular aspect, in a less invasive manner than transplantation [135–138].

Several studies deals with HA based devices composed of other biopolymers such as heparin, silk fibroin[108], chitosan [12,133,139–142], collagen [133,143,144], alginate [11,145]or synthetic ones like poly(methylvinylether-alt-maleic acid [146], polycaprolactone [147,148], PDLLA [149], PEG [150], poloxamer [96,127–129]. These composite scaffolds made of natural polymers are biocompatible systems that exhibit interesting properties for tissue engineering applications such as structure, porosity, stiffness and correct controlled degradation rates [14,151]. Natural macromolecules exhibit abilities for site-specific cell adhesion, and given that HA is the main component of the brain ECM, neural cells can interact with a matrix which mimics their natural environment[3,10,14]. The most recent studies are presented, these systems have been developed for various applications such as GB treatment, peripheral nerve regeneration, and brain tissue engineering (Table S1, Table S2, Table S3).

Since they exhibit shear-thinning properties in rheological studies as well as when being injected, some hydrogels have been applied as fillers in nerve guide channels (NGCs) in order to induce regeneration of peripheral nerve tissue [49,142,152,153]

Other lyophilized or dried biopolymer scaffolds have been administered locally for drug delivery, cell encapsulation or cell tissue colonization [108,138,141,146,148,154,155]. They have various applications such as cartilage, brain tissue, bone regeneration or treatment. They provide structural support for cell attachment and subsequent tissue growth. They consist of biological substitutes to restore, replace or regenerate defective tissues, and mimic tissue-specific ECM [113–116].

Biomaterial scaffolds are one of the most important factors in promoting cell differentiation and proliferation to form new tissues of interest. Tissue-engineered scaffolds must have multiple functions, including proper porosity, optimized mechanical properties, well-controlled biodegradability, non-destructive sterilization, and biocompatibility with treated tissue [156–158].

Electrospun fibers have applications such as drug delivery, tissue engineering, wound dressing and cosmetics[99,109,159]. Electrospinning is a type of electrospray process and consists of strong electrical forces that overcome the weak surface tension of polymer solutions at specific thresholds to emit a jet of liquid that can be rooted in the process of electrospray forming small solid polymer droplets and/or fibers [79,99,109,159,160].

A nanogel is a three-dimensional nano-sized hydrogel material composed of a cross-linked swellable hydrophilic polymer network with high water storage capacity, without actually dissolving in an aqueous medium. Nanogels can be made from a variety of natural, synthetic, or polymer combinations [161–164].

Nerve guidance conduits are tubular devices made of wide-range biomaterials that guide axial regeneration from the injured proximal nerve to the distal stump. It is a type of bridging that helps avoid nerve grafting and nerve healing which are both llimited [48,49,165].

Scaffolds specifications:

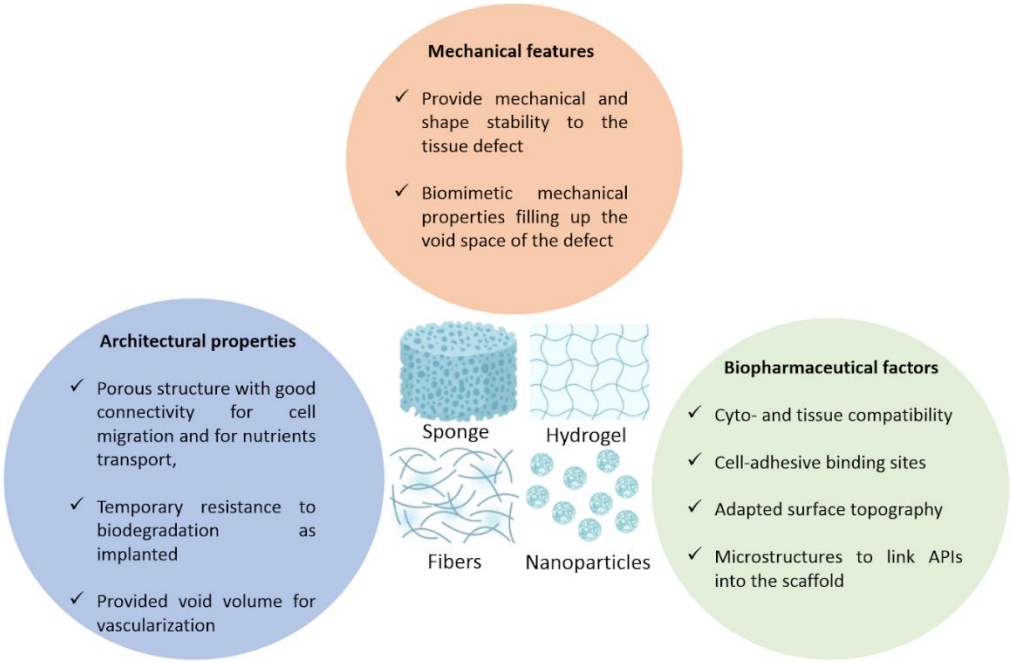


Figure 8: Scaffold specifications depending on various parameters

The scaffolds described in the tables 2, 3 and 4 must show some features, firstly architectural features, in other words, a suitable porosity in case of cell encapsulation or a system requiring cell trapping and migration, short-term resistance to biodegradation, and a void volume for blood vessels ramification. Secondly, mechanical properties, like shape stability and biomechanical mimicking the treated tissue, for instance by having a close Young modulus also called Elastic modulus (kPa). Lastly, biopharmaceutical features required are cyto and histocompatibility, surface topography, cell-anchoring sites, and microstructures for the drug to bind into the scaffold, which is helpful for controlled drug release.

5.1 HA based scaffolds for glioma application

The first authors to provide anti-inflammatory and anti-cancer natural molecules using HA nanohydrogels are [166]. It is a combination of quercetin and temozolomide for the treatment of GB. In this study, it was shown that quercetin nanohydrogel promotes preferential uptake of CD44 and significantly enhances the therapeutic effect of temozolomide in GB cells, possibly through an anti-inflammatory mechanism [166]. Moreover, other results suggest that doxorubicin-loaded modified hyaluronic acid nanogels are an excellent candidate to effectively achieve glioma targeting [164].

Another study showed that the efficacy of HA-coupled micelles was increased by stronger inhibition of glioma proliferation and induction of apoptosis. Overall, these findings demonstrated the benefit of GBM associated chemotherapy using HA-coupled micelles [97]. Besides, HA-CF / CB hydrogel has the potential to be a strong candidate for drug delivery vehicles, especially for the treatment of GB. Injections of DOX -loaded HA-CF / CB hydrogel into GB *ex vivo* human tissue samples showed efficient attachment of the gel within diffusion and release of the compound into surrounding tissue [167]. Another system for GB treatment consisted of a polymer-drug conjugate, releasing DOX and has shown decrease in cell viability and inhibition of tumor

growth [168]. Drug delivery systems composed of HA, intended for GB treatment, have also shown promising *in vitro* on GB cell lines and *in vivo* on mice and rat models results, in terms of bioperformance, biocompatibility, biomimetism and controlled drug release of DOX, PXL and/or TMZ [114,164,169–171].

3D hydrogel cultures of patient-derived GB cells showed good viability and proliferation rates equivalent or superior to when cultured as standard neurospheres. The hydrogel system also allowed the incorporation of ECM mimetic peptides to reduce the effects of specific cell-ECM interactions [141,144,172,173]. Besides, the system described by other authors [150], provides a useful PEG-HA and PCL+/-BC/GEL-HA 3D *in vitro* mechanomimetic with stiffness tunability, a model for elucidating the underlying mechanisms of GBM progression in a more physiologically appropriate and controlled manner and assessing the efficacy of potential drug candidates [148,172,174]. In another similar study, HA brain-mimicking hydrogel network resulted in significant dose-dependent changes in markers of glioma malignancies compared to unmodified 3D gelatin or PEG hydrogels [148,174,175]. The HA-modified hydrogel system provided a clear and reproducible extracellular microenvironment for studying the development of gliomas [175].

The scaffold Gliadel® underwent clinical trials and has been FDA approved. It is a polyanhydride copolymer wafer loaded with Carmustin or BCNU. This post-resection treatment is the only GB implantable device on the market and shows effective bio performance with a few side effects [35,176]. Alternative systems have been developed with biopolymers such as silk fibroin, hyaluronic acid and heparin [68,108]. Such as formulating sponges loaded with SDF-1α chemoattractant cytokine that acts as tumor trap for CXCR4 receptor-positive cells. This strategy has also been explored in a recent study[177], using chitosan-based electrospun fibers charged with SDF-1α loaded PLGA nanoparticles for GB treatment. It was shown that a 7-day follow-up study of Fischer rats with implanted devices had no side effects *in vivo* [177]. Moreover, the nanofiber structure of the scaffold provided excellent fixation sites to aid the adhesion of human GB cells. Some improvement must be achieved to better shape the resection cavity and optimize the drug quantity that can reach sites of interest, in order to increase the bioperformance and efficacy of the system [177].

5.2 Systems for CNS application

Discussion of hydrogels:

HA-PDL hydrogels has been explored to repair brain tissue defects and showed a good bridging property helping tissue ingrowth and vascularization *in vitro* and *in vivo* in Sprague-Dawley rat models [178]. In other studies, amino acid-based hydrogels have been prepared and improved tissue restructuration through, angiogenesis, and axonal growth in Sprague-Dawley rats models [179,180]. These formulated HA hydrogels also prevented glial scar formation by lowering glial cell proliferation also in Sprague-Dawley rats models [133]. Tam et al. [181] developed HA-MC hydrogel to deliver NSPCs(Neural stem/progenitor cells) that allow OLG (oligodendrocyte) differentiation. Besides, respectively formulated HA nanocomposite hydrogels loaded with BDNF [182] and VEGF [183] *in vitro* SP embryo cell lines, showing a stable release of biological factors, allowing cell survival and growth and HA-laminin hydrogel charged with SDF-1α *in vitro* and *in vivo* C57BL/6 mouse model enhance retention and migration of NPSC grafts post SDF-1α treatment in a signal-dependent manner through the SDF-1α-CXCR4 axis.

HA-poly(N-isopropylacrylamide) has shown to support cell survival and differentiation, have good biomimetic rheological properties, and stimulates ECM network production [184]. Iron oxide (Fe3O4)-HA nanogels intended for the treatment of Alzheimer, via a theranostic tool containing metal complex associated to HA nanogels, have shown a good biocompatibility to astrocyte cells and as a contrast agent of quality in

MRI imaging *in vitro* [161]. This theranostic system could be a promising choice for neurodegenerative disease theranostics *in vitro* and *in vivo* [161].

Discussion of scaffolds:

Other studies, developed scaffolds composed of biopolymers like collagen, alginate, and PCL have shown interesting bioperformance and biocompatibility. These scaffolds had mechanical properties mostly Young modulus ranging from 0.1-10kPa which is in concordance with the brain tissue young modulus interval [143,185,186]

Moreover, it has been shown through *in vitro* and *in vivo* assays that NSCs embedded in HA collagen biomaterials can ameliorate the recovery of damaged facial nerves and artificial conduction of NSCs may bring potential for the treatment of peripheral nerve damage. Aligned nanofibers allow guiding the growth of neurites [143].

Diverse developed collagen-HA-based scaffolds were tested *in vitro*. It has been shown that their system promoted the differentiation of neural stem cells (NSCs) into neurons *in vitro* [185].

5.3 Systems for PNS application

HA has been very successful in neural tissue engineering and supports the growth, differentiation and proliferation of neurites on a variety of substrates [153,187]. HA hydrogel amends the viability and proliferation of neural progenitor cells [153]. This indicates the potential therapeutic approaches for peripheral nerve regeneration and CNS therapies. HA hydrogels' mechanical properties have been adapted for the differentiation of neural progenitors, an up-and-coming strategy for neurodegenerative diseases treatment.
HA can be blended with different biopolymers, especially collagen, since they both enter in the composition of the ECM and are biocompatible and biomimetic when formulated in scaffolds. For example, some used neural stem cells embedded in the HA / collagen conduit to regenerate a 5 mm facial nerve gap in a rabbit model [143]. In addition, a blend of HA with biodegradable synthetic polymers such as PLGA and poly-L-lysine has shown great potential for controlled delivery of drugs, targeting axonal regeneration after spinal cord injury *in vitro* and *in vivo* [188].

The high biocompatibility of HA is crucial in reducing the inflammatory response produced by conductive polymers in nervous tissue engineering. For instance, PEDOT-doped HA nanoparticles are integrated into chitosan / gelatin scaffolds and exhibit excellent PC12 cell adhesion and growth, while pyrrole / HA conjugates mask conductive electrodes from adverse reactions of glial cells during implantation [189]. Nanofiber-aligned PCL / Gel / HA scaffolds have been shown to promote axon growth and elongation and help support intracellular communication [147]. Based on these results, the PCL / gel / HA composite scaffold is an excellent candidate for a biomimetic matrix for GBM and tumor testing.

Discussion of conduits systems

Many studies have developed composite HA-based conduits for nerve regeneration. Most of them performed experiments on preclinical models, such as SD rats, CD-1 mice, and NZ rabbits, that helped validate these systems [143,149,187,190]. Besides, some of the systems have not shown significant regeneration. HA / collagen conduits have been developed but showed limited results with unmyelinated nerve fibers remaining, according to the authors, the scaffold needed to be amended since myelin degeneration and swelling can be observed [143]. For other authors, a similar system has shown good stability, cell growth and adhesion, and neurosphere development on the conduit scaffold, making possible the differentiation and nerve tissue regeneration [187].

Discussion of hydrogels

Some hydrogels have shown good results in terms of biocompatibility, architectural properties, mechanical features, bioperformance *in vitro* and *in vivo*. The sustained release of NGF from these chitosan and HA-based hydrogels was well-controlled [153,191,192]. Porosity and viscoelastic properties of their systems are interesting for cell attachment. Moreover, these hydrogels enhance neural regeneration and tissue repair but also cell differentiation and migration [153,191,192].

PDLLA / βTCP nerve conduits containing CS-HA / NGF hydrogel have also been described in the literature [149]. These devices enhanced nerve regeneration and myelination in contrast to the void PDLLA / βTCP nerve channels and autologous transplant group [149]. This suggests that injectable CS–HA / NGF hydrogels can successfully enhance nerve regeneration and are therefore a good candidate in the field of neural tissue engineering [149].

6. Conclusion

HA is a promising material for GB, CNS and PNS injuries treatment due to its biomimetic, biomechanical, biocompatible, biodegradable, tunable with chemical modifications and associable to other polymers making it possible to create a simple scaffold for cell encapsulation, allowing glial, neural cells and nerve fibers regeneration. More complex systems such as thermosensitive, (nano) composite systems for targeted drug delivery and local administration are also developed.

Indeed, treatments aimed to treat pathologies other than CNS and PNS ones, are available on the market, using other administration routes, such as Orthovisc® is a topical preparation of highly modified HA, that has shown a successful osteoarthritis(OA) treatment [193–195]. Hyalone® treats osteoarthritis and targets lower back pain [196], Cartistem® for ligament and cartilage degeneration including Degenerative OA [197]. Hyalofast® for chondral and osteochondral lesion treatment [198]. Hence, these systems can be adapted for better targeting and biomimetic properties to target GB, CNS and PNS impairments (figure 9).

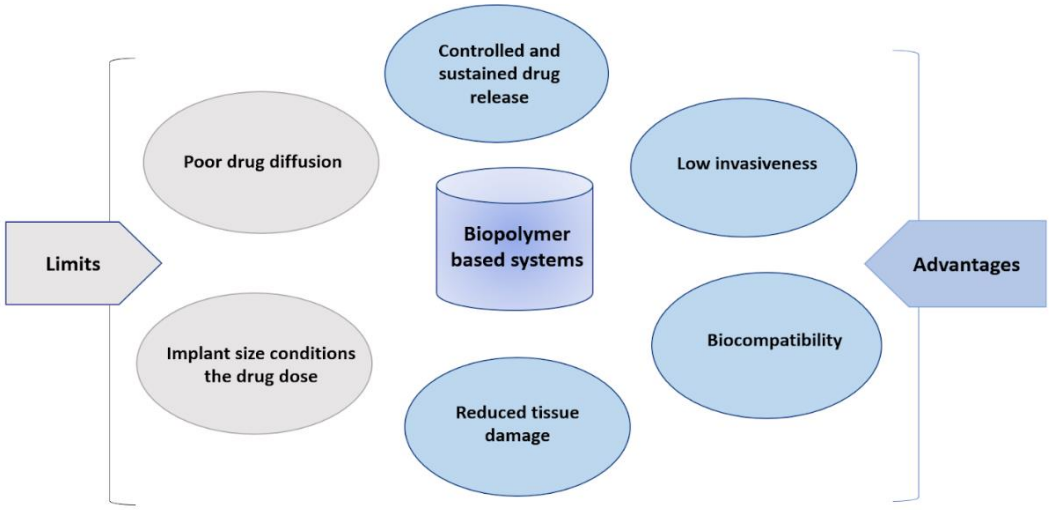


Figure 9: Characteristics of polymer-based devices for central nervous system delivery

In conclusion, HA-based devices present qualities like biocompatibility, low invasiveness, controlled drug release, reduction of tissue damage, and permit, in most cases, local administration of APIs. The efficacy of such systems is conditioned on the drug quantity initially put in the scaffold, and the size of the scaffold.

Supplementary Materials: The following supporting information can be downloaded at: www.mdpi.com/xxx/s1,; Table S1: title; Table S2: title; Table S3: title;

Author Contributions: A.D. F.B. RMP. EG. contributed to conception of the review. A.D. F.B. and N.F. and I.O retrieved the main articles included in the review. A.D, I.O, R.M.P, N.F wrote the first draft of the manuscript. A.D. and F.B. supervised the project and finalized the manuscript. Review and editing F.B, E.G; Visualization, R.M.P, N.F. All authors contributed to manuscript revision, read, and approved the submitted version. All authors have read and agreed to the published version of the manuscript.

Funding and Acknowledgments: This work was carried out with support from by La Ligue Con-tre le Cancer (grant number TARC21174 to A.D.). It was also supported by the Institut National de la Santé et de la Recherche Médicale (INSERM) and by the University of Angers (Angers, France). The work was in addition related : (i) to the Region Pays-de-la-Loire programs to F.B. : Bioimplants for Bone Regeneration (BILBO) part of the BIOREGATE Research-Training-Innovation consortium (RFI) and NanoFar + (International Strategy) and (ii) to the French Na-tional Research Agency (ANR) under the frame of EuroNanoMed III (project GLIOSILK) and through the LabEx IRON (Innovative Radiopharmaceuticals in Oncology and Neurology) as part of the French government Investissements d'Avenir program (ANR-11-LABX-0018 to E.G.).

Institutional Review Board Statement: Not applicable.

Informed Consent Statement: Not applicable.

Data Availability Statement: Not applicable.

Conflicts of Interest: The authors declare no conflict of interest.

References:

[1] Jre F, Tc L, Ubg L. Hyaluronan: its nature, distribution, functions and turnover 1997:7.

[2] Passi A, Vigetti D. Hyaluronan: Structure, Metabolism, and Biological Properties. In: Cohen E, Merzendorfer H, editors. Extracellular Sugar-Based Biopolymers Matrices, vol. 12, Cham: Springer International Publishing; 2019, p. 155–86. https://doi.org/10.1007/978-3-030-12919-4_4.

[3] Vercruysse KP. Chapter 9. Hyaluronan: a Simple Molecule with Complex Character. In: Williams PA, editor. Polymer Chemistry Series, Cambridge: Royal Society of Chemistry; 2011, p. 261–91. https://doi.org/10.1039/9781849733519-00261.

[4] Vigetti D, Karousou E, Viola M, Deleonibus S, De Luca G, Passi A. Hyaluronan: Biosynthesis and signaling. Biochimica et Biophysica Acta (BBA) - General Subjects 2014;1840:2452–9. https://doi.org/10.1016/j.bbagen.2014.02.001.

[5] Bukhari SNA, Roswandi NL, Waqas M, Habib H, Hussain F, Khan S, et al. Hyaluronic acid, a promising skin rejuvenating biomedicine: A review of recent updates and pre-clinical and clinical investigations on cosmetic and nutricosmetic effects. International Journal of Biological Macromolecules 2018;120:1682–95. https://doi.org/10.1016/j.ijbiomac.2018.09.188.

[6] Ma W, Suh WH. Cost-Effective Cosmetic-Grade Hyaluronan Hydrogels for ReNcell VM Human Neural Stem Cell Culture. Biomolecules 2019;9. https://doi.org/10.3390/biom9100515.

[7] Kogan G, Šoltés L, Stern R, Gemeiner P. Hyaluronic acid: a natural biopolymer with a broad range of biomedical and industrial applications. Biotechnol Lett 2006;29:17–25. https://doi.org/10.1007/s10529-006-9219-z.

[8] Jensen G, Holloway JL, Stabenfeldt SE. Hyaluronic Acid Biomaterials for Central Nervous System Regenerative Medicine. Cells 2020;9:2113. https://doi.org/10.3390/cells9092113.

[9] Borzacchiello A, Russo L, Malle BM, Schwach-Abdellaoui K, Ambrosio L. Hyaluronic Acid Based Hydrogels for Regenerative Medicine Applications. BioMed Research International 2015;2015:1–12. https://doi.org/10.1155/2015/871218.

[10] Kogan G, Šoltés L, Stern R, Mendichi R. HYALURONIC ACID: A BIOPOLYMER WITH VERSATILE PHYSICO-CHEMICAL AND BIOLOGICAL PROPERTIES. Hyaluronic Acid n.d.:47.

[11] Draget KI, Skjåk-Bræk G. Chapter 7. Alginates: Existing and Potential Biotechnological and Medical Applications. In: Williams PA, editor. Polymer Chemistry Series, Cambridge: Royal Society of Chemistry; 2011, p. 186–209. https://doi.org/10.1039/9781849733519-00186.

[12] Kean T, Thanou M. Chapter 10. Chitin and Chitosan: Sources, Production and Medical Applications. In: Williams PA, editor. Polymer Chemistry Series, Cambridge: Royal Society of Chemistry; 2011, p. 292–318. https://doi.org/10.1039/9781849733519-00292.

[13] Shibata T. Chapter 3. Cellulose and Its Derivatives in Medical Use. In: Williams PA, editor. Polymer Chemistry Series, Cambridge: Royal Society of Chemistry; 2011, p. 48–87. https://doi.org/10.1039/9781849733519-00048.
[14] Williams PA. Chapter 1. Natural Polymers: Introduction and Overview. In: Williams PA, editor. Polymer Chemistry Series, Cambridge: Royal Society of Chemistry; 2011, p. 1–14. https://doi.org/10.1039/9781849733519-00001.
[15] Adamson C, Kanu OO, Mehta AI, Di C, Lin N, Mattox AK, et al. Glioblastoma multiforme: a review of where we have been and where we are going. Expert Opinion on Investigational Drugs 2009;18:1061–83. https://doi.org/10.1517/13543780903052764.
[16] Galgano M, Toshkezi G, Qiu X, Russell T, Chin L, Zhao L-R. Traumatic Brain Injury: Current Treatment Strategies and Future Endeavors. Cell Transplant 2017;26:1118–30. https://doi.org/10.1177/0963689717714102.
[17] Clarke D, Richardson P. Peripheral nerve injury. Curr Opin Neurol 1994;7:415–21. https://doi.org/10.1097/00019052-199410000-00009.
[18] Nau R, Sörgel F, Eiffert H. Penetration of drugs through the blood-cerebrospinal fluid/blood-brain barrier for treatment of central nervous system infections. Clin Microbiol Rev 2010;23:858–83. https://doi.org/10.1128/CMR.00007-10.
[19] Hersh DS, Wadajkar AS, Roberts N, Perez JG, Connolly NP, Frenkel V, et al. Evolving Drug Delivery Strategies to Overcome the Blood Brain Barrier. Curr Pharm Des 2016;22:1177–93. https://doi.org/10.2174/1381612822666151221150733.
[20] Caldarella A, Crocetti E, Paci E. Is the incidence of brain tumors really increasing? A population-based analysis from a cancer registry. J Neurooncol 2011;104:589–94. https://doi.org/10.1007/s11060-011-0533-5.
[21] Alifieris C, Trafalis DT. Glioblastoma multiforme: Pathogenesis and treatment. Pharmacology & Therapeutics 2015;152:63–82. https://doi.org/10.1016/j.pharmthera.2015.05.005.
[22] Louis DN, Perry A, Wesseling P, Brat DJ, Cree IA, Figarella-Branger D, et al. The 2021 WHO Classification of Tumors of the Central Nervous System: a summary. Neuro Oncol 2021;23:1231–51. https://doi.org/10.1093/neuonc/noab106.
[23] Bradshaw A, Wickremesekera A, Brasch HD, Chibnall AM, Davis PF, Tan ST, et al. Cancer Stem Cells in Glioblastoma Multiforme. Front Surg 2016;3. https://doi.org/10.3389/fsurg.2016.00048.
[24] Strobel H, Baisch T, Fitzel R, Schilberg K, Siegelin MD, Karpel-Massler G, et al. Temozolomide and Other Alkylating Agents in Glioblastoma Therapy. Biomedicines 2019;7. https://doi.org/10.3390/biomedicines7030069.
[25] Zhang J, Stevens MFG, Bradshaw TD. Temozolomide: mechanisms of action, repair and resistance. Curr Mol Pharmacol 2012;5:102–14. https://doi.org/10.2174/1874467211205010102.
[26] Wu W, Klockow JL, Zhang M, Lafortune F, Chang E, Jin L, et al. Glioblastoma multiforme (GBM): An overview of current therapies and mechanisms of resistance. Pharmacol Res 2021;171:105780. https://doi.org/10.1016/j.phrs.2021.105780.
[27] Binello E, Germano IM. Targeting glioma stem cells: A novel framework for brain tumors. Cancer Science 2011;102:1958–66. https://doi.org/10.1111/j.1349-7006.2011.02064.x.
[28] Ahmed SI, Javed G, Laghari AA, Bareeqa SB, Farrukh S, Zahid S, et al. CD133 Expression in Glioblastoma Multiforme: A Literature Review. Cureus 2018. https://doi.org/10.7759/cureus.3439.
[29] Wang D, Starr R, Chang W-C, Aguilar B, Alizadeh D, Wright SL, et al. Chlorotoxin-directed CAR T cells for specific and effective targeting of glioblastoma. Sci Transl Med 2020;12:eaaw2672. https://doi.org/10.1126/scitranslmed.aaw2672.
[30] Fisher JP, Adamson DC. Current FDA-Approved Therapies for High-Grade Malignant Gliomas. Biomedicines 2021;9:324. https://doi.org/10.3390/biomedicines9030324.
[31] Agrahari V. The exciting potential of nanotherapy in brain-tumor targeted drug delivery approaches. Neural Regen Res 2017;12:197–200. https://doi.org/10.4103/1673-5374.200796.
[32] Duskey JT, Rinaldi A, Ottonelli I, Caraffi R, De Benedictis CA, Sauer AK, et al. Glioblastoma Multiforme Selective Nanomedicines for Improved Anti-Cancer Treatments. Pharmaceutics 2022;14:1450. https://doi.org/10.3390/pharmaceutics14071450.

[33] Ashby LS, Smith KA, Stea B. Gliadel wafer implantation combined with standard radiotherapy and concurrent followed by adjuvant temozolomide for treatment of newly diagnosed high-grade glioma: a systematic literature review. World J Surg Onc 2016;14:225. https://doi.org/10.1186/s12957-016-0975-5.
[34] Dang W, Daviau T, Brem H. Morphological Characterization of Polyanhydride Biodegradable Implant Gliadel® During in Vitro and in Vivo Erosion Using Scanning Electron Microscopy. Pharm Res 1996;13:683–91. https://doi.org/10.1023/A:1016035229961.
[35] Perry J, Chambers A, Spithoff K, Laperriere N, on behalf of the Neuro-Oncology Disease Site Group§ of Cancer Care Ontario's Program in Evidence-Based Care. Gliadel Wafers in the Treatment of Malignant Glioma: A Systematic Review. Current Oncology 2007;14:189–94. https://doi.org/10.3747/co.2007.147.
[36] NISHIKAWA R, IWATA H, SAKATA Y, MURAMOTO K, MATSUOKA T. Safety of Gliadel Implant for Malignant Glioma: Report of Postmarketing Surveillance in Japan. Neurol Med Chir (Tokyo) 2021;61:536–48. https://doi.org/10.2176/nmc.oa.2021-0024.
[37] Salle F, Lahiani W, Spagnuolo E, Palfi S. Adverse Event with the Use of Carmustine Wafers and Postoperative Radiochemotherapy for the Treatment of High-grade Glioma. Asian J Neurosurg 2018;13:1171–4. https://doi.org/10.4103/ajns.AJNS_235_16.
[38] De Bonis P, Anile C, Pompucci A, Fiorentino A, Balducci M, Chiesa S, et al. Safety and efficacy of Gliadel wafers for newly diagnosed and recurrent glioblastoma. Acta Neurochirurgica 2012;154:1371–8. https://doi.org/10.1007/s00701-012-1413-2.
[39] Thomas KE, Stevens JA, Sarmiento K, Wald MM. Fall-related traumatic brain injury deaths and hospitalizations among older adults--United States, 2005. J Safety Res 2008;39:269–72. https://doi.org/10.1016/j.jsr.2008.05.001.
[40] Georges A, M Das J. Traumatic Brain Injury. StatPearls, Treasure Island (FL): StatPearls Publishing; 2022.
[41] Galgano M, Toshkezi G, Qiu X, Russell T, Chin L, Zhao L-R. Traumatic Brain Injury. Cell Transplant 2017;26:1118–30. https://doi.org/10.1177/0963689717714102.
[42] Margulies S, Hicks R, Combination Therapies for Traumatic Brain Injury Workshop Leaders. Combination therapies for traumatic brain injury: prospective considerations. J Neurotrauma 2009;26:925–39. https://doi.org/10.1089/neu.2008.0794.
[43] Hall ED, Vaishnav RA, Mustafa AG. Antioxidant therapies for traumatic brain injury. Neurotherapeutics 2010;7:51–61. https://doi.org/10.1016/j.nurt.2009.10.021.
[44] Boahene KDO, Lim M, Chu E, Quinones-Hinojosa A. Transpalpebral Orbitofrontal Craniotomy: A Minimally Invasive Approach to Anterior Cranial Vault Lesions. Skull Base 2010;20:237–44. https://doi.org/10.1055/s-0030-1249247.
[45] Clavreul A, Aubin G, Delion M, Lemée J-M, Minassian A, Menei P. What effects does awake craniotomy have on functional and survival outcomes for glioblastoma patients? Journal of Neuro-Oncology 2021;151. https://doi.org/10.1007/s11060-020-03666-7.
[46] Alastra G, Aloe L, Baldassarro VA, Calzà L, Cescatti M, Duskey JT, et al. Nerve Growth Factor Biodelivery: A Limiting Step in Moving Toward Extensive Clinical Application? Frontiers in Neuroscience 2021;15.
[47] Kochanek PM, Jackson TC, Ferguson NM, Carlson SW, Simon DW, Brockman EC, et al. Emerging therapies in traumatic brain injury. Semin Neurol 2015;35:83–100. https://doi.org/10.1055/s-0035-1544237.
[48] Arslantunali D, Dursun T, Yucel D, Hasirci N, Hasirci V. Peripheral nerve conduits: technology update. Med Devices (Auckl) 2014;7:405–24. https://doi.org/10.2147/MDER.S59124.
[49] Yoo J, Park JH, Kwon YW, Chung JJ, Choi IC, Nam JJ, et al. Augmented peripheral nerve regeneration through elastic nerve guidance conduits prepared using a porous PLCL membrane with a 3D printed collagen hydrogel. Biomater Sci 2020;8:6261–71. https://doi.org/10.1039/D0BM00847H.
[50] Dahlin LB, Wiberg M. Nerve injuries of the upper extremity and hand. EFORT Open Rev 2017;2:158–70. https://doi.org/10.1302/2058-5241.2.160071.
[51] Burnett MG, Zager EL. Pathophysiology of peripheral nerve injury: a brief review. Neurosurg Focus 2004;16:E1. https://doi.org/10.3171/foc.2004.16.5.2.
[52] Menorca RMG, Fussell TS, Elfar JC. Peripheral Nerve Trauma: Mechanisms of Injury and Recovery. Hand Clin 2013;29:317–30. https://doi.org/10.1016/j.hcl.2013.04.002.

[53] Barichello T, Collodel A, Hasbun R, Morales R. An Overview of the Blood-Brain Barrier. In: Barichello T, editor. Blood-Brain Barrier, vol. 142, New York, NY: Springer New York; 2019, p. 1–8. https://doi.org/10.1007/978-1-4939-8946-1_1.
[54] Daneman R, Prat A. The Blood–Brain Barrier. Cold Spring Harb Perspect Biol 2015;7:a020412. https://doi.org/10.1101/cshperspect.a020412.
[55] Rhea EM, Banks WA. Role of the Blood-Brain Barrier in Central Nervous System Insulin Resistance. Frontiers in Neuroscience 2019;13.
[56] Zlokovic BV. The blood-brain barrier in health and chronic neurodegenerative disorders. Neuron 2008;57:178–201. https://doi.org/10.1016/j.neuron.2008.01.003.
[57] Gabathuler R. Approaches to transport therapeutic drugs across the blood-brain barrier to treat brain diseases. Neurobiol Dis 2010;37:48–57. https://doi.org/10.1016/j.nbd.2009.07.028.
[58] Pardridge WM. Blood-brain barrier drug targeting: the future of brain drug development. Mol Interv 2003;3:90–105, 51. https://doi.org/10.1124/mi.3.2.90.
[59] Gong Q, Gao X, Liu W, Hong T, Chen C. Drug-Loaded Microbubbles Combined with Ultrasound for Thrombolysis and Malignant Tumor Therapy. Biomed Res Int 2019;2019:6792465. https://doi.org/10.1155/2019/6792465.
[60] Chen K-T, Wei K-C, Liu H-L. Focused Ultrasound Combined with Microbubbles in Central Nervous System Applications. Pharmaceutics 2021;13:1084. https://doi.org/10.3390/pharmaceutics13071084.
[61] Ren S, Si R, Sun P, Wu T, Dai A, Chen L, et al. Ultrasound combined with microbubbles enhances the renoprotective effects of methylprednisolone in rats with adriamycin-induced nephropathy. Eur J Pharm Sci 2021;159:105714. https://doi.org/10.1016/j.ejps.2021.105714.
[62] Crowe TP, Greenlee MHW, Kanthasamy AG, Hsu WH. Mechanism of intranasal drug delivery directly to the brain. Life Sci 2018;195:44–52. https://doi.org/10.1016/j.lfs.2017.12.025.
[63] Kiparissides C, Vasileiadou A, Karageorgos F, Serpetsi S. A Computational Systems Approach to Rational Design of Nose-to-Brain Delivery of Biopharmaceutics. Ind Eng Chem Res 2020;59:2548–65. https://doi.org/10.1021/acs.iecr.9b04885.
[64] Yuki Y, Uchida Y, Sawada S-I, Nakahashi-Ouchida R, Sugiura K, Mori H, et al. Characterization and Specification of a Trivalent Protein-Based Pneumococcal Vaccine Formulation Using an Adjuvant-Free Nanogel Nasal Delivery System. Mol Pharm 2021;18:1582–92. https://doi.org/10.1021/acs.molpharmaceut.0c01003.
[65] Khan A, Imam SS, Aqil M, Ahad A, Sultana Y, Ali A, et al. Brain Targeting of Temozolomide via the Intranasal Route Using Lipid-Based Nanoparticles: Brain Pharmacokinetic and Scintigraphic Analyses. Mol Pharmaceutics 2016;13:3773–82. https://doi.org/10.1021/acs.molpharmaceut.6b00586.
[66] Clementino AR, Pellegrini G, Banella S, Colombo G, Cantù L, Sonvico F, et al. Structure and Fate of Nanoparticles Designed for the Nasal Delivery of Poorly Soluble Drugs. Mol Pharmaceutics 2021;18:3132–46. https://doi.org/10.1021/acs.molpharmaceut.1c00366.
[67] Sayed S, Elsharkawy FM, Amin MM, Shamsel-Din HA, Ibrahim AB. Brain targeting efficiency of intranasal clozapine-loaded mixed micelles following radio labeling with Technetium-99m. Drug Delivery 2021;28:1524–38. https://doi.org/10.1080/10717544.2021.1951895.
[68] Najberg M, Haji Mansor M, Boury F, Alvarez-Lorenzo C, Garcion E. Reversing the Tumor Target: Establishment of a Tumor Trap. Front Pharmacol 2019;10. https://doi.org/10.3389/fphar.2019.00887.
[69] Atkinson AJ. Intracerebroventricular drug administration. Transl Clin Pharmacol 2017;25:117–24. https://doi.org/10.12793/tcp.2017.25.3.117.
[70] Shah N, Padalia D. Intrathecal Delivery System. StatPearls, Treasure Island (FL): StatPearls Publishing; 2022.
[71] Smith HS, Deer TR, Staats PS, Singh V, Sehgal N, Cordner H. Intrathecal drug delivery. Pain Physician 2008;11:S89–104.
[72] Bottros MM, Christo PJ. Current perspectives on intrathecal drug delivery. J Pain Res 2014;7:615–26. https://doi.org/10.2147/JPR.S37591.
[73] Fowler M, Cotter J, Knight B, Sevick-Muraca E, Sandberg D, Sirianni R. Intrathecal Drug Delivery in the Era of Nanomedicine. Adv Drug Deliv Rev 2020;165–166:77–95. https://doi.org/10.1016/j.addr.2020.02.006.

[74] Mehta AM, Sonabend AM, Bruce JN. Convection-Enhanced Delivery. Neurotherapeutics 2017;14:358–71. https://doi.org/10.1007/s13311-017-0520-4.
[75] Debinski W, Tatter SB. Convection-enhanced delivery for the treatment of brain tumors. Expert Rev Neurother 2009;9:1519–27. https://doi.org/10.1586/ern.09.99.
[76] Lonser RR, Sarntinoranont M, Morrison PF, Oldfield EH. Convection-enhanced delivery to the central nervous system. JNS 2015;122:697–706. https://doi.org/10.3171/2014.10.JNS14229.
[77] Vogelbaum MA, Iannotti CA. Chapter 23 - Convection-enhanced delivery of therapeutic agents into the brain. In: Aminoff MJ, Boller F, Swaab DF, editors. Handbook of Clinical Neurology, vol. 104, Elsevier; 2012, p. 355–62. https://doi.org/10.1016/B978-0-444-52138-5.00023-2.
[78] Hoffman AS. Hydrogels for biomedical applications. Advanced Drug Delivery Reviews 2012;64:18–23. https://doi.org/10.1016/j.addr.2012.09.010.
[79] Lu P, Ding B. Applications of electrospun fibers. Recent Pat Nanotechnol 2008;2:169–82. https://doi.org/10.2174/187221008786369688.
[80] Wang Y, Tan H, Hui X. Biomaterial Scaffolds in Regenerative Therapy of the Central Nervous System. BioMed Research International 2018;2018:1–19. https://doi.org/10.1155/2018/7848901.
[81] Fakhari A, Nugent S, Elvecrog J, Vasilakos J, Corcoran M, Tilahun A, et al. Thermosensitive Gel–Based Formulation for Intratumoral Delivery of Toll-Like Receptor 7/8 Dual Agonist, MEDI9197. Journal of Pharmaceutical Sciences 2017;106:2037–45. https://doi.org/10.1016/j.xphs.2017.04.041.
[82] Fan R, Cheng Y, Wang R, Zhang T, Zhang H, Li J, et al. Thermosensitive Hydrogels and Advances in Their Application in Disease Therapy. Polymers (Basel) 2022;14:2379. https://doi.org/10.3390/polym14122379.
[83] Chatterjee S, Hui PC, Kan C. Thermoresponsive Hydrogels and Their Biomedical Applications: Special Insight into Their Applications in Textile Based Transdermal Therapy. Polymers (Basel) 2018;10:480. https://doi.org/10.3390/polym10050480.
[84] Zhang K, Xue K, Loh XJ. Thermo-Responsive Hydrogels: From Recent Progress to Biomedical Applications. Gels 2021;7:77. https://doi.org/10.3390/gels7030077.
[85] Tian ML, Zhou JF, Qi X, Shen R. Thermo-sensitive hydrogel and their biomedical applications. IOP Conf Ser: Earth Environ Sci 2021;714:032062. https://doi.org/10.1088/1755-1315/714/3/032062.
[86] Gong C, Qi T, Wei X, Qu Y, Wu Q, Luo F, et al. Thermosensitive polymeric hydrogels as drug delivery systems. Curr Med Chem 2013;20:79–94.
[87] Mukerji R, Schaal J, Li X, Bhattacharyya J, Asai D, Zalutsky MR, et al. Spatiotemporally photoradiation-controlled intratumoral depot for combination of brachytherapy and photodynamic therapy for solid tumor. Biomaterials 2016;79:79–87. https://doi.org/10.1016/j.biomaterials.2015.11.064.
[88] Wei X, Senanayake TH, Warren G, Vinogradov SV. Hyaluronic acid-based nanogel-drug conjugates with enhanced anticancer activity designed for targeting of CD44-positive and drug-resistant tumors. Bioconjug Chem 2013;24:658–68. https://doi.org/10.1021/bc300632w.
[89] Cohen-Pfeffer JL, Gururangan S, Lester T, Lim DA, Shaywitz AJ, Westphal M, et al. Intracerebroventricular Delivery as a Safe, Long-Term Route of Drug Administration. Pediatric Neurology 2017;67:23–35. https://doi.org/10.1016/j.pediatrneurol.2016.10.022.
[90] Cook AM, Mieure KD, Owen RD, Pesaturo AB, Hatton J. Intracerebroventricular administration of drugs. Pharmacotherapy 2009;29:832–45. https://doi.org/10.1592/phco.29.7.832.
[91] Jandial R, editor. 14 - Supraorbital (Keyhole) Craniotomy With Optional Orbital Osteotomy. Core Techniques in Operative Neurosurgery (Second Edition), Philadelphia: Elsevier; 2020, p. 69–73. https://doi.org/10.1016/B978-0-323-52381-3.00014-9.
[92] Zubair A, De Jesus O. Ommaya Reservoir. StatPearls, Treasure Island (FL): StatPearls Publishing; 2022.
[93] Krishnaswamy VR, Benbenishty A, Blinder P, Sagi I. Demystifying the extracellular matrix and its proteolytic remodeling in the brain: structural and functional insights. Cell Mol Life Sci 2019;76:3229–48. https://doi.org/10.1007/s00018-019-03182-6.
[94] Ruoslahti E. Brain extracellular matrix. Glycobiology 1996;6:489–92. https://doi.org/10.1093/glycob/6.5.489.
[95] Reichardt LF, Tomaselli KJ. Extracellular Matrix Molecules and their Receptors: Functions in Neural Development. Annu Rev Neurosci 1991;14:531–70. https://doi.org/10.1146/annurev.ne.14.030191.002531.

[96] Yang R, Chen M, Yang X, Sun W, Lu C, Hui Q, et al. Modified poloxamer 407 and hyaluronic acid thermosensitive hydrogel-encapsulated keratinocyte growth factor 2 improves knee osteoarthritis in rats. Materials & Design 2021;210:110086. https://doi.org/10.1016/j.matdes.2021.110086.
[97] Liu X, Li W, Chen T, Yang Q, Huang T, Fu Y, et al. Hyaluronic Acid-Modified Micelles Encapsulating Gem-C12 and HNK for Glioblastoma Multiforme Chemotherapy. Mol Pharmaceutics 2018;15:1203–14. https://doi.org/10.1021/acs.molpharmaceut.7b01035.
[98] Wei Y-T, He Y, Xu C-L, Wang Y, Liu B-F, Wang X-M, et al. Hyaluronic acid hydrogel modified with nogo-66 receptor antibody and poly-L-lysine to promote axon regrowth after spinal cord injury. Journal of Biomedical Materials Research Part B: Applied Biomaterials 2010;95B:110–7. https://doi.org/10.1002/jbm.b.31689.
[99] Chen S, Li R, Li X, Xie J. Electrospinning: An enabling nanotechnology platform for drug delivery and regenerative medicine. Advanced Drug Delivery Reviews 2018;132:188–213. https://doi.org/10.1016/j.addr.2018.05.001.
[100] Charlet A, Bono F, Amstad E. Mechanical reinforcement of granular hydrogels. Chem Sci 2022;13:3082–93. https://doi.org/10.1039/D1SC06231J.
[101] Qazi TH, Burdick JA. Granular hydrogels for endogenous tissue repair. Biomaterials and Biosystems 2021;1:100008. https://doi.org/10.1016/j.bbiosy.2021.100008.
[102] Weltman A, Yoo J, Meng E. Flexible, Penetrating Brain Probes Enabled by Advances in Polymer Microfabrication. Micromachines 2016;7:180. https://doi.org/10.3390/mi7100180.
[103] Polacheck WJ, Zervantonakis IK, Kamm RD. Tumor cell migration in complex microenvironments. Cell Mol Life Sci 2013;70:1335–56. https://doi.org/10.1007/s00018-012-1115-1.
[104] Engler AJ, Sen S, Sweeney HL, Discher DE. Matrix elasticity directs stem cell lineage specification. Cell 2006;126:677–89. https://doi.org/10.1016/j.cell.2006.06.044.
[105] Brekken RA, Stupack D, editors. Extracellular Matrix in Tumor Biology. Springer International Publishing; 2017. https://doi.org/10.1007/978-3-319-60907-2.
[106] Bilston LE. Brain Tissue Mechanical Properties. In: Miller K, editor. Biomechanics of the Brain, New York, NY: Springer; 2011, p. 69–89. https://doi.org/10.1007/978-1-4419-9997-9_4.
[107] Miller K, Chinzei K. Mechanical properties of brain tissue in tension. Journal of Biomechanics 2002;35:483–90. https://doi.org/10.1016/S0021-9290(01)00234-2.
[108] Najberg M, Haji Mansor M, Taillé T, Bouré C, Molina-Peña R, Boury F, et al. Aerogel sponges of silk fibroin, hyaluronic acid and heparin for soft tissue engineering: Composition-properties relationship. Carbohydrate Polymers 2020;237:116107. https://doi.org/10.1016/j.carbpol.2020.116107.
[109] Jiang T, Carbone EJ, Lo KW-H, Laurencin CT. Electrospinning of polymer nanofibers for tissue regeneration. Progress in Polymer Science 2015;46:1–24. https://doi.org/10.1016/j.progpolymsci.2014.12.001.
[110] van Dommelen JAW, van der Sande TPJ, Hrapko M, Peters GWM. Mechanical properties of brain tissue by indentation: Interregional variation. Journal of the Mechanical Behavior of Biomedical Materials 2010;3:158–66. https://doi.org/10.1016/j.jmbbm.2009.09.001.
[111] Sundaresh SN, Finan JD, Elkin BS, Lee C, Xiao J, Morrison B. Viscoelastic characterization of porcine brain tissue mechanical properties under indentation loading. Brain Multiphysics 2021;2:100041. https://doi.org/10.1016/j.brain.2021.100041.
[112] Rashid B, Destrade M, Gilchrist MD. Mechanical characterization of brain tissue in compression at dynamic strain rates. Journal of the Mechanical Behavior of Biomedical Materials 2012;10:23–38. https://doi.org/10.1016/j.jmbbm.2012.01.022.
[113] Prange M, Meaney D, Margulies S. Defining brain mechanical properties: effects of region, direction, and species. Stapp Car Crash Journal 2000. https://doi.org/10.4271/2000-01-SC15.
[114] Parkins CC, McAbee JH, Ruff L, Wendler A, Mair R, Gilbertson RJ, et al. Mechanically matching the rheological properties of brain tissue for drug-delivery in human glioblastoma models. Biomaterials 2021;276:120919. https://doi.org/10.1016/j.biomaterials.2021.120919.
[115] Budday S, Nay R, de Rooij R, Steinmann P, Wyrobek T, Ovaert TC, et al. Mechanical properties of gray and white matter brain tissue by indentation. Journal of the Mechanical Behavior of Biomedical Materials 2015;46:318–30. https://doi.org/10.1016/j.jmbbm.2015.02.024.

[116] Chen J-WE, Pedron S, Shyu P, Hu Y, Sarkaria JN, Harley BAC. Influence of Hyaluronic Acid Transitions in Tumor Microenvironment on Glioblastoma Malignancy and Invasive Behavior. Front Mater 2018;5:39. https://doi.org/10.3389/fmats.2018.00039.
[117] Budday S, Ovaert TC, Holzapfel GA, Steinmann P, Kuhl E. Fifty Shades of Brain: A Review on the Mechanical Testing and Modeling of Brain Tissue. Arch Computat Methods Eng 2020;27:1187–230. https://doi.org/10.1007/s11831-019-09352-w.
[118] Chatelin S, Constantinesco A, Willinger R. Fifty years of brain tissue mechanical testing: from in vitro to in vivo investigations. Biorheology 2010;47:255–76. https://doi.org/10.3233/BIR-2010-0576.
[119] Hoare TR, Kohane DS. Hydrogels in drug delivery: Progress and challenges. Polymer 2008;49:1993–2007. https://doi.org/10.1016/j.polymer.2008.01.027.
[120] Hsu S-H, Leu Y-L, Hu J-W, Fang J-Y. Physicochemical Characterization and Drug Release of Thermosensitive Hydrogels Composed of a Hyaluronic Acid/Pluronic F127 Graft. Chemical & Pharmaceutical Bulletin 2009;57:453–8. https://doi.org/10.1248/cpb.57.453.
[121] Russo E, Villa C. Poloxamer Hydrogels for Biomedical Applications. Pharmaceutics 2019;11. https://doi.org/10.3390/pharmaceutics11120671.
[122] Dumortier G, Grossiord JL, Agnely F, Chaumeil JC. A Review of Poloxamer 407 Pharmaceutical and Pharmacological Characteristics. Pharm Res 2006;23:2709–28. https://doi.org/10.1007/s11095-006-9104-4.
[123] Zarrintaj P, Ramsey JD, Samadi A, Atoufi Z, Yazdi MK, Ganjali MR, et al. Poloxamer: A versatile tri-block copolymer for biomedical applications. Acta Biomaterialia 2020;110:37–67. https://doi.org/10.1016/j.actbio.2020.04.028.
[124] Dimer F, Pereira G, Guterres S, Cardozo N, Kechinski C, Granada J. Formulation and characterization of poloxamer 407®: Thermoreversible gel containing polymeric microparticles and hyaluronic acid. Química Nova 2013;36:1121–5. https://doi.org/10.1590/S0100-40422013000800008.
[125] Gioffredi E, Boffito M, Calzone S, Giannitelli SM, Rainer A, Trombetta M, et al. Pluronic F127 Hydrogel Characterization and Biofabrication in Cellularized Constructs for Tissue Engineering Applications. Procedia CIRP 2016;49:125–32. https://doi.org/10.1016/j.procir.2015.11.001.
[126] Akkari ACS, Papini JZB, Garcia GK, Franco MKKD, Cavalcanti LP, Gasperini A, et al. Poloxamer 407/188 binary thermosensitive hydrogels as delivery systems for infiltrative local anesthesia: Physico-chemical characterization and pharmacological evaluation. Materials Science and Engineering: C 2016;68:299–307. https://doi.org/10.1016/j.msec.2016.05.088.
[127] Hsieh H-Y, Lin W-Y, Lee A, Li Y-C, Chen Y-J, Chen K-C, et al. Hyaluronic acid on the urokinase sustained release with a hydrogel system composed of poloxamer 407: HA/P407 hydrogel system for drug delivery. PLOS ONE 2020;15:e0227784. https://doi.org/10.1371/journal.pone.0227784.
[128] Li X, Li A, Feng F, Jiang Q, Sun H, Chai Y, et al. Effect of the hyaluronic acid-poloxamer hydrogel on skin-wound healing: in vitro and in vivo studies. Animal Models and Experimental Medicine 2019;2:107–13. https://doi.org/10.1002/ame2.12067.
[129] Mayol L, Quaglia F, Borzacchiello A, Ambrosio L, La Rotonda MI. A novel poloxamers/hyaluronic acid in situ forming hydrogel for drug delivery: rheological, mucoadhesive and in vitro release properties. Eur J Pharm Biopharm 2008;70:199–206. https://doi.org/10.1016/j.ejpb.2008.04.025.
[130] Giuliano E, Paolino D, Cristiano M, Fresta M, Cosco D. Rutin-Loaded Poloxamer 407-Based Hydrogels for In Situ Administration: Stability Profiles and Rheological Properties. Nanomaterials 2020;10:1069. https://doi.org/10.3390/nano10061069.
[131] Jung Y, Park W, Park H, Lee D-K, Na K. Thermo-sensitive injectable hydrogel based on the physical mixing of hyaluronic acid and Pluronic F-127 for sustained NSAID delivery. Carbohydrate Polymers 2017;156:403–8. https://doi.org/10.1016/j.carbpol.2016.08.068.
[132] Alonso JM, Andrade del Olmo J, Perez Gonzalez R, Saez-Martinez V. Injectable Hydrogels: From Laboratory to Industrialization. Polymers (Basel) 2021;13:650. https://doi.org/10.3390/polym13040650.
[133] Lin Y-C, Tan F, Marra KG, Jan S-S, Liu D-C. Synthesis and characterization of collagen/hyaluronan/chitosan composite sponges for potential biomedical applications. Acta Biomaterialia 2009;5:2591–600. https://doi.org/10.1016/j.actbio.2009.03.038.
[134] Bucatariu S-M, Constantin M, Varganici C-D, Rusu D, Nicolescu A, Prisacaru I, et al. A new sponge-type hydrogel based on hyaluronic acid and poly(methylvinylether-alt-maleic acid) as a 3D platform for tumor

cell growth. International Journal of Biological Macromolecules 2020;165:2528–40. https://doi.org/10.1016/j.ijbiomac.2020.10.095.
[135] Chan BP, Leong KW. Scaffolding in tissue engineering: general approaches and tissue-specific considerations. Eur Spine J 2008;17:467–79. https://doi.org/10.1007/s00586-008-0745-3.
[136] El-Sherbiny IM, Yacoub MH. Hydrogel scaffolds for tissue engineering: Progress and challenges. Glob Cardiol Sci Pract 2013;2013:316–42. https://doi.org/10.5339/gcsp.2013.38.
[137] Entekhabi E, Haghbin Nazarpak M, Shafieian M, Mohammadi H, Firouzi M, Hassannejad Z. Fabrication and in vitro evaluation of 3D composite scaffold based on collagen/hyaluronic acid sponge and electrospun polycaprolactone nanofibers for peripheral nerve regeneration. Journal of Biomedical Materials Research Part A 2021;109:300–12. https://doi.org/10.1002/jbm.a.37023.
[138] Entcheva E, Bien H, Yin L, Chung C-Y, Farrell M, Kostov Y. Functional cardiac cell constructs on cellulose-based scaffolding. Biomaterials 2004;25:5753–62. https://doi.org/10.1016/j.biomaterials.2004.01.024.
[139] Chen C-H, Chen S-H, Mao S-H, Tsai M-J, Chou P-Y, Liao C-H, et al. Injectable thermosensitive hydrogel containing hyaluronic acid and chitosan as a barrier for prevention of postoperative peritoneal adhesion. Carbohydrate Polymers 2017;173. https://doi.org/10.1016/j.carbpol.2017.06.019.
[140] Erickson AE, Levengood SKL, Sun J, Chang F-C, Zhang M. Fabrication and Characterization of Chitosan–Hyaluronic Acid Scaffolds with Varying Stiffness for Glioblastoma Cell Culture. Advanced Healthcare Materials 2018;7:1800295. https://doi.org/10.1002/adhm.201800295.
[141] Wang K, Kievit FM, Erickson AE, Silber JR, Ellenbogen RG, Zhang M. Culture on 3D Chitosan-Hyaluronic Acid Scaffolds Enhances Stem Cell Marker Expression and Drug Resistance in Human Glioblastoma Cancer Stem Cells. Advanced Healthcare Materials 2016;5:3173–81. https://doi.org/10.1002/adhm.201600684.
[142] Xu H, Zhang L, Bao Y, Yan X, Yin Y, Li Y, et al. Preparation and characterization of injectable chitosan–hyaluronic acid hydrogels for nerve growth factor sustained release. Journal of Bioactive and Compatible Polymers 2017;32:146–62. https://doi.org/10.1177/0883911516662068.
[143] Zhang H, Wei YT, Tsang KS, Sun CR, Li J, Huang H, et al. Implantation of neural stem cells embedded in hyaluronic acid and collagen composite conduit promotes regeneration in a rabbit facial nerve injury model. J Transl Med 2008;6:67. https://doi.org/10.1186/1479-5876-6-67.
[144] Rao SS, Dejesus J, Short AR, Otero JJ, Sarkar A, Winter JO. Glioblastoma behaviors in three-dimensional collagen-hyaluronan composite hydrogels. ACS Appl Mater Interfaces 2013;5:9276–84. https://doi.org/10.1021/am402097j.
[145] Abdi SIH, Choi JY, Lee JS, Lim HJ, Lee C, Kim J, et al. In Vivo study of a blended hydrogel composed of pluronic F-127-alginate-hyaluronic acid for its cell injection application. Tissue Eng Regen Med 2012;9:1–9. https://doi.org/10.1007/s13770-012-0001-0.
[146] Bucatariu S-M, Constantin M, Varganici C-D, Rusu D, Nicolescu A, Prisacaru I, et al. A new sponge-type hydrogel based on hyaluronic acid and poly(methylvinylether-alt-maleic acid) as a 3D platform for tumor cell growth. International Journal of Biological Macromolecules 2020. https://doi.org/10.1016/j.ijbiomac.2020.10.095.
[147] Xue J, He M, Liu H, Niu Y, Crawford A, Coates PD, et al. Drug loaded homogeneous electrospun PCL/gelatin hybrid nanofiber structures for anti-infective tissue regeneration membranes. Biomaterials 2014;35:9395–405. https://doi.org/10.1016/j.biomaterials.2014.07.060.
[148] Unal S, Arslan S, Yilmaz BK, Oktar FN, Ficai D, Ficai A, et al. Polycaprolactone/Gelatin/Hyaluronic Acid Electrospun Scaffolds to Mimic Glioblastoma Extracellular Matrix. Materials 2020;13:2661. https://doi.org/10.3390/ma13112661.
[149] Yan X, Wang J, He Q, Xu H, Tao J, Koral K, et al. PDLLA/β-TCP/HA/CHS/NGF Sustained-release Conduits for Peripheral Nerve Regeneration. J Wuhan Univ Technol Mater Sci Ed 2021;36:600–6. https://doi.org/10.1007/s11595-021-2450-6.
[150] Wang C, Tong X, Yang F. Bioengineered 3D Brain Tumor Model To Elucidate the Effects of Matrix Stiffness on Glioblastoma Cell Behavior Using PEG-Based Hydrogels. Mol Pharmaceutics 2014;11:2115–25. https://doi.org/10.1021/mp5000828.

[151] Nayak A, Olatunji O, Bhusan Das D, Vladisavljević G. Pharmaceutical Applications of Natural Polymers. In: Olatunji O, editor. Natural Polymers: Industry Techniques and Applications, Cham: Springer International Publishing; 2016, p. 263–313. https://doi.org/10.1007/978-3-319-26414-1_9.
[152] Chen MH, Wang LL, Chung JJ, Kim Y-H, Atluri P, Burdick JA. Methods To Assess Shear-Thinning Hydrogels for Application As Injectable Biomaterials 2017:15.
[153] Xu H, Yu Y, Zhang L, Zheng F, Yin Y, Gao Y, et al. Sustainable release of nerve growth factor for peripheral nerve regeneration using nerve conduits laden with Bioconjugated hyaluronic acid-chitosan hydrogel. Composites Part B: Engineering 2022;230:109509. https://doi.org/10.1016/j.compositesb.2021.109509.
[154] Ma L, Li Y, Wu Y, Yu M, Aazmi A, Gao L, et al. 3D bioprinted hyaluronic acid-based cell-laden scaffold for brain microenvironment simulation. Bio-Design and Manufacturing 2020;3. https://doi.org/10.1007/s42242-020-00076-6.
[155] Rivet CJ, Zhou K, Gilbert RJ, Finkelstein DI, Forsythe JS. Cell infiltration into a 3D electrospun fiber and hydrogel hybrid scaffold implanted in the brain. Biomatter 2015;5:e1005527. https://doi.org/10.1080/21592535.2015.1005527.
[156] Eswarappa V, Bhatia SK. Biomaterial and Therapeutic Applications. Naturally Based Biomaterials and Therapeutics 2012:27–79. https://doi.org/10.1007/978-1-4614-5386-4_3.
[157] Bhat S, Kumar A. Biomaterials and bioengineering tomorrow's healthcare. Biomatter 2013;3:e24717. https://doi.org/10.4161/biom.24717.
[158] Lee EJ, Kasper FK, Mikos AG. Biomaterials for Tissue Engineering. Ann Biomed Eng 2014;42:323–37. https://doi.org/10.1007/s10439-013-0859-6.
[159] Nune SK, Rama KS, Dirisala VR, Chavali MY. Chapter 11 - Electrospinning of collagen nanofiber scaffolds for tissue repair and regeneration. In: Ficai D, Grumezescu AM, editors. Nanostructures for Novel Therapy, Elsevier; 2017, p. 281–311. https://doi.org/10.1016/B978-0-323-46142-9.00011-6.
[160] Nune SK, Rama KS, Dirisala VR, Chavali MY. Electrospinning of collagen nanofiber scaffolds for tissue repair and regeneration. Nanostructures for Novel Therapy, Elsevier; 2017, p. 281–311. https://doi.org/10.1016/B978-0-323-46142-9.00011-6.
[161] Chen X, Guo X, Hao S, Yang T, Wang J. Iron oxide nanoparticles-loaded hyaluronic acid nanogels for MRI-aided Alzheimer's disease theranostics. Arabian Journal of Chemistry 2022;15:103748. https://doi.org/10.1016/j.arabjc.2022.103748.
[162] Grimaudo MA, Concheiro A, Alvarez-Lorenzo C. Nanogels for regenerative medicine. Journal of Controlled Release 2019;313:148–60. https://doi.org/10.1016/j.jconrel.2019.09.015.
[163] Soni KS, Desale SS, Bronich TK. Nanogels: an overview of properties, biomedical applications and obstacles to clinical translation. J Control Release 2016;240:109–26. https://doi.org/10.1016/j.jconrel.2015.11.009.
[164] Zhang M, Asghar S, Tian C, Hu Z, Ping Q, Chen Z, et al. Lactoferrin/phenylboronic acid-functionalized hyaluronic acid nanogels loading doxorubicin hydrochloride for targeting glioma. Carbohydrate Polymers 2021;253:117194. https://doi.org/10.1016/j.carbpol.2020.117194.
[165] Yucel D, Kose GT, Hasirci V. Polyester based nerve guidance conduit design. Biomaterials 2010;31:1596–603. https://doi.org/10.1016/j.biomaterials.2009.11.013.
[166] Barbarisi M, Iaffaioli RV, Armenia E, Schiavo L, De Sena G, Tafuto S, et al. Novel nanohydrogel of hyaluronic acid loaded with quercetin alone and in combination with temozolomide as new therapeutic tool, CD44 targeted based, of glioblastoma multiforme. Journal of Cellular Physiology 2018;233:6550–64. https://doi.org/10.1002/jcp.26238.
[167] Rowland MJ, Parkins CC, McAbee JH, Kolb AK, Hein R, Loh XJ, et al. An adherent tissue-inspired hydrogel delivery vehicle utilised in primary human glioma models. Biomaterials 2018;179:199–208. https://doi.org/10.1016/j.biomaterials.2018.05.054.
[168] Malfanti A, Catania G, Degros Q, Wang M, Bausart M, Préat V. Design of Bio-Responsive Hyaluronic Acid–Doxorubicin Conjugates for the Local Treatment of Glioblastoma. Pharmaceutics 2022;14:124. https://doi.org/10.3390/pharmaceutics14010124.
[169] Velasco-Rodriguez B, Diaz-Vidal T, Rosales-Rivera LC, García-González CA, Alvarez-Lorenzo C, Al-Modlej A, et al. Hybrid Methacrylated Gelatin and Hyaluronic Acid Hydrogel Scaffolds. Preparation and Systematic Characterization for Prospective Tissue Engineering Applications. International Journal of Molecular Sciences 2021;22:6758. https://doi.org/10.3390/ijms22136758.

[170] Kasapidou PM, de Montullé EL, Dembélé K-P, Mutel A, Desrues L, Gubala V, et al. Hyaluronic acid-based hydrogels loaded with chemoattractant and anticancer drug – new formulation for attracting and tackling glioma cells. Soft Matter 2021;17:10846–61. https://doi.org/10.1039/D1SM01003D.
[171] Rezazadeh M, Akbari V, Amuaghae E, Emami J. Preparation and characterization of an injectable thermosensitive hydrogel for simultaneous delivery of paclitaxel and doxorubicin. Res Pharm Sci 2018;13:181–91. https://doi.org/10.4103/1735-5362.228918.
[172] Xiao W, Ehsanipour A, Sohrabi A, Seidlits SK. Hyaluronic-Acid Based Hydrogels for 3-Dimensional Culture of Patient- Derived Glioblastoma Cells. Journal of Visualized Experiments 2018:9.
[173] Heffernan JM, Overstreet DJ, Le LD, Vernon BL, Sirianni RW. Bioengineered Scaffolds for 3D Analysis of Glioblastoma Proliferation and Invasion. Ann Biomed Eng 2015;43:1965–77. https://doi.org/10.1007/s10439-014-1223-1.
[174] Unal S, Arslan S, Yilmaz BK, Oktar FN, Sengil AZ, Gunduz O. Production and characterization of bacterial cellulose scaffold and its modification with hyaluronic acid and gelatin for glioblastoma cell culture. Cellulose 2021;28:117–32. https://doi.org/10.1007/s10570-020-03528-5.
[175] Pedron S, Becka E, Harley BAC. Regulation of glioma cell phenotype in 3D matrices by hyaluronic acid. Biomaterials 2013;34:7408–17. https://doi.org/10.1016/j.biomaterials.2013.06.024.
[176] Hart MG, Garside R, Rogers G, Somerville M, Stein K, Grant R. Chemotherapy wafers for high grade glioma. Cochrane Database of Systematic Reviews 2011. https://doi.org/10.1002/14651858.CD007294.pub2.
[177] Molina-Peña R, Haji Mansor M, Najberg M, Thomassin J-M, Gueza B, Alvarez-Lorenzo C, et al. Nanoparticle-containing electrospun nanofibrous scaffolds for sustained release of SDF-1α. International Journal of Pharmaceutics 2021;610:121205. https://doi.org/10.1016/j.ijpharm.2021.121205.
[178] Tian W m., Hou S p., Ma J, Zhang C l., Xu Q y., Lee I s., et al. Hyaluronic Acid–Poly-D-Lysine-Based Three-Dimensional Hydrogel for Traumatic Brain Injury. Tissue Engineering 2005;11:513–25. https://doi.org/10.1089/ten.2005.11.513.
[179] Cui FZ, Tian WM, Hou SP, Xu QY, Lee I-S. Hyaluronic acid hydrogel immobilized with RGD peptides for brain tissue engineering. J Mater Sci: Mater Med 2006;17:1393–401. https://doi.org/10.1007/s10856-006-0615-7.
[180] Wei YT, Tian WM, Yu X, Cui FZ, Hou SP, Xu QY, et al. Hyaluronic acid hydrogels with IKVAV peptides for tissue repair and axonal regeneration in an injured rat brain. Biomed Mater 2007;2:S142–6. https://doi.org/10.1088/1748-6041/2/3/S11.
[181] Tam RY, Cooke MJ, Shoichet MS. A covalently modified hydrogel blend of hyaluronan–methyl cellulose with peptides and growth factors influences neural stem/progenitor cell fate. J Mater Chem 2012;22:19402. https://doi.org/10.1039/c2jm33680d.
[182] Wang Y, Wei YT, Zu ZH, Ju RK, Guo MY, Wang XM, et al. Combination of Hyaluronic Acid Hydrogel Scaffold and PLGA Microspheres for Supporting Survival of Neural Stem Cells. Pharm Res 2011;28:1406–14. https://doi.org/10.1007/s11095-011-0452-3.
[183] Addington CP, Dharmawaj S, Heffernan JM, Sirianni RW, Stabenfeldt SE. Hyaluronic acid-laminin hydrogels increase neural stem cell transplant retention and migratory response to SDF-1α. Matrix Biology 2017;60–61:206–16. https://doi.org/10.1016/j.matbio.2016.09.007.
[184] Guo W, Douma L, Hu MH, Eglin D, Alini M, Šećerović A, et al. Hyaluronic acid-based interpenetrating network hydrogel as a cell carrier for nucleus pulposus repair. Carbohydrate Polymers 2022;277:118828. https://doi.org/10.1016/j.carbpol.2021.118828.
[185] Wang T-W, Spector M. Development of hyaluronic acid-based scaffolds for brain tissue engineering. Acta Biomaterialia 2009;5:2371–84. https://doi.org/10.1016/j.actbio.2009.03.033.
[186] McMurtrey RJ. Patterned and functionalized nanofiber scaffolds in three-dimensional hydrogel constructs enhance neurite outgrowth and directional control. J Neural Eng 2014;11:066009. https://doi.org/10.1088/1741-2560/11/6/066009.
[187] Sakai Y, Matsuyama Y, Takahashi K, Sato T, Hattori T, Nakashima S, et al. New artificial nerve conduits made with photocrosslinked hyaluronic acid for peripheral nerve regeneration. Biomed Mater Eng 2007;17:191–7.

[188] Sequeira JAD, Santos AC, Serra J, Veiga F, Ribeiro AJ. Chapter 10 - Poly(lactic-co-glycolic acid) (PLGA) matrix implants. In: Grumezescu AM, editor. Nanostructures for the Engineering of Cells, Tissues and Organs, William Andrew Publishing; 2018, p. 375–402. https://doi.org/10.1016/B978-0-12-813665-2.00010-7.
[189] Wang S, Guan S, Zhu Z, Li W, Liu T, Ma X. Hyaluronic acid doped-poly(3,4-ethylenedioxythiophene)/chitosan/gelatin (PEDOT-HA/Cs/Gel) porous conductive scaffold for nerve regeneration. Materials Science and Engineering: C 2017;71:308–16. https://doi.org/10.1016/j.msec.2016.10.029.
[190] Gisbert Roca F, Lozano Picazo P, Pérez-Rigueiro J, Guinea Tortuero GV, Monleón Pradas M, Martínez-Ramos C. Conduits based on the combination of hyaluronic acid and silk fibroin: Characterization, in vitro studies and in vivo biocompatibility. Int J Biol Macromol 2020;148:378–90. https://doi.org/10.1016/j.ijbiomac.2020.01.149.
[191] Xu H, Zhang L, Bao Y, Yan X, Yin Y, Li Y, et al. Preparation and characterization of injectable chitosan-hyaluronic acid hydrogels for nerve growth factor sustained release. Journal of Bioactive and Compatible Polymers 2016;32. https://doi.org/10.1177/0883911516662068.
[192] Li R, Liu H, Huang H, Bi W, Yan R, Tan X, et al. Chitosan conduit combined with hyaluronic acid prevent sciatic nerve scar in a rat model of peripheral nerve crush injury. Mol Med Rep 2018;17:4360–8. https://doi.org/10.3892/mmr.2018.8388.
[193] Brandt KD, Block JA, Michalski JP, Moreland LW, Caldwell JR, Lavin PT. Efficacy and safety of intraarticular sodium hyaluronate in knee osteoarthritis. ORTHOVISC Study Group. Clin Orthop Relat Res 2001:130–43. https://doi.org/10.1097/00003086-200104000-00021.
[194] Neustadt D, Caldwell J, Bell M, Wade J, Gimbel J. Clinical effects of intraarticular injection of high molecular weight hyaluronan (Orthovisc) in osteoarthritis of the knee: a randomized, controlled, multicenter trial. J Rheumatol 2005;32:1928–36.
[195] DePuy Mitek. A Comparison of Orthovisc® to Corticosteroid Injection in Shoulder Osteoarthritis: Orthovisc Randomized Clinical Trial. clinicaltrials.gov; 2017.
[196] Migliore A, Massafra U, Frediani B, Bizzi E, Sinelnikov Yzchaki E, Gigliucci G, et al. HyalOne® in the treatment of symptomatic hip OA - data from the ANTIAGE register: seven years of observation. Eur Rev Med Pharmacol Sci 2017;21:1635–44.
[197] Medipost Co Ltd. Evaluation of Safety and Exploratory Efficacy of CARTISTEM®, a Cell Therapy Product for Articular Cartilage Defects: A Phase I/IIa Clinical Trial in Patients With Focal, Full-thickness Grade 3-4 Articular Cartilage Defects of the Knee. clinicaltrials.gov; 2021.
[198] Anika Therapeutics, Inc. A Prospective, Randomized, Active Treatment-controlled, Evaluator-blinded Multicenter Study to Establish the Superiority of Hyalofast® With BMAC in the Treatment of Articular Knee Cartilage Defect Lesions in Comparison to Control. clinicaltrials.gov; 2022.

List of abbreviations:

BBB Blood Brain Barrier
BC Bacterial cellulose
BCNU Carmustin or β-chloro-nitrosourea
BDNF Brain-Derived Neurotrophic Factor
CB Cucurbit[n]uril
CED Convection Enhanced Diffusion
CNS Central Nervous System
CS Chitosan
CXCR4 C-X-C Motif Chemokine Receptor 4
DOX Doxorubicin
ECM Extra Cellular Matrix
ELP Elastin-like polypeptide
FDA Food and Drug Administration
FU focused ultrasound
GAG Glycosaminoglycan

GB Glioblastoma
GEL Gelatin
GRAS Generally Recognized As Safe
HA Hyaluronic Acid
LCGT lower critical gelation temperature
MC Methylcellulose
MRI Magnetic Resonance Imaging
NGCs Nerve guide channels
NGF Nerve Growth Factor
NSCs Neural Stem Cells
OLG Oligodendrocyte
P407 Poloxamer 407
PCL Polycaprolactone
PDLLA Poly-d,l-lactic acid
PEG Polyethylene glycol
PEOx polyethylene oxide
PG Propylene glycol
PNNs Perineuronal nets
PNS Peripheral Nervous System
PPO Poly Propylene Oxide
PXL Paclitaxel
ROS Reactive Oxygen Species
SDF-1α *Stromal cell-derived factor 1*
TMZ Temozolomide
UCGT Upper critical gelation temperature
VEGF Vascular Endothelial Growth Factor

Supplementary data :

Table 2: Devices development for Glioblastoma application

Table 3: Systems developed for CNS injuries application

Table 4: Systems developed for PNS injuries applications

Table 2. Devices development for Glioblastoma application

Device	Matrix composition	Proposed mechanism	Study model *(In vitro, in vivo, ex vivo)*	Major Findings	Reference
Hydrogel system	HA-functionalized Methacrylate gelatin/poly(ethylene glycol) (PEG)4A	Mimic the microenvironment matrix for GBM cells	2-3D cultures, patient-derived GBM cells	HA-dose-dependent alterations in GBM malignancy-associated markers. HA can lead to a specific interaction in EGFR+ cells via CD44.	[Pedron et al., 2013] 10.1016/j.biomaterials.2013.06.024
Composite hydrogel	Collagen-Hyaluronan	Mimic the microenvironment matrix for GBM cells	3D culture, patient-derived GBM cells	Cell morphology, spreading and migration were influenced by collagen type and HA concentration.	[Rao et al., 2013] 10.1021/am402097j
Hydrogels	HA-Gelatin thiol-reactive PEG diacrylate (PEGDA)/PEG divinyl sulfone (PEGDVS) crosslinked	Mimic the microenvironment matrix for GBM cells and develop a better analytical analysis *in vitro*	Single-cells, 3D culture, U118, U87R cell lines	Potential to identify differences in the invasive behaviour of the cell and analyse the cellular response to biophysical signals in the extracellular environment.	[Heffernan et al., 2014] 10.1007/s10439-014-1223-1
Composite scaffold	Chitosan-HA scaffold	Mimic the microenvironment matrix for GBM cells	Single-cells, 2D culture, GSC GBM6 cell lines	Better cellular morphology, growth patterns, and malignant behaviour than adherent monolayers.	[Wang et al., 2016] 10.1002/adhm.201600684
Micelles	HA-Modified Micelles lauroyl-gemcitabine (Gem-C12) and honokiol (HNK) encapsulated	Nanocarriers for targeting drug delivery of combined chemotherapeutics	Single-cells, 3D culture, U87 cell line Subcutaneous glioma-bearing mice; orthotopic xenograft GBM	Deep penetration into spheroids, endocytosis mediated by the CD44 receptor, and increased cytotoxicity of the combined treatment. Enhanced animal survival rate.	[Liu et al., 2018] 10.1021/acs.molpharmaceut.7b01035

Thermosensitive hydrogel	Doxorubicin/paclitaxel embedded Pluronic F127/HA hydrogel system (freeze-dried micelles)	Intratumoral administration of combined chemotherapy	Degradation rate, drug release Injection force determination, Chicken meat model	Controlled release of both chemotherapeutics and great stability. The formulation also showed easy injectability.	[Rezazadeh et al., 2018] 10.4103/1735-5362.228918
Hydrogel	HA/ poly(ethylene glycol) (PEG)	Mimic the microenvironment matrix for GBM cells	3D culture, patient-derived GBM cells	Cell viability and proliferation rates are as good as or better than standard glioma spheres culture. Compatible results for use in molecular and cellular analyses.	[Xiao et al., 2018] 10.3791/58176
Aerogel sponge	Stromal cell derived factor-1α loaded in Silk fibroin-HA-Heparin	Chemoattractant loaded scaffold trap for brain tumor cells	Single-cells, NIH3T3 cell line	Cytocompatible material with adequate mean pore diameter (60 μm) and connectivity for welcoming cells. Texture similar to brain tissue (6–13 kPa Young's Modulus), slower biodegradation and 93% retention of SDF-1α.	[Najberg et al., 2019] 10.1016/j.carbpol.2020.116107
Nanofibers scaffold	Polycaprolactone (PCL) /gelatin (Gel) / hyaluronic acid (HA)	Mimic GBM extracellular matrix	Single-cells, U251 cell line	The topography and surface chemistry (hydrophilic) played an important role in the biomechanical , proliferative, and morphological properties of the cells.	[Unal et al., 2020] 10.3390/ma13112661
Drug loaded Hydrogel	Crosslinked-HA-adipic acid dihydrazide (ADH) loaded with human urotensin (hUII) peptide and doxorubicin (DOX) or temozolomide (TMZ)	Chemoattractant matrix to trap and eradicate GBM cells	Single-cells, U87MG cell line	Cell migration and invasion into the hydrogel in response to the hUII. Significant cytotoxicity of DOX-loaded hydrogels for U87MG cells.	[Kasapidou et al., 2021] 10.1039/d1sm01003d
Drug-loaded hydrogel	Peptide functionalized HA (HACF) cross-linked by cucurbit[8]uril (CB[8])	Drug delivery reservoir for resection cavity	Single-cells, patient-derived GBM cells	Biocompatible, adaptable, and adjustable to local tissue stiffness. 45% improvement in patient survival.	[Parkins et al., 2021] 10.1016/j.biomaterials.2021.120919

			Patient-derived xenograft (PDX) rats		
Hydrogel	Methacryloyl-modified HA (HAMA)	Tissue engineering application	-	Suitable structure, porosity, and stiffness for tissue engineering purposes. Also, it showed to be resistant to collagenase biodegradation.	[Velasco-Rodriguez et al., 2021] 10.3390/ijms22136758
Composite scaffold	HA/gelatin (Gel) modified bacterial cellulose (BC)	Mimic GBM extracellular matrix	3D culture, U251 cell line	Good cell vitality, forming multi-layers and cell clusters in the scaffolds.	[Unal et al., 2021] 10.1007/s10570-020-03528-5
Drug loaded Nanogel	Lactoferrin (Lf)/phenylboronic acid (PBA)-functionalized HA nanogels crosslinked with disulfide-bond and doxorubicin hydrochloride (DOX)-loaded	Drug delivery and dual-targeting GBM	Single-cells and coculture, G422, bEnd.3 cell lines SD rats - pharmacokinetics, ICR mice - biodistribution	Controlled release of the drug, effective BBB penetration, and precise glioma dual-targeting (PBA and HA), presenting strong cytotoxicity against G422 cells.	[Zhang et al., 2021] 10.1016/j.cjche.2021.08.029
Polymer-drug conjugate	HA-Hydrazone-DOX	GBM local treatment	2-3D culture GL261, U87MG, B16F10 cell lines GL261-bearing mice	Increased tumor cell mortality and inhibition of the tumor growth. Bio-responsive linker was crucial for the observed bioperformance.	[Malfanti et al., 2022] 10.3390/pharmaceutics14010124

Table 3. Systems developed for CNS injuries application

Device	Matrix composition	Proposed mechanism	Porosity connectivity diameter	Mechanical properties	Study model *(In vitro, in vivo, ex vivo)*	Major Findings	Reference
Hydrogel	HA –PDL hydrogel	Scaffold material for the repair of defects brain tissue	Good connectivity and adherence	-	• Human DRG cell line and NSCs • 3 months old Sprague Dawley rats	After implantation, the polymer hydrogel rightly bridged the tissue defect, establishing a permissive interface with the host tissue to aid cell ingrowth and angiogenesis.	[Tian et al.2005] 10.1089/ten.2005.11.513
Hydrogel	HA-arginine-glycine-aspartic acid (RGD)	Tissue engineering for brain regeneration	-	-	• Sprague-Dawley rats, cortex implantation	HA-RGD hydrogel provided a structural, 3D continuity across the cortex and favoured reorganisation of local wound-repair cells, angiogenesis, and axonal growth.	[Cui et al., 2006] 10.1007/s10856-006-0615-7
Hydrogel	HA- Poly-D-lysine (PLL)/ nogo-66 receptor antibody (antiNgR)	Tissue engineering for nerve regeneration	10 to 100 µm interconnected network	-	• Sprague-Dawley rats, lateral hemisection of spinal cord	Inhibited the glial scar formation, support angiogenesis, and promote axonal extension.	[Wei et al., 2007] 10.1002/jbm.b.31689
Sponge-like scaffold	Collagen type I and II/HA	Neurogenic induction of cells seeded into a construct for brain regeneration	80-200µm pore size(75% to 91%)	1-6.3kPa Young modulus	• 2-3D, primary cell culture	The scaffolds favour the differentiation of neural stem cells (NSCs) to neuronal cells *in vitro*.	[Wang et al., 2009] 10.1016/j.actbio.2009.03.033

Gel	HA	Matrix to reduce the marginal glial scarring	120 to 182 μm porosity	Tensile strength: 4.1-6.3 N/mm2	• Sprague-Dawley rats	Inhibited the glial scar formation by decreasing the thickness of gliosis and by reducing the number of the glial cells.	[Lin et al.2009] 10.1016/j.wneu.2009.09.004
Hydrogel-microspheres composite	HA hydrogel / recombinant human brain-derived neurotrophic factor (BDNF) and vascular endothelial growth factor (VEGF)-poly(lactic-co-glycolic acid) microspheres loaded	Delivery system for NSCs	-	-	• 2-3D, primary and single-cells cultures (Sprague-Dawley embryos forebrain cells)	Stable releasing of the biofactors, promoting cells survival and growth. The soft property was suitable for CNS tissue. Biocompatible material, with great adhesion and cell proliferation.	[Wang et al.2011] 0.1007/s11095-011-0452-3
Hydrogel	HA-Modified methylcellulose	NSPCs cells delivery vehicle	-	-	• Rat NSPCs cells	Increased oligodendrocytes differentiation.	[Tam et al.,2012] 10.1039/c2jm33680d
Electrospun nanofiber scaffold	HA-laminin-coated polycaprolactone (PCL) nanofibers	Neural tissue engineering for restore damaged tissue	Fiber diameters: 600–1200 nm	-	• 2-3D cell culture, eGFP neuronal SH-SY5Y cell line	The aligned nanofibers permitted the guidance of neurite outgrowth.	[McMurtrey, 2014] 10.1088/1741-2560/11/6/066009

Hydrogel	HA-laminin/SDF-1α loaded	Matrix to enhance neural transplant retention and migration delivery system	-	-	• 3D, primary cell culture; NPSCs • C57BL/6 mice, brain injection	SDF-1α signalling critically mediates NPSC transplant chemotactic migration, and the matrix increases NPSCs transplant retention.	[Addington et al., 2017] 10.1016/j.matbio.2016.09.007
Microporous annealed particle hydrogel	HA/K-peptide/Q-peptide/RGD	Matrix to promote brain tissue repair after stroke	-	-	• C57BL/6, stroke-induced	Reduced inflammatory response following stroke and increased peri-infarct vascularization.	[Nih et al., 2017] 10.1002/adma.201606471
Drug delivery scaffold	SA and HA loaded device	Microenvironnement to embed stem cells in traumatic brain injury	200 µm to tens of µm	0.1 kPa to 1 kPa Young Modulus	• HUC-MSCs • SD rats	NSCs embedded in HA collagen biomaterials may promote reinnervation of damaged facial nerves, and artificial conduction of NSCs may provide a potential treatment for peripheral nerve injury.	[Zhang et al.2008] 10.1039/C7TB03213G
Hydrogel	Glycidyl methacrylate-HA and Methacrylic anhydride-HA/Collagen I and laminin functionalized	Engineered scaffold for tissue regeneration	1 µm pore size	2-6kPa Young modulus	• Schwann Cells and dorsal root ganglia (DRGs) cell lines • Rat isolated tissue (sciatic nerve, brain and spinal cord)	The material can be tuned to numerous soft tissues, and supported 3D axonal elongation of DRGs cultures.	[Spearman et al., 2020] 10.1002/jbm.a.36814.

Hydrogel	HA-galactose oxidase (GalOx)-horseradish peroxidase (HRP)/ bone mesenchymal stem cells (BMSC) and nerve growth factors (NGF) encapsulated	Implant or cell/drug delivery vehicle for tissue repair	<100um pore size loose and porous structure	Low elastic modulus <0.1kPa	• 3D and single-cells models; BMSC cells • Traumatic Brain Injury (TBI) model, C57BL/6 mice	Good biocompatibility, stability, and biodegradability. Suitable for cell survival and proliferation, accelerated brain repair process.	[Wang et al., 2022] 10.1016/j.mtbio.2021.100201
Hydrogel	HA-poly(N-isopropylacrylamide)	Hybrid interpenetrating polymer network as cell carrier for nucleus pulposus (NP) repair	-	0.1kPa-8kPa Elastic modulus	• Primary culture, NP cells • Cartilage and intervertebral disc (IVD) organ culture	The matrix supported the cell viability and the phenotype expression of the encapsulated cells.	[Guo et al., 2022] 10.1016/j.carbpol.2021.118828
Nanogel	Iron oxide (Fe_3O_4)-HA	Theranostic material for Alzheimer's disease	–	-	• Single-cells culture, C8-D1A cell line	Non-cytotoxic matrix. Efficient generation of negative contrast in MRI.	[Chen et al., 2022] 10.1016/j.arabjc.2022.103748

Table 4. Systems developed for PNS injuries application

Device	Matrix composition	Proposed mechanism	Porosity and connectivity	Mechanical properties	Study model *(In vitro, in vivo, ex vivo)*	Major Findings	Reference
Composite Conduit	HA / collagen	Tissue engineering for nerve regeneration	Diameter 1.2 mm Porosity 50 µm	-	• Rat SCs and neurospheres • NSCs from neural cortex of SD rat embryos	Cultured rat Schwann cells and neurospheres grow *in vitro* on new artificial HA-based nerve conduits. After 3 weeks of culture, conduits stayed circular with a round lumen, and cell-conduits conserved their original structure.	[Sakai et al. 2007]PMID: 17502696
Composite conduit	HA / collagen	Tissue engineering for nerve regeneration	7 mm in length	-	• Normal adult New Zealand rabbits	NSC-embedded NT-3 HA-collagen composite scaffold, has shown that a number of nerve fibers were still unmyelinated. Degeneration and swelling of myelin lamellae were also visible.	[Zhang et al. 2008] 10.1186/1479-5876-6-67
Composite Conduit	HA-Silk Fibroin composite device	Tissue engineering for nerve regeneration	79% of porosity	G'/G': 6 to 7 viscoelasticity	• Rat Schwann cells (rSCs) • Male CD-1 mice	Both HA and HA-SF scaffolds were received by the host with no residual immune response at 8 weeks. The results show that SF incorporation improves the mechanical properties of the material and leads to promising biocompatible conduits for tubing strategies.	[Gisbert et al. 2020]10.1016/j.ijbiomac.2020.01.149

Composite Conduit	PDLLA/*β*-TCP/HA/CHS/NGF	Polymer based scaffold for controlled release of NGF	Semi-permeable, pore size less than 10 μm	13-60 kPa Elastic modulus	• PDLLA/*β*-TCP nerve conduits • Sciatic nerve defect in SD rat	Substantial enhancements in nerve regeneration were noticed after using the PDLLA/β-TCP/HA/CHS/NGF NGCs based on the different assessments. In vivo studies show that the PDLLA/ β-TCP/ HA/ CHS/NGF sustained-release NGCs can significantly stimulate peripheral nerve regeneration, and the effect is comparable to that of autograft.	[Yan et al. 2021]10.1007/s11595-021-2450-6
Scaffold	PEDOT-doped HA NPs/ CS / Gel matrix	Tissue engineering for nerve regeneration	200– 300 μm pore size 83-92% porosity	13-60 kPa Elastic modulus	• PC12 cell line	8% PEDOT-HA/Cs/Gel scaffold had a higher cell adhesive efficiency and cell viability in comparison to the other conductive scaffolds. It also has shown a higher expression of synapse growth genes of GAP43 and SYP compared with the Cs/Gel control group.	[Wang et al. 2017] 10.1016/j.msec.2016.10.029
Hydrogel	HA-CS composite system	Hydrogels for nerve growth factor(NGF) sustained release and nerve regeneration	Porosity: 20 to 100μm	2 to 4 kPa Elastic modulus	• RSC96 rat SCs and PC12 cell lines • Healthy adult Sprague-Dawley (SD) rats	• The good mechanical, porous, and swelling properties play a synergistic role in enhancing nerve regeneration. The CS-HA/NGF hydrogels through a sustained release are favorable for promoting cell adhesion, spreading, and differentiation • Chitosan and HA inhibited extraneural scarring, promoted nerve regeneration, raised the nerve conduction velocity and amended the recovery of nerve function. Combined together they	[Xu et al. 2016] 10.1177/0883911516662068 [Li et al. 2018] 10.3892/mmr.2018.8388

						enhance neural regeneration and repair.	
Hydrogel	HA-CS/NGF hydrogel	Injectable hydrogels aimed to sustained release of nerve growth factor (NGF)	Pore size 53-73µm Porosity(82-87%)	2.3-4.5kPa Elastic modulus	• BMMSCs, RSC96 rat SCs cells and PC12 cell line	PDLLA/β-TCP nerve conduits formulated with CS-HA/NGF hydrogels improved the axon regeneration and myelination, contrasted to the PDLLA/β-TCP hollow nerve conduits and the autograft group. These findings imply that the CS-HA/NGF injectable hydrogel can successfully upgrade nerve regeneration, hence, it is a good candidate in the field of neural tissue engineering.	[Xu et al. 2022] 10.1016/j.compositesb.2021.109509

Chapter 4

Encapsulation of BMP-4 into polymer-based nanoparticles

4. ENCAPSULATION OF BMP-4 INTO POLYMER-BASED NANOPARTICLES

pharmaceuticals

MDPI

Article

Development of BMP-4 loaded PLGA nanoparticles via a non-toxic phase separation process

Amel Djoudi*[1], Rodolfo Molina-Peña[1], Natalia Ferreira[1], Sylvie Avril[1], Emmanuel Garcion[1], Frank Boury*[1]

[1] Université d'Angers, Inserm UMR 1307, CNRS UMR 6075, Nantes Université, CRCINA, F-49000 -Angers - France

* Correspondence: djoudi-amel@hotmail.fr, frank.boury@univ-angers.fr

Citation: Djoudi, A.; Molina-Pena, R.; Ferreira, N. Development of BMP-4 loaded PLGA nanoparticles via a non-toxic phase separation process. *Pharmaceuticals* **2022**, *15*, x. https://doi.org/10.3390/xxxxx

Academic Editor: Firstname Lastname

Received: date
Accepted: date
Published: date

Publisher's Note: MDPI stays neutral with regard to jurisdictional claims in published maps and institutional affiliations.

Copyright: © 2022 by the authors. Submitted for possible open access publication under the terms and conditions of the Creative Commons Attribution (CC BY) license (https://creativecommons.org/licenses/by/4.0/).

Abstract: The current project aims to develop PLGA NPs with non-toxic and biocompatible solvents via a phase separation process, to achieve a controlled release of BMP-4, a cytokine involved in early differentiation of the embryo establishment of the dorsoventral axis and differentiation processes (cartilage, bone, sympathetic neurons). In this work, BMP-4 and lysozyme as a model protein, were initially precipitated to favor their stability upon encapsulation. Blank PLGA-based nanoparticles (NPs) showed an average size of 250 ± 20 nm, the loaded ones a size of 480nm+/-10nm and a high encapsulation efficiency intended to for a GB application. The encapsulated BMP-4 kept its biological activity after the formulation process as assessed by its capacity to activate the SMAD pathway and to modify F98 and U87MG gliomasphere number. The nanoparticles allowed sustained release of BMP-4 α for 4 weeks. Using NIH3T3 and L929 mouse fibroblasts, we showed that the nanoparticles had high cytocompatibility *in vitro*.

Keywords: Glioblastoma; nanoprecipitation; phase separation; controlled drug release

1. Introduction

Glioblastoma (GB) and malignant gliomas are the most common primary malignant brain tumors [1–3].They are characterized by an annual incidence of 5.26 per 100,000 population or 17,000 new cases each year. These kinds of tumors are a poor quality of life and prognosis for the patients [1,2].

Glioblastoma is a IV grade glioma and is the most lethal and frequent malignant intrinsic and primary brain tumor. On the contrary to other solid tumor cell types GB widely invades the surrounding brain but rarely metastasizes to other organs [1,2]. The injunctive therapy is surgical resection of the majority of the tumor followed by radiotherapy and chemotherapy with temozolomide according to Stupp protocol [4–7]. In most of the cases patients experiment with relapse and only a few therapeutic possibilities are available including surgery and chemoradiotherapy. Despite this huge therapeutic arsenal, patient median survival only reaches around 15 months [1,2]. The main issue in this type of cancers, is a specific population of cancer stem cells (CSCs) which are called tumor initiating stem cells; these cells have a tumorigenic potential and are able to proliferate in an asymmetric way [8–10]. In 90% of cases, GB is recurrent because of CSCs that remain close to the resection cavity after surgery []. A treatment already in the market called Gliadel® is a carmustine loaded wafer used for the treatment of GB post-resection [11–14]. This treatment has shown a few promising results for patients, does not fill the whole exeresis cavity and has various side effects [11–14]. In 90% of cases, GB is recurrent because of CSCs that remain close to the resection cavity after surgery [8,9]. A treatment already in the market called Gliadel® is a carmustine loaded wafer used for the treatment of GB post-resection [11–14]. This treatment has shown a few promising results for patients, does not fill the whole exeresis cavity and has various side effects [15–17].

Therapeutic strategy and BMP-4 features

Despite advances in various fields including immunotherapy [18,19], gene therapy [20–22] or improved methods of administering various anti-cancer agents including biological agents [23,24], chemical inhibitors[25,26] or radiopharmaceuticals[27,28], the prognosis remains bleak [1,2,29]. Also the differentiating strategy has been little investigated until now, while several biological compounds that include retinoic acid [30–32] or BMP-4 [33–35] demonstrated strong activities and interesting possibilities of application. Hence, our therapeutic strategy is based on the use of BMP-4 to allow locoregional CSCs to leave the CSCs compartment and give them increased radiosensitivity [33,36–38]. Bone morphogenic protein 4 (BMP4) is a cytokine that belongs to the TGF-β superfamily, it is a structural homology of Bone morphogenic protein 2 (BMP-2) protein [39–44].

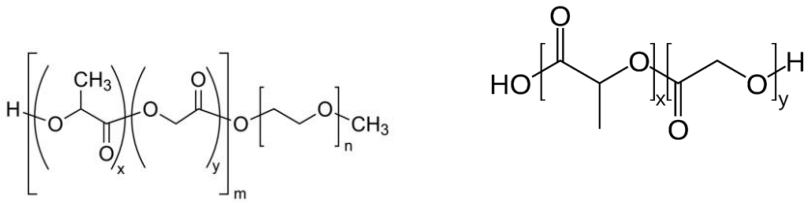
BMP-4 and BMP-2 cytokines are involved in early differentiation processes (cartilage, bone and sympathetic neurons) and dorso-ventral axis establishment [34,35,45,46]. Moreover, it has been found to be a key regulator of embryogenesis and development, and also in maintaining adult tissue homeostasis [34,35].
Indeed, BMP-4 has been shown to regulate the development of mesoderm, and more precisely in the specification of the vascular and hematopoietic systems. It is also an important regulator of the growth of hematopoietic stem cells (HSC), participating in the control of their proliferation, migration and differentiation [33–35,47,48]. It has been highlighted to participate in embryonic skeletal development too. According to other studies, BMP-4 sensitizes GB tumor-initiating cells and reverses multidrug resistance. Indeed, it drives GCSCs to differentiate into cells with increased sensitivity to conventional therapy, which improves therapeutic efficacy, and hence patient prognosis [22–27].

BMP-4 also triggers antiproliferative and antisecretory action of pharmaceuticals with possible treatment of Cushing disease like retinoic acid and somatostatin analogs [49–51]. Besides, BMP-2 is also used in various research projects that involve bone tissue through sustained release of BMP-2 from biodegradable nanoparticles for bone regeneration [42,52]. Therefore, BMP-4 is the main cytokine investigated in this paper

with reference to previous works, but BMP-2 has also been tested as a comparison treatment in the *in vitro* gliomasphere assays to evaluate *in vitro* its effect on GB .

Our therapeutic strategy consists on firstly, developing BMP-4 loaded NPs and secondly, include them in injectable hydrogels for a locoregional administration. A differentiation strategy through BMP-4, would lead these CSCs to become specialized hence less tumorigenic and proliferate less, making these cells radiosensitive and more likely to be eliminated by a concomitant treatment with external radiotherapy and chemotherapy with temozolomide.

PLGA relevance in this system



(**a**) (**b**)

Figure 10: Chemical structure of PLGA-PEG (a) and capped PLGA-COOR (b)

Lactic-co-glycolic acid (PLGA) acid is a copolymer of lactic acid and glycolic acid (Figure 10). It is a biodegradable, biocompatible polymer, and allows to formulate controlled drug release systems [53–56]. FDA-approved, it is therefore extensively used in the research field for diagnosis and treatment administration applied to vectorize drugs [53]. Commercially, various grades of PLGA are reliant on their inherent viscosity, lactic acid to glycolic acid ratio and their molecular weight [53]. PLGA types with ester end groups are more resistant to hydrolytic degradation, hence, a delay in release profile is observable for some active pharmaceutical ingredients (APIs) [57].

PLGA nanoparticles have become one of the most promising delivery modes of macromolecular drug delivery by parenteral, mucosal, and local routes [58–60].

Implantable or injectable PLGA systems for sustained protein delivery have been extensively studied to overcome the need for repeated administration of therapeutic proteins [61–63]. It has been used to overcome limited pharmacokinetics profiles of conventional therapies. These devices can be either nanoparticles, microparticles, implants, or patches, depending on the condition and route of administration. In addition, the release rate can be adjusted from weeks to months by controlling the polymer composition, the shape of the device, or the introduction of additives while manufacturing the device [64,65].

Polyethylene glycol PEG-PLGA systems and extensive research efforts have allowed the development of a variety of functional PLGA-based nanoparticle delivery systems. Typical examples are Pegylated micelles / nanoparticles , polyplexes, polymersomes, core-shell lipid-PLGA hybrids, cell-PLGA hybrids, receptor-specific ligands-PLGA conjugates, theranostic agents (Figure 10) [61,62,64,66–68].

In this article, PLGA nanoparticles are formulated through a phase separation process. Aqueous non-solvent is added to the dissolved polymer and separates the solvent from the polymer that reduces the solubility of the polymer. The phase separation of the polymer from its solution contributes to the formation of polymer-

rich liquid phase (coacervate) surrounding the inner part aqueous phase containing the drug [67]. After the phase separation process, the coacervate solidifies to produce drug-loaded particles, The main disadvantage of this process is the need of large volumes of organic solvent [67,69,70]. Recent work proposed the use of water-miscible organic solvents to dissolve the polymer such as Glycofurol (GF) and Dimethyl isosorbide (DMI). Therefore the need for organic solvents to induce phase separation is no longer necessary, hence, water can be used to extract the polymer solvent [67].

2. Results and discussion

2.1.1. Precipitation and Encapsulation efficiency assessment

According to figures 11 the size and shape of protein nanoprecipitates BMP-4 are homogenous in TEM. Size is monodisperse with 92nm+/-5nm and shape is round with tiny white points that could correspond either to the protein and/or/Poloxamer 188 aggregates. These nanoprecipitates are directly encapsulated given that protein is stabilized in this state and its native conformation is kept. Moreover P188 helps to stabilize the protein by reducing repulsive interactions and facilitating salting-out processes. In addition, the whole process of precipitation is done in ice; lowering the temperature means lowering kinetic energy of the protein molecules, and thus faster aggregation and subsequent precipitation. A main study states that similar precipitation efficiency could be achieved at 4°C or room temperature ; a choice to lower the temperature was made for possible protein protective effects [55,67,68]

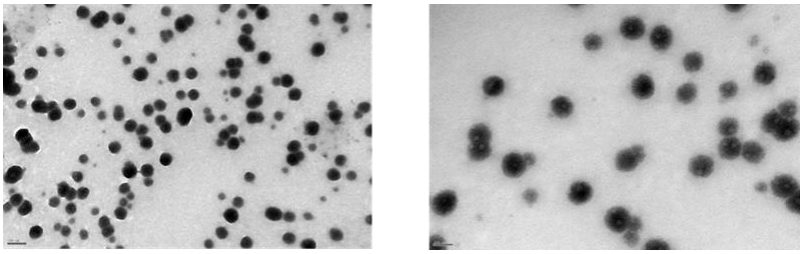


Figure 11 TEM images of the formulations. Nanoprecipitates of BMP-4 with a size distribution of 92nm+/-5nm

Precipitation efficiencies (PE) obtained for Lysozyme, used here as a model protein, are close to previous published studies [55,67,68]. 0.15M concentration is NaCl salt is the most suitable for Lysozyme precipitation with 98% of PE followed by 0.30M, 0M and 0.45M NaCl concentration (Table 5). Indeed the highest concentration of NaCl leads to protein aggregates observable in TEM, leading to a poor precipitation whereas no salt presence can precipitate lysozyme though aggregation limits the salting out process. Consequently, the preparation is not cloudy with less and more heterogenous objects observable in TEM (Figure 11). The salting out process seems successful in presence of HEPES buffer that could be explained by its SO3- group interacting with positively charged aminoacids via electrostatic interactions.

The other protein studied is BMP-4, has never been precipitated to our best knowledge. However, proteins with close physico-chemical properties such as TGF-β1 [62,68], BSA [71] lysozyme, peroxidase, beta galactosidase, alpha chymotrypsin [55], c(CytC)[47] [72] and lastly BMP-2 [39,73] were successfully precipitated.

Table 5: Precipitation efficiency (PE) of Lysozyme and BMP-4 with variation of the NaCl concentration

NaCl concentration	Lysozyme	BMP-4
0M	63+/-4	N/P
0.15M	98+/-11	N/P
0.30M	75+/-5	N/P
0.45M	51+/-8	N/P
0.15M and 2M HEPES	N/P	103+/-9%

[1] N/P corresponds to no precipitation obtained nor observed in TEM

2.1.2 Dynamic Light Scattering and Protein quantification and activity:

DLS and SEM, TEM results for blank and loaded NPs are in accordance with those obtained in previous studies [55,67,68]. Figure 12 represents BMP-4 loaded PLGA nanoparticles with an average size of 320+/- 50 nm and a round shape with a dark and dense core, suggesting the obtention of nanospheres [74], that consist on an entanglement of PEG-PLGA and PLGA-COOR polymers with protein nanoprecipitates, with an interesting asset: controlled drug release matrixes [67,70,75,76].

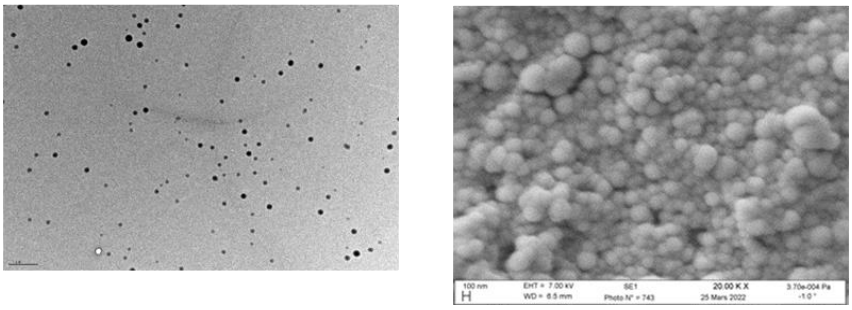


Figure 12: TEM (left) and SEM(right) images of the formulations. BMP4 -Loaded nanoparticles of PLGA with a size distribution of 320nm+/-50nm

The smallest size is obtained with the blank NPs followed by lysozyme-loaded ones and then BMP-4 loaded NPs. The ratio of PLGA-COOR/PLGA-PEG has an impact on size. Indeed, when the amount of PLGA-PEG is increased, NPs size rises. This has been described in previous studies [70,75,76]. When protein nanoprecipitates are encapsulated in PLGA NPs, we observe an increase of NPs size especially by a 1.5 fold rise for Lysozyme loaded ones and by a 2 fold rise for BMP-4 loaded NPs which can be explained by the size of the respective proteins 14kDa and 25kDa that might affect the entanglement of PLGA polymers chains. In comparison to previous studies where SDF1-alpha was encapsulated in similar conditions, size of NPs was not affected by protein due to the size of 8kDa of the protein. Polydisperse index (PDI) of all formulations is inferior to 0.4 so the nanosuspensions are quite monodisperse. In addition, the zeta potential is between -0mV and +10mV, suggesting that PLGA NPs are neutral (Table 6) [67,68]. To achieve adequate colloidal stability, zeta potential levels over +30 mV or less than +30 mV are typically considered optimal, since this guarantees strong electrostatic repulsive interactions between the nanoparticles [77]. The inclusion of the exterior PEG layer in our study obviously reduced the zeta potential magnitude of the PLGA/PEG-PLGA nanoparticles. Despite the loss of electrostatic stability, the nanoparticle suspension would benefit from the PEG chains steric stabilization [67].

When the pH is adjusted around the protein isoelectric point, protein molecules have a reduced net electrical charge and hence lower aqueous solubility (pI). The findings in Table 6 confirmed this idea since both lysozyme and BMP-4 were most efficiently encapsulated when the pH of the aqueous phase was adjusted closest to their respective pI. Lysozyme has a 11.35 pI, BMP-4 7.6 pI. This may reduce protein loss into the aqueous phase during the formulation process, therefore, increasing encapsulation efficiency.

Besides lowering water solubility, the lower net charge is assumed to have reduced electrostatic repulsions between protein molecules, allowing the protein loaded to be compressed and entrapped inside the nanoparticles [78,79].For such reasons, the pH of the aqueous phase in subsequent encapsulations was always tuned to the protein pI.

The EE% in table 6,of the formulations 4 and 6 are the highest because a lower amount of PLGA-COOR was used, increasing therefore the interactions with the protein. This has been studied in a previous work, and have shown that PLGA-COOR based NPs exhibit lower EE% than PLGA-COOH but in terms of release kinetics, this latter is slower and more sustained [67].

Table 6: Encapsulation efficiency of Lysozyme (3 and 4) and BMP-4 (5 and 6) in different conditions: 70/30 %(1, 3, 5) and 50/50% (2, 4, 6) ratio of PLGA-COOR/PLGA-PEG. All experiments were done in triplicates

Formulation	Size(nm)	PDI	Zeta Potential (mV)	EE (%)
Blank 1 70/30%	199+/-10	0,20+/-0,09	-2,5+/-0,4	-
Blank 2 50/50%	264+/- 6	0,15+/- 0,06	-3,6+/- 0,4	-
Formulation 3 70/30%	289+/-3	0.26 +/-0.11	-3.4+/-0.2	76 ± 6
Formulation 4 50/50%	368+/-5	0.31+/-0.10	-4.1+/-0.1	90± 7
Formulation 5 70/30%	381 +/- 12	0,28 +/- 0,1	-3,4+/-0,6	71+/-3
Formulation 6 50/50%	588+/- 10	0,20+/- 0,06	-2,5+/- 0,3	86+/-5

2.1.3. ATR-FTIR

Figure 13 depicts the ATR-FTIR spectra of the polymers used in our formulations. The peaks located at 2995 cm-1 and at 2883 cm-1 are O-H stretching ; those at 1747 cm-1 and 1749 cm-1correspond to C=O stretching of ester. The peak located at 2883 cm-1is O-H stretching and 1749 cm-1 peak corresponds to C=O stretching of ester. This spectrum is comparable to the literature [80].

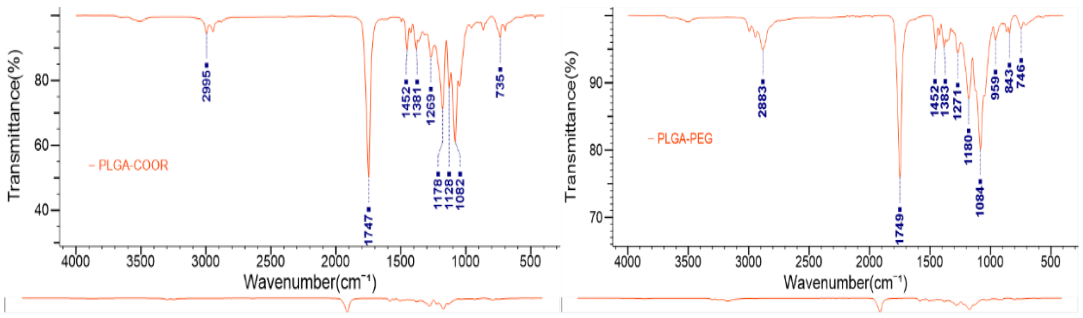


Figure 13: ATR-FTIR spectrum of capped PLGA-COOR (a) and PLGA-PEG (b), transmittance (%) representation in function of the wavenumber (cm-1) in the whole region (3600–650 cm−1) and the fingerprint region (1800–650 cm−1)

2.1.4. Stability study of nanoparticles with pH variation and post lyophilization with HβBCD

Stability study described in the Material and Method section consisted in varying the pH of the measurement medium of blank NPs. Hence, depending on the pH, blank PLGA NPs are similarly stable at pH 4 and pH 7 with zeta potential respectively equal to -3mV and -5mV for both formulations whereas, they are also stable at pH 10 with a ZP equal to -28mV and -32mV for the 2 formulations (Figure 14). As previously highlighted, to reach adequate colloidal stability, zeta potential levels over +30 mV or less than +30 mV are typically considered optimal, since this permits strong electrostatic repulsive interactions between the nanoparticles.

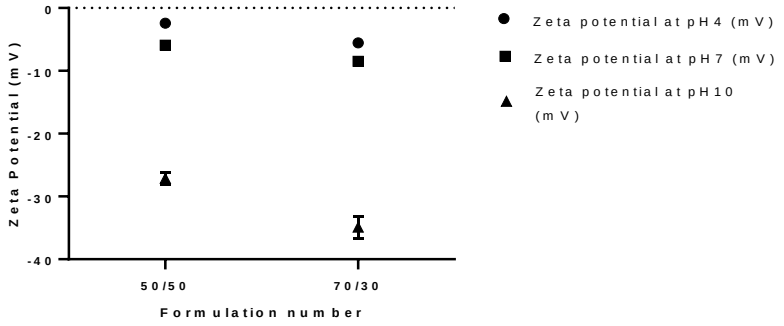


Figure 14: Stability study of blank NPs in different pH conditions

In order to evaluate the effect of lyophilization on the NPs behavior, the size and the PDI of blank NPs formulation with different ratios of PLGA-PEG and capped PLGA-COOR were measured in presence of HβCD used as cryoprotectant before (i) and after (f) freeze-drying (Table 8). A previous study has observed the effect of a cryoprotectant on NPs size and PDI but this time the polymer ratio is the parameter that has been changed[55,67,68]. According to the following result in Table 7, both NPs formulations do not exhibit a size variation prior (Si) and after (Sf) freeze-drying. It is observable through the Sf/Si and the PDIf/ PDIi slight difference between formulations and the increase in size after lyophilization is not significant. For the formulation without cryoprotectant, no data was obtained, because the sample collapsed due to a lower degree of porosity of the freeze-dried product, thus, reducing its surface area to volume ratio and hydration rate [81].

The volume contraction caused by the collapse of other cryoprotectants such as sucrose and trehalose matrices is believed to have minimized the distance between the nanoparticles, allowing the PEG layers of agglomerated particles to interact and create stable crystalline bridges, as described in the literature [67,82,83]

Table 7 Stability study of blank NPs formulations pre and post-lyophilisation in presence of HβBCD

Formulation	Si(nm)	PDIi	Sf(nm)	PDIf	Sf/Si	PDIf/PDIi
Formulation 1 70/30	167±3	0,07±0,02	168±1	0,08±0,02	1,005	1.15
Formulation 2 50/50	183±4	0,098±0,04	189±7	0,11±0,01	1,04	1.12

2.1.5. Release profiles

Protein release was investigated by placing the nanoparticles in a buffer solution and centrifuging the supernatant at pre-determined time intervals for protein analysis (Figure 15 A and B). Originally, lysozyme release patterns in several buffer solutions were investigated. The fraction of PLGA-COOR in the nanoparticles was demonstrated to impact the amount of lysozyme release at the physiologically relevant pH 7.4 [67]

Protein leakage from PLGA particles with uncapped carboxylic end groups has previously been described in these articles as too fast [62,67,84,85], that is why we have chosen to formulate the NPs only with capped PLGA-COOR and PLGA-PEG.

Lysozyme release from Tris HCl at 7.4 pH and through 30 days for both formulations 3 and 4 is shown in figure 15A. In formulation 3 the presence of PLGA-COOR, with the COOH groups neutralized by esterification, may explain the higher released protein amount observed for lysozyme release during the first 48 hours in comparison to formulations made only with uncapped PLGA. Uncapped PLGA has been shown to have an incomplete release due to partial neutralization of carboxylate groups by medium cations, preventing complete lysozyme release. Aside from pH, another element that may influence lysozyme-PLGA

electrostatic interactions is the concentration of cations in the release media, since these ions can also displace lysozyme molecules from the PLGA carboxylic acid groups. To minimize protein-polymer interactions we presented protein in the presence of poloxamer 188 [55,67,68] and encapsulated in PEG-PLGA co-polymer to enhance the quantity of released protein.

Previous research found that PLGA-COOH had a high encapsulation efficiency but a slow *in vitro* release profile, whereas PLGA-COOR had a lower encapsulation efficiency but a rapid release profile. Lysozyme release seems faster for the 70/30%ratio than the 50/50%, this can be explained by the higher PLGA-COOR amount that has been shown to accelerate protein release [67,86].

BMP-4 release profile has been done in the PBS buffer at pH7.4 during 1 month. Both formulations 5 and 6 correspond to 70%/30% ratio formulation and 50%/50% ratio formulation. Formulation 5 seems to have a faster release than formulation 6. This can be explained by the higher amount of PLGA-PEG in the formulation 6 that can slow down the release of BMP-4 given that PLGA-PEG will interact more with BMP-4 through electrostatic interactions. Therefore, increasing the adsorbed BMP-4 at the surface and reducing the kinetic of release but also reducing the burst effect that tend to release the majority of the protein for various known systems [67,68,87,88]. Not all the protein is released, 86 % for formulation 5 and 54% for the formulation 6. In regards of release rate, adding a PEO derivative to the PLGA matrix, like PEG, reduced the undesirable burst effect more efficiently than the more hydrophilic PLGA-poloxamer combination [59,67,89]. The incomplete release of BMP-4 and Lysozyme might be explained by the hydrolysis of ester bonds of capped PLGA-COOR resulting in a contact between protein positive charges and negatively charged carboxylate that might prevent the protein from being liberated.

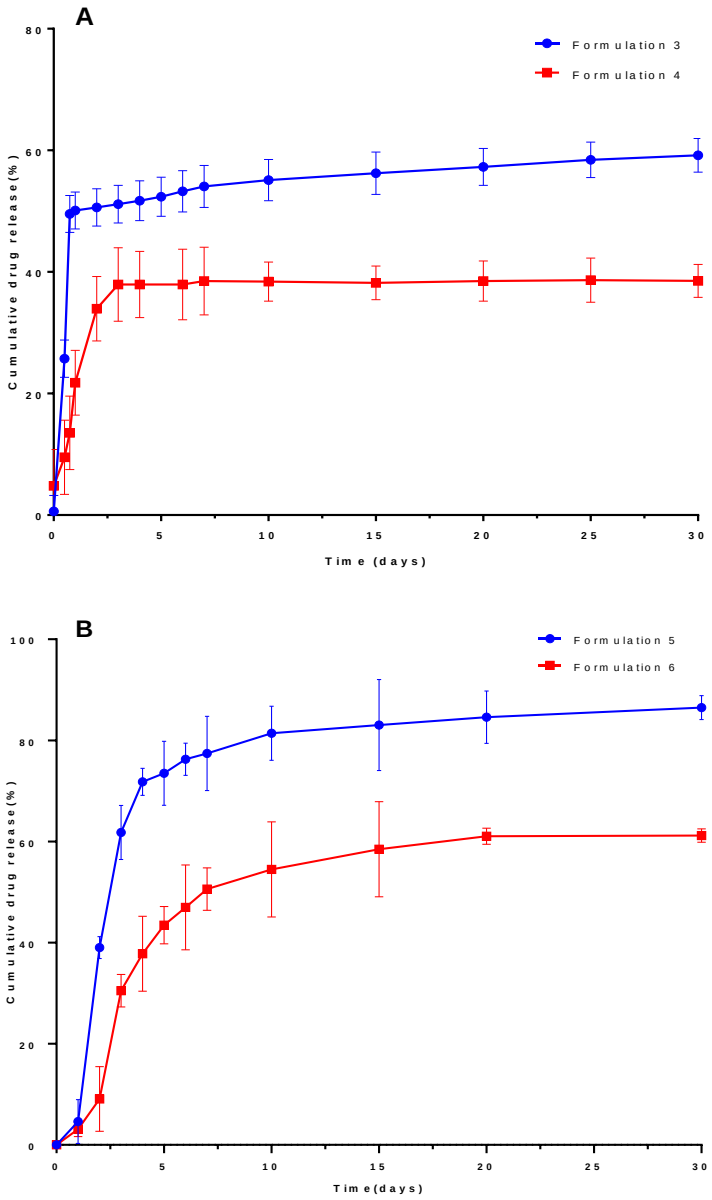


Figure 15 (A) Release profiles from PLGA nanoparticles of lysozyme in Tris-HCl, Formulation 3 and 4 correspond respectively to 70%/30% and 50%/50% ratios of PLGA-COOR/PLGA-PEG loaded with Lysozyme. (B) Release profiles from PLGA nanoparticles of BMP-4 in PBS. Formulation 5 and 6 correspond respectively to 70%/30% and 50%/50% ratios of PLGA-COOR/PLGA-PEG loaded with BMP-4 Each data point with error bar represents mean ± SD, Triplicates have been done n = 3 for each formulation.

2.1.6. Nanoparticles cytotoxicity assay

According to cytotoxicity results and statistical analysis, blank nanoparticles with PLGA-COOR/PEG-PLGA 50%/50% and 70%/30% polymer ratios do not seem to be toxic for the NIH3T3 an L929 cell lines after 24h, 48h and 72h (Figures 41-46 in annexes). Besides, there is an increase in cell viability for cell lines incubated with low concentration suspension, this could be due to a higher amount of medium that stimulates the growth

mostly at 72h. These findings are consistent with results found previously in the literature related PLGA NPs [67,68,90–92]. Moreover, NPs are not toxic even at the highest concentration 1mg/mL. Many parameters may affect the cell proliferation like as the methodology of NPs formulation, remaining solvent and cell lines types. Varying the ration between PLGA-COOR and PLGA-PEG varies the size of the NPs, hence, this parameter does not seem to have an impact on cell viability. In the framework of other applications, these NPs could be useful like other CNS and PNS disease.

2.2. In vitro assays:

2.2.1. Western Blot of SMAD pathway activation

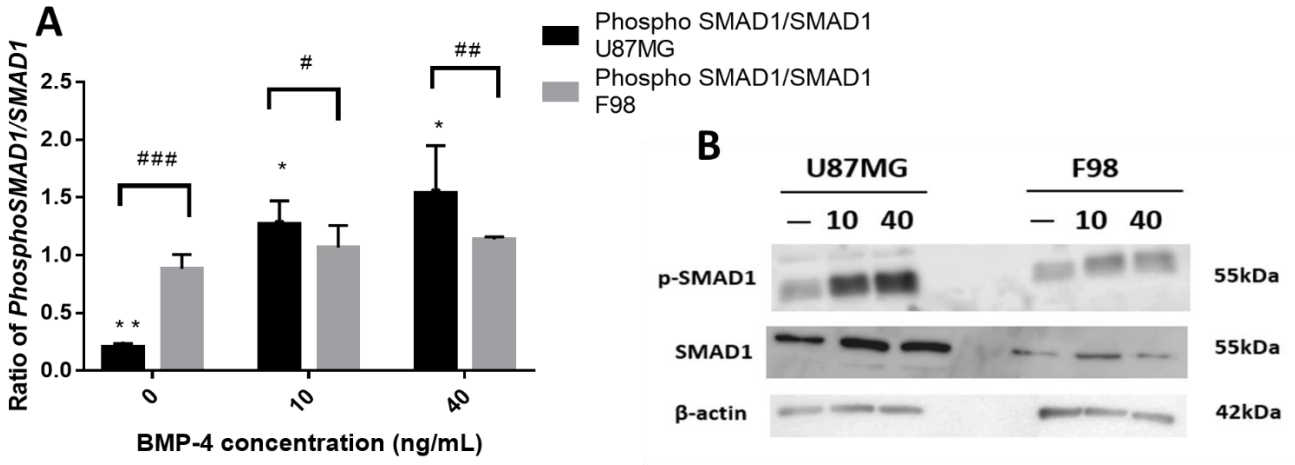


Figure 16. (A) Western Blot graphic of PSmad1 and Smad1 in U87MG and F98 cell lines. (B) Western Blot of U87MG and F98 cell lines with and without treatment with BMP-4 in ng/mL during 1 hour. Statistical analysis: n=2. * P<0, 05, ** P<0, 01 treated versus corresponding non- treated cells condition; # P<0, 05, ## P<0, 05 treated condition compared to the same treatment

This assay helps to validate the cell models F98 and U87MG through the activation of SMAD pathway by BMP-4. Measuring Smad1 and p-Smad1 after treating the U87-MG and F98 adherent lines with BMP-4 for 48 hours, we observe what seems to be a dose-dependent regression in the amount of intracellular Smad1 under the conditions treated with BMP-4 (Figure 16) for both cell lines, with a less pronounced effect noticed in U87-MG line. These data seem to support the consumption of Smad1, by phosphorylation after activation of the BMP pathway by BMP-4.

Besides, we observe an increase in the signal of p-Smad1 for the U87-MG line when the concentrations of BMP-4 increase, due to the activation of the signaling pathway. In addition, the untreated condition appears to exhibit a strong presence of constitutively activated Smad1. This trend seems to be validated for the F98 line but to a lesser extent, where we observe a weak presence of p-Smad1 in the untreated condition, and less presence in the treated conditions. The results suggest that our cells express the receptor since the treatment with BMP-4 seems to unmodify the amount of Smad1 and increase the amount of p-Smad1. This suggests an activation of the BMP-4 pathway (Figure 16).

2.2.2 Proliferation assay

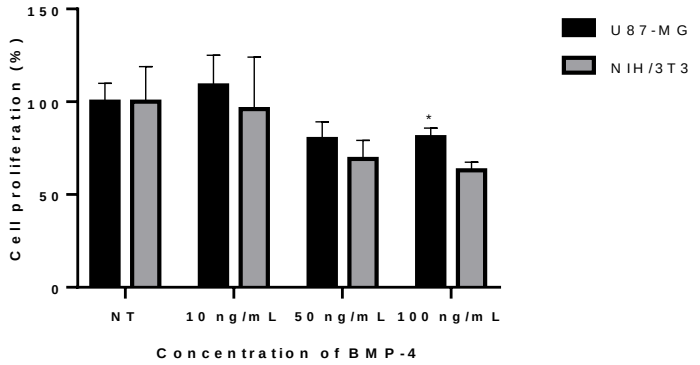


Figure 17. Cell viability at different concentrations of BMP-4 on U87-MG and NIH3T3. Values are presented as means ± standard deviation, n=4. * P<0, 05 versus corresponding non-treated (NT) condition (0 ng/mL), ## P<0, 01, ### P<0,001 versus treatment to same concentration of different BMPs.

In both cell lines (figure 17), proliferation tends to decrease after treatments with 50 ng/mL of BMP-4 and 100 ng/mL condition in a similar way. BMP-4 at 100 ng/mL significantly decreases cell proliferation on the U87-MG cell line (80, 92% of non-treated proliferation). These results suggest that BMP-4 alone would be able to slow down the cell growth of tumor cells. Evaluation of the effects of BMP-4 released from PLGA NPs are in course and unfortunately cannot be shown at this stage.

2.2.3. Assessment of BMP-4 and BMP2 bioactivity

The results depicted in figure 18 suggested by the activity assay reveal some useful data. For the U87-MG line, treatment with BMP-2 or -4 does not seem to influence the development of spheres for concentrations under 70 ng/mL of BMPs. We notice an unexpected increase of gliomasphere formation with 70 ng/mL BMP-4. Concerning the F98 line, it appears that BMP-4 does not significantly modify gliomasphere number; it considerably increases the number of spheres formed from 20 ng/mL, up to doubling the number of spheres at 70 ng/mL treatment (404 gliomasphere versus 209 gliomasphere for non-treated). However, BMP-2 at 100 ng/mL reveals a rise in the number of spheres which is less important compared to the other conditions mentioned, or even a decrease in the number of spheres in the line U87-MG.

To avoid toxicity phenomena, this concentration will no longer constitute a dose of therapeutic interest in future trials. Moreover, 0, 4 and 4 ng/mL concentrations won't be considered for later experiments because of their lack of effect on both cell lines for both of the two molecules tested. Here also, evaluation of the effects of BMP-4 released from PLGA NPs are in course and may give complementary information.

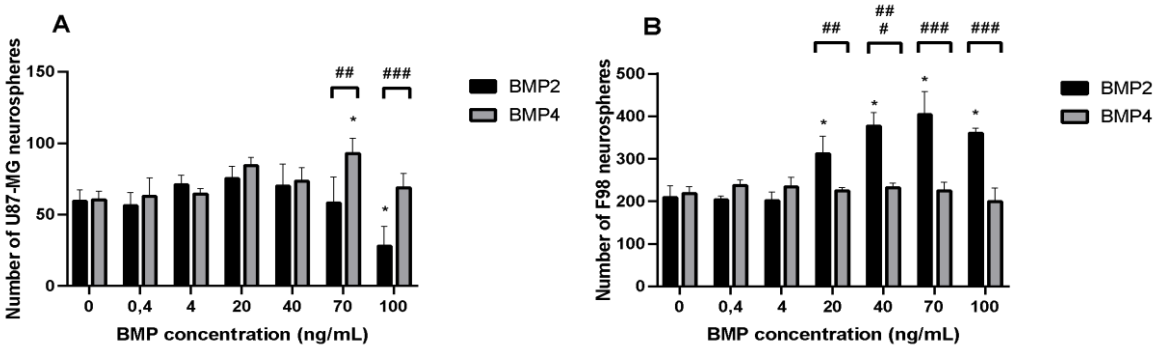


Figure 18. (A) Activity of BMPs at different concentrations on U87-MG and (B) F98 gliomasphere formation after 7 days of treatment. Values are presented as means ± standard deviation, n=4. * P<0, 05 versus corresponding

non-treated (NT) condition (0 ng/mL), ## P<0, 01, ### P<0,001 versus treatment to same concentration of different BMPs

2.2.4 Limiting dilution assay of gliomaspheres with BMP-4 and BMP-2

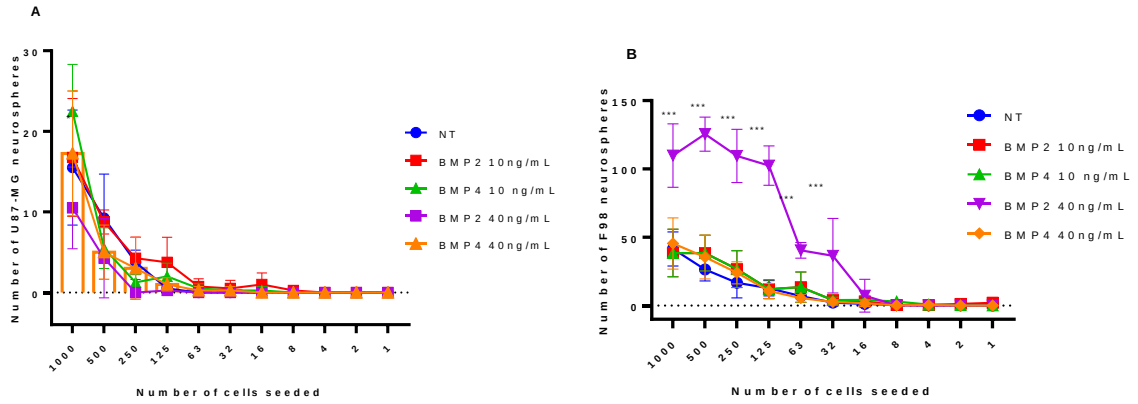


Figure 19. (A) Activity of BMPs on U87-MG and (B) F98 gliomasphere formation at 10 ng/mL and 40 ng/mL concentrations after 7 days of treatment. Values are presented as means ± standard deviation, n=4.
* P<0, 05, *** P<0,001 versus corresponding non-treated (NT) condition.

Limiting dilution assays (figure 19) were carried out to observe and quantify the formation of spheres in function of the number of seeded cells and the BMP concentration with which the wells were treated (10 ng/mL and 40 ng/mL). The curve profiles observed for the different treatment conditions in the U87-MG line are rather similar.

Most notable in the F98 cell line is the almost three-fold increase in the number of spheres with the condition treated with BMP-2 at 40 ng/mL (110 gliomaspheres versus 42 for non-treated). This also confirms the preliminary results obtained in the activity assay. Excluding this condition, there is no difference between the other conditions.

The results obtained for non-treated (NT) condition for both cell lines confirm our observation that F98 cells proliferate to a greater extent and form more spheres than U87-MG cells (42 F98 spheres and 16 U87-MG spheres at 1000 seeded cells). In addition, the F98 cells are able to form spheres with a minimum of 16 cells seeded per well, compared to 63 for the U87-MG line.

2.2.5. Radiosenzitising effect of BMP-4 and BMP-2 on gliomasphere model

We coupled the usual previous treatment to X-ray irradiation. U87-MG and F98 cells were treated at 10 ng/mL or 40 ng/mL of BMP-2 or BMP-4, and were then irradiated at 4 or 16 Gy. The control condition corresponds to untreated cells non-irradiated at the same doses. These results do not demonstrate an increase in sensitivity to radiotherapy. On the contrary, the tendency is to show that the cells seem to have proliferated more, if not the same, than in the untreated condition(Figure 20).

Concerning U87-MG cell line (Figure 20A), we find again this tendency of BMP-2 to increase cell proliferation, mainly at low X-ray dose irradiation (4 Gy), which could explain a non-decrease in cell proliferation even after irradiation at 16 Gy. However, BMP-4 increases cell proliferation under higher irradiation at 16 Gy (120% of non- treated proliferation at 10 ng/mL and 121% at 40 ng/mL).

Our results do not provide any difference in cell proliferation for the F98 cell line (Fig 20B), except from the condition treated with BMP-2 at 40 ng/mL and irradiated at 16 Gy which shows a proliferation increase (120%

of non-treated proliferation). These results tend to suggest a possible radioresistance induced by treatment with BMPs [51, 52], which is in contradiction with literature studies that has shown a pro-differenciating and sensitizing effect of BMP-4 on CSC and GB cell lines [17, 20, 23, 25]. Hence, an observational analysis of the phenotype of the gliomaspheres has been done 24 hours after treatment with BMPs highlights the fact that the irradiated U87-MG and F98 spheres dissociate and return to their state of individualized adherent cells (Figure 39 and 40 in annexes). In these pictures, U87MG are less in gliomasphere phenotype post treatment and radiotherapy: U87MG cells adhere to the plates, but the F98 cell line has dissociated gliomasphere shown through floating cells (Figure 39 and 40 in annexes).

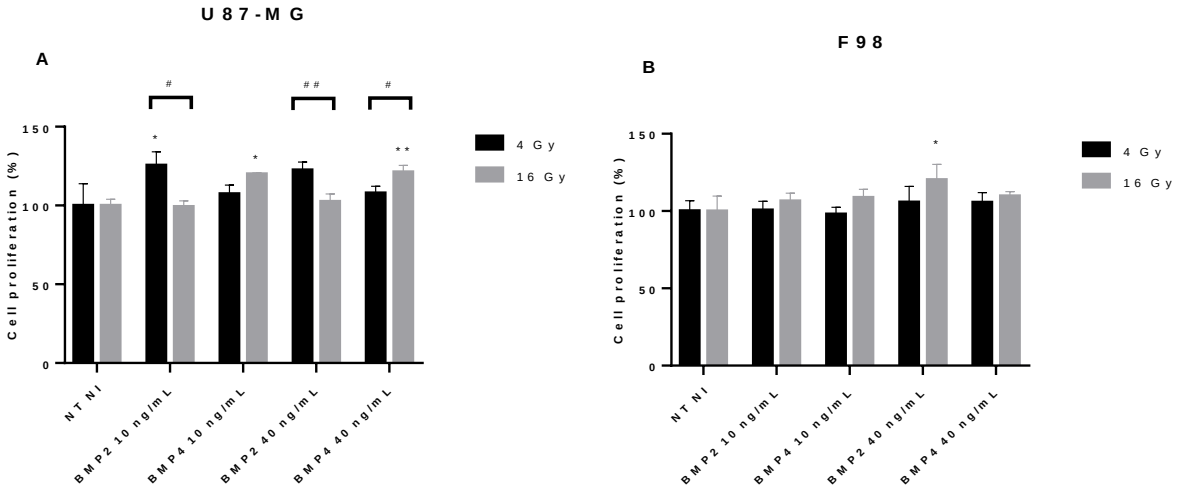


Figure 20 U87-MG (A) and F98 (B) cell proliferation assay 24 hours after X-ray irradiation at 4 Gy or 16 Gy and treatment with BMP-2 and -4. Values are presented as means ± standard deviation, n=4. * P<0, 05, ** P<0, 01 versus corresponding non- treated and non-irradiated (NT NI) condition; # P<0, 05, ## P<0, 05 versus treated condition compared to the same treatment

3. Conclusion

This study allows us to obtain high precipitation efficiencies of BMP-4 comparable to other studies and to protect the protein from degradation [42,44]. The encapsulation process has also been optimized and EE% are promising for future studies.

In terms of release profile, the study has shown a controlled release profile with a faster release for formulations 5 and 3. This has been shown in other studies but similarly, the released amount is not entire, in general between 50 and 85% of the drug is released in less than 10 day, which could be optimized with a more optimised PLGA polymer composition, by modifying the release medium, changing the physico-chemistry of NPs by chemically pegylating their surface to enhance the drug release and tuning the pH of the release compartment. The particle composition improved protein encapsulation efficiency while reducing protein release rate significantly. Furthermore, the model proteins were optimally incorporated at pH levels near to their isoelectric point. In terms of release kinetics, adding a PEO derivative like PEG to the PLGA matrix decreased the unwanted early burst effect more effectively than the more hydrophilic PLGA-poloxamer combination [59,89].

Besides, the blank NPs seem to be non cytotoxic after 24, 48 and 72 hours of incubation with direct contact with fibroblast cells, a result that is in accordance with the literature. Stability study of blank NPs also has shown a good stability post-lyophilisation with the presence of a cryoprotectant; and the stability study done with pH variation kept a constant zeta potential for pH4 and pH7 media, which is promising for their stability *in vivo* at a 7.4 pH. These precipitation and encapsulation results are interesting for scaling up to BMP-2 protein for a bone regeneration application.

In vitro results have shown an efficacy of BMP-4 and BMP-2 on gliomasphere models, and permit to compare two structurally close BMPs and see their result on 3D cell models and therefore their effect on tumorigenicity. Some results obtained in radiotherapy experimentations are counterintuitive with the literature, but a modification in the cell phenotype after treatment and irradiation compared to the control. This has been completed through differentiation markers study in flow cytometry on gliomasphere after treatment with BMP-4. Short term and long-term *in vivo* studies on rat models are in progress too in order to have a proof of concept concerning the biocompatibility and efficacy through histological and immunofluorescence assays. Experiments with BMP-4 loading PLGA NPs are in course and will complete soon this set of results.

Finally, this study will be continued with a second article consisting on a nanocomposite hydrogel loaded with the same developed PLGA NPs containing BMP-4 and its detailed characterization with *in vitro* studies (release, erosion test, cytotoxicity) and physico-chemical ones (DSC, Rheology, SAXS, SEM, ATR-FTIR, injectability) for a potential GB application.

4. Materials and Methods

4.1 Reagents

Ester-capped PLGA (Mn = 5.5 kDa) and PEG-PLGA copolymer (MnPEG = 5 kDa, MnPLGA = 25.7 kDa) were synthesized by a ring- opening polymerization method according to protocol described by (Haji Mansor et al., 2018). Glycofurol (Tetraglycol BioXtra®), isosorbide dimethyl ether. Lysozyme of chicken egg white, Micrococcus lysodeikticus, dimethyl sulfoxide (DMSO), sodium chloride, poloxamer 188 (Lutrol® F68),poloxamer 407,(Pluronic F-127) glycine, sucrose, 37% hydrochloric acid, 10 M sodium hydroxide, tris(hydroxymethyl)aminomethane (Tris) base (Trizma®), HEPES salt were obtained from Sigma-Aldrich (Saint Quentin Fallavier, France). Bovine serum albumin fraction V was obtained from Roche Diagnostics (Mannheim, Germany), human BMP-4 from Miltenyi Biotech (Paris, France), hydroxypropyl-β-cyclodextrin (Kleptose® HPBCD) from Roquette (Lestrem, France), Dulbecco's phosphate-buffered saline (Biowhittaker®) from Lonza (Verviers, Belgium), and Dulbecco's Modified Eagle's Medium (Gibco® DMEM) from Thermo Fisher Scientific (Villebon sur Yvette, France). Ultrapure water dispensed from a Milli-Q® Advantage A10 system (Millipore, Paris, France) was used in all experiments.

Dulbecco's modified Eagle's medium (DMEM) with 4.5 g/L Glucose, L-Glutamine and sodium pyruvate, Ham's F12 with L-Glutamine, Phosphate Buffered Saline (PBS), Hanks' Balanced Salt Solution (HBSS) were acquired from Lonza (Verviers, Belgium). Trypsin-EDTA (0,5 g porcine trypsin and 0,2 g EDTA), trypan blue, antibiotic solution (A5955, 10000 units penicillin, 10 mg streptomycin and 25 µg amphotericin B per mL) and heparin (H1027, ≥180 USP units/mg) were purchased from Sigma Aldrich (Saint-Louis, USA). Anti-phosphorylated Smad1/5/8 (AB3848-I, Ser463/465) antibody was acquired from Merck Millipore (Burlington, USA), anti-Smad1 (A1101) from ABclonal (Woburn, United States) and anti-rabbit HRP conjugate (111-035-003) was obtained from Jackson ImmunoResearch (Cambridgeshire, United Kingdom). B27 (17504-044) was purchased from Invitrogen (Gibco, Invitrogen, Carlsbad, New Mexico, USA), fetal bovine serum (FBS) from Eurobio (AbCys, Les Ulis, France), and human recombinant EGF and FGF-2 from Miltenyi Biotech (Bergisch Gladbach, Germany).Human U87MG and rat F98 GB cell lines , NIH3T3T and L929 fibroblast cell lines purchased from the American type Culture Collection (ATCC, LGC Standards, Molsheim, France)

4.2 Nanoprecipitation and encapsulation processes:

Let GF at 4°C for 30 min, to maintain the protein in its functional and native conformation and to limit its mobility in solution. Dissolve P188 in a suitable buffer and mix with the protein. Add the mixture of BMP-4-P188 in the cold GF then let it for 20 min at 4° C. After that, vortex gently o and put for 10 min more at 4°C. After nanoprecipitation follows an encapsulation process based on coacervation also called phase separation process (figure 21). Precipitation efficiency is determined dosing the pellet protein content and encapsulation efficiency has been determined using the following formula:

Precipitation efficiency method

$$EE\ (\%) = \frac{Mass\ of\ protein\ quantified\ after\ precipitation}{Initial\ mass\ of\ protein\ used\ for\ formulation} \times 100$$

Encapsulation efficiency via the direct method

$$EE\ (\%) = \frac{Mass\ of\ protein\ quantified\ in\ formulation}{Initial\ mass\ of\ protein\ used\ for\ formulation} \times 100$$

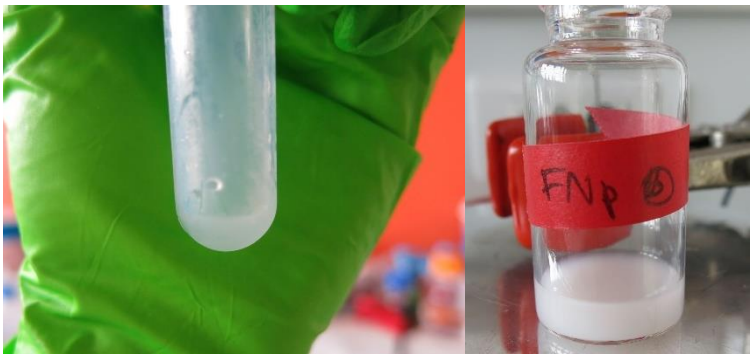


Figure 21: BMP-4 protein nanoprecipitation (left) and PLGA nanoparticles obtained by phase inversion method (right)

4.2.1 Protein quantification and activity:

Lysozyme was quantified using Micrococcus Leidococcus cell suspension as a substrate as described in the literature [67,84]. Micro BCA assay was used to quantify total protein amount. For encapsulation efficiency and release studies BMP-4 activity and quantification were assessed using ELISA (enzyme-linked immunosorbent assay) DuoSet Kit for BMP-4 from R&D Systems. Lysozyme has a 11.35 pI and Mw of 14kDa according to Sigma Aldrich provider; BMP-4 7.6 pI and 26.2kDa according to the protein data bank and the provider Miltenyi Biotech

Regarding the supplier's instructions (R&D Systems, Lille, France). In summary, BMP-4 capture antibody solution was added to a Nunc Maxisorp® 96-well microplate (Thermo Fisher Scientific) and incubated overnight for wells' coating. The microplate was then washed with 0.05% (w/v) Tween® 20 in phosphate-buffered saline (PBS) solution (pH 7.4), followed by a 1-hour incubation with PBS solution (pH 7.4) containing 1% (w/v) BSA to block non-specific sites. After washing, the kit standard and samples diluted in PBS (pH 7.4) containing 1% (w/ v) BSA were added to the microplate for a 2-h incubation. Then, the microplate was washed before addition of a detection antibody solution for another 2-h incubation. The washing step was afterwards repeated before incubation with a streptavidin-horseradish peroxidase solution for 20 min. After the final wash, substrate solution was added for another 20-min incubation. Finally, 2N sulphuric acid was added to terminate the enzymatic reaction followed by immediate measurement of absorbance at 450 nm. All incubations were done at room temperature.

4.3 Physicochemical characterization of nanoparticles and nanoprecipitates:

4.3.1 Dynamic Light Scattering:

The DLS measurements were performed using a Malvern Zetasizer and its software. Measurements were performed at 25°C. The results were presented in the table. Zeta potentials were derived from electrophoretic mobility values using Smoluchowski's approximation. Nanoparticle samples were prepared by dilution in water or 0.01 M NaCl solution for size and zeta-potential measurements respectively, to obtain concentrations suitable for analyses in a Nanosizer® ZS (Malvern) such that the attenuator value was in the range of 5–7. Each sample was measured in triplicate, with each measurement representing an average value of at least 10 runs. All measurements were made at 25 °C under automatic mode. Besides average particle size, the DLS protocol of Nanosizer® ZS produced a PDI value ranging between 0 and 1 that estimates the width of the size distribution. Datas were processed with GraphPad Prism 9.

4.3.2 TEM and SEM:

The nanoparticle and nanoprecipitates' morphology was visualized under TEM (JEM 1400, JEOL Paris, France). A 5 μL drop of purified nanoparticle suspension at a concentration of 200 μg/mL was added onto the

center of a mica slide (for SEM) or carbon-coated nickel grid (for TEM), and left to dry overnight at room temperature. Images have been analyzed using ImageJ software. The observation has been done using the SEM (ZEISS EVO/LS10). For SEM, the sample was coated with a gold layer of 5 nm thickness before observation whereas no coating was applied to TEM. Images have been analyzed using ImageJ software.

4.3.3 ATR-FTIR

Studies of the polymers structure have been done on a range of 400-4000cm-1 at room temperature on semi-solid samples, solid and liquid samples on a BRUKER Vertex 70 spectrometer. Data has been processed and baseline corrections done with the software KnowItAll Informatics System 2021 from Wiley Science Solutions.

4.3.4 Nanoparticles stability study

Lyophilisation has been performed using a Lyovac STERIS GT2 cryodessicator, coupled to an Alcatel vacuum pump and a cryothermostat HUBER CC-505. Size, Zeta Potential and PDI of the nanoparticles has been investigated before and after lyophilisation with sucrose and HPBCD.

4.4 *In vitro* assays:

4.4.1 Adherent Cell culture:

U87-MG cells are routinely cultured at 10^4 cells/cm² in Dulbecco's modified Eagle's medium (DMEM) containing 4.5 g/L glucose and L-glutamine supplemented with 10 % (v/v) fetal bovine serum (FBS) and 1% antibiotic solution. F98 cells are routinely cultured at 8.10^3 cells/cm² in Dulbecco's modified Eagle's medium (DMEM) containing 4.5 g/L glucose and L-glutamine supplemented with 10 % (v/v) fetal bovine serum (FBS) and 1% antibiotic solution. NIH/3T3 cells are routinely cultured at 10^4 cells/cm² in Dulbecco's modified Eagle's medium (DMEM) containing 4.5 g/L glucose and L-glutamine supplemented with 10 % (v/v) fetal bovine serum (FBS) and 1% antibiotic solution. All Cells were maintained at 37 °C in a humidified 5 % CO_2 atmosphere.

4.4.2 Neurosphere culture

F98 (8.10^3 cells/cm²) and U87-MG (10^4 cells/cm²) were cultured in spheres using neurosphere medium, composed of a basis of DMEM: F12 (1:1), supplemented with 1‰ heparin, 2‰ EGF and FGF-2 and 2% B27. On the third day of culture, one half of the medium is replaced by a new medium. Spheres are dissociated the seventh day using HBSS. Proliferation assays have been done using the CyQUANT® proliferation assay

4.4.4 Limiting dilution

F98 and U87-MG spheres were cultured for 7 days, and then dissociated into single cells to be seeded again for 7 days in 96-well plates at various cell concentration : 1000, 500, 250, 125, 63, 32, 16, 8, 4, 2 and 1 cell in 200 µL of neurosphere medium. Cells were either treated with BMP-2 or BMP-4, both at 10 and 40 ng/mL, or non-treated. Each condition has been done in quadruplicate, and the number of spheres formed is counted with ImageJ from fields of a surface of 8.25 mm² (a quarter of a well). Are only counted the spheres which contain at least 6 cells. The spheres that have merged or are in the process of merging are counted individually as far as possible (2 merged spheres count for 2 spheres)

4.4.5 Assessment of BMP-4 bioactivity:

F98 and U87-MG spheres were cultured for 7 days, and then dissociated into single cells to be seeded again for 7 days in 96-well plates (both cell lines at $1{,}0x10^3$ cells/well) and treated with various cell concentrations of BMP-2 or BMP-4 : 0 (non-treated), 0.4, 4, 10, 20, 40, 70 and 100 ng/mL in 200 µL of gliomasphere medium. Each condition has been done in quadruplicate, and the number of spheres formed is precisely counted with ImageJ

after whole photo reconstitution of each well. Are only counted the spheres which contain at least 6 cells. The spheres that have merged or are in the process of merging are counted individually as far as possible (2 merged spheres count for 2 spheres).

4.4.6 Western blotting

F98 ($2.0x10^5$ cells/flask) and U87-MG ($2.5x10^5$ cells/flask) were cultured in flasks for 48 hours, starved at 24h. Lysate supernatants (20 µg of protein) were separated electrophoretically and transferred to PVDF membranes (Cytiva, Thermofisher Scientific, USA). After blocking, membranes were incubated overnight using anti-Smad1 (A1101, 1:1000) or anti-phosphorylated Smad1/5/8 (AB3848-I, 1:1000) antibodies. Membranes were then incubated with the secondary anti-rabbit antibody (111-035-003, 1:10000) for 1 hour.

4.4.7 X-Ray radiation

F98 (8.10^3 cell/cm^2) and U87-MG (10^4 cell/cm^2) cells were cultured for 72 hours. Cells were treated at 24 hours with 100 µL of BMP-2 or BMP-4 diluted in serum free DMEM, both at 10 and 40 ng/mL. The untreated control condition corresponds to the addition of 100 µL of medium alone and no irradiation. Each condition has been done in quadruplicate. Cells were irradiated at 72 hours using Edimex FAXITRON (160 kV, 6,3 mA) at a dose of 4 Gray or 16 Gray. Cell proliferation was then evaluated 48 hours after irradiation using MTS proliferation assay.

4.4.8 In *vitro* cytotoxicity of blank nanoparticles:

The proliferation ability of cells was assessed using (3-(4, 5-dimethylthiazol-2-yl)-5-(3-carboxymethyl phenyl)-2-(4-sulfophenyl)-2H-tetrazolium) (MTS reagent) (Promega, Madison, USA). For each condition to be tested, medium was removed and replaced with a mixture of 100 µL MTS reagent and 500 µl DMEM containing 10% FBS. After 3 hours of incubation, 100 µl of the supernatant was transferred in 96-well plate following the manufacturer's instructions. The absorbance of each well was detected at 490 nm with the Multiskan (Thermofisher Scientific, USA) microplate reader. Each condition has been done in quadruplicate.

Statistical analysis

Three independent experiments were performed to confirm the reproducibility of the results. Graph Pad Software Inc. (San Diego, CA, USA) was used for statistical evaluation. Results were compared through two-way analysis of variance (ANOVA) and t-test. Differences between datasets with $p<0.05$ were considered statistically significant. Statistical analyses were performed comparing all treatments to the control.

Concluding remark of Chapter 4:

This paper describes the development of novel BMP-4 nanocarriers made of PLGA-COOR and a PEG-PLGA co-polymer. BMP-4 was efficiently precipitated and loaded into these nanoparticles under mild formulation conditions after optimization with lysozyme as a model protein. BMP-4 was also gradually released in its bioactive form. Moreover, by changing the ratio of PLGA-COOR / PLGA-PEG capped carboxylic acid groups in the PLGA core, the unique formulation approach permits the generation of nanoparticles with variable physicochemical characteristics that impact encapsulation efficiency and the degree of protein release. Furthermore, the use of non-toxic polymers and solvents guaranteed that the synthesized nanoparticles were highly biocompatible. Hence, the innovative BMP-4 nanocarriers show promise for future cancer cell trapping applications and will be put into a suitable hydrogel for researching glioblastoma cell development.

A unique formulation approach generating homogenous nanoparticles with high BMP-4 encapsulation efficiency and strong cytocompatibility was established in this section of the investigation. Because of its versatility, PLGA was employed as the principal material polymer in the production of the nanoparticles. It is a lactic acid and glycolic acid co-polymer, which means that its molecular chain always terminates with a carboxyl group, which offers a site for chemical conjugation or physical contact with other polymers or protein

molecules (figure 22). For example, PLGA may be conjugated with a hydrophilic polymer like PEG to generate an amphiphilic di-block (as developed in this work) or tri-block co-polymer [87] that can be utilized to replace surfactant molecules, which are frequently required in the manufacture of micro/nanoparticles.

Once the carboxyl groups are uncapped, they can engage electrostatically with basic protein molecules, contributing to high encapsulation efficiencies. Because it is a hydrophobic polymer, PLGA degrades slowly in water [93]. This feature is anticipated to be useful in the creation of polymer-based carriers designed to facilitate prolonged protein release. Because the lactide component of PLGA has a methyl side group, it is more hydrophobic than the glycolide residue. A high lactide-to-glycolide ratio is thus beneficial in reducing the hydrolytic breakdown of PLGA [94].

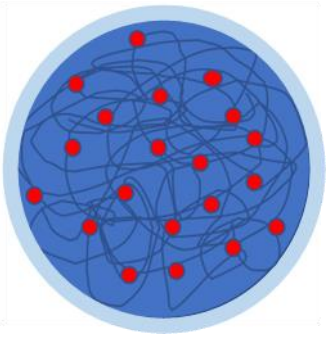


Figure 22 Model structure of the BMP-4-loaded PLGA-COOR/PEG-PLGA nanoparticles developed in this study.

The lactide-to-glycolide ratio of the PLGA-COOR and PEG-PLGA used in this study was 75:25. The formulated nanoparticles were projected to degrade slowly as a result of this. Actually, the degradation period of PLGA 75:25 has been observed to be many months [95,96]. Despite this, when maintained in proper release medium, the produced nanoparticles were demonstrated to release the majority of their protein content rather quickly (about 48 hours). While the rate of particle disintegration appears to be a key predictor of release kinetics, it is not the only factor that influences the rate of diffusion of water molecules into the polymer matrix and the consequent dissolution of the protein load [97].

Remaining organic solvents like GF and DMI may diffuse out of the matrix material during the extraction step has frequently resulted in the creation of porous nanoparticles [98]. These holes might enhance the overall surface area accessible to the release media and hasten the dissolution of surface-adsorbed or partly embedded protein molecules in the polymer matrix. This explains why the created nanoparticle technology produced such a large burst discharge. Furthermore, the porous interior structure may minimize the distance of diffusion necessary for the embedded protein molecules to escape from the polymer matrix, reducing the overall latency of protein release [62,67,68].

Because of the fast protein release from the nanoparticles, the bioperformance on GBM cells in the brain is anticipated to be limited. GBMs are known to be very invasive and can spread across the brain parenchyma. An autopsy research identified infiltrating GBM cells up to 14 mm distant from the tumor boundary as defined by magnetic resonance imaging (MRI) [99,100]. Because surgical excision of GBM is often identified by contrast-enhanced regions in MRI, these infiltrating GBM cells were frequently left in the brain and might grow to re-form the tumor [101]. In fact, 96% of GBM recurrences occurred within 20 mm of the tumor boundary as determined by MRI [67,102].

Acknowledgments: This work was carried out with support from by La Ligue Contre le Cancer (grant number TARC21174 to A.D.). It was also supported by the Institut National de la Santé et de la Recherche Médicale (INSERM) and by the University of Angers (Angers, France). The work was in addition related : (i) to the Region Pays-de-la-Loire programs to F.B. : Bioimplants for Bone Regeneration (BILBO) part of the BIOREGATE Research-Training-Innovation

consortium (RFI) and NanoFar + (International Strategy) and (ii) to the French Na-tional Research Agency (ANR) under the frame of EuroNanoMed III (project GLIOSILK) and through the LabEx IRON (Innovative Radiopharmaceuticals in Oncology and Neurology) as part of the French government Investissements d'Avenir program (ANR-11-LABX-0018 to E.G.).". Romain Mallet of the SCIAM (Common service for Imaging and microscopy analysis, Angers, France) for SEM and TEM analyses. Olivier Laeveque from MOLTECH (plateau CARMA / SFR MATRIX) for ATR-FTIR analyses Olivier Thomas from MINT for DLS and freeze-drying.

References:

[1] Alifieris C, Trafalis DT. Glioblastoma multiforme: Pathogenesis and treatment. Pharmacology & Therapeutics 2015;152:63–82. https://doi.org/10.1016/j.pharmthera.2015.05.005.

[2] Adamson C, Kanu OO, Mehta AI, Di C, Lin N, Mattox AK, et al. Glioblastoma multiforme: a review of where we have been and where we are going. Expert Opinion on Investigational Drugs 2009;18:1061–83. https://doi.org/10.1517/13543780903052764.

[3] Louis DN. The 2016 World Health Organization Classification of Tumors of the Central Nervous System: a summary. Acta Neuropathol 2016:18.

[4] Stupp R, Weller M, Belanger K, Bogdahn U, Ludwin SK, Lacombe D, et al. Radiotherapy plus Concomitant and Adjuvant Temozolomide for Glioblastoma. The New England Journal of Medicine 2005:10.

[5] Stupp R, Brada M. High-grade glioma: ESMO Clinical Practice Guidelines for diagnosis, treatment and follow-up. Annals of Oncology 2014;25:9.

[6] Zhang J, Stevens MFG, Bradshaw TD. Temozolomide: mechanisms of action, repair and resistance. Curr Mol Pharmacol 2012;5:102–14. https://doi.org/10.2174/1874467211205010102.

[7] Strobel H, Baisch T, Fitzel R, Schilberg K, Siegelin MD, Karpel-Massler G, et al. Temozolomide and Other Alkylating Agents in Glioblastoma Therapy. Biomedicines 2019;7. https://doi.org/10.3390/biomedicines7030069.

[8] Alves ALV, Gomes INF, Carloni AC, Rosa MN, da Silva LS, Evangelista AF, et al. Role of glioblastoma stem cells in cancer therapeutic resistance: a perspective on antineoplastic agents from natural sources and chemical derivatives. Stem Cell Research & Therapy 2021;12:206. https://doi.org/10.1186/s13287-021-02231-x.

[9] Bradshaw A, Wickremesekera A, Brasch HD, Chibnall AM, Davis PF, Tan ST, et al. Cancer Stem Cells in Glioblastoma Multiforme. Front Surg 2016;3. https://doi.org/10.3389/fsurg.2016.00048.

[10] Altaner C. Glioblastoma and stem cells. Neoplasma 2008;55:369–74.

[11] Perry J, Chambers A, Spithoff K, Laperriere N, on behalf of the Neuro-Oncology Disease Site Group§ of Cancer Care Ontario's Program in Evidence-Based Care. Gliadel Wafers in the Treatment of Malignant Glioma: A Systematic Review. Current Oncology 2007;14:189–94. https://doi.org/10.3747/co.2007.147.

[12] Perry J, Chambers A, Spithoff K, Laperriere N. Gliadel wafers in the treatment of malignant glioma: a systematic review. Curr Oncol 2007;14:189–94. https://doi.org/10.3747/co.2007.147.

[13] Ashby LS, Smith KA, Stea B. Gliadel wafer implantation combined with standard radiotherapy and concurrent followed by adjuvant temozolomide for treatment of newly diagnosed high-grade glioma: a systematic literature review. World J Surg Onc 2016;14:225. https://doi.org/10.1186/s12957-016-0975-5.

[14] Dang W, Daviau T, Brem H. Morphological Characterization of Polyanhydride Biodegradable Implant Gliadel® During in Vitro and in Vivo Erosion Using Scanning Electron Microscopy. Pharm Res 1996;13:683–91. https://doi.org/10.1023/A:1016035229961.

[15] d'Avella D, DellaPuppa A. Safety and efficacy of Gliadel wafers for newly diagnosed and recurrent glioblastomas. Acta Neurochir 2012;154:1379–81. https://doi.org/10.1007/s00701-012-1414-1.

[16] NISHIKAWA R, IWATA H, SAKATA Y, MURAMOTO K, MATSUOKA T. Safety of Gliadel Implant for Malignant Glioma: Report of Postmarketing Surveillance in Japan. Neurol Med Chir (Tokyo) 2021;61:536–48. https://doi.org/10.2176/nmc.oa.2021-0024.

[17] De Bonis P, Anile C, Pompucci A, Fiorentino A, Balducci M, Chiesa S, et al. Safety and efficacy of Gliadel wafers for newly diagnosed and recurrent glioblastoma. Acta Neurochirurgica 2012;154:1371–8. https://doi.org/10.1007/s00701-012-1413-2.

[18] Silva J, Miranda A, Sousa J, Pais A, Vitorino C. Impact of Immunotherapy in the Treatment of Glioblastoma. IntechOpen; 2018. https://doi.org/10.5772/intechopen.78603.

[19] Tivnan A. Advances in immunotherapy for the treatment of glioblastoma. J Neurooncol 2017:9.

[20] Banerjee K, Núñez FJ, Haase S, McClellan BL, Faisal SM, Carney SV, et al. Current Approaches for Glioma Gene Therapy and Virotherapy. Frontiers in Molecular Neuroscience 2021;14.
[21] Okura H, Smith CA, Rutka JT. Gene therapy for malignant glioma. Mol Cell Ther 2014;2:21. https://doi.org/10.1186/2052-8426-2-21.
[22] Tobias A, Ahmed A, Moon K-S, Lesniak MS. The art of gene therapy for glioma: a review of the challenging road to the bedside. J Neurol Neurosurg Psychiatry 2013;84:213–22. https://doi.org/10.1136/jnnp-2012-302946.
[23] Oliver R. Principles and practice of the biologic therapy of cancer (third edition). Br J Cancer 2002;86:662–3. https://doi.org/10.1038/sj.bjc.6600090.
[24] Schirrmacher V. From chemotherapy to biological therapy: A review of novel concepts to reduce the side effects of systemic cancer treatment (Review). Int J Oncol 2018;54:407–19. https://doi.org/10.3892/ijo.2018.4661.
[25] Mellinghoff IK, Schultz N, Mischel PS, Cloughesy TF. Will Kinase Inhibitors Make it as Glioblastoma Drugs? Curr Top Microbiol Immunol 2012;355:135–69. https://doi.org/10.1007/82_2011_178.
[26] Kim G, Ko YT. Small molecule tyrosine kinase inhibitors in glioblastoma. Arch Pharm Res 2020;43:385–94. https://doi.org/10.1007/s12272-020-01232-3.
[27] Sgouros G. RADIOPHARMACEUTICAL THERAPY. Health Phys 2019;116:175–8. https://doi.org/10.1097/HP.0000000000001000.
[28] Bolcaen J, Kleynhans J, Nair S, Verhoeven J, Goethals I, Sathekge M, et al. A perspective on the radiopharmaceutical requirements for imaging and therapy of glioblastoma. Theranostics 2021;11:7911–47. https://doi.org/10.7150/thno.56639.
[29] Lacroix M, Abi-Said D, Fourney DR, Gokaslan ZL, Shi W, DeMonte F, et al. A multivariate analysis of 416 patients with glioblastoma multiforme: prognosis, extent of resection, and survival. J Neurosurg 2001;95:190–8. https://doi.org/10.3171/jns.2001.95.2.0190.
[30] Dreyfus M, El-Atifi M, Court M, Bidart M, Coutton C, Leclech C, et al. Reprogramming glioma cell cultures with retinoic acid: Additional arguments for reappraising the potential of retinoic acid in the context of personalized glioma therapy. Glioma 2018;1:66. https://doi.org/10.4103/glioma.glioma_3_18.
[31] Campos B, Weisang S, Osswald F, Ali R, Sedlmeier G, Bageritz J, et al. Retinoid resistance and multifaceted impairment of retinoic acid synthesis in glioblastoma. Glia 2015;63:1850–9. https://doi.org/10.1002/glia.22849.
[32] Campos B, Centner F-S, Bermejo JL, Ali R, Dorsch K, Wan F, et al. Aberrant expression of retinoic acid signaling molecules influences patient survival in astrocytic gliomas. Am J Pathol 2011;178:1953–64. https://doi.org/10.1016/j.ajpath.2011.01.051.
[33] Piccirillo SGM, Reynolds BA, Zanetti N, Lamorte G, Binda E, Broggi G, et al. Bone morphogenetic proteins inhibit the tumorigenic potential of human brain tumour-initiating cells. Nature 2006;444:761–5. https://doi.org/10.1038/nature05349.
[34] Nayak S, Mahenthiran A, Yang Y, McClendon M, Mania-Farnell B, James CD, et al. Bone Morphogenetic Protein 4 Targeting Glioma Stem-Like Cells for Malignant Glioma Treatment: Latest Advances and Implications for Clinical Application. Cancers 2020;12:516. https://doi.org/10.3390/cancers12020516.
[35] Xi G, Best B, Mania-Farnell B, James CD, Tomita T. Therapeutic Potential for Bone Morphogenetic Protein 4 in Human Malignant Glioma. Neoplasia 2017;19:261–70. https://doi.org/10.1016/j.neo.2017.01.006.
[36] Piccirillo S, Combi R, Cajola L, Patrizi A, Redaelli S, Bentivegna A, et al. Distinct pools of cancer stem-like cells coexist within human glioblastomas and display different tumorigenicity and independent genomic evolution. Oncogene 2009;28:1807–11. https://doi.org/10.1038/onc.2009.27.
[37] Hughes JH, Ewy JM, Chen J, Wong SY, Tharp KM, Stahl A, et al. Transcriptomic analysis reveals that BMP4 sensitizes glioblastoma tumor-initiating cells to mechanical cues. Matrix Biol 2020;85–86:112–27. https://doi.org/10.1016/j.matbio.2019.06.002.
[38] Koguchi M, Nakahara Y, Ito H, Wakamiya T, Yoshioka F, Ogata A, et al. BMP4 induces asymmetric cell division in human glioma stem-like cells. Oncology Letters 2020;19:1247–54. https://doi.org/10.3892/ol.2019.11231.
[39] Sundermann J, Zagst H, Kuntsche J, Wätzig H, Bunjes H. Bone Morphogenetic Protein 2 (BMP-2) Aggregates Can be Solubilized by Albumin—Investigation of BMP-2 Aggregation by Light Scattering and Electrophoresis. Pharmaceutics 2020;12:1143. https://doi.org/10.3390/pharmaceutics12121143.

[40] Persano L, Pistollato F, Rampazzo E, Della Puppa A, Abbadi S, Frasson C, et al. BMP2 sensitizes glioblastoma stem-like cells to Temozolomide by affecting HIF-1α stability and MGMT expression. Cell Death Dis 2012;3:e412. https://doi.org/10.1038/cddis.2012.153.
[41] Chen D, Zhao M, Mundy GR. Bone Morphogenetic Proteins. Growth Factors 2004;22:233–41. https://doi.org/10.1080/08977190412331279890.
[42] Fawwaz Abdullah M, Muhamad M, Ab-Rahim S. The role of bone morphogenetic protein 2 in the reprogramming of cancer stem cells. Biomedicalresearch 2019;30. https://doi.org/10.35841/biomedicalresearch.30-19-039.
[43] Barati D, Shariati SRP, Moeinzadeh S, Melero-Martin JM, Khademhosseini A, Jabbari E. Spatiotemporal release of BMP-2 and VEGF enhances osteogenic and vasculogenic differentiation of human mesenchymal stem cells and endothelial colony-forming cells co-encapsulated in a patterned hydrogel. Journal of Controlled Release 2016;223:126–36. https://doi.org/10.1016/j.jconrel.2015.12.031.
[44] Cai H, Zou J, Wang W, Yang A. BMP2 induces hMSC osteogenesis and matrix remodeling. Molecular Medicine Reports 2021;23:1–1. https://doi.org/10.3892/mmr.2020.11764.
[45] Miyazono K, Kamiya Y, Morikawa M. Bone morphogenetic protein receptors and signal transduction. Journal of Biochemistry 2009;147:35–51. https://doi.org/10.1093/jb/mvp148.
[46] Wang RN, Green J, Wang Z, Deng Y, Qiao M, Peabody M, et al. Bone Morphogenetic Protein (BMP) signaling in development and human diseases. Genes & Diseases 2014;1:87–105. https://doi.org/10.1016/j.gendis.2014.07.005.
[47] Beederman M, Lamplot JD, Nan G, Wang J, Liu X, Yin L, et al. BMP signaling in mesenchymal stem cell differentiation and bone formation. JBiSE 2013;06:32–52. https://doi.org/10.4236/jbise.2013.68A1004.
[48] Beier D, Hau P, Proescholdt M, Lohmeier A, Wischhusen J, Oefner PJ, et al. CD133 $^{+}$ and CD133 $^{-}$ Glioblastoma-Derived Cancer Stem Cells Show Differential Growth Characteristics and Molecular Profiles. Cancer Res 2007;67:4010–5. https://doi.org/10.1158/0008-5472.CAN-06-4180.
[49] Giacomini D, Páez-Pereda M, Theodoropoulou M, Gerez J, Nagashima AC, Chervin A, et al. Bone morphogenetic protein-4 control of pituitary pathophysiology. Front Horm Res 2006;35:22–31. https://doi.org/10.1159/000094262.
[50] Giacomini D, Acuña M, Gerez J, Nagashima AC, Silberstein S, Páez-Pereda M, et al. Pituitary Action of Cytokines: Focus on BMP-4 and gp130 Family. NEN 2007;85:94–100. https://doi.org/10.1159/000100428.
[51] Tsukamoto N, Otsuka F, Miyoshi T, Yamanaka R, Inagaki K, Yamashita M, et al. Effects of bone morphogenetic protein (BMP) on adrenocorticotropin production by pituitary corticotrope cells: involvement of up-regulation of BMP receptor signaling by somatostatin analogs. Endocrinology 2010;151:1129–41. https://doi.org/10.1210/en.2009-1102.
[52] Nie H, Ho M-L, Wang C-K, Wang C-H, Fu Y-C. BMP-2 plasmid loaded PLGA/HAp composite scaffolds for treatment of bone defects in nude mice 2009:10.
[53] Sequeira JAD, Santos AC, Serra J, Veiga F, Ribeiro AJ. Chapter 10 - Poly(lactic-co-glycolic acid) (PLGA) matrix implants. In: Grumezescu AM, editor. Nanostructures for the Engineering of Cells, Tissues and Organs, William Andrew Publishing; 2018, p. 375–402. https://doi.org/10.1016/B978-0-12-813665-2.00010-7.
[54] Feczkó T, Tóth J, Dósa G, Gyenis J. Optimization of protein encapsulation in PLGA nanoparticles. Chemical Engineering and Processing 2011:9.
[55] Giteau A, Venier-Julienne M-C, Marchal S, Courthaudon J-L, Sergent M, Montero-Menei C, et al. Reversible protein precipitation to ensure stability during encapsulation within PLGA microspheres. Eur J Pharm Biopharm 2008;70:127–36. https://doi.org/10.1016/j.ejpb.2008.03.006.
[56] Cerqueira BBS, Lasham A, Shelling AN, Al-Kassas R. Development of biodegradable PLGA nanoparticles surface engineered with hyaluronic acid for targeted delivery of paclitaxel to triple negative breast cancer cells. Materials Science and Engineering C 2017:8.
[57] Chavan YR, Tambe SM, Jain DD, Khairnar SV, Amin PD. Redefining the importance of polylactide-co-glycolide acid (PLGA) in drug delivery. Annales Pharmaceutiques Françaises 2021. https://doi.org/10.1016/j.pharma.2021.11.009.
[58] Bramwell VW, Perrie Y. Particulate delivery systems for vaccines. Crit Rev Ther Drug Carrier Syst 2005;22:151–214. https://doi.org/10.1615/critrevtherdrugcarriersyst.v22.i2.20.

[59] Santander-Ortega MJ, Csaba N, González L, Bastos-González D, Ortega-Vinuesa JL, Alonso MJ. Protein-loaded PLGA–PEO blend nanoparticles: encapsulation, release and degradation characteristics. Colloid Polym Sci 2010;288:141–50. https://doi.org/10.1007/s00396-009-2131-z.
[60] Allahyari M. Peptide/protein vaccine delivery system based on PLGA particles. HUMAN VACCINES n.d.:24.
[61] Molina-Peña R, Haji Mansor M, Najberg M, Thomassin J-M, Gueza B, Alvarez-Lorenzo C, et al. Nanoparticle-containing electrospun nanofibrous scaffolds for sustained release of SDF-1α. International Journal of Pharmaceutics 2021;610:121205. https://doi.org/10.1016/j.ijpharm.2021.121205.
[62] Swed A. Sustained release of TGF-β1 from biodegradable microparticles prepared by a new green process in CO2 medium. International Journal of Pharmaceutics 2015:9.
[63] Pratiwi RD, Agustiyanti DF, Agustiani F, Warsito MF, Mustopa AZ. Encapsulation of proteins with high/low pI in PLGA-particles for oral delivery. IOP Conf Ser: Mater Sci Eng 2021;1011:012026. https://doi.org/10.1088/1757-899X/1011/1/012026.
[64] Lee PW, Pokorski JK. PLGA Devices: Production and Applications for Sustained Protein Delivery. Wiley Interdiscip Rev Nanomed Nanobiotechnol 2018. https://doi.org/10.1002/wnan.1516.
[65] Fredenberg S, Wahlgren M, Reslow M, Axelsson A. The mechanisms of drug release in poly(lactic-co-glycolic acid)-based drug delivery systems—A review. International Journal of Pharmaceutics 2011:19.
[66] Sah H, Thoma L, Desu H, Sah E, Wood G. Concepts and practices used to develop functional PLGA-based nanoparticulate systems. International Journal of Nanomedicine 2013;8:747–65. https://doi.org/10.2147/IJN.S40579.
[67] Haji Mansor M, Najberg M, Contini A, Alvarez-Lorenzo C, Garcion E, Jérôme C, et al. Development of a non-toxic and non-denaturing formulation process for encapsulation of SDF-1α into PLGA/PEG-PLGA nanoparticles to achieve sustained release. Eur J Pharm Biopharm 2018;125:38–50. https://doi.org/10.1016/j.ejpb.2017.12.020.
[68] Swed A, Cordonnier T, Fleury F, Boury F. Protein Encapsulation into PLGA Nanoparticles by a Novel Phase Separation Method Using Non-Toxic Solvents. Journal of Nanomedicine & Nanotechnology 2014;6. https://doi.org/10.4172/2157-7439.1000241.
[69] van de Witte P, Dijkstra PJ, van den Berg JWA, Feijen J. Phase separation processes in polymer solutions in relation to membrane formation. Journal of Membrane Science 1996;117:1–31. https://doi.org/10.1016/0376-7388(96)00088-9.
[70] Ruiz JM, Busnel JP, Benoît JP. Influence of average molecular weights of poly(DL-lactic acid-co-glycolic acid) copolymers 50/50 on phase separation and in vitro drug release from microspheres. Pharm Res 1990;7:928–34. https://doi.org/10.1023/a:1015945806917.
[71] Tarhini M, Benlyamani I, Hamdani S, Agusti G, Fessi H, Greige-Gerges H, et al. Protein-Based Nanoparticle Preparation via Nanoprecipitation Method. Materials 2018;11:394. https://doi.org/10.3390/ma11030394.
[72] Morales-Cruz M. Two-step nanoprecipitation for the production of protein-loaded PLGA nanospheres. Results in Pharma Sciences 2012:7.
[73] Schwartz D, Sofia S, Friess W. Integrity and stability studies of precipitated rhBMP-2 microparticles with a focus on ATR-FTIR measurements. Eur J Pharm Biopharm 2006;63:241–8. https://doi.org/10.1016/j.ejpb.2005.12.011.
[74] Teixeira M, Alonso MJ, Pinto MMM, Barbosa CM. Development and characterization of PLGA nanospheres and nanocapsules containing xanthone and 3-methoxyxanthone. Eur J Pharm Biopharm 2005;59:491–500. https://doi.org/10.1016/j.ejpb.2004.09.002.
[75] Husmann M, Schenderlein S, Lück M, Lindner H, Kleinebudde P. Polymer erosion in PLGA microparticles produced by phase separation method. Int J Pharm 2002;242:277–80. https://doi.org/10.1016/s0378-5173(02)00187-4.
[76] Thomasin C, Merkle HP, Gander B. Drug microencapsulation by PLA/PLGA coacervation in the light of thermodynamics. 2. Parameters determining microsphere formation. J Pharm Sci 1998;87:269–75. https://doi.org/10.1021/js970048j.
[77] Honary S, Zahir F. Effect of Zeta Potential on the Properties of Nano-Drug Delivery Systems - A Review (Part 1). Tropical Journal of Pharmaceutical Research 2013;12:255–64. https://doi.org/10.4314/tjpr.v12i2.19.

[78] Bilati U, Allémann E, Doelker E. Nanoprecipitation versus emulsion-based techniques for the encapsulation of proteins into biodegradable nanoparticles and process-related stability issues. AAPS PharmSciTech 2005;6:E594–604. https://doi.org/10.1208/pt060474.
[79] Gibson TJ, Mccarty K, Mcfadyen IJ, Cash E, Dalmonte P, Hinds KD, et al. Application of a high-throughput screening procedure with PEG-induced precipitation to compare relative protein solubility during formulation development with IgG1 monoclonal antibodies. J Pharm Sci 2011;100:1009–21. https://doi.org/10.1002/jps.22350.
[80] Pereira E, Cerruti R, Fernandes E, icart L, Saez V, Pinto J, et al. Influence of PLGA and PLGA-PEG on the dissolution profile of oxaliplatin. Polímeros 2016;26. https://doi.org/10.1590/0104-1428.2323.
[81] Patel SM, Doen T, Pikal MJ. Determination of End Point of Primary Drying in Freeze-Drying Process Control. AAPS PharmSciTech 2010;11:73. https://doi.org/10.1208/s12249-009-9362-7.
[82] F DJ, E A, J F, T K, E D, R G. Freeze-drying and lyopreservation of diblock and triblock poly(lactic acid)-poly(ethylene oxide) (PLA-PEO) copolymer nanoparticles. Pharmaceutical Development and Technology 2000;5. https://doi.org/10.1081/pdt-100102031.
[83] F DJ, E A, Jc L, W S, J F, E D, et al. Formulation and lyoprotection of poly(lactic acid-co-ethylene oxide) nanoparticles: influence on physical stability and in vitro cell uptake. Pharmaceutical Research 1999;16. https://doi.org/10.1023/a:1018826103261.
[84] Morille M, Van-Thanh T, Garric X, Cayon J, Coudane J, Noël D, et al. New PLGA–P188–PLGA matrix enhances TGF-β3 release from pharmacologically active microcarriers and promotes chondrogenesis of mesenchymal stem cells. Journal of Controlled Release 2013;170:99–110. https://doi.org/10.1016/j.jconrel.2013.04.017.
[85] White LJ, Kirby GTS, Cox HC, Qodratnama R, Qutachi O, Rose FRAJ, et al. Accelerating protein release from microparticles for regenerative medicine applications. Mater Sci Eng C Mater Biol Appl 2013;33:2578–83. https://doi.org/10.1016/j.msec.2013.02.020.
[86] Li X, Wei Y, Wen K, Han Q, Ogino K, Ma G. Novel insights on the encapsulation mechanism of PLGA terminal groups on ropivacaine. European Journal of Pharmaceutics and Biopharmaceutics 2021;160:143–51. https://doi.org/10.1016/j.ejpb.2021.01.015.
[87] Buske J, König C, Bassarab S, Lamprecht A, Mühlau S, Wagner KG. Influence of PEG in PEG–PLGA microspheres on particle properties and protein release. European Journal of Pharmaceutics and Biopharmaceutics 2012:7.
[88] Giteau A, Venier-Julienne MC, Aubert-Pouëssel A, Benoit JP. How to achieve sustained and complete protein release from PLGA-based microparticles? International Journal of Pharmaceutics 2008;350:14–26. https://doi.org/10.1016/j.ijpharm.2007.11.012.
[89] Park J, Fong PM, Lu J, Russell KS, Booth CJ, Saltzman WM, et al. PEGylated PLGA nanoparticles for the improved delivery of doxorubicin. Nanomedicine: Nanotechnology, Biology and Medicine 2009;5:410–8. https://doi.org/10.1016/j.nano.2009.02.002.
[90] Chittasupho C, Xie S-X, Baoum A, Yakovleva T, Siahaan TJ, Berkland CJ. ICAM-1 targeting of doxorubicin-loaded PLGA nanoparticles to lung epithelial cells. Eur J Pharm Sci 2009;37:141–50. https://doi.org/10.1016/j.ejps.2009.02.008.
[91] Mura S, Hillaireau H, Nicolas J, Le Droumaguet B, Gueutin C, Zanna S, et al. Influence of surface charge on the potential toxicity of PLGA nanoparticles towards Calu-3 cells. Int J Nanomedicine 2011;6:2591–605. https://doi.org/10.2147/IJN.S24552.
[92] Zhang X, Sun M, Zheng A, Cao D, Bi Y, Sun J. Preparation and characterization of insulin-loaded bioadhesive PLGA nanoparticles for oral administration. Eur J Pharm Sci 2012;45:632–8. https://doi.org/10.1016/j.ejps.2012.01.002.
[93] Wnek G, Bowlin G, editors. Polylactic-Co-Glycolic Acid (PLGA) / Konstantinos Avgoustakis. Encyclopedia of Biomaterials and Biomedical Engineering. 0 ed., CRC Press; 2008, p. 2291–301. https://doi.org/10.1201/9780429154065-216.
[94] Makadia HK, Siegel SJ. Poly Lactic-co-Glycolic Acid (PLGA) as Biodegradable Controlled Drug Delivery Carrier. Polymers 2011;3:1377–97. https://doi.org/10.3390/polym3031377.
[95] Guarecuco R, Lu J, McHugh KJ, Norman JJ, Thapa LS, Lydon E, et al. Immunogenicity of pulsatile-release PLGA microspheres for single-injection vaccination. Vaccine 2018;36:3161–8. https://doi.org/10.1016/j.vaccine.2017.05.094.

[96] Middleton JC, Tipton AJ. Synthetic biodegradable polymers as orthopedic devices. Biomaterials 2000;21:2335–46. https://doi.org/10.1016/s0142-9612(00)00101-0.
[97] Ulery BD, Nair LS, Laurencin CT. Biomedical applications of biodegradable polymers. Journal of Polymer Science Part B: Polymer Physics 2011;49:832–64. https://doi.org/10.1002/polb.22259.
[98] Zhao J, Liu C-S, Yuan Y, Tao X-Y, Shan X-Q, Sheng Y, et al. Preparation of hemoglobin-loaded nano-sized particles with porous structure as oxygen carriers. Biomaterials 2007;28:1414–22. https://doi.org/10.1016/j.biomaterials.2006.10.012.
[99] Yamahara T, Numa Y, Oishi T, Kawaguchi T, Seno T, Asai A, et al. Morphological and flow cytometric analysis of cell infiltration in glioblastoma: a comparison of autopsy brain and neuroimaging. Brain Tumor Pathol 2010;27:81–7. https://doi.org/10.1007/s10014-010-0275-7.
[100] Roder C, Bisdas S, Ebner FH, Honegger J, Naegele T, Ernemann U, et al. Maximizing the extent of resection and survival benefit of patients in glioblastoma surgery: high-field iMRI versus conventional and 5-ALA-assisted surgery. Eur J Surg Oncol 2014;40:297–304. https://doi.org/10.1016/j.ejso.2013.11.022.
[101] Louis DN, Perry A, Wesseling P, Brat DJ, Cree IA, Figarella-Branger D, et al. The 2021 WHO Classification of Tumors of the Central Nervous System: a summary. Neuro Oncol 2021;23:1231–51. https://doi.org/10.1093/neuonc/noab106.
[102] Gaspar LE, Fisher BJ, Macdonald DR, Leber DV, Halperin EC, Schold SC, et al. Supratentorial malignant glioma: Patterns of recurrence and implications for external beam local treatment. International Journal of Radiation Oncology*Biology*Physics 1992;24:55–7. https://doi.org/10.1016/0360-3016(92)91021-E.

Chapter 5
Development of nanocomposite hydrogels for Glioblastoma application

5. DEVELOPMENT OF NANOCOMPOSITE HYDROGELS FOR GB APPLICATION

gels

MDPI

Article

Formulation of BMP-4 loaded nanocomposite hydrogel as a potential Glioblastoma treatment

Amel Djoudi[1], Rodolfo Molina-Peña[1], Natalia Ferreira[1], Sylvie Avril[1], Emmanuel Garcion[1], Frank Boury[1]

Citation: Djoudi, A.; Molina-Pena, R.; Ferreira, N. Formulation of BMP-4 loaded nanocomposite hydrogel as a potential Glioblastoma treatment, *Gels* **2022**, *15*, x. https://doi.org/10.3390/xxxxx

Academic Editor: Firstname Lastname

Received: date
Accepted: date
Published: date

Publisher's Note: MDPI stays neutral with regard to jurisdictional claims in published maps and institutional affiliations.

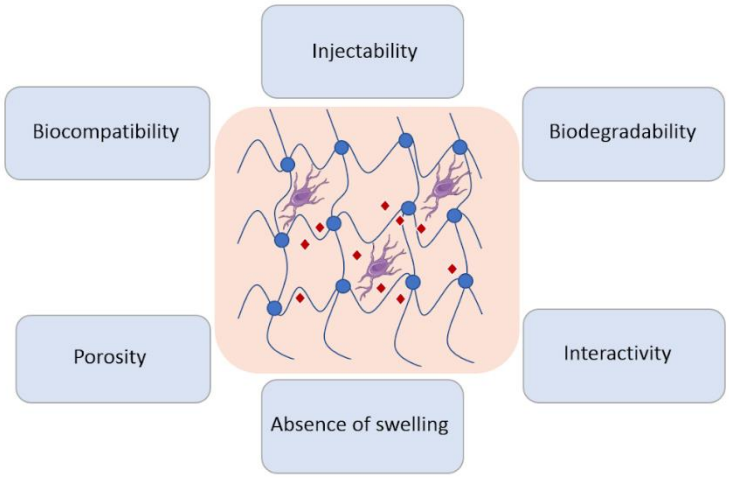
Copyright: © 2022 by the authors. Submitted for possible open access publication under the terms and conditions of the Creative Commons Attribution (CC BY) license (https://creativecommons.org/licenses/by/4.0/).

Université d'Angers, Inserm UMR 1307, CNRS UMR 6075, Nantes Université, CRCI2NA, F-49000 Angers - France

* Correspondance: djoudi-amel@hotmail.fr, frank.boury@univ-angers.fr

The current project aims to formulate protein loaded polymeric nanoparticles (NPs). PLGA NPs are prepared via non-toxic and biocompatible solvents and are incorporated into nanocomposite hydrogels to achieve a controlled release of BMP-4, a cytokine involved in early differentiation of the embryo establishment of the dorsoventral axis and differentiation processes (cartilage, bone, and sympathetic neurons). Herein, a differentiation strategy is applied to lead GB cancer cells and more precisely cancer stem cells to acquire a less aggressive phenotype that may increase their radiotherapy sensitivity. Since the brain microenvironment is composed of a Hyaluronic acid (HA) enriched extracellular matrix (ECM), we have developed an injectable, biocompatible, bioadhesive and biodegradable HA scaffold. HA is thus a good candidate since it possesses all those functionalities. Moreover these nanoparticles have been suspended in a hydrogel composed of a synthetic polymer called poloxamer 407 and a biopolymer, high molecular weight hyaluronic acid. A proof of concept regarding cytotoxicity has been obtained on NIH3T3 cell line. This developed system is biocompatible and has been characterized via an erosion assay, rheology, IR spectroscopy, DSC, SEM, injectability texturometer and SAXS methods. Bioperformance and biocompatibility *in vivo* evaluation of our device on preclinical models are ongoing.

Keywords: hyaluronic acid; sustained release nanocomposite hydrogels, thermosensitive hydrogel



Graphical abstract on the specifications of the nanocomposite hydrogel

1. Introduction

Hydrogels as biomimetic scaffolds

Hydrogels are three-dimensional lattice structures capable of absorbing large amounts of water [1,2]. They are generally insoluble due to chemical or physical crosslinking and/or chain entanglement. They exist naturally as a network of polymers such as hyaluronic acid, collagen, agarose or can be synthetic [1,2]. Environmentally sensitive hydrogels can serve a variety of applications due to their ability to respond to environmental changes, likewise, they show volume changes [1–3]. The traditional stimuli that induce hydrogel reactions are temperature, ionic strength and pH [4–7]. Because of their tunable properties and flexible manufacturing methods, hydrogel materials have found applications in a wide range of biomedical and engineering applications, such as tissue engineering and regenerative medicine [1–3]. Since then, hydrogels have been used as controlled drug delivery systems, to facilitate local, sustained, and prolonged drug release, thereby reducing frequency of administration, avoiding side effects [1–3,8]

Various biopolymer based hydrogels have been developed [1–3,8], and include hyaluronic acid the main polymer used in this study along with poloxamer 407 triblock polymer (POL407) (Figure 24) [7,9–12]. These two polymers offer many interesting properties. For instance, HA has been chosen because of its biocompatibility, biodegradability, biomimetism, bioadhesive properties [3,13–15], and poloxamer 407 is biocompatible, biodegradable, shows good drug controlled release, with thermosensitive features, and self-assembly behavior [7,9–12,16–18].

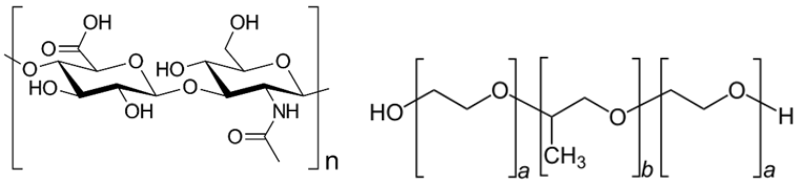


Figure 23: Hyaluronic acid (right) and poloxamer 407 (left) polymers chemical structure

This research project aims to associate BMP-4 loaded nanoparticles to a hydrogel and therefore obtain a nanocomposite hydrogel. This system has various characteristics like biocompatibility, biomimetic stiffness, high water content, porosity and controlled release properties. This protein has been encapsulated in nanoparticles, in suspension in a hydrogel that is more suitable as a scaffold, being injectable in the resection cavity.

2. Results and Discussion

2.1. Hydrogel development

2.1.1. Tube inversion test

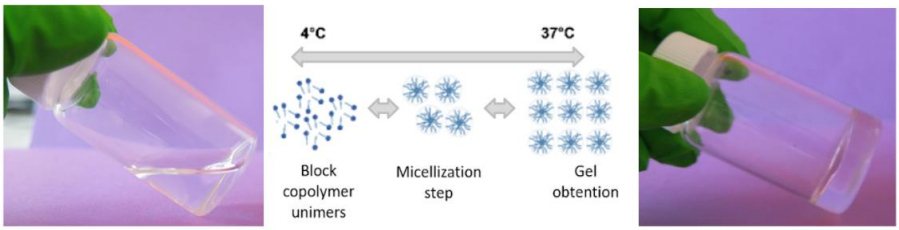


Figure 24 : Thermogelation by tube inversion method: at 4°C (left) and 37°C(right) The hydrogel 4°C still flows and the gel is liquid and mobile. At 37°C it completely gelifies. Gelation time is 30s for HA+Poloxamer hydrogel and 1 min for Poloxamer alone.

This preliminary test helps us get an idea of the gelling temperature at 4°C which is the formulation temperature and 37°C as the physiological conditions (Figure 24).
The tube is inclined to see if the hydrogel flows or not and the time of gelation of each hydrogel tested is measured using a chronometer. The gelation time of POL alone took around 1 min whereas HA+POL took 30 seconds, this could be explained by the fact that HA could decrease the gelling temperature therefore the hydrogel containing HA gelifies faster, at a lower temperature [5–7]. Gelation process is divided in 3 steps, block copolymer unimers, the micellization step and the gel network obtention.

2.1.2 ATR-FTIR

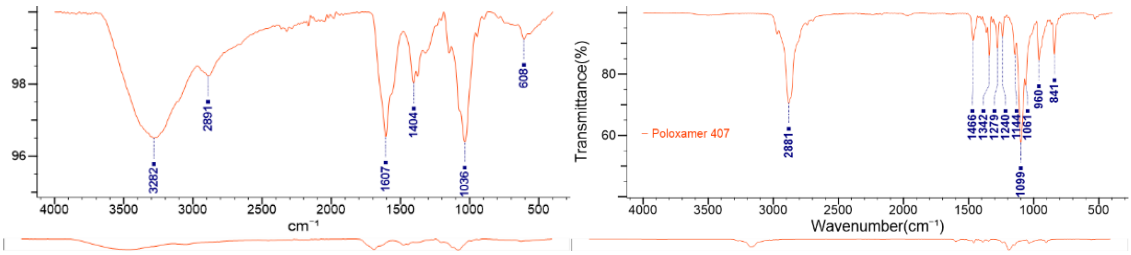


Figure 25: ATR-FTIR spectrum of Hyaluronic acid (left) and Poloxamer 407 (right), transmittance (%) representation in function of the wavenumber (cm-1) in the whole region (3600–650 cm−1) and the fingerprint region (1800–650 cm−1).

From figure 25, ATR-FTIR provides information on the molecular composition of the both polymers. Hyaluronic acid raw material spectrum shows characteristic transmittance peaks at 3282 cm-1 O-H stretching of the carboxylic group, 2891 cm-1 C-H stretch , 1607 cm-1 corresponds to the C-H anti asymmetric stretch vibration, 1404 cm-1 is attributed to the symmetric vibration stretch COO-. This spectrum is comparable to the literature [19,20]. Poloxamer 407 raw material spectrum shows characteristic transmittance peaks at 2881cm-1 medium intensity is ν(-CH3) stretching and 1099 high intensity peak is C-O stretching and 960 cm-1 ν(C-O-C) linkage. These peaks are similar to those found in the literature [21,22].

2.1.3 Small Angle X-Ray Scattering

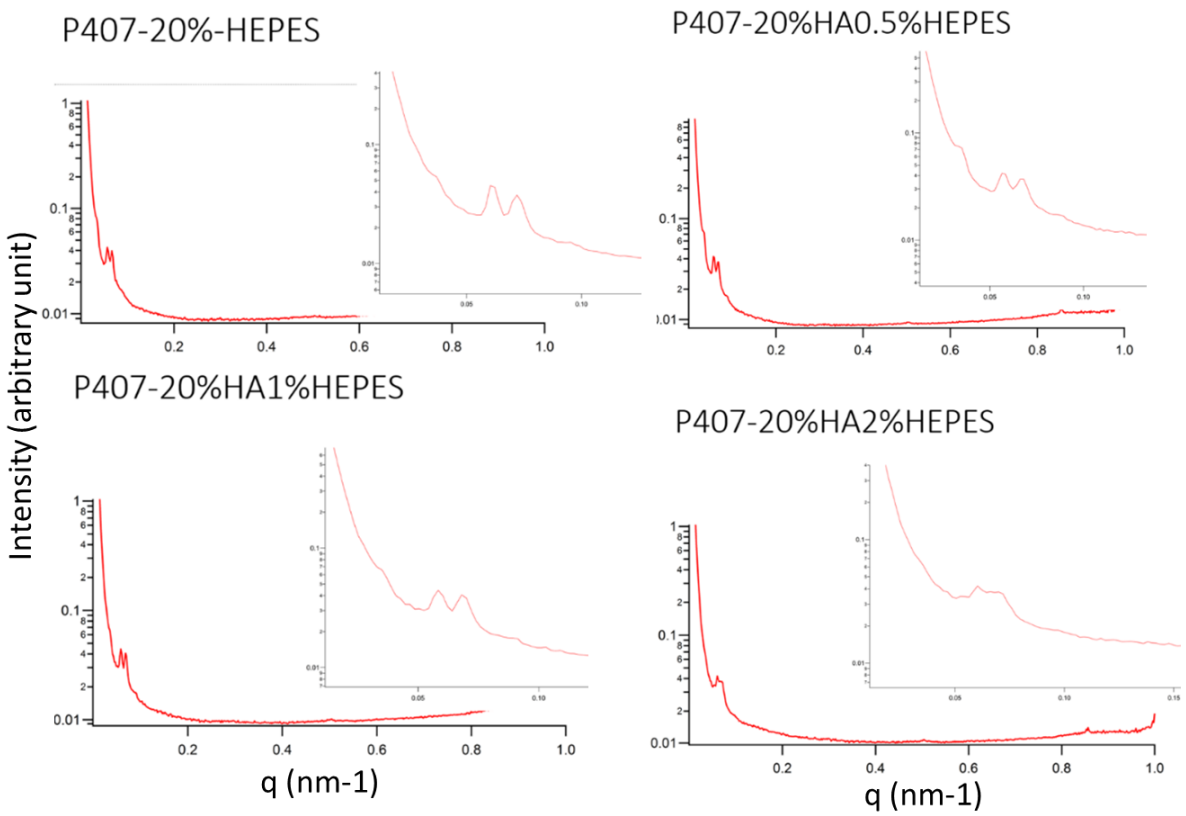


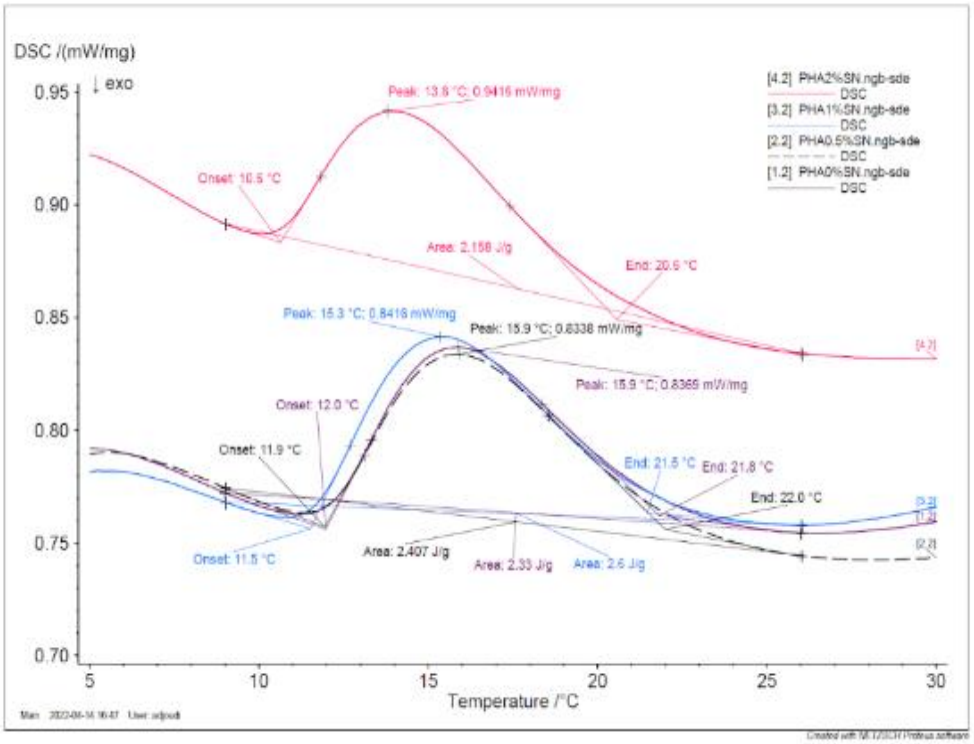
Figure 26: : Small-Angle X-Ray Scattering (SAXS) diffraction patterns obtained from the four cubic phase samples of Hydrogel formulations containing 20%w/v Poloxamer 0, 0.5, 1, 2%w/v HA.

The scattering patterns are shown in figure 27 At 25 °C. All systems presented lamellar structure with spacing D = 2π/q* ~17.5 nm, for PL 407 20%. However, considering the temperature at 40 °C, they exhibited a phase organization in cubic structure, as can be seen from the peak positions at q*, rac(2)q*, 2q* and 71/2q*, with q* ~0.34 nm for PL 407 20% and q* ~0.36 nm−1 for PL 407 20% HA0.5% q* ~0.4 nm−1 for PL 407 20% HA1% q* ~0.46 nm−1 for PL 407 20% HA2%, corresponding to a distance of respectively 18.48 nm, 17.45nm, 15.71 nm, 13.65 nm between micellar centers in both systems (Figure 27). The resolution decreases with the increase of the HA concentration but the Bragg peaks are still observable and indexable. The first peak is characteristic of the micelle shape form and the thin and long peaks are Bragg peaks typical of the cubic phase. A few studies have studied the supramolecular organization of poloxamer hydrogels using SAXS, such as ones using P85 and F88 that are similar in terms of structure and physical-chemical properties, that have been shown to be a packing of micelles under a hexagonal compact structure for P85 and a cubic phase for F88 [11]. Nascimento et al. has shown [23] that the presence of HA seems to increase the size of POL407 micelles. Pluronic F-127 and Pluronic F-108 has shown a cubic and hexagonal phases for these polymers. Park[24] has shown a cubic packing of the Pluronic F108, which suggests a similar organization as our system. Another study characterized their hydrogel composed of glycerol monooleate (MO), propylene glycol (1,2-propanediol, PG), and water; consisted on a cubic phase too [25]. A main point between all the cubic packing systems, when a drug was encapsulated, knowing that POL407 [9,17,26] and other polymers such as propylene glycol [27] allowed sustained release properties, which is interesting in terms of drug delivery. The reduction in micellar centers distance when increasing the HA amount, suggests a more packed structure which could help to obtain a slower release rate. HA seems to interact more closely with POL407 at highest concentration.

2.1.4 Differential Scanning Calorimetry

The critical micellization temperature (CMT) onset and endset temperatures (Tonset and Tend) and area under the curve (AUC) have been determined. A temperature ramp from -5°C to 50 °C has been done and the endothermic event can be seen in the area between 10°C and 30°C. For formulations POL40720% 1% to 2%w/v of HA without nanoparticles (SN) have shown a variation of the Tonset, Tendset, AUC, and CMT when increasing the concentration of HA. For formulations POL20% 0% 0.5 and 1%w/v of HA, temperature don't vary in a significative way (Figure 28 and Table 9) . There is a shift of these temperatures for POL407-20% HA2%w/v. Therefore, the most concentrated HA hydrogel seems to have an effect on the thermal events of the hydrogel. Again, the gelation seems to occur at a lower temperature, hence, earlier for the highest concentrations of HA. This is in accordance with the tube inversion assay aforementioned. This behavior can be explained by a higher interactions between POL407 and HA molecules when in present in a higher concentration.
The addition of nanoparticles to POL20% 0% to 2%w/v of HA varies in a significant way the Tonset, Tendset, AUC, and CMT in comparison to the SN condition. The events happen at lower temperatures for the highly concentrated hydrogels, whereas for the least concentrated they take place higher concentrations. Moreover, all the CMT temperature, Tonset and Toffset are increased when combined with NPs. This could be due to the presence of from its repeating methylene units contained in PEG-PLGA. NPs might delay the thermal events by interacting with PPO polymer chains and/or hyaluronic acid through multivalent hydrophobic interaction [28].
The reduction in CMT in the POL407 gels might explain the rapidity of gel degradation. Incorporating HA to pure POL407 gels resulted in a decrease in CMT [29] . Researchers demonstrated that the amount of HA added has no linear relationship with the enhancement of the viscoelastic characteristics of poloxamers gel [29]. The reduction of CMT and other parameters reported in this investigation can be explained by the fact that at 1% to 2% w/w, high molecular weight HA solution functions as an entangled network with topological interactions among the molecules [30,31]. Micelle mobility and packing are hindered in these conditions, competing with the poloxamer gelation process alone. A similar observation was made with the fibrillogenesis of collagen gels [32].

A



B

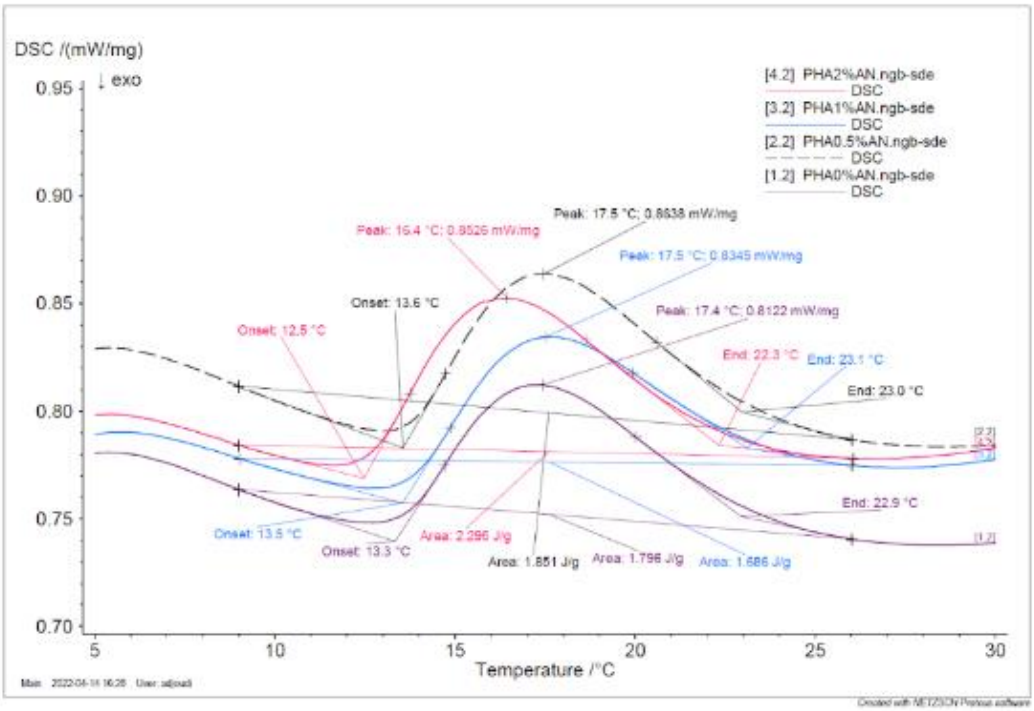


Figure 27: Differential Scanning Calorimetry of POL20%w/v +/- HA 0.5/1/2% w/v without (A) and with blank PEG-PLGA NPs (B) with a concentration 1mg/mL with a mean size of 250nm with a zeta potential of -3.2 mV.

Table 8: Transition Temperatures for the Different Poloxamer hydrogel with and without blank PLGA nanoparticles. Gelation temperatures from SAXS experiments and gelation temperatures from rheology experiments. N/D no data were obtained

Formulation POL407/HA	Ratio of POL/HA w/w%	Tonset(+/- 0.5°C)	Tend(+/-1°C)	CMT (+/- 1°C)	AUC(J/g)	Rheology Tsol-gel
P407/HA	20%/0%	12.0	21.8	15.9	1.796	20
	20%/0.5 %	11.9	22.0	15.9	2.407	23
	20%/1%	11.5	21.5	15.3	2.6	24
	20%/2%	10.6	20.6	13.8	2.158	36
	20%/0% + NPs	13.3	22.9	17.4	1.296	19
	20%/0.5 % + NPs	13.6	23.0	17.5	1.851	N/D
	20%/1%+ NPs	13.5	23.1	17.5	1.686	N/D
	20%/2%+ NPs	12.5	22.3	16.4	2.296	20 & 32

2.1.5 Scanning Electron Microscopy

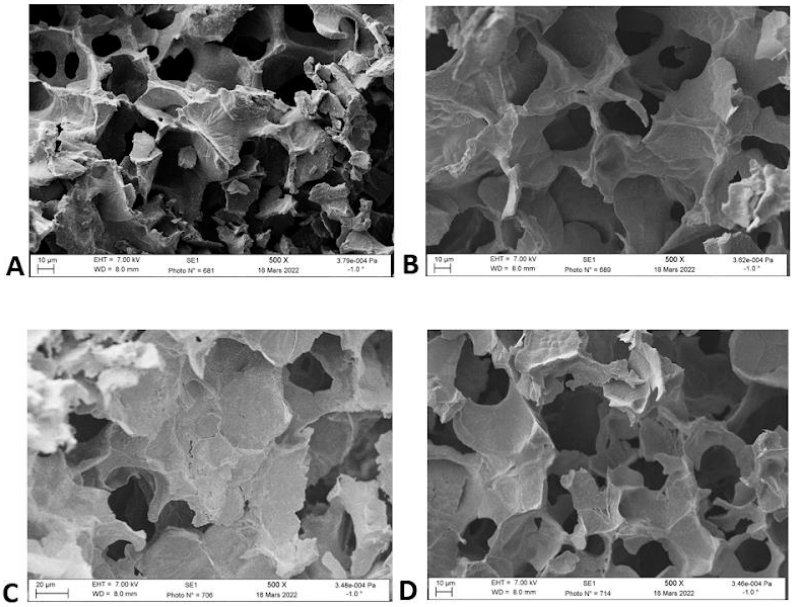


Figure 28: SEM Images of 0 % (A) 0.5%(B) 1%(C) and 2%(D) POL/HA lyophilized hydrogels in 500X Pore size varies from 10µm to 200µm

These images were obtained after lyophilization of hydrogels (Figure 28). This process lead to a porogen effect of crystalline structures are visible in hydrogels at 500x and porosity is present in all freeze-dried hydrogels. The pore size is similar from a gel to another according to ImageJ treatment of images. But the hydrogel that shows more than 80% of porosity and a homogenous porosity is POL407-20% HA 2%w/v, with also good connectivity, and a sponge-like microarchitecture that is similar to some studies with HA [33]. Moreover, the pore size similar from 0, 0.5, 1 and 2%HA w/v concentrations. POL20%HA0%, POL20%HA0.5%, POL20%HA1% and POL20%HA2% have mean pore sizes 10-200 µm. Pore diameter is more visible in this study compared in the literature where the pores are more elongated, smaller and less monodisperse [9]. The microstructure of pure P407 gels were shown to be porous and sponge-like in SEM pictures. The inclusion of HA, on the other hand, did not change the pore size but resulted in a more compact porous structure, indicating that HA may have a protective role in this hydrogel system [9]. Hyaluronic Mw and poloxamer types used can have an impact on the porosity of the hydrogel and on the frequency and connectivity of the pores [9,34]. This porosity feature gained by lyophilisation may have an asset for cell incorporation or cell-HA interactions *in vivo* [35].

2.1.6 Rheology study:

Viscosity study

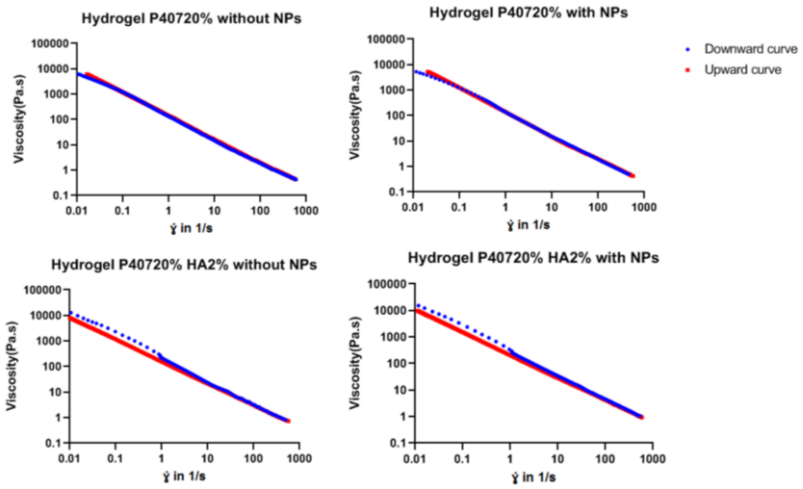


Figure 29: Viscosity studies of Hydrogels POL407 20%w/v +/- HA 2%w/v at 37°C

Viscosity studies in figure 29 have consisted of doing a downward and a forward curve by doing two cycles of shear rates from 0.01-800s-1 and 800-0.01s-1 at 37°C. The downward curve exhibits a shear-thinning behavior, suggesting that the polymer chains of POL407 and HA at rest or low shear rate are entangled and highly interacting, whereas when a high shear rate is applied, they disentangle and stretch (Figure 31). When applying a decreasing shear rate, the material recovers its initial viscosity; this can be seen by the overlapping of both curves in hydrogel POL407 with and without NPs. This hydrogel is therefore not a thixotropic material. The other hydrogel POL407 20% and HA2% with and without NPs has shown the same behavior, because the curves are overlayed between 800s-1 and 1s-1. There is a gap between the downward and upward curves from 0.01s-1 and 1s-1 suggesting that this formulation is thixotropic. These results are comparable to other ones El Kechai et al has also shown a thixotropic behavior of nanocomposite hydrogels composed of POL407 and HA containing liposomes [36,37].

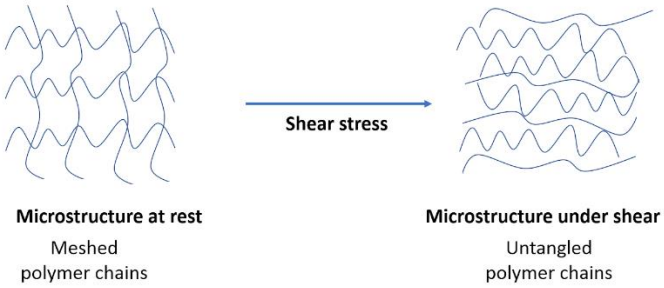


Figure 30: Shear-thining of polymer-based hydrogel

HA addition in the formulation seem to prevent overlapping of both curves, therefore, HA+POL hydrogel seem to be thixotropic whereas the hydrogel with POL alone is not.

Thermogelation Sol-Gel transition

Cross-over point or sol-gel transition has been determined with rheology software for each formulation (figure 32). The hydrogel POL20% and HA0% has a Tsol-gel at 20°C, POL20% and HA0.5% has a Tsol-gel at 23°C, POL20% and HA1% has a Tsol-gel at 24°C, POL20% and HA2% has a Tsol-gel at 36°C (with no observed cross-over). Several sol-gel transitions have been assessed in the literature; Li et al developed hydrogels intended for skin wound healing applications where POL407 was used with high molecular weight hyaluronic acid where the sol-gel transition went from 37°C with POL407 to 30°C with POL407+HA. The transition observed here is less significant than the one observed in this study [16]. 32 and 37°C were sol-gel temperatures obtained in another study by Mayol et al, F68 and F127 (POL407) in different proportions and low HA concentrations [17]. In our work we wanted a more HA concentrated hydrogel in order to have biomechanical properties

similar to the brain ones [36,38]. For all the hydrogels formulated the Young modulus is 10-20kDa that is in the range of brain Young modulus.

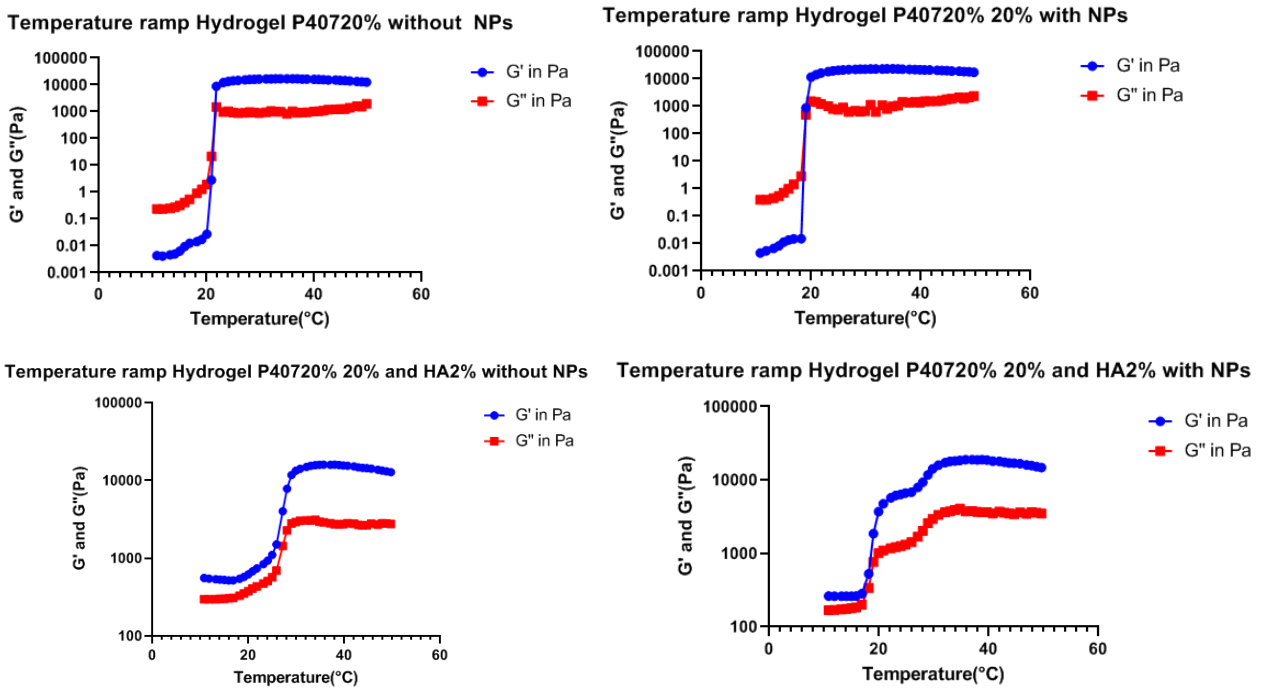


Figure 31: Temperature ramp studies of Hydrogels POL407 20%w/v +/- HA 2%w/v and +/- blank NPs at 1mg/mL with 250nm size at 37°C

In figure 31, the hydrogels with POL20% and HA0% without NPs has a Tsol-gel at 20°C, POL20% and HA0% with NPs has a Tsol-gel at 19°C. The temperature effect can be explained by interactions between NPs and polymer chains, lowering the gelation temperature.
Hydrogel with POL20% and HA2% without NPs has a Tsol-gel at 23°C, POL20% and HA2% with NPs has a Tsol-gel at 20°C (effect of NPs) at 32°C with the presence of double plateau related to the effect on micellization, and viscosity and structural organization of the polymer network involving ionic interactions. This phenomenon suggests that the sol-gel transition takes place in two steps due to the presence of the PEG-PLGA NPs.
P407 is distinguished by its thermosensitive self-assembling and thermo-gelling properties. As the temperature rises, the aqueous P407 solution switches to an intermediate gel state due to a decrease in the solubility of PPO blocks, which causes aggregation to occur to reduce their contact with water molecules at 20°C [18,23,39]. The collected hydrophobic blocks create the micelle center, while the PEO blocks form the outside layer of hydrophilic shell that is covalently bonded to the water molecules. The temperature of the solution-to-gel change varies with concentration and the NPs composed of an outershell of PEG, may interact with the PPO through hydrophobic interactions leading to a more packed structure, hence to a gelation at 32°C and also through H bonds between HA and Poloxamer PEO moieties [9,40,41].

Amplitude sweep study

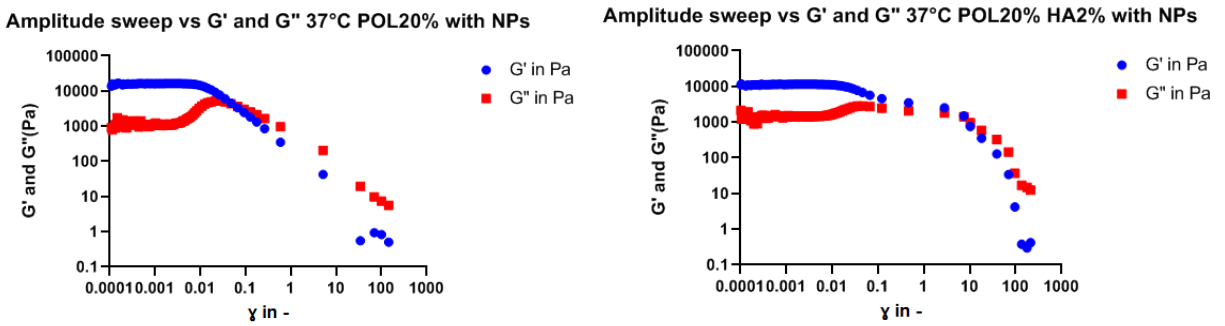


Figure 32: Amplitude sweep studies of Hydrogels POL407 20%w/v +/- HA 2%w/v with blank NPs at 1mg/mL with 250nm size at 37°C

The linear regimen is the zone where the hydrogel does not undergo irreversible structural modifications (figure 32). Amplitude sweep studies at 37°C in figure 33, have shown a linear regime between 0.0001 and 0.1% for the POL20% and HA0% with NPs and between 0.0001 and 1% for POL20% and HA2% with NPs; in this domain, the sample does not show irreversible structural modifications and the interval 0.05-10Hz was chosen for frequency sweep at a 10Pa strain stress for the frequency sweep. This study has also been done by El Kechai on the same strain interval, and have shown a similar linear regimen [36].

Frequency sweep study

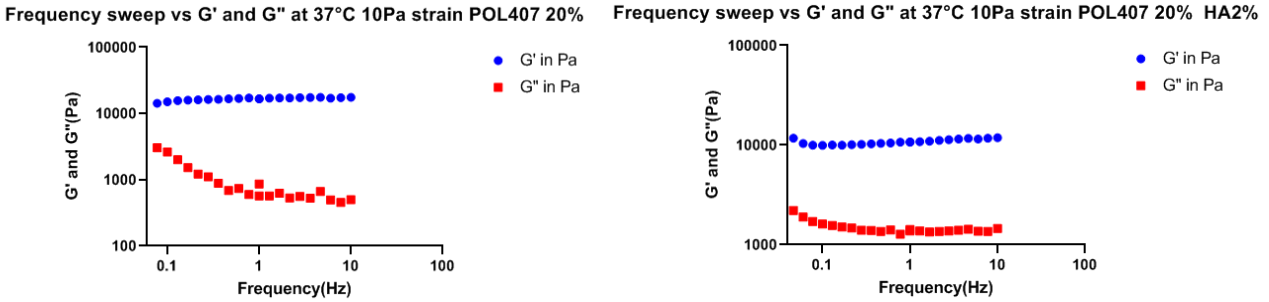


Figure 33: Frequency sweep studies of Hydrogels POL407 20%w/v +/- HA 2%w/v with blank NPs at 1mg/mL with 250nm size at 37°C

The frequency sweep obtained in figure 33, from 0.05 to 10Hz has shown a gel behavior from 0.05 to 10Hz that can be seen through the parallel curves of G' and G'', the material is equally a solid elastic and a viscous liquid, in other words a hydrogel. Mayol et al have investigated the frequency sweep showing that at a frequency range between 0.001 and 10Hz the G' is higher to G'', suggesting an elastic dominant behavior in both hydrogels POL407 only and POL407+HA2% [17].

2.1.7 Injectability studies

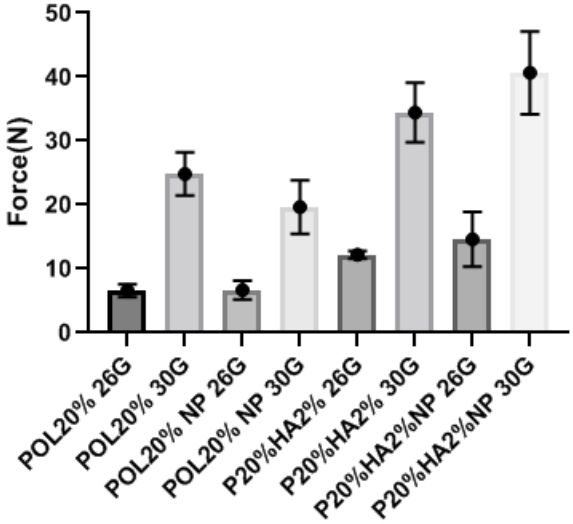


Figure 34: Injectability study of POL/HA and POL hydrogels with and without NPs

Injectability has been done following the following protocol [36] (See Material and Methods). Results in figure 34, show a variation in injection force in the different formulations. 30G needles tend to significantly increase the force of injection because of the smaller inner diameter of the needle. It is also due to the needle length. The presence of NPs is also another parameter involved in a higher injection force. The increase of the injection

force is due to the higher viscosity of the NP loaded hydrogel and also due to the potential of NPs to aggregate and form a phase that could increase pressure in the syringe and therefore make a bulk. The hydrogel has been characterized as a shear thinning material and therefore this property can help the injectability process. The injection rate can also influence the syringeability but in this study it was kept constant, following previous works [26,36]. The adapted 26G gauge was selected for the injection of the formulation POL20%+HA2%w/v containing NPs.

2.2. Hydrogel in vitro assays

2.2.1 Erosion assay *in vitro*

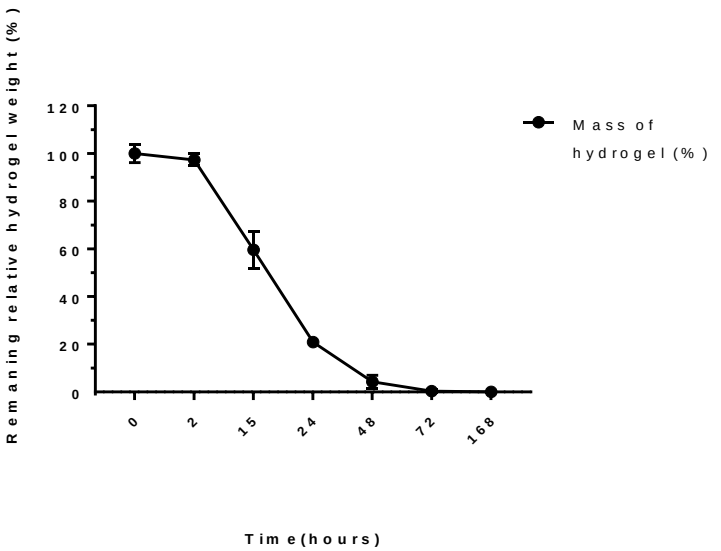


Figure 35: The mass erosion behaviors of POL/HA hydrogel system. Data are represent as the mean ± standard deviation (n = 3).

Erosion assay has shown a degradation of the hydrogel in contact with PBS starting day 1 and after 15 hours more than 40% of the hydrogel has been degraded (figure 35). Then, at day 1, 80% of it have been dissolved in PBS, and at day 7 all the hydrogel is eroded (Figure 36). This assay has been inspired from the literature and done during a week [9]. This property of hydrolysis in physiological conditions might facilitate release profile of BMP-4 especially for hydrophilic drugs like proteins. In contrast to another study that found a considerable swelling, the addition of HA did not appreciably delay the occurrence of gel erosion in the 20% POL407 gels. They described an increase in hydrogel swelling as a result of the COO- groups inside the HA/POL407 hydrogels, which generated the repulsive force, increasing water penetration and prolonged the gel erosion process [9]. Even though, *in vitro* gel dissolution tests revealed no substantial delay in gel erosion when HA was added to 25% P407. Swelling may not be the primary deciding element of the gel erosion process [42,43].

2.2.2 Release study of Lysozyme and BMP-4

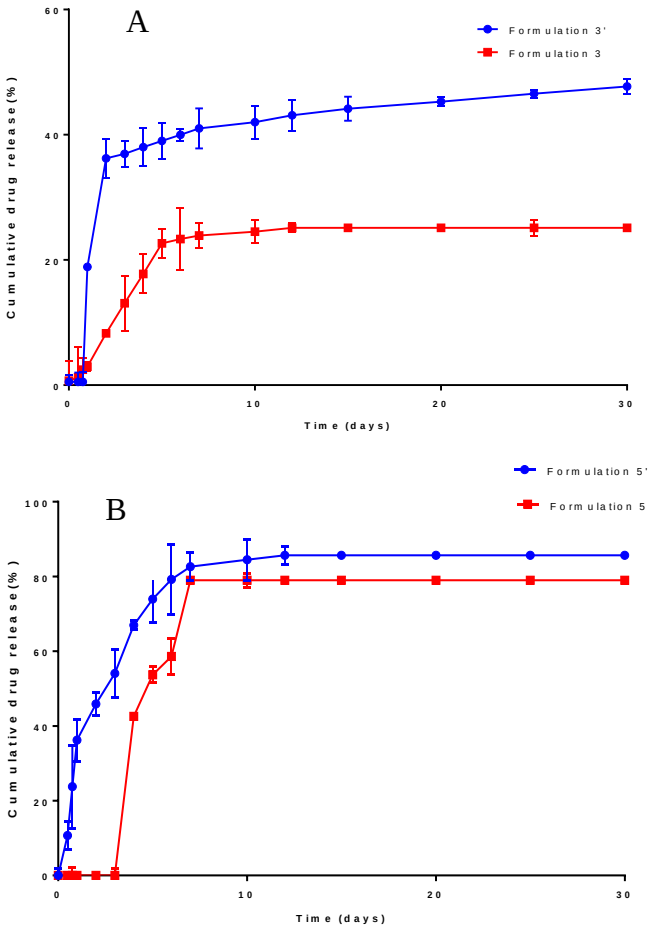


Figure 36: Release profile of Lysozyme in TrisHCl buffer at pH 7.4 (A) and BMP4 in PBS at pH 7.4.(B) Formulation 3 is the POL40720%w/w% + HA2%w/v hydrogel with lysozyme loaded NPs with a ratio 70/30% of PLGA-COOR/PLGA-PEG. Formulation 3' is the the POL40720%w/w% + HA2%w/v hydrogel with free Lysozyme; Formulation 5 is the POL40720%w/w% + HA2%w/v hydrogel with BMP-4 loaded NPs with a ratio 70/30% of PLGA-COOR/PLGA-PEG; Formulation 5' is the the POL40720%w/w% + HA2%w/v hydrogel with free BMP-4. All release experiments have been done in triplicates and SD is represented for each formulation.

According to figure 36, formulation 3 with Lysozyme loaded NPs shows an incomplete release with only less than 25% of the protein quantified in the recipient compartment. Indeed, the release does not show a marked burst effect that could be due to the hydrogel structures that have been described in the previous studies of SAXS and DSC; POL407 possess nanostructuration that could delay the protein release, initially imbedded in the NPs. The amount of not released protein might have interacted with the Tris HCl salts through ionic interactions and also the protein could also interact and be depleted by PLGA polymer trough electrostatic interactions. Moreover, through this method of release, the NPs tended to sediment at the bottom of the inserts which might have affected the release kinetics. In the case of hydrophilic hydrogels, gel erosion and drug diffusion run in parallel, therefore, slower gel erosion frequently induce slower drug release [44,45]. Another hypothesis is the interaction of NPs with the POL407 and HA may delay the erosion phenomenon and in consequently protein release.

In the case of formulation 3', where Lysozyme is freely present in the hydrogel , the release is marked by a burst effect after 15 hours that correspond to the erosion of 60% of the hydrogel and making the diffusion of Lysozyme more straightforward, the Lysozyme might not have strong interactions with HA due to the basic amino acids that compose it.

For BMP-4 release after 10 hours, similar proteins amount released were detected by ELISA in the formulation 5 and 5' respectively of 80% and 85%. Besides, there is a delay of liberation of BMP-4 for formulation 5 from 0h to day 4 that could be due to the presence of the PLGA NPs having interactions with the POL407-HA

network and affecting its erosion. A burst effect is observed on day 5 where more than 40% of the protein is liberated followed by a plateau reached at day 8. Opposed to Lysozyme that has more basic amino acids, BMP-4 is mainly composed of an equal amount of acid and basic amino acid making it a neutral protein at physiological conditions with less interactions with PLGA that could also explain the gap in the release kinetics.
For the free BMP-4 in formulation 5', the release is linear in the first part of the curve then reaches a plateau at day 8. This more progressive release might be due to the erosion process that starts at 15 hours and keeps on going until the 7th day where the plateau is reached.
A recent research found that adding high molecular weight HA to a poloxamer mix reduced the final gel strength, resulting in quicker drug release from the gel, which could also explain the fast release from HA-POL407 formulations 3' and 5' [29].
Barichello et al have developed insulin loaded POL407 hydrogels for a subcutaneous administration , and have shown that one of the major limitations that restricts the use of poloxamer gels as drug delivery platforms is their fast dilution when exposed to high quantities of aqueous solutions [39,46]. This results in inadequate control over the drug release rate, which is often excessively rapid [39,46]. Release of drug from these thermosensitive gels occurs via a mixed diffusion/dissolution process, and the capacity of high molecular weight HA to strengthen the poloxamer gel structure is mirrored in the gel's ability to better regulate and prolong protein release.

2.2.3 Cytotoxicity hydrogel assay:

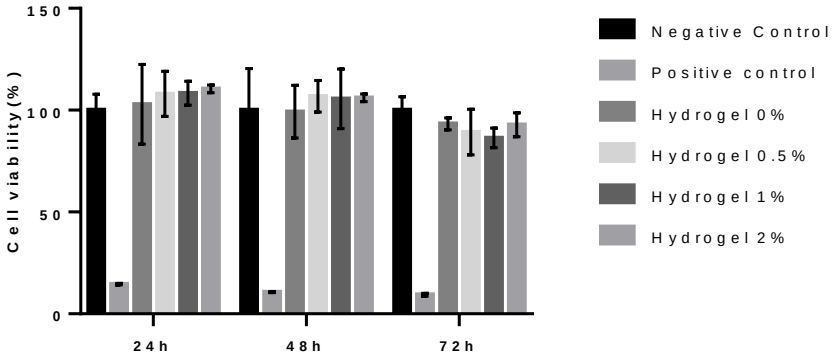


Figure 37: NIH3T3 Cell line cytotoxicity assay at 24h, 48h and 72h. All experiments has been done in triplicates and statistical analysis with ANOVA was made.

Hydrogels from 0 to 2% does not seem to be toxic to the NIH3T3 cell line compared to the control at 24h and 48h (figure 37). From 72h the cell viability seems to decrease but not in a significant way. Hence, the hydrogel with 2% of HA and POL40720% is cytocompatibility on fibroblast cells and meets the main specifications of the literature for drug delivery [1,2,9].

3. Conclusion

This research part complete our understanding of the impact of polymeric nanoparticles on the behavior of HA gels. It also emphasizes the importance of combining rheological, thermal, and syringeability tests to thoroughly analyze the in-use characteristics of such formulations during and after injection. The shear-thinning characteristic of HA nanocomposite gels enabled appropriate injectability regardless of the needles used. Furthermore, the viscoelasticity and self-healing properties of these gels should encourage rapid immobilization and an extended residence duration following injection. We established that the composition and microstructure of hydrogels are important criteria regulating their thermosensitivity and microstructure. They seemed to be biocompatible for 72 hours study on NIH3T3 fibroblast cell line. Their erosion in a week shows that the release takes place in parallel. The controlled drug kinetics are different for Lysozyme and BMP-4, and might be explained by interactions between proteins and POL407 and HA and/or between proteins and PLGA polymer that could delay the release. PLGA NPs in HA gels should promote the continuous release of encapsulated proteins and the interactions between NPs and HA play a significant role in the strengthening of the formulations 3D structure.

Additional physicochemical studies are needed to properly understand the structure of PLGA NPs-HA-POL407 hydrogels. Finally, our study demonstrates that nanocomposite gels may be used as a safe and versatile formulation platform for a variety of applications in the field of local drug administration. Other studies are being conducted to assess the *in vitro* and *in vivo* efficacy of HA-POL407 hydrogels containing PEG-PLGA NPs encapsulating BMP-4 for locoregional injection.

4. Materials and Methods

4.1 Hydrogels preparation and characterizations:

Hydrogels were formulated with Poly(ethylene glycol)-*block*-poly(propylene glycol)-*block*-poly(ethylene glycol)) triblock polymer: Kolliphor® P407 (Poloxamer 407, (Sigma Aldrich, Saint-Louis, USA) and high molecular weight (990 kDa average) hyaluronic acid (Contipro, Dolní Dobrouč, Czech Republic) at concentration between 0 and 2% w/v by cold thermogelation, according to the literature [36]. Poloxamer 407 solution is prepared by gradually dissolving the poloxamer 407 powder (20% w / v) in HEPES / NaCl buffer, pH 7.4 with magnetic stirring in an ice bath until a clear solution is obtained [9,10]. Besides, HA / poloxamer gels were formulated by adding HA (0, 0.5, 1 and 2% w / v) to the poloxamer 407 solution. Stirring was maintained for 2 hours in an ice bath and cold room [36]. Prepared different gel lots. All gels were stored at 4 ° C for at least 12 hours prior to analysis to obtain complete hydration of the polymer. Formulation 3 is the POL40720%w/w% + HA2%w/v hydrogel with lysozyme loaded NPs with a ratio 70/30% of PLGA-COOR/PLGA-PEG. Formulation 3' is the the POL40720%w/w% + HA2%w/v hydrogel with free Lysozyme; Formulation 5 is the POL40720%w/w% + HA2%w/v hydrogel with BMP-4 loaded NPs with a ratio 70/30% of PLGA-COOR/PLGA-PEG; Formulation 5' is the the POL40720%w/w% + HA2%w/v hydrogel with free BMP-4.

NIH/3T3 cells were cultured in 24-well plates for 24 hours and then treated for 48 hours with each gel using 24-well transwell insert (Cellqart, Northeim, Germany). Each condition has been done in triplicate. Cytotoxicity was assessed using MTS assay. The gelation process has been investigated with the tube inversion method, SAXS, DSC, rheology, texturometer-injectability system, erosion assay. Release study has been done using ELISA assay and Micrococcus Leidococcus assays for respectively BMP-4 and Lysozyme. Porosity was evaluated with SEM. Chemical structure was studied using ATR-FTIR. The nanoparticles preparation protocol is similar to the one described in Chapter 4.

4.2 ATR-FTIR

Studies of the structure of hydrogels have been done on a range of 400-4000cm-1 at room temperature on semi-solid samples and solid samples on a BRUKER Vertex 70 spectrometer. Data has been processed with the software KnowItAll Informatics System 2021 from Wiley Science Solutions.

4.3 Small Angle X-Ray Scattering

Structure of the samples was evaluated by X-ray scattering with a homemade setup. X-ray scattering results were collected with a Pilatus 300 K (Dectris, Switzerland), mounted on a microsource X-ray generator GeniX 3D (Xenocs, France) operating at 30 W. The monochromatic CuKa radiation was of l = 1.541 Å. The results were recorded in a reciprocal space q = (4p.sin u)/l in a range of repetitive distances from 0.01 to 1.72 Å1. The 4 samples were introduced into 1.5 mm quartz capillaries, then centrifuged and sealed with candle wax[47]. For analysis, samples were placed in a capillary holder with 7 capillaries. Measurement of 15 samples during 15 minutes each at room temperature and at 40°C , 1 point per sampleat 1mm, vertical position, exposition time of 600s. Each capillary was probed at two Y positions to confirm sample uniformity and the analysis performed 7 points per capillary. The purpose of this analysis was to determine the temperature at which the micelles of the heat-sensitive hydrogel were observed. This study focused on the type of structure with small-angle X-ray scattering (SAXS) (long-range order) and the type of packing with wide-angle X-ray scattering (WAXS) (short-range order). The results were collected by a homemade program and analyzed by Igor Pro 7.0 software (Wavemetrics, USA) [47].

4.4 Scanning Electron Microscopy:

Porosity of the hydrogels has been studied using SEM. Samples have been frozen at -20°C and lyophilized with a cryodessicator Steris_02 Lyovac GT2, in order to preserve the cross-section of samples, and metalized with gold on SEM specimen holders. The observation has been done using the SEM (ZEISS EVO/LS10). For

SEM, the sample was coated with a gold layer of 5 nm thickness before observation whereas no coating was applied to TEM. Images have been analyzed using ImageJ software.

4.5 Differential Scanning Calorimetry:
Analysis has been done using Netzsch DSC 3500 *Sirius.* The following cycle has been applied to samples: 0°C to 50°C then 50°C to 0°C, afterwards DSC recording was done from 0°C to 50°C the onset, peak, AUC and onset temperatures has been investigated to show the entropy event which is micellization for 0, 0.5, 1 and 2% Pol/HA hydrogels in presence and absence of nanoparticles. Datas have been processed using NETZSCH-Proteus-80 software.

4.6 Rheology study:
Hydrogels were analyzed by rheometer, Flow and oscillatory measurements have been performed. Viscosity of hydrogels has been measured at 37° C in inward and backward curves with increasing shear rates from 0.01 to 1000 Pa. The most common type of non-Newtonian behavior is shear thinning or pseudoplastic flow, in which the fluid viscosity decreases with increasing shear. The thixotropy of the hydrogel was evaluated in the backward-inward curves. For most liquids shear thinning is reversible and the liquids will eventually recover their original viscosity when the shearing force is removed. When this recovery process is sufficiently time dependent the fluid is considered to be thixotropic.
Oscillatory regimen was used for visco-elasticity study and determination of sol-gel transition at 1Hz frequency in an ascending ramp from 10°C to 50°C. All measurements have been performed in triplicates.

4.7 Injectability studies
Injectability or syringeability is the force required to inject a pharmaceutical product at a given infusion rate through a given gauge and length of needle. The injectability of the gel was determined using the method previously described in the literature [48].
The device was coupled to a Texture Analyzer in compression mode and equipped with a force transducer calibrated with a 5kg sensor. The principle is to apply a specific displacement rate to a gel-filled syringe plunger and measure the resulting injection input. Samples were placed in 1mL luer-lock syringe syringes and let at RT for at least 20 min. Needles of 26G and 30G has been placed at the edge of each syringe.
The displacement rate of the plunger was 0.5 mm/s corresponding to a flow rate of 0.4 mL/min, in a 1mL luer-lock syringe which is close to a manual injection rate [48] All measurements were made in triplicates at room temperature (23°C) for each lot of gel. The feasibility of manual injection of all formulations using different needles was also systematically checked.

4.8 Degradation study of hydrogels:
Hydrogels were placed in microtubes and directly covered with a PBS buffer to mimic physiological conditions at 37°C under stirring. They were weighed for a week after each incubation time and fresh PBS was renewed. Weight loss of the samples is represented in the function of time in hours. All experiments were made in triplicates.(POL + 0% and 2% HA hydrogels)

4.9. Release study of Lysozyme and BMP-4 from HA-POL407 hydrogel
Release study has been assessed using a transwell method where the hydrogel in an indirect contact with the recipient release medium. The transwell porosity is 8um and permits to the proteins to migrate through the pores, given that their respective molecular weights are 14 kDa and 25 kDa. The quantification of Lysozyme have been done using Micrococcus Leidococcus kit by Sigma Aldrich, and the following protocols [49–51] and BMP-4 have been detected via the ELISA DuoSet Kit from R&D Systems.

4.10 Cytotoxicity hydrogel assay:
The assessment of hydrogel toxicity has been done, using an indirect method where cells are grown on a 24 well plate and inserts of 8um of porosity have been placed upon each well and hydrogel injected in the insert. Incubation was performed during 24, 48 and 72hrs in 37% 5%CO2 on fibroblast NIH3T3 cell lines, in an incubator. MTS assay was used to quantify cell viability, plates were read on a multiplate reader at 590 nm wavelength.

Conclusion of Chapter 5:

This paper describes the creation of Hyaluronic acid-Poloxamer 407-based nanocomposite gels incorporating BMP-4-loaded PLGA-based nanoparticles in order to achieve prolonged BMP-4 release. To the state of the art, this is the first case of a composite polymer-based vehicle being used for intracerebral delivery of protein biomolecules. As a result, the feasibility of using these scaffolds to transport proteins with similar physicochemical properties to BMP-4 should be investigated. Besides, because the scaffold displayed great *in vitro* cytocompatibility as well as acceptable rheological and injectability features, the *in vivo* assessment of their safety profile is justified. Finally, when the bulk tumor has been removed from the brain, the implantation of the scaffolds into the tumor resection cavity might offer tremendous potential as an efficient treatment method (figure 39).

The goal of this chapter, was to develop thermosensitive and injectable polymeric technology composed of poloxamer, HA blends and high molecular weight HA with acceptable Tgel, biocompatible system, viscoelastic qualities, and controlled release functionality. One prospective application of these systems in drug delivery systems is to improve drug residence duration and bioavailability, hence overcoming the disadvantages associated with the use of traditional dosage forms. The practicality of these platforms for intracerebral administration was investigated in particular by loading Lysozyme as a reference protein and BMP-4 as the therapeutic medication and evaluating its *in vitro* release under healthy settings. Furthermore, physical characteristics such as SAXS, DSC, ATR-FTIR, Rheology, injectability, erosion assay, and *in vitro* like cytotoxicity assay have been developed.

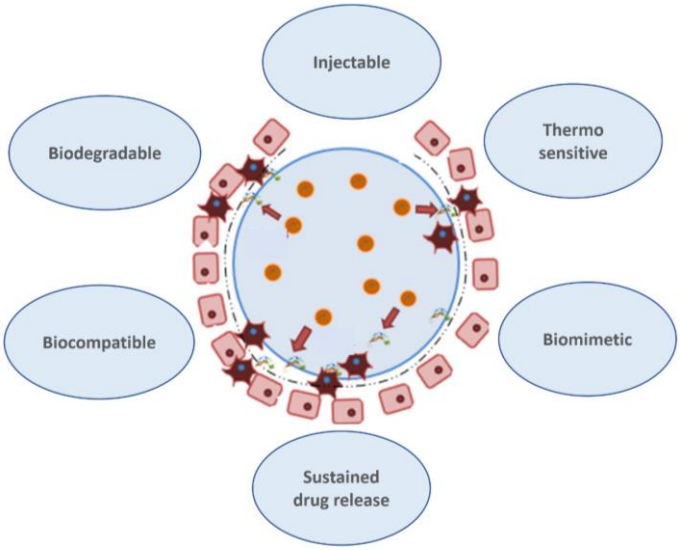


Figure 38: Nanocomposite hydrogel model for locoregional treatment of GB (Adapted from Haji Mansor et al. 2019)

Other experimentations are in course such as biocompatibility study *in vivo* and bio performance assays in order to confirm a potential therapeutic effect of BMP-4 in a suitable and validated animal model.

Funding and Acknowledgement: This work was carried out with support from by La Ligue Contre le Cancer (grant number TARC21174 to A.D.). It was also supported by the Institut National de la Santé et de la Recherche Médicale (INSERM) and by the University of Angers (Angers, France). The work was in addition related : (i) to the Region Pays-de-la-Loire programs to F.B. : Bioimplants for Bone Regeneration (BILBO) part of the BIOREGATE Research-Training-Innovation consortium (RFI) and NanoFar + (International Strategy) and (ii) to the French National Research Agency (ANR) under the frame of EuroNanoMed III (project GLIOSILK) and through the LabEx IRON (Innovative Radiopharmaceuticals in Oncology and Neurology) as part of the French government Investissements d'Avenir program (ANR-11-LABX-0018 to E.G.). Romain Mallet of the SCIAM (Common service for Imaging and microscopy analysis, Angers, France) for SEM analyses. Franck Artzner from IPR-Rennes for SAXS analysis. Olivier Aleveque from MOLTECH (plateau CARMA / SFR MATRIX) for ATR-FTIR analyses and Magali Allain from MOLTECH for DSC. Olivier Thomas from MINT for freeze-drying. François Loll and Thierry Rouillon for rheology and injectability studies from the RMeS team in the Odontology department of Nantes University.

References:

[1] Hoffman AS. Hydrogels for biomedical applications. Advanced Drug Delivery Reviews 2012;64:18–23. https://doi.org/10.1016/j.addr.2012.09.010.

[2] Hoare TR, Kohane DS. Hydrogels in drug delivery: Progress and challenges. Polymer 2008;49:1993–2007. https://doi.org/10.1016/j.polymer.2008.01.027.

[3] Borzacchiello A, Russo L, Malle BM, Schwach-Abdellaoui K, Ambrosio L. Hyaluronic Acid Based Hydrogels for Regenerative Medicine Applications. BioMed Research International 2015;2015:e871218. https://doi.org/10.1155/2015/871218.

[4] Klouda L, Mikos AG. Thermoresponsive hydrogels in biomedical applications - a review. Eur J Pharm Biopharm 2008;68:34–45. https://doi.org/10.1016/j.ejpb.2007.02.025.

[5] Chatterjee S, Hui PC, Kan C. Thermoresponsive Hydrogels and Their Biomedical Applications: Special Insight into Their Applications in Textile Based Transdermal Therapy. Polymers (Basel) 2018;10:480. https://doi.org/10.3390/polym10050480.

[6] Chatterjee S, Hui P, Kan C-W, Wang J. Dual-responsive (pH/temperature) Pluronic F-127 hydrogel drug delivery system for textile-based transdermal therapy. Scientific Reports 2019;9:11658. https://doi.org/10.1038/s41598-019-48254-6.

[7] Giuliano E, Paolino D, Cristiano M, Fresta M, Cosco D. Rutin-Loaded Poloxamer 407-Based Hydrogels for In Situ Administration: Stability Profiles and Rheological Properties. Nanomaterials 2020;10:1069. https://doi.org/10.3390/nano10061069.

[8] Ahmed EM. Hydrogel: Preparation, characterization, and applications: A review. J Adv Res 2015;6:105–21. https://doi.org/10.1016/j.jare.2013.07.006.

[9] Hsieh H-Y, Lin W-Y, Lee A, Li Y-C, Chen Y-J, Chen K-C, et al. Hyaluronic acid on the urokinase sustained release with a hydrogel system composed of poloxamer 407: HA/P407 hydrogel system for drug delivery. PLOS ONE 2020;15:e0227784. https://doi.org/10.1371/journal.pone.0227784.

[10] Akkari ACS, Papini JZB, Garcia GK, Franco MKKD, Cavalcanti LP, Gasperini A, et al. Poloxamer 407/188 binary thermosensitive hydrogels as delivery systems for infiltrative local anesthesia: Physico-chemical characterization and pharmacological evaluation. Materials Science and Engineering: C 2016;68:299–307. https://doi.org/10.1016/j.msec.2016.05.088.

[11] Artzner F, Geiger S, Olivier A, Allais C, Finet S, Agnely F. Interactions between Poloxamers in Aqueous Solutions: Micellization and Gelation Studied by Differential Scanning Calorimetry, Small Angle X-ray Scattering, and Rheology. Langmuir 2007;23:5085–92. https://doi.org/10.1021/la062622p.

[12] Dimer F, Pereira G, Guterres S, Cardozo N, Kechinski C, Granada J. Formulation and characterization of poloxamer 407®: Thermoreversible gel containing polymeric microparticles and hyaluronic acid. Química Nova 2013;36:1121–5. https://doi.org/10.1590/S0100-40422013000800008.

[13] Jre F, Tc L, Ubg L. Hyaluronan: its nature, distribution, functions and turnover 1997:7.

[14] Passi A, Vigetti D. Hyaluronan: Structure, Metabolism, and Biological Properties. In: Cohen E, Merzendorfer H, editors. Extracellular Sugar-Based Biopolymers Matrices, vol. 12, Cham: Springer International Publishing; 2019, p. 155–86. https://doi.org/10.1007/978-3-030-12919-4_4.

[15] Vercruysse KP. Chapter 9. Hyaluronan: a Simple Molecule with Complex Character. In: Williams PA, editor. Polymer Chemistry Series, Cambridge: Royal Society of Chemistry; 2011, p. 261–91. https://doi.org/10.1039/9781849733519-00261.

[16] Li X, Li A, Feng F, Jiang Q, Sun H, Chai Y, et al. Effect of the hyaluronic acid-poloxamer hydrogel on skin-wound healing: in vitro and in vivo studies. Animal Models and Experimental Medicine 2019;2:107–13. https://doi.org/10.1002/ame2.12067.

[17] Mayol L, Quaglia F, Borzacchiello A, Ambrosio L, La Rotonda MI. A novel poloxamers/hyaluronic acid in situ forming hydrogel for drug delivery: rheological, mucoadhesive and in vitro release properties. Eur J Pharm Biopharm 2008;70:199–206. https://doi.org/10.1016/j.ejpb.2008.04.025.

[18] Yang R, Chen M, Yang X, Sun W, Lu C, Hui Q, et al. Modified poloxamer 407 and hyaluronic acid thermosensitive hydrogel-encapsulated keratinocyte growth factor 2 improves knee osteoarthritis in rats. Materials & Design 2021;210:110086. https://doi.org/10.1016/j.matdes.2021.110086.

[19] Saraswathy M, Sreenivasan K. Conjugation of curcumin onto hyaluronic acid enhances its aqueous solubility and stability. Journal of Colloid and Interface Science 2011;359:318–25. https://doi.org/10.1016/j.jcis.2011.03.071.

[20] Chen H, Qin J, Hu Y. Efficient Degradation of High-Molecular-Weight Hyaluronic Acid by a Combination of Ultrasound, Hydrogen Peroxide, and Copper Ion. Molecules 2019;24:617. https://doi.org/10.3390/molecules24030617.
[21] Pontremoli C, Boffito M, Fiorilli S, Laurano R, Torchio A, Bari A, et al. Hybrid injectable platforms for the in situ delivery of therapeutic ions from mesoporous glasses. Chemical Engineering Journal 2018;340. https://doi.org/10.1016/j.cej.2018.01.073.
[22] Laurano R, Abrami M, Grassi M, Ciardelli G, Boffito M, Chiono V. Using Poloxamer® 407 as Building Block of Amphiphilic Poly(ether urethane)s: Effect of its Molecular Weight Distribution on Thermo-Sensitive Hydrogel Performances in the Perspective of Their Biomedical Application. Frontiers in Materials 2020;7.
[23] Nascimento MHM, Franco MKKD, Yokaichyia F, de Paula E, Lombello CB, de Araujo DR. Hyaluronic acid in Pluronic F-127/F-108 hydrogels for postoperative pain in arthroplasties: Influence on physico-chemical properties and structural requirements for sustained drug-release. International Journal of Biological Macromolecules 2018;111:1245–54. https://doi.org/10.1016/j.ijbiomac.2018.01.064.
[24] Park H, Treich G, Helming Z, Morgan J, Ryu C, Hwang H, et al. Micellar Packing of Pluronic Block Copolymer Solutions: Polymeric Impurity Effects. Macromolecular Research 2015;23:13–20. https://doi.org/10.1007/s13233-015-3014-4.
[25] Peng X, Wen X, Pan X, Wang R, Chen B, Wu C. Design and In Vitro Evaluation of Capsaicin Transdermal Controlled Release Cubic Phase Gels. AAPS PharmSciTech 2010;11:1405–10. https://doi.org/10.1208/s12249-010-9481-1.
[26] Bermudez J, Grau R. Injectable Thermosensitive Gels Based in Poloxamer as Modified Drug Release Systems for Veterinary Use. LATIN AMERICAN JOURNAL OF PHARMACY 2010;29:1377–82.
[27] Abdul Rasool B, Abu-Gharbieh E, Awni R, Rasool A. In Vitro Release Study of Nystatin from Chitosan Buccal Gel. Jordan Journal of Pharmaceutical Sciences 2010;3:2010–44.
[28] Liu B, Huang P-JJ, Zhang X, Wang F, Pautler R, Ip ACF, et al. Parts-per-million of polyethylene glycol as a non-interfering blocking agent for homogeneous biosensor development. Anal Chem 2013;85:10045–50. https://doi.org/10.1021/ac4024654.
[29] Wei G, Xu H, Ding PT, Li SM, Zheng JM. Thermosetting gels with modulated gelation temperature for ophthalmic use: the rheological and gamma scintigraphic studies. J Control Release 2002;83:65–74. https://doi.org/10.1016/s0168-3659(02)00175-x.
[30] AMBROSIO L, BORZACCHIELLO A, NETTI PA, NICOLAIS L. Rheological Study on Hyaluronic Acid and Its Derivative Solutions. Journal of Macromolecular Science, Part A 1999;36:991–1000. https://doi.org/10.1080/10601329908951195.
[31] Maltese A, Borzacchiello A, Mayol L, Bucolo C, Maugeri F, Nicolais L, et al. Novel polysaccharides-based viscoelastic formulations for ophthalmic surgery: rheological characterization. Biomaterials 2006;27:5134–42. https://doi.org/10.1016/j.biomaterials.2006.05.036.
[32] Xin X, Borzacchiello A, Netti PA, Ambrosio L, Nicolais L. Hyaluronic-acid-based semi-interpenetrating materials. Journal of Biomaterials Science, Polymer Edition 2004;15:1223–36. https://doi.org/10.1163/1568562041753025.
[33] Najberg M, Haji Mansor M, Taillé T, Bouré C, Molina-Peña R, Boury F, et al. Aerogel sponges of silk fibroin, hyaluronic acid and heparin for soft tissue engineering: Composition-properties relationship. Carbohydr Polym 2020;237:116107. https://doi.org/10.1016/j.carbpol.2020.116107.
[34] Entekhabi E, Haghbin Nazarpak M, Moztarzadeh F, Sadeghi A. Design and manufacture of neural tissue engineering scaffolds using hyaluronic acid and polycaprolactone nanofibers with controlled porosity. Materials Science and Engineering: C 2016;69:380–7. https://doi.org/10.1016/j.msec.2016.06.078.
[35] Lam J, Truong NF, Segura T. Design of cell–matrix interactions in hyaluronic acid hydrogel scaffolds. Acta Biomaterialia 2014;10:1571–80. https://doi.org/10.1016/j.actbio.2013.07.025.
[36] El Kechai N, Bochot A, Huang N, Nguyen Y, Ferrary E, Agnely F. Effect of liposomes on rheological and syringeability properties of hyaluronic acid hydrogels intended for local injection of drugs. International Journal of Pharmaceutics 2015;487:187–96. https://doi.org/10.1016/j.ijpharm.2015.04.019.
[37] El Kechai N, Mamelle E, Nguyen Y, Huang N, Nicolas V, Chaminade P, et al. Hyaluronic acid liposomal gel sustains delivery of a corticoid to the inner ear. Journal of Controlled Release 2016;226:248–57. https://doi.org/10.1016/j.jconrel.2016.02.013.

[38] Kechai NE. Gels d'acide hyaluronique contenant des liposomes pour la libération prolongée d'un corticoïde dans l'oreille interne n.d.:242.
[39] Barichello JM, Morishita M, Takayama K, Nagai T. Absorption of insulin from Pluronic F-127 gels following subcutaneous administration in rats. International Journal of Pharmaceutics 1999;184:189–98. https://doi.org/10.1016/S0378-5173(99)00119-2.
[40] Alexandridis P, Alan Hatton T. Poly(ethylene oxide)◎poly(propylene oxide)◎poly(ethylene oxide) block copolymer surfactants in aqueous solutions and at interfaces: thermodynamics, structure, dynamics, and modeling. Colloids and Surfaces A: Physicochemical and Engineering Aspects 1995;96:1–46. https://doi.org/10.1016/0927-7757(94)03028-X.
[41] Alexandridis P, Hatton TA, Holzwarth JF. Micellization of poly(ethylene oxide)-poly(propylene oxide)-poly(ethylene oxide) triblock copolymers in aqueous solutions: Thermodynamics of copolymer association. Macromolecules; (United States) 1994;27:9. https://doi.org/10.1021/ma00087a009.
[42] Li J, Mooney DJ. Designing hydrogels for controlled drug delivery. Nat Rev Mater 2016;1:16071. https://doi.org/10.1038/natrevmats.2016.71.
[43] Gratieri T, Gelfuso GM, Rocha EM, Sarmento VH, de Freitas O, Lopez RFV. A poloxamer/chitosan in situ forming gel with prolonged retention time for ocular delivery. Eur J Pharm Biopharm 2010;75:186–93. https://doi.org/10.1016/j.ejpb.2010.02.011.
[44] Bhardwaj R, Blanchard J. Controlled-release delivery system for the alpha-MSH analog melanotan-I using poloxamer 407. J Pharm Sci 1996;85:915–9. https://doi.org/10.1021/js960097g.
[45] Zhang K, Shi X, Lin X, Yao C, Shen L, Feng Y. Poloxamer-based in situ hydrogels for controlled delivery of hydrophilic macromolecules after intramuscular injection in rats. Drug Deliv 2015;22:375–82. https://doi.org/10.3109/10717544.2014.891272.
[46] Chun KW, Lee JB, Kim SH, Park TG. Controlled release of plasmid DNA from photo-cross-linked pluronic hydrogels. Biomaterials 2005;26:3319–26. https://doi.org/10.1016/j.biomaterials.2004.07.055.
[47] Hubert C, Meriadec C, Panizza P, Artzner F, de Clermont-Gallerande H. Comparison between a wax/volatile oil mixture and vegetable butters in a long-lasting make-up formula: A rheological and structural study compared to product performance. OCL 2020;27:42. https://doi.org/10.1051/ocl/2020035.
[48] Burckbuchler V, Mekhloufi G, Giteau AP, Grossiord JL, Huille S, Agnely F. Rheological and syringeability properties of highly concentrated human polyclonal immunoglobulin solutions. European Journal of Pharmaceutics and Biopharmaceutics 2010;76:351–6. https://doi.org/10.1016/j.ejpb.2010.08.002.
[49] Haji Mansor M, Najberg M, Contini A, Alvarez-Lorenzo C, Garcion E, Jérôme C, et al. Development of a non-toxic and non-denaturing formulation process for encapsulation of SDF-1α into PLGA/PEG-PLGA nanoparticles to achieve sustained release. Eur J Pharm Biopharm 2018;125:38–50. https://doi.org/10.1016/j.ejpb.2017.12.020.
[50] Morille M, Van-Thanh T, Garric X, Cayon J, Coudane J, Noël D, et al. New PLGA–P188–PLGA matrix enhances TGF-β3 release from pharmacologically active microcarriers and promotes chondrogenesis of mesenchymal stem cells. Journal of Controlled Release 2013;170:99–110. https://doi.org/10.1016/j.jconrel.2013.04.017.
[51] Swed A. Sustained release of TGF-β1 from biodegradable microparticles prepared by a new green process in CO2 medium. International Journal of Pharmaceutics 2015:9.

Chapter 6
General discussion and perspectives

6.General discussion and perspectives

6.1 General discussion

Glioblastoma tumors, now known as glioblastoma (GB), continue to be a source of concern for both physicians and researchers with a very poor prognosis for patients. Since 2021, Louis et al have actualized the classification of CNS tumors. Hence, Glioblastoma is now GB and no longer called Glioblastoma Multiforme [1,2]. Among adult-type diffuse gliomas, the most frequency primary brain tumors in neuro-oncology practice is GB- IDH wild type and still holds the grade 4 [1]. Due to the fact that GB can advance extremely quickly, surgical technique has been established as the first-line treatment for this illness due to its effectiveness in instantly lowering the bulk tumor volume and minimizing its aggressiveness. In reality, this method has been the standard method for a while [3–6]. Having said that, it's worth mentioning that surgical removal of brain tumors has been studied and improved since 1879 [4,7]. However, true excitement about the procedure's curative potential would not arise until almost a century later. The growing anticipation was fueled by significant advances in *in vivo* imaging, such as computed tomography (CT) scanning and magnetic resonance imaging (MRI) [8,9].

Adjuvant therapies such as radiation and chemotherapy are used after surgery to eliminate the remaining tumor cells. When these therapies are combined, the median survival time for GB patients after diagnosis is only about 15 months [4,7]. The bad prognosis is caused by a small fraction of remaining tumor cells that survive despite the damaging impact of post-surgical therapy and grow to produce a tumor with even more aggressive characteristics. Incomplete death of remaining tumor cells might be attributed to chemoresistance or evasion owing to anatomical limits [10–12].
To complicate things, the poorly targeted modes of action of chemoradiation therapy can frequently result in significant harm to the healthy brain tissues with which they come into contact [4,13]. Patient' conditions are deteriorating not just as a result of tumor recurrence, but also as a result of the adverse effects of the therapies they got [14,15]. As a result, we were encouraged to investigate the method of differentiating remaining tumor cells into a less tumorigenic and resistant phenotype to permit more selective and thorough elimination of this cell population [16,17].

GB is a severe cancer to treat due to its aggressiveness, high chance of recurrence, and resistance caused by CSC. CSCs include a plethora of markers for this cell type (CD24, CD34, Nestin, Sox2). Because of gene mutations, CSCs can survive apoptosis, retain the parental phenotype, and reduce sensitivity to differentiation cues [11,15,18]. Several signaling pathways are being studied in order to develop drugs that can destroy CSCs and prevent disease recurrence [12].

Despite the fact known that GB stem cells can differentiate, it is less clear if they can commit to persistent differentiation and achieve the terminal cell cycle. Clinical transfer of BMP-based differentiation treatment may thus be difficult [10,17]. Firstly, there are considerable variances in responses between cell lines, which is to be expected in patients [17]. Secondly, although induction is rapid, methylation changes are slow and need continuous exposure to treatment [19]. Finally, acquired mutations are not persistent, and reversal, de-differentiation, or selection of differentiation-resistant clones are still possible [12,14].

Therefore, overcoming these obstacles at the beginning will be a big effort in the design of differentiation therapies. Implementing differentiation therapy for GB demands a deeper understanding of the methods by which tumor cells resist differentiation commitment [12,14]. These CSCs can persist more than one centimeter out from the resection cavity boundary [18]. As a result, extended BMP-4 release will be essential for extending the treatment duration. In light of this consideration, the goal of this thesis was to create scaffolds that may offer continuous delivery of bioactive BMP-4, and the experimental approach was focused on two goals:

• Encapsulating BMP-4 in polymer-based nanoparticles to produce main carriers of this cytokine

• Incorporating BMP-4-loaded nanoparticles into an injectable hydrogel to offer a secondary barrier to BMP-4 release

Objective 1: To prepare BMP-4 loaded polymer nanoparticles

Protein delivery using PLGA nanoparticles is of relevance for a variety of applications, including the production of innovative, more effective, and safer tissue engineering procedures. Moreover, the fragility, lack of cell selectivity, toxicity, and oncogenic potential of growth factors need the creation of such delivery methods that allow for the targeted and sustained release of these macromolecules [20,21]. Nevertheless, the destabilizing conditions applied to the proteins during the formation of these systems, as well as the breakdown of the polymers during storage, incubation, limit their development [22,23].
Nanoparticles made of polymers have been utilized to transport a variety of protein molecules. Various formulation procedures, such as phase separation, may be used to easily create nanoparticles from a broad variety of polymers [24–27]. Although their extensive use, neither of these nanoparticle formulation methods can easily encapsulate all forms of proteins. The encapsulation procedure must frequently be carefully selected based on the physicochemical parameters of the protein to be encapsulated [28]. Aside from determining the best formulation technique, selecting the proper type of polymer is critical. After this, different process and polymeric parameters should be verified to obtain appropriate encapsulating efficiencies and release kinetics. In this work, we adapted an existing process for encapsulating proteins in particulate polymeric systems utilizing non-toxic solvents for use in GB application [24–26,29].
Because therapeutic proteins are expensive, we decided to start by proving the notion of the proposed methods by assessing the encapsulation ability of a model protein. Due to the sensitivity of detecting its enzymatic activity, lysozyme was chosen as a model protein to readily measure the quantity of protein encapsulated and released in active form from protein loaded particles [24,25,29]. Nanoprecipitation process was used for both Lysozyme and BMP-4 to protect them during encapsulating step. Indeed, This reduces the requirement of protein solution emulsification in the polymer phase, which can frequently result in protein molecule unfolding at the water-oil interface [24,30]. Protein molecules fold *in vivo* to shield their hydrophobic residues from watery conditions [24,30]. If confronted to an oil-water interface, they can undertake structure and conformation rearrangements in order to obtain the state of lowest free energy. The non-polar residues might be accessible and engage interactions with the oil phase, causing a protein's three-dimensional structure to change and possibly affect its bioactivity [24,30]. Protein molecules possess restricted conformational mobility once precipitated, reducing their ability to unfold when in contact with organic solvents [24,30].

A mixture of PLGA-COOR and PEG-PLGA was employed in this study to create nanoparticles through a phase separation approach. The creation of a polymer-rich liquid phase (coacervate) all around inner protein-containing aqueous phase is aided by the polymer's phase separation from its solution. Because more non-solvent is introduced, the coacervate hardens to form protein-loaded nanoparticles [31–33]. The need for a substantial amount of organic solvent to produce phase separation is an evident disadvantage of this approach [25,34,35]. To overcome this, isosorbide dimethyl ether (DMI) was employed to dissolve PLGA and PEG-PLGA. DMI is a non-halogenated, non-volatile solvent with a great *in vivo* safety profile [36]. Furthermore, it is a water-miscible solvent, which means that the phase separation stage may be activated by aqueous solvents like water.

Utilization of such a harmless solvent, as well as the large reduction in the overall amount of organic solvents used, serves to eliminate the need for any specific devices or facilities to safeguard the operators [36]. Thus, the formulation process was purposefully created to be straightforward so that it could be executed by anyone else.
We demonstrated that encapsulating BMP-4 precipitates in PLGA solutions before the phase separation showed no observable loss of biological activity. We also demonstrated that factors like protein content and

ionic strength can influence the effectiveness of the precipitation process in regards to the quantity and bioactivity of the precipitates obtained. As a result, if the established formulation technique is utilized to encapsulate additional forms of protein in the future, the precipitation parameters will need to be re-optimized.

Regardless of the apparent ease of the formulation process, there are several aspects that might affect the final protein encapsulation efficiency. Due to their high water solubility, protein molecules prone to segregate into the aqueous phase during phase separation process, causing a low encapsulation efficiency. The pH of the aqueous phase was buffered near to the isoelectric point (pI) of the protein being loaded, which alleviated the issue. The net charge of the protein molecules that came into touch with the buffer solution will be near to zero as a result, making the protein less water-soluble.
A neutral Tris-HCl buffer solution was utilized throughout the phase separation process since BMP-4 has a pI of 7.6. Aside from modifying the pH, adding salts or other agents can reduce the aqueous phase protein solvation capability. When salts like ammonium sulfate and hydrophilic polymers like PEG are introduced to an aqueous solvent, they can interact with water molecules that would otherwise be accessible for protein solvation [37,38]. As a result, they may be effective in reducing protein loss from the organic phase throughout the phase separation process.

Encapsulation efficiency can be influenced by polymer characteristics in addition to process factors. It has been demonstrated that employing PLGA with uncapped, so ionizable, carboxylic terminals resulted in improved encapsulation [24]. It has been shown previously, that the high amount of carboxyl groups in uncapped PLGA nanoparticles may bind significantly with protein molecules, increasing its encapsulation efficiency and inhibiting their release [24]. As a result, according to previous studies, we chose PLGA with capped terminals encapsulation efficiency in exchange for more complete protein release. The encapsulation efficiency for Formulation 6 (86%) was higher than the Formulation 5 (71%).
Encapsulation efficiency for BMP-4 was 71% using Formulation 5 and less than 80% was released and 86% of protein was encapsulated in the Formulation 6 but less than 60% of BMP-4 was released at the end of the 30-day release study period. The degradation of the PLGA ester bonds, which produced ionizable carboxyl groups that may then interact forcefully, may account for the lack of completely complete BMP-4 release.

Because PLGA is prone to hydrolysis, it is critical to keep PLGA-based nanoparticles dry. Lyophilization, also known as freeze-drying, is a typical procedure for eliminating water from PLGA-based nanoparticle aqueous dispersions. Because this approach can cause large physical stresses on the nanoparticles, di/oligosaccharides are frequently incorporated to the nanoparticle dispersion to generate a spacing matrix to avoid nanoparticle aggregation [24,39]. However, it should be mentioned that the performance of these so-called "protectants" varies between publications [24,39,40].

Many of these papers either omitted to specify the specific parameters (temperature and pressure) of the freeze-drying settings or failed to demonstrate why a particular combination of circumstances was selected [24,39]. We demonstrated in our study that the efficacy of freeze-drying in terms of retaining the size and polydispersity of the nanoparticles is contingent on the drying temperature being lower than the collapse temperature of the added protectant. As a result, it is critical to select a cryoprotectant types with a high collapse temperature or to reduce the drying temperature as much as conceivable [39]. Here, we selected HP-beta-CD which has been shown in a previous study to be the most suitable for a long-term storage and an efficient conservation of PDI and size [24].

Moreover, zeta potential of the blank nanoparticles in different pH have shown a better stability at a physiological pH which is suitable for our locoregional application. The biocompatibility has also been proven through the cytotoxicity study made on the NIH3T3 and L929 cell lines.
However, the *in vitro* studies on three-dimensional gliomasphere models have shown a poor bioactivity of BMP-4, it did not seem to reduce the gliomasphere formation in comparison to the control and to BMP-2 treatment. On the contrary, this latter has shown a stimulation of the gliomasphere number on F98 cell line. Figures 31 and 32 have shown an effect on U87MG linked to phenotype changing but F98 exhibited a cell necrosis effect that have been confirmed with FACS study. The results are being completed with an

immunofluorescence study and checking differentiation markers with flow cytometry method. Other experiments are in course *in vivo* biocompatibility, bioperformance, and *in vivo* BMP-4 detection through histological and immunofluorescence method. Those studies are ongoing and are not finalized yet, therefore where not present in manuscript.

Objective 2: To incorporate BMP-4-loaded nanoparticles into a HA-Poloxamer407 hydrogel

Since the BMP-4-loaded nanoparticles enable only transitory protein release, they were then integrated into a cold thermogelated Hyaluronic acid-Poloxamer 407 hydrogel to extend the release time and maintain the protein at 4°C to avoid denaturation.

Due to its physicochemical qualities and biological features such as biocompatibility and biomimetism, HA was chosen as the polymer of choice for the hydrogel formation process. Poloxamer 407 also has interesting and comparable features, as well as additional ones such as controlled release and thermosensitivity.
Crucial features in this study were the shear-thinning property and injectability. Compared to systems like chitosan nanocomposite electrospun fibers developed by Haji Mansor et al. or HA- Silk fibroin- Heparin sponges developped by Najberg et al., both intended for GB, or Gliadel wafer that is commercialized for GB treatment, our thermosensitive nanocomposite hydrogels can be easily injected into an *in vivo* resection cavity and fill it entirely which can increase contact surface and protein reaching its target, the CSCs [24,41–44].
In the first objective, the majority of the protein encapsulated was released between 48 and 72 hours, but after incorporating the BMP-4 loaded NPs into the HA-POL407 hydrogel it has shown a delay of the release, with a majority of the protein release between 5 and 7 days. To prolong the release rate, HA should be crosslinked, modifying the surface of the NPs or optimizing the content of the release medium.

As previously stated, BMP-4 can be released freely when the cations Na+ in the release media neutralize any ionized carboxyl groups in the nanoparticles. The easy availability of the release medium to the nanoparticles, on the other hand, might contribute to the hydrolysis of the PLGA ester bonds, resulting in a high number of ionized carboxyl groups, which can limit future release of the encapsulated BMP-4. This explains why nanoparticles release BMP-4 for such a short period of time.
The incorporation of these nanoparticles into HA-POL407 hydrogels slows the infiltration of release media into the nanoparticles, avoiding the initial burst release and a rapid rise in the amount of ionized carboxyl groups, both of which contribute to more continuous BMP-4 release. We also demonstrated that BMP-4 molecules placed directly into the HA-POL407 hydrogel were promptly released following incubation in an adequate release environment. Because of the quick release of bare BMP-4 and the delayed release of its encapsulated equivalent from the hydrogel, the pace of BMP-4 distribution at the site of implantation may be tailored to optimize the amount of GB cells treated. Moreover, the release profile is also linked to the erosion kinetics of the hydrogel in physiological conditions.

Other characterizations such as the rheology and injectability studies have shown a shear thinning behavior, a thixotropic system that after undergoing a shear stress, can recover its initial properties, which is a useful property for the injection step in the resection cavity. The sol-gel transition results of the selected formulation HA2%POL407 20% has a gelation at 32°C close to the physiological temperature and a Young Modulus that reaches 10kPa, close to the human brain value which is around 1-10kPa, thus, giving the hydrogel biomimetic properties [45]. For the injectability force assessment, the hydrogel HA2%POL407 20% with NPs could be injected with a 1mL luer-lock 26G needle with a good control over the volume and with a constant rate. Finally, hydrogel have shown a good cytocompatibility, making it a good candidate for further applications.

6.2 Conclusion and perspectives

The goal of this thesis study was to tune a non-toxic process for encapsulating therapeutic proteins in PLGA particles and integrate them in a HA-POL407 hydrogel for the treatment of Glioblastoma. This study thereby connects two significant fields of biomedical research, galenic development and tissue engineering. The work

done for the thesis is organized around three major axes: A bibliographical examination of the state of the art in the differentiation approach, therapeutic protein vectorization. This paper explains the phase separation and nanoprecipitation encapsulation process in particulate polymeric systems, the organic solvents utilized, and the formation of thermosensitive hydrogels made of hyaluronic acid and poloxamer 407.

Lastly, a review of hyaluronic acid-based systems for the treatment of central and peripheral nervous system diseases, as well as glioblastoma, fulfills this bibliographic study. The first experimental investigation on the encapsulation of a model protein (lysozyme) and a therapeutic protein (BMP-4) in PLGA nanoparticles using the phenomena of phase separation and non-toxic solvents DMI and GF. A second research focused on the phase separation encapsulation of lysozyme and BMP-4 in PLGA nanoparticles embedded in an injectable hyaluronic acid and Poloxamer 407 hydrogel, as well as the physicochemical and biological evaluation of this system.

In summary, the major goal of this research was accomplished by creating two methods for encapsulating a protein BMP-4 in PLGA nanoparticles without the use of a harmful solvent. Furthermore, we established the promise of these systems for glioblastoma treatment by designing an injectable biomaterial capable of targeted and sustained release of functional therapeutic proteins. This study yielded encouraging results and opened up new avenues of inquiry. In addition, the scaffolds exhibit excellent *in vivo* biocompatibility.
It appears conceivable to test the developed biomaterial ability to stimulate the differentiation of cancer stem cells and to investigate therapeutic effectiveness *in vivo* utilizing an animal model.

Yet, in order to obtain a continuous and full release, the protein release kinetics from these particulate structures would need to be improved. More hydrophilic copolymers, such as PLGA-PEG-PLGA, are possible and will be the focus for future research projects. Finally, preliminary results show that our techniques are capable of encapsulating additional proteins such as BMP-2, which would allow us to broaden the areas of use such as bone regeneration in the dental sector in partnership with another team. *In vivo* biocompatibility and bioefficacy of our nanocomposite system on an animal model studies are in course and supplementary experiments are being assessed for the *in vitro* part.

To summarize, the work done in this project led to the creation of a tool that may be employed in the tumor differentiation strategy and might allow future proof-of-concept step. The study also advanced the area of nanomedicine and drug delivery from a physicochemical standpoint by developing novel polymer-based systems for local delivery of protein therapeutics. The created scaffolds tumor differentiation ability and selectivity will be deeply tested next.

Many partnerships involving multidisciplinary researchers will be required to answer basic issues about the tumor differentiation strategy's potential as a therapy for GB. In addition, feedback from neurosurgeons and patient group advocates will be required to examine the clinical feasibility of this method. Hence, this thesis might serve as a foundation for the creation of a therapeutic tool for GB treatment.

References:

[1] Louis DN, Perry A, Wesseling P, Brat DJ, Cree IA, Figarella-Branger D, et al. The 2021 WHO Classification of Tumors of the Central Nervous System: a summary. Neuro Oncol 2021;23:1231–51. https://doi.org/10.1093/neuonc/noab106.
[2] Clavreul A, Soulard G, Lemée J-M, Rigot M, Fabbro-Peray P, Bauchet L, et al. The French glioblastoma biobank (FGB): a national clinicobiological database. Journal of Translational Medicine 2019;17:133. https://doi.org/10.1186/s12967-019-1859-6.
[3] Barone DG, Lawrie TA, Hart MG. Image guided surgery for the resection of brain tumours. Cochrane Database Syst Rev 2014:CD009685. https://doi.org/10.1002/14651858.CD009685.pub2.
[4] Stupp R, Brada M. High-grade glioma: ESMO Clinical Practice Guidelines for diagnosis, treatment and follow-up. Annals of Oncology 2014;25:9.
[5] Gogos A, Young J, Morshed R, Hervey-Jumper S, Berger M. Awake glioma surgery: technical evolution and nuances. Journal of Neuro-Oncology 2020;147. https://doi.org/10.1007/s11060-020-03482-z.

[6] Stummer W, Pichlmeier U, Meinel T, Wiestler OD, Zanella F, Reulen H-J, et al. Fluorescence-guided surgery with 5-aminolevulinic acid for resection of malignant glioma: a randomised controlled multicentre phase III trial. Lancet Oncol 2006;7:392–401. https://doi.org/10.1016/S1470-2045(06)70665-9.
[7] Stupp R, Weller M, Belanger K, Bogdahn U, Ludwin SK, Lacombe D, et al. Radiotherapy plus Concomitant and Adjuvant Temozolomide for Glioblastoma. The New England Journal of Medicine 2005:10.
[8] Kuhnt D, Becker A, Ganslandt O, Bauer M, Buchfelder M, Nimsky C. Correlation of the extent of tumor volume resection and patient survival in surgery of glioblastoma multiforme with high-field intraoperative MRI guidance. Neuro Oncol 2011;13:1339–48. https://doi.org/10.1093/neuonc/nor133.
[9] Roder C, Bisdas S, Ebner FH, Honegger J, Naegele T, Ernemann U, et al. Maximizing the extent of resection and survival benefit of patients in glioblastoma surgery: high-field iMRI versus conventional and 5-ALA-assisted surgery. Eur J Surg Oncol 2014;40:297–304. https://doi.org/10.1016/j.ejso.2013.11.022.
[10] Wu W, Klockow JL, Zhang M, Lafortune F, Chang E, Jin L, et al. Glioblastoma multiforme (GBM): An overview of current therapies and mechanisms of resistance. Pharmacol Res 2021;171:105780. https://doi.org/10.1016/j.phrs.2021.105780.
[11] Altaner C. Glioblastoma and stem cells. Neoplasma 2008;55:369–74.
[12] Alves ALV, Gomes INF, Carloni AC, Rosa MN, da Silva LS, Evangelista AF, et al. Role of glioblastoma stem cells in cancer therapeutic resistance: a perspective on antineoplastic agents from natural sources and chemical derivatives. Stem Cell Research & Therapy 2021;12:206. https://doi.org/10.1186/s13287-021-02231-x.
[13] Schirrmacher V. From chemotherapy to biological therapy: A review of novel concepts to reduce the side effects of systemic cancer treatment (Review). Int J Oncol 2018;54:407–19. https://doi.org/10.3892/ijo.2018.4661.
[14] Barker HE, Paget JTE, Khan AA, Harrington KJ. The Tumour Microenvironment after Radiotherapy: Mechanisms of Resistance and Recurrence. Nat Rev Cancer 2015;15:409–25. https://doi.org/10.1038/nrc3958.
[15] Xie XP, Laks DR, Sun D, Ganbold M, Wang Z, Pedraza AM, et al. Quiescent human glioblastoma cancer stem cells drive tumor initiation, expansion, and recurrence following chemotherapy. Dev Cell 2022;57:32-46.e8. https://doi.org/10.1016/j.devcel.2021.12.007.
[16] Stockhausen M-T, Kristoffersen K, Stobbe L, Poulsen HS. Differentiation of glioblastoma multiforme stem-like cells leads to downregulation of EGFR and EGFRvIII and decreased tumorigenic and stem-like cell potential. Cancer Biol Ther 2014;15:216–24. https://doi.org/10.4161/cbt.26736.
[17] Carén H, Beck S, Pollard SM. Differentiation therapy for glioblastoma – too many obstacles? Mol Cell Oncol 2015;3:e1124174. https://doi.org/10.1080/23723556.2015.1124174.
[18] Gimple RC, Bhargava S, Dixit D, Rich JN. Glioblastoma stem cells: lessons from the tumor hierarchy in a lethal cancer. Genes Dev 2019;33:591–609. https://doi.org/10.1101/gad.324301.119.
[19] Feldheim J, Kessler AF, Monoranu CM, Ernestus R-I, Löhr M, Hagemann C. Changes of O6-Methylguanine DNA Methyltransferase (MGMT) Promoter Methylation in Glioblastoma Relapse—A Meta-Analysis Type Literature Review. Cancers (Basel) 2019;11:1837. https://doi.org/10.3390/cancers11121837.
[20] Bialy IE. Formulation, Delivery and Stability of Bone Morphogenetic Proteins for Effective Bone Regeneration n.d.:19.
[21] Manning MC, Chou DK, Murphy BM, Payne RW, Katayama DS. Stability of protein pharmaceuticals: an update. Pharm Res 2010;27:544–75. https://doi.org/10.1007/s11095-009-0045-6.
[22] Swed A. Encapsulation de protéines dans des systèmes polymériques particulaires par des procédés sans solvants toxiques pour l'ingénierie tissulaire du cartilage n.d.:156.
[23] Bilati U, Allémann E, Doelker E. Nanoprecipitation versus emulsion-based techniques for the encapsulation of proteins into biodegradable nanoparticles and process-related stability issues. AAPS PharmSciTech 2005;6:E594–604. https://doi.org/10.1208/pt060474.
[24] Haji Mansor M, Najberg M, Contini A, Alvarez-Lorenzo C, Garcion E, Jérôme C, et al. Development of a non-toxic and non-denaturing formulation process for encapsulation of SDF-1α into PLGA/PEG-PLGA nanoparticles to achieve sustained release. Eur J Pharm Biopharm 2018;125:38–50. https://doi.org/10.1016/j.ejpb.2017.12.020.
[25] Swed A, Cordonnier T, Fleury F, Boury F. Protein Encapsulation into PLGA Nanoparticles by a Novel Phase Separation Method Using Non-Toxic Solvents. Journal of Nanomedicine & Nanotechnology 2014;6. https://doi.org/10.4172/2157-7439.1000241.

[26] Giteau A, Venier-Julienne M-C, Marchal S, Courthaudon J-L, Sergent M, Montero-Menei C, et al. Reversible protein precipitation to ensure stability during encapsulation within PLGA microspheres. Eur J Pharm Biopharm 2008;70:127–36. https://doi.org/10.1016/j.ejpb.2008.03.006.
[27] Husmann M, Schenderlein S, Lück M, Lindner H, Kleinebudde P. Polymer erosion in PLGA microparticles produced by phase separation method. Int J Pharm 2002;242:277–80. https://doi.org/10.1016/s0378-5173(02)00187-4.
[28] Brudar S, Hribar-Lee B. Effect of Buffer on Protein Stability in Aqueous Solutions: A Simple Protein Aggregation Model. J Phys Chem B 2021;125:2504–12. https://doi.org/10.1021/acs.jpcb.0c10339.
[29] Morille M, Van-Thanh T, Garric X, Cayon J, Coudane J, Noël D, et al. New PLGA–P188–PLGA matrix enhances TGF-β3 release from pharmacologically active microcarriers and promotes chondrogenesis of mesenchymal stem cells. Journal of Controlled Release 2013;170:99–110. https://doi.org/10.1016/j.jconrel.2013.04.017.
[30] Sah H. Protein instability toward organic solvent/water emulsification: implications for protein microencapsulation into microspheres. PDA J Pharm Sci Technol 1999;53:3–10.
[31] Makadia HK, Siegel SJ. Poly Lactic-co-Glycolic Acid (PLGA) as Biodegradable Controlled Drug Delivery Carrier. Polymers 2011;3:1377–97. https://doi.org/10.3390/polym3031377.
[32] Sinha VR, Trehan A. Biodegradable microspheres for protein delivery. J Control Release 2003;90:261–80. https://doi.org/10.1016/s0168-3659(03)00194-9.
[33] Ding D, Zhu Q. Recent advances of PLGA micro/nanoparticles for the delivery of biomacromolecular therapeutics. Mater Sci Eng C Mater Biol Appl 2018;92:1041–60. https://doi.org/10.1016/j.msec.2017.12.036.
[34] van de Witte P, Dijkstra PJ, van den Berg JWA, Feijen J. Phase separation processes in polymer solutions in relation to membrane formation. Journal of Membrane Science 1996;117:1–31. https://doi.org/10.1016/0376-7388(96)00088-9.
[35] Ruiz JM, Busnel JP, Benoît JP. Influence of average molecular weights of poly(DL-lactic acid-co-glycolic acid) copolymers 50/50 on phase separation and in vitro drug release from microspheres. Pharm Res 1990;7:928–34. https://doi.org/10.1023/a:1015945806917.
[36] Dudeck O, Jordan O, Hoffmann KT, Okuducu AF, Tesmer K, Kreuzer-Nagy T, et al. Organic Solvents as Vehicles for Precipitating Liquid Embolics: A Comparative Angiotoxicity Study with Superselective Injections of Swine Rete Mirabile. AJNR Am J Neuroradiol 2006;27:1900–6.
[37] Yamniuk AP, Ditto N, Patel M, Dai J, Sejwal P, Stetsko P, et al. Application of a kosmotrope-based solubility assay to multiple protein therapeutic classes indicates broad use as a high-throughput screen for protein therapeutic aggregation propensity. J Pharm Sci 2013;102:2424–39. https://doi.org/10.1002/jps.23618.
[38] Gibson TJ, Mccarty K, Mcfadyen IJ, Cash E, Dalmonte P, Hinds KD, et al. Application of a high-throughput screening procedure with PEG-induced precipitation to compare relative protein solubility during formulation development with IgG1 monoclonal antibodies. J Pharm Sci 2011;100:1009–21. https://doi.org/10.1002/jps.22350.
[39] F DJ, E A, J F, T K, E D, R G. Freeze-drying and lyopreservation of diblock and triblock poly(lactic acid)-poly(ethylene oxide) (PLA-PEO) copolymer nanoparticles. Pharmaceutical Development and Technology 2000;5. https://doi.org/10.1081/pdt-100102031.
[40] Patel SM, Doen T, Pikal MJ. Determination of End Point of Primary Drying in Freeze-Drying Process Control. AAPS PharmSciTech 2010;11:73. https://doi.org/10.1208/s12249-009-9362-7.
[41] Najberg M, Haji Mansor M, Taillé T, Bouré C, Molina-Peña R, Boury F, et al. Aerogel sponges of silk fibroin, hyaluronic acid and heparin for soft tissue engineering: Composition-properties relationship. Carbohydr Polym 2020;237:116107. https://doi.org/10.1016/j.carbpol.2020.116107.
[42] Ashby LS, Smith KA, Stea B. Gliadel wafer implantation combined with standard radiotherapy and concurrent followed by adjuvant temozolomide for treatment of newly diagnosed high-grade glioma: a systematic literature review. World J Surg Onc 2016;14:225. https://doi.org/10.1186/s12957-016-0975-5.
[43] Dang W, Daviau T, Brem H. Morphological Characterization of Polyanhydride Biodegradable Implant Gliadel® During in Vitro and in Vivo Erosion Using Scanning Electron Microscopy. Pharm Res 1996;13:683–91. https://doi.org/10.1023/A:1016035229961.
[44] d'Avella D, DellaPuppa A. Safety and efficacy of Gliadel wafers for newly diagnosed and recurrent glioblastomas. Acta Neurochir 2012;154:1379–81. https://doi.org/10.1007/s00701-012-1414-1.

[45] Morin F, Chabanas M, Courtecuisse H, Payan Y. Biomechanical Modeling of Brain Soft Tissues for Medical Applications. Biomechanics of Living Organs: Hyperelastic Constitutive Laws for Finite Element Modeling, 2017, p. 127–46. https://doi.org/10.1016/B978-0-12-804009-6.00006-7.

Table of figures :

Figure 1: GB different niches and microenvironments elements. Barthel, Lennart et al. "Glioma: molecular signature and crossroads with tumor microenvironment." Cancer metastasis reviews vol. 41,1 (2022): 53-75. doi:10.1007/s10555-021-09997-9 (Authorization in course) 4
Figure 2: SMAD pathway triggered by BMP-4 Beederman, M. et al. BMP signaling in mesenchymal stem cell differentiation and bone formation. Journal of Biomedical Science and Engineering 6, 32–52 (2013).(Autorisation in course) 8
Figure 3: Figure 3: Common types of polymer-based delivery systems 9
Figure 4 Phase separation process of PLGA NPs. Adapted from Haji Mansor, M. et al. Eur J Pharm Biopharm 125, 38–50 (2018). 12
Figure 5: Parameters affecting the ability of drugs to cross the blood brain barrier (BBB) 33
Figure 6: Routes of administration into the CNS. A) Enhanced administration of molecules and nanobodies by osmotic or focused ultrasound (FU) disruption of the BBB. B) Direct administration: 1.1. Intraparenchymal injection. A brain tumor case is schematized where hydrogel injection might be performed intratumorally or after resection around the cavity edges. 1.2. Intraparenchymal injection assisted by CED (convection-enhanced delivery). Depicted is the case where soluble compounds are evenly distributed by CED within the tumor before a gelation reaction is induced by photoirradiation. The resulting embedded gel can be used as a platform for the sustained release of active compounds [87]. 2. Intracerebroventricular administration of drugs directly into the cerebrospinal fluid (CSF). The Ommaya reservoir consists of a catheter connected to one lateral ventricle and a reservoir implanted under the scalp [92]. 3. Intrathecal injection. Lumbar puncture showing the direct administration of a drug directly into the CSF. 4. Intranasal delivery. 4.1 Intranasal application of modified HA in the nasal endothelium. Upon in situ polymerization the generated patch might be used as a reservoir for sustained release of compounds [63]. 4.2 After permeation of the nasal barrier, HA nanogels may be used to enhance intracellular trafficking of drugs in CD44 expressing cells [88]. 5. Keyhole surgery [44,91] might be used as an alternative access route to the implantation of hydrogels into the brain. Credits: figures were reused with authorization of the authors and or editors. 36
Figure 7: Hyaluronic acid chemical structure 38
Figure 8: Scaffold specifications depending on various parameters 41
Figure 9: Characteristics of polymer-based devices for central nervous system delivery 44
Figure 10: Chemical structure of PLGA-PEG (a) and capped PLGA-COOR (b) 71
Figure 11 TEM images of the formulations. Nanoprecipitates of BMP-4 with a size distribution of 92nm+/-5nm 72
Figure 12: TEM (left) and SEM(right) images of the formulations. BMP -Loaded nanoparticles of PLGA with a size distribution of 320nm+/-50nm 73
Figure 13: ATR-FTIR spectrum of capped PLGA-COOR (a) and PLGA-PEG (b), transmittance (%) representation in function of the wavenumber (cm-1) in the whole region (3600–650 cm−1) and the fingerprint region (1800–650 cm−1) 74
Figure 14: Stability study of blank NPs in different pH conditions 75
Figure 15. A. Western Blot graphic of PSmad1 and Smad1 in U87MG and F98 cell lines. B. Western Blot of U87MG and F98 cell lines with and without treatment with BMP-4 in ng/mL. Statistical analysis: n=2. * P<0, 05, ** P<0, 01 treated versus corresponding non- treated cells condition; # P<0, 05, ## P<0, 05 treated condition compared to the same treatment 78
Figure 16. Cell viability at different concentrations of BMP-4 on U87-MG and NIH3T3. Values are presented as means ± standard deviation, n=4. * P<0, 05 versus corresponding non-treated (NT) condition (0 ng/mL), ## P<0, 01, ### P<0,001 versus treatment to same concentration of different BMPs. 79

Figure 17. Activity of BMPs at different concentrations on U87-MG (A) and F98 (B) gliomasphere formation after 7 days of treatment. Values are presented as means ± standard deviation, n=4. * P<0, 05 versus corresponding non-treated (NT) condition (0 ng/mL), ## P<0, 01, ### P<0,001 versus treatment to same concentration of different BMPs 79
Figure 18. Activity of BMPs on U87-MG (A) and F98 (B) gliomasphere formation at 10 ng/mL and 40 ng/mL concentrations after 7 days of treatment. Values are presented as means ± standard deviation, n=4. * P<0, 05, *** P<0,001 versus corresponding non-treated (NT) condition. 80
Figure 19 U87-MG (A) and F98 (B) cell proliferation assay 24 hours after X-ray irradiation at 4 Gy or 16 Gy and treatment with BMP-2 and -4. Values are presented as means ± standard deviation, n=4. * P<0, 05, ** P<0, 01 versus corresponding non- treated and non-irradiated (NT NI) condition; # P<0, 05, ## P<0, 05 versus treated condition compared to the same treatment 81
Figure 20: BMP-4 protein nanoprecipitation (left) and PLGA nanoparticles obtained by phase inversion method (right) 84
Figure 21: Model structure of the BMP-4-loaded PLGA-COOR/PEG-PLGA nanoparticles developed in this study. **Erreur ! Signet non défini.**
Figure 22: Hyaluronic acid (right) and poloxamer 407(left) polymers chemical structure 97
Figure 23 : Thermogelation by tube inversion method: at 4°C (left) and 37°C(right) The hydrogel 4°C still flows and the gel is liquid and mobile. At 37°C it completely gelifies. Gelation time is 30s for HA+Poloxamer hydrogel and 1 min for Poloxamer alone. 98
Figure 24: ATR-FTIR spectrum of Hyaluronic acid (left) and Poloxamer 407 (right), transmittance (%) representation in function of the wavenumber (cm-1) in the whole region (3600–650 cm−1) and the fingerprint region (1800–650 cm−1) 98
Figure 25: : Small-Angle X-Ray Scattering (SAXS) diffraction patterns obtained from the four cubic phase samples of Hydrogel formulations containing 20%w/v Poloxamer 0, 0.5, 1, 2%w/v HA. This diffractogram represents intensity (arbitrary unit) in function of q (nm-1) 99
Figure 26: Differential Scanning Calorimetry of POL20%w/v +/- HA 0.5/1/2% w/v without (left) and with blank PEG-PLGA NPs with a concentration 1mg/mL with a mean size of 250nm with a zeta potential of -3.2 mV. 101
Figure 27: SEM Images of 0 % (A) 0.5%(B) 1%(C) and 2%(D) POL/HA lyophilized hydrogels in 500X Pore size varies from 10µm to 200µm 102
Figure 28: Viscosity studies of Hydrogels POL407 20%w/v +/- HA 2%w/v at 37°C 103
Figure 29: Shear-thining of polymer-based hydrogel 103
Figure 30: Temperature ramp studies of Hydrogels POL407 20%w/v +/- HA 2%w/v and +/- blank NPs at 1mg/mL with 250nm size at 37°C 104
Figure 31: Amplitude sweep studies of Hydrogels POL407 20%w/v +/- HA 2%w/v with blank NPs at 1mg/mL with 250nm size at 37°C 104
Figure 32: Frequency sweep studies of Hydrogels POL407 20%w/v +/- HA 2%w/v with blank NPs at 1mg/mL with 250nm size at 37°C 105
Figure 33: Injectability study of POL/HA and POL hydrogels with and without NPs 105
Figure 34: The mass erosion behaviors of POL/HA hydrogel system. Data are represent as the mean ± standard deviation (n = 3). 106
Figure 35: Release profile of Lysozyme in TrisHCl buffer at pH 7.4 (left) and BMP4 in PBS at pH 7.4. Formulation 3 is the POL40720%w/w% + HA2%w/v hydrogel with lysozyme loaded NPs with a ratio 70/30% of PLGA-COOR/PLGA-PEG. Formulation 3' is the the POL40720%w/w% + HA2%w/v hydrogel with free Lysozyme; Formulation 5 is the POL40720%w/w% + HA2%w/v hydrogel with BMP-4 loaded NPs with a ratio 70/30% of PLGA-COOR/PLGA-PEG; Formulation 5' is the the POL40720%w/w% + HA2%w/v hydrogel with free BMP-4. All release experiments have been done in triplicates and SD is represented for each formulation. 107
Figure 36: NIH3T3 Cell line cytotoxicity assay at 24h, 48h and 72h. All experiments has been done in triplicates and statistical analysis with ANOVA was made. 108
Figure 37: Nanocomposite hydrogel model for locoregional treatment of GB (Adapted from Haji Mansor et al. 2019) 111
Figure 38: U87MG cell line 48 hours after treatment with BMP-4 or BMP4 and radiotherapy without RT or with 4Gy and 16 Gy 128

Figure 39: F98 cell line 48 hours after treatment with BMP-4 or BMP4 and radiotherapy without RT or with 4Gy and 16 Gy 129
Figure 40: Cell viability NIH3T3 after 24hrs of incubation in presence of blank NPs 130
Figure 41: Cell viability NIH3T3 after 48hrs of incubation in presence of blank NPs 130
Figure 42: Cell viability NIH3T3 after 72hrs of incubation in presence of blank NPs 131
Figure 43: Cell viability L929 after 24hrs of incubation in presence of blank NPs 131
Figure 44: Cell viability L929 after 48hrs of incubation in presence of blank NPs 132
Figure 45: Cell viability L929 after 72hrs of incubation in presence of blank NPs 132

Table 1: Solvent characteristics tested in in vivo models 13
Table 2: Devices development for Glioblastoma application(Table S1) 56
Table 3: Systems developed for CNS injuries application (Table S2) 56
Table 4: Systems developed for PNS injuries applications (Table S3) 56
Table 1:Precipitation efficiency(PE) of Lysozyme and BMP-4 with variation of the NaCl concentration 72
Table 2: Encapsulation efficiency of Lysozyme(3 and 4) and BMP-4(5 and 6) in different conditions: 70/30%(1, 3, 5) and 50/50% (2, 4, 6) ratio of PLGA-COOR/PLGA-PEG. All experiments were done in triplicates 74
Table 3: Stability study of blank NPs formulations pre and post-lyophilisation in presence of HβBCD

Supplementary figures

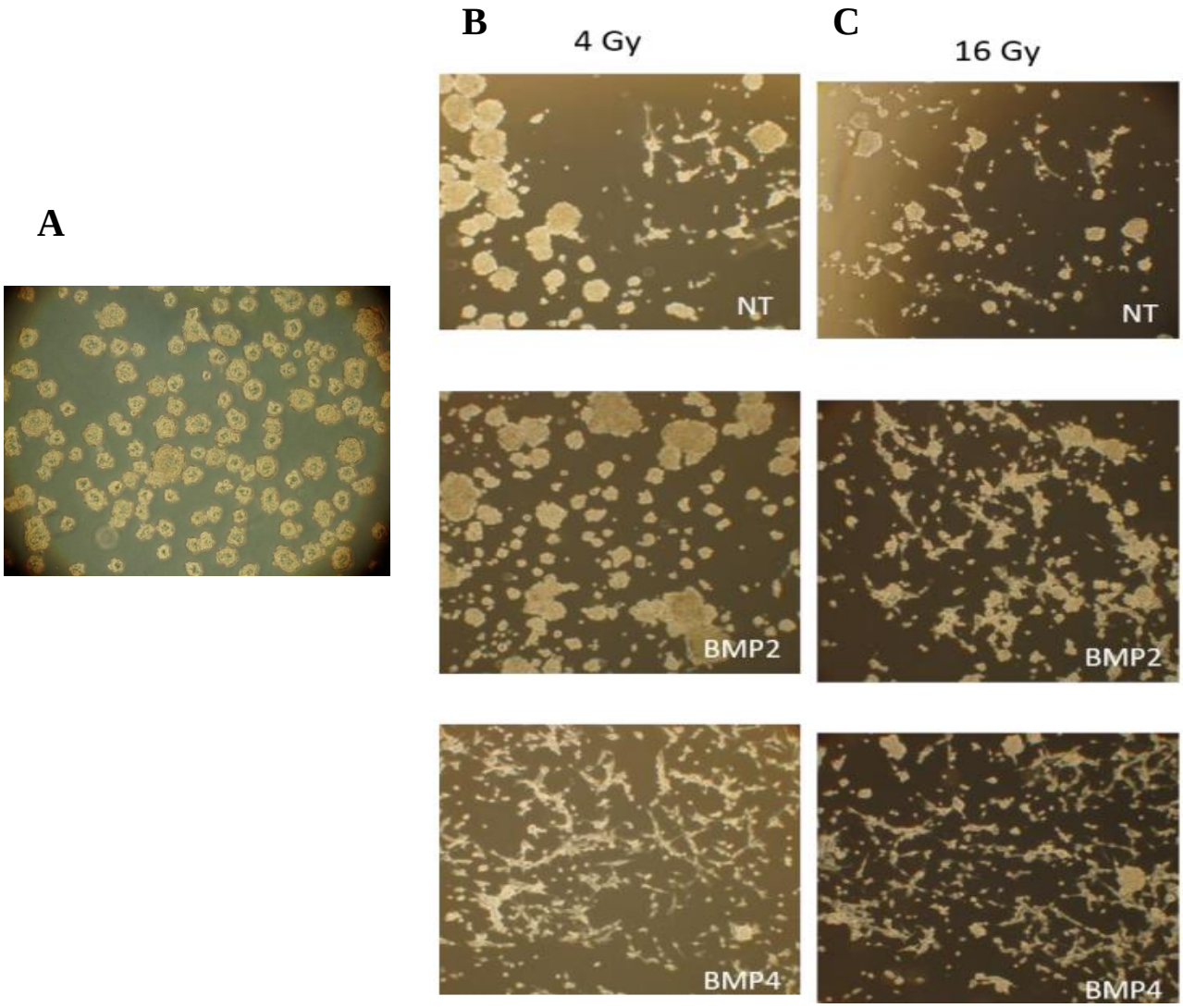


Figure 39: U87MG cell line 48 hours after treatment with BMP-4 or BMP4 and radiotherapy without RT or with 4Gy and 16 Gy

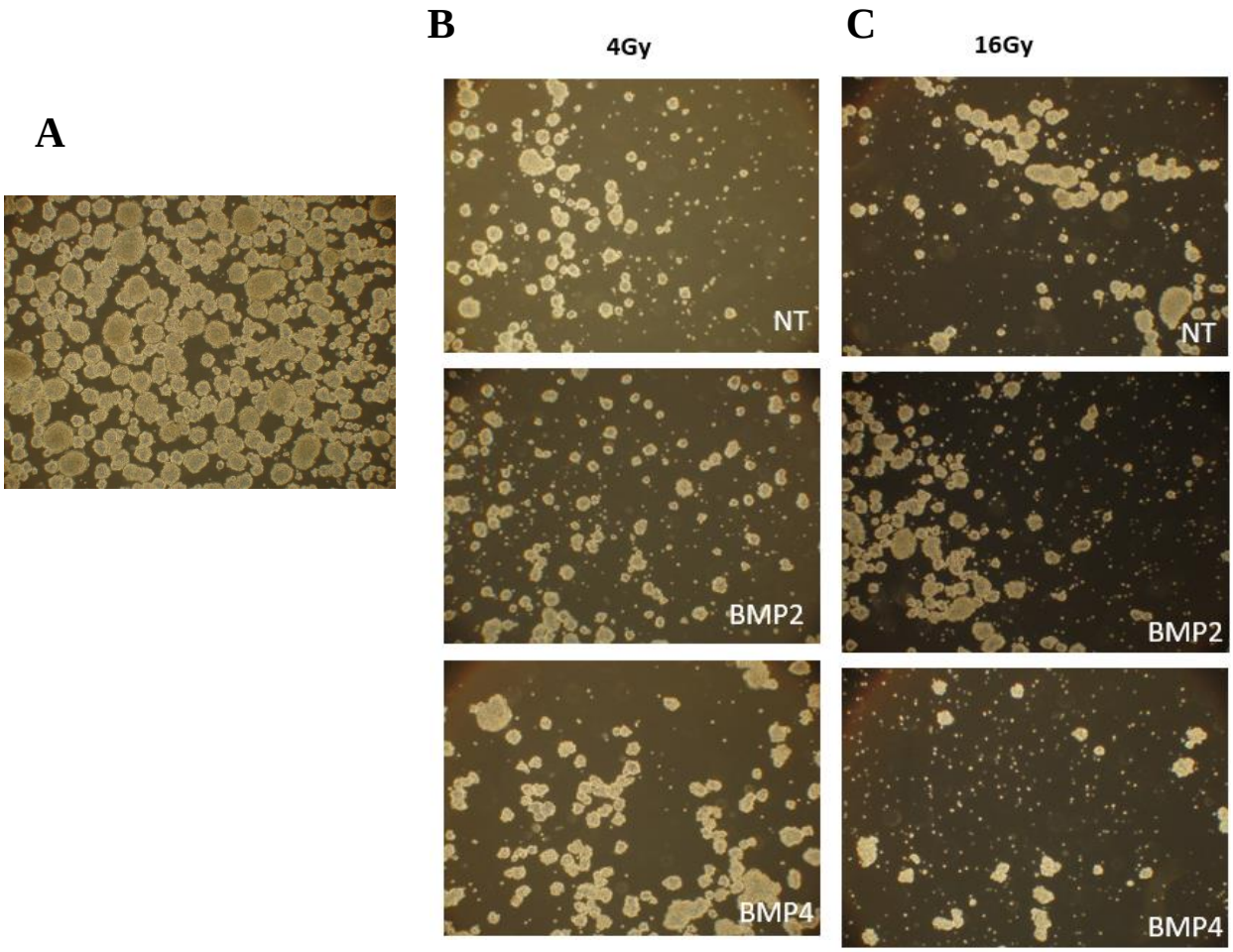


Figure 40: F98 cell line 48 hours after treatment with BMP-4 or BMP4 and radiotherapy without RT or with 4Gy and 16 Gy

Cytotoxicity assay of PLGA blank nanoparticles at 24hrs, 48hrs and 72hrs on NIH3T3 cell lines

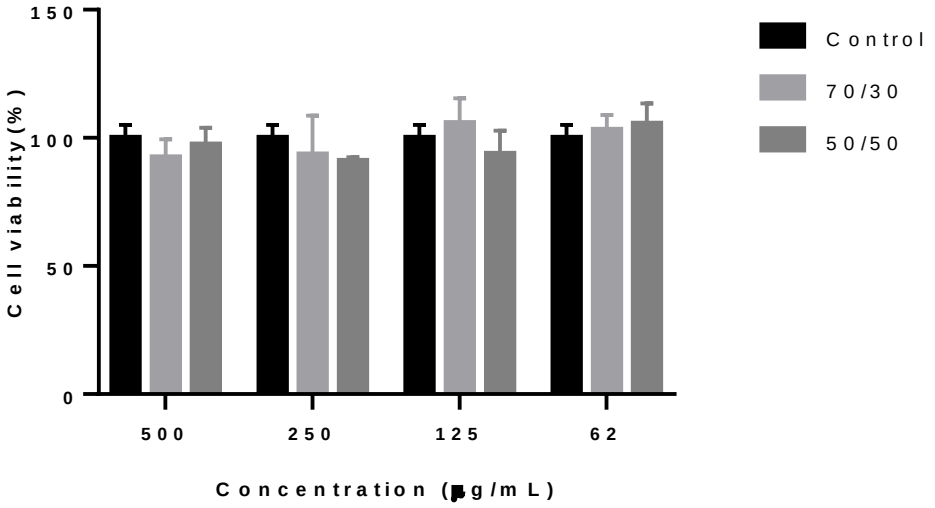


Figure 41: Cell viability NIH3T3 after 24hrs of incubation in presence of blank NPs

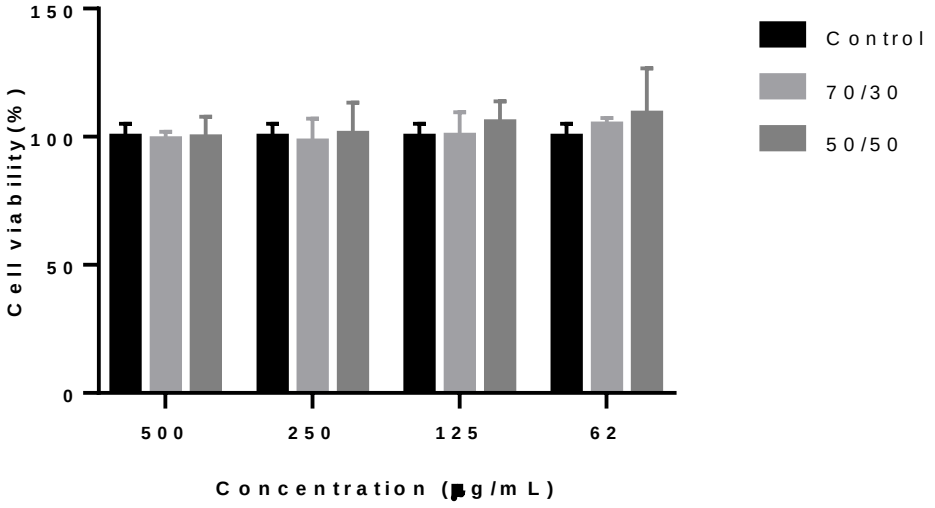


Figure 42: Cell viability NIH3T3 after 48hrs of incubation in presence of blank NPs

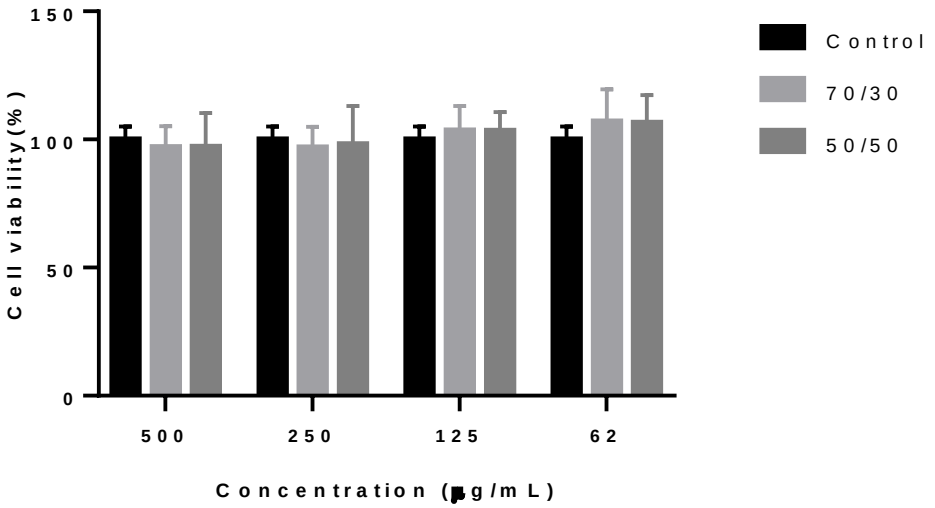


Figure 43: Cell viability NIH3T3 after 72hrs of incubation in presence of blank NPs

Cytotoxicity assay of PLGA blank nanoparticles at 24hrs, 48hrs and 72hrs on L929 cell lines

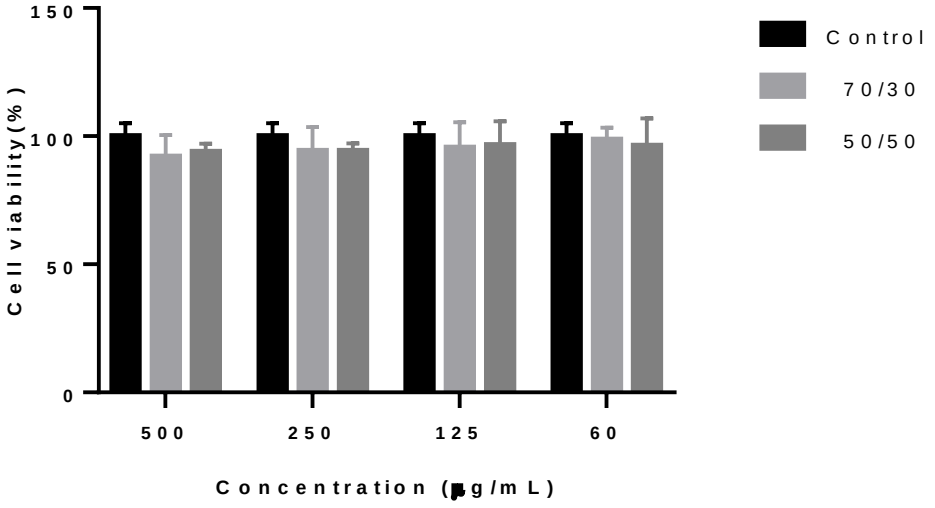


Figure 44: Cell viability L929 after 24hrs of incubation in presence of blank NPs

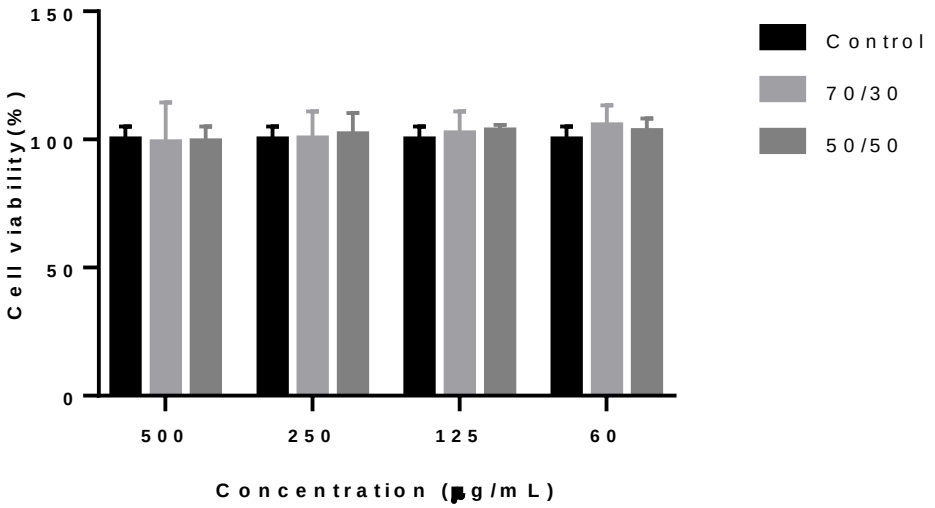


Figure 45: Cell viability L929 after 48hrs of incubation in presence of blank NPs

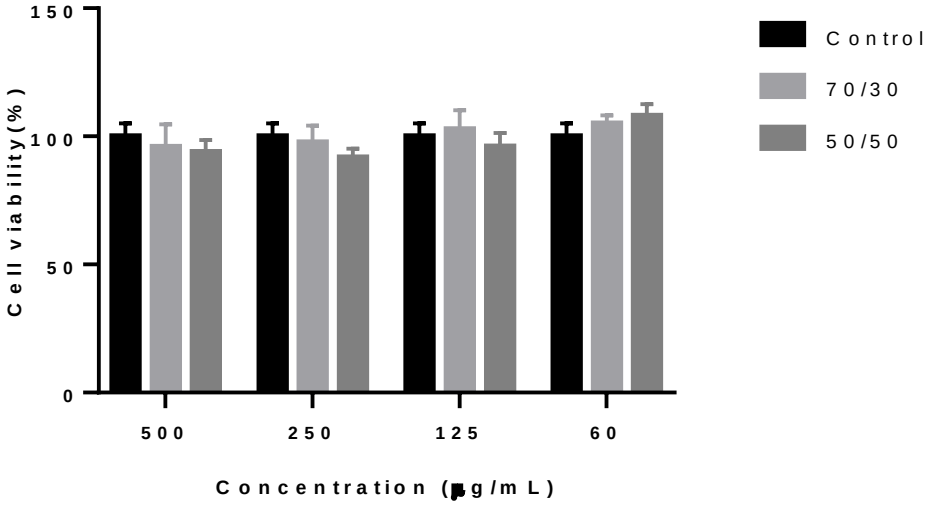


Figure 46: Cell viability L929 after 72hrs of incubation in presence of blank NPs

Annexes

frontiers in Bioengineering and Biotechnology

ORIGINAL RESEARCH
published: 25 February 2021
doi: 10.3389/fbioe.2020.602998

Rapamycin-Loaded Lipid Nanocapsules Induce Selective Inhibition of the mTORC1-Signaling Pathway in Glioblastoma Cells

*Delphine Séhédic[1], Loris Roncali[1], Amel Djoudi[1], Nela Buchtova[1], Sylvie Avril[1], Michel Chérel[2], Frank Boury[1], Franck Lacoeuille[1], François Hindré[1] and Emmanuel Garcion[1]**

[1] Univ Angers, Université de Nantes, Inserm, CRCINA, SFR ICAT, Angers, France, [2] Université de Nantes, Inserm, CNRS, CRCINA, Nantes, France

Inhibition of the PI3K/Akt/mTOR signaling pathway represents a potential issue for the treatment of cancer, including glioblastoma. As such, rapamycin that inhibits the mechanistic target of rapamycin (mTOR), the downstream effector of this signaling pathway, is of great interest. However, clinical development of rapamycin has floundered due to the lack of a suitable formulation of delivery systems. In the present study, a novel method for the formulation of safe rapamycin nanocarriers is investigated. A phase inversion process was adapted to prepare lipid nanocapsules (LNCs) loaded with the lipophilic and temperature sensitive rapamycin. Rapamycin-loaded LNCs (LNC-rapa) are ~110 nm in diameter with a low polydispersity index (<0.05) and the zeta potential of about −5 mV. The encapsulation efficiency, determined by spectrophotometry conjugated with filtration/exclusion, was found to be about 69%, which represents 0.6 wt% of loading capacity. Western blot analysis showed that LNC-rapa do not act synergistically with X-ray beam radiation in U87MG glioblastoma model *in vitro*. Nevertheless, it demonstrated the selective inhibition of the phosphorylation of mTORC1 signaling pathway on Ser2448 at a concentration of 1 μM rapamycin in serum-free medium. Interestingly, cells cultivated in normoxia (21% O_2) seem to be more sensitive to mTOR inhibition by rapamycin than those cultivated in hypoxia (0.4% O_2). Finally, we also established that mTOR phosphorylation inhibition by LNC-rapa induced a negative feedback through the activation of Akt phosphorylation. This phenomenon was more noticeable after stabilization of HIF-1α in hypoxia.

Keywords: rapamycin, nanoparticles, radiation, hypoxia, mTOR, Akt, HIF-1α, cancer

OPEN ACCESS

Edited by:
Guillermo Raul Castro, Consejo Nacional de Investigaciones Científicas y Técnicas (CONICET), Argentina

Reviewed by:
Maria Do Carmo Pereira, University of Porto, Portugal
Antonio Giordano, Temple University, United States

***Correspondence:**
Emmanuel Garcion
emmanuel.garcion@univ-angers.fr

Specialty section:
This article was submitted to Nanobiotechnology, a section of the journal Frontiers in Bioengineering and Biotechnology

Received: *07 September 2020*
Accepted: *29 December 2020*
Published: *25 February 2021*

Citation:
Séhédic D, Roncali L, Djoudi A, Buchtova N, Avril S, Chérel M, Boury F, Lacoeuille F, Hindré F and Garcion E (2021) Rapamycin-Loaded Lipid Nanocapsules Induce Selective Inhibition of the mTORC1-Signaling Pathway in Glioblastoma Cells. Front. Bioeng. Biotechnol. 8:602998. doi: 10.3389/fbioe.2020.602998

INTRODUCTION

Glioblastoma (GB) is the most common and deadly primary brain tumor in adults (Ostrom et al., 2017). Despite remarkable advances in surgical techniques and treatment options including chemotherapy and radiotherapy, the prognosis of this disease remains very poor with a median survival under 15 months (Stupp et al., 2005, 2009). Therefore, the understanding of the molecular mechanisms that drive malignancy in glioblastoma is seriously needed for the development of new agents specifically targeting tumor cells and the tumor microenvironment (Touat et al., 2017; Najberg et al., 2019).

The phosphatidylinositol 3-kinase (PI3K)/protein kinase B (Akt)/mechanistic target of rapamycin (mTOR) intracellular signaling pathway plays a central role in the regulation of cell proliferation, growth, differentiation, and survival (Sonoda et al., 2001; Bjornsti and Houghton, 2004; Knobbe et al., 2005; Castellino and Durden, 2007; Jiang and Liu, 2009). Stimulation of this pathway results in the activation of a receptor tyrosin kinase (RTK) by a cytokine or a growth factor, which drive a sequential phosphorylation of PI3K, Akt, and mTOR. mTOR regulates cell growth and survival *via* two different multiprotein complexes, mTORC1 and mTORC2. The complex mTORC1 is composed of mTOR, regulatory-associated protein of mTOR (Raptor), mammalian lethal with Sec13 protein 8 (mLST8), proline-rich AKT substrate 40 kDa (PRAS40), and DEP-domain-containing mTOR-interacting protein (Deptor) (Saxton and Sabatini, 2017). mTORC1 activates the eukaryotic initiation factor 4E (eIF4E)-binding protein, releasing the transcription factor eIF4E and the p70 ribosomal S6 kinase 1 (S6K1 or p70S6K) implicated in translation (Heimberger et al., 2005).

This pathway can be activated through numbers of mechanisms, including growth factors, overexpression or amplification of Akt family members, inactivation of the inhibitory effects of PTEN (phosphatase and tensin homolog) tumor suppressor or by non-canonical Wnt pathway (Saxton and Sabatini, 2017). Furthermore, radiation can also activate mTOR signaling in vascular endothelium and in glioblastoma cell lines (Eshleman et al., 2002; Shinohara et al., 2005; Anandharaj et al., 2011). Consequently, mutations in the PI3K or AKT genes, loss of PTEN, epigenetic modifications, or constitutive activation of upstream tyrosine kinase receptors will lead to dysregulation of this pathway in a variety of tumors, including GB (Engelman, 2009; Bai et al., 2011; Wick et al., 2011; Mao et al., 2012). As such, there are marked associations between alterations in the PI3K/AKT/mTOR pathway and the poor clinical survival (Engelman, 2009). Therefore, inhibition of the PI3K/Akt/mTOR signaling pathway has been widely investigated as a potential therapy for cancer including glioblastoma (Li et al., 2016). Interestingly, tumor cells in which the PI3K/Akt/mTOR pathway is dysregulated are more susceptible to the inhibition of mTOR, the downstream effector of this signaling pathway, than normal cells (Courtney et al., 2010). Hence, mTOR inhibitors such as rapamycin and its derivatives provide a new class of active agents and therapeutics for GB.

Rapamycin (Sirolimus) is a natural macrolide antibiotic (firstly isolated from samples of Streptomyces hygroscopicus found on Easter Island), which binds to FK506 binding protein 12 (FKBP12). The rapamycin-FKBP12 complex inhibits mTOR and prevents further phosphorylation of proteins involved in the transcription, translation, and cell cycle control (Heimberger et al., 2005). Anandharaj et al. studied three PTEN-null GB cell lines and demonstrated that rapamycin combined with radiotherapy inhibited the inhibitor of apoptosis protein (IAP) family protein surviving through repression of phospho-Akt. Thus, targeting Akt through mTOR with rapamycin increased the radiation sensitivity (Anandharaj et al., 2011). Preclinical trials showed that PTEN deficient tumors and those dependent on PI3K overexpression were most sensitive to rapamycin (Bjornsti and Houghton, 2004). These results provide a strong basis for investigation of mTOR inhibitors as potential tumor-selective therapeutic agents. Rapamycin and its derivatives, CCI-779 and RAD001, specifically inhibit the function of mTOR by blocking the phosphorylation of downstream molecules, such as p70S6 kinase (p70S6K) and eukaryotic initiation factor 4E-binding protein 1 (4E-BP1), leading to G1-phase cell cycle arrest. Accumulating evidence from preclinical and early clinical studies suggests that these mTOR inhibitors, alone or in combination, would be directly and indirectly effective as growth inhibitors against a broad range of tumors including GB (Mecca et al., 2018; Hsu et al., 2020; Wanigasooriya et al., 2020).

Despite the potency of rapamycin in preclinical studies, clinical development of rapamycin floundered due to the lack of suitable formulations. The low oral bioavailability (<15%) (Yatscoff et al., 1995) precludes tablet formulation except for low dosage treatments such as immunosuppression. Rapamycin's poor solubility in water, ca. 2.6 µg/mL, and common excipients make intravenous (i.v.) formulation difficult (Simamora et al., 2001). In addition, pharmacokinetic studies found that rapamycin strongly partition into the erythrocytes (Kd ca. 20) from where it may not readily access to solid tumors (Yatscoff et al., 1995). This led to the development of ester derivatives, e.g., Temsirolimus or CCI-779, which were more easily formulated. Despite the promise of CCI-779 for mTOR inhibition, intravenous formulations required ethanol that may cause hemolysis (Raymond et al., 2004). Furthermore, phase I trials established that the CCI-779 prodrug was rapidly hydrolyzed in the plasma back into rapamycin thus favoring again potential partition into erythrocytes and unsupportive for tumor accumulation. More recent evolutions with the derivative Everolimus in phase II leads to increase treatment-related toxicities (Chinnaiyan et al., 2018).

In order to improve rapamycine biodistribution, nanovectorization strategies have been developed. They provide a physical protection and allow freeing from solubility problems. In this work, lipid nanocapsules loaded with rapamycin (LNC-rapa) were developed as new nanocarriers for the treatment of GB. We demonstrated that encapsulated rapamycin keeps its biological effect and efficiently inhibits mTOR phosphorylation. LNC-rapa were more cytotoxics than rapamycin alone but, in association with 8Gy radiation, no synergistic effect were observed. This result could be explained by the complexity of the PI3k/Akt/mTOR in GB as demonstrated by activation of phosphorylated Akt with mTOR inhibition and dependence from oxic status.

MATERIALS AND METHODS

Materials

Lipoïd® S75-3 (soybean lecithin at 69% of phosphatidylcholine) and Solutol® HS15 (a mixture of polyethylene glycol 660 and polyethylene glycol 660 hydroxystearate) were kindly provided by LipoïdGmbh (Ludwigshafen, Germany) and BASH (Ludwigshafen, Germany), respectively. NaCl and DMSO were provided by Sigma Aldrich (St-Quentin, Fallavier, France). Deionized water was obtained from a Milli-Q plus

system (Millipore, Paris, France). Lipophilic Labrafac® CC (caprylic-capric acid triglycerides) was provided by Gattefosse S.A. (Saint-Priest, France). Rapamycin was purchased from Interchim (Montluçon, France).Captex® 8000 (Triglyceride of caprylic acid), Transcutol® HP (Diethylene glycol monoethyl ether), and Miglyol® 812 (caprylic/capric triglyceride) were purchased, respectively, from Abitec (Janesville, WI, USA), Gattefosse S.A. (Saint-Priest, France) and Sasol Germany GmbH (Marl, Germany).

Reagents and Antibodies

Rapamycin was dissolved in DMSO. The final concentration of DMSO in the culture medium did not exceed 0.2%. Anti-phospho-mTOR (ab109268, diluted 1:2,000) and anti-HIF-1α (ab51608, diluted 1:2,000) were from Abcam (Cambridge, UK). Anti-phospho-Akt (#4058, diluted 1:1,000) was from Cell Signaling Technology (Beverly, MA, USA) and anti-HSC70 (sc7298, diluted 1:10,000) was from Santa Cruz biotechnology (Dallas, TX, USA). Peroxidase-conjugated anti-mouse (#32430, diluted 1:2,000) and anti-rabbit (#32460, diluted 1:2,000) secondary antibody were from ThermoScientific (Waltham, MA, USA). Lysis buffer: [50 mM Hepes (pH 7.5), 150 mM sodium chloride, 1 mM EDTA (pH 8), 2.5 mM EGTA (pH 7.4), 0.1% Tween 20, 10% glycerol, 0.1 mM sodium orthovanadate, 1 mM sodium fluoride and 10 mM β-glycerophosphate] plus Protease inhibitor cocktail (#539134 Calbiochem, Darmstadt, Germany), PMSF and Phosphatase inhibitor Cocktail Set II (#524636 Calbiochem).

Solubility Assays

Rapamycin solubility assays were performed in different oils: Captex® 8000, Labrafac® CC and Miglyol® 812. Five microgram of rapamycine were dissolved in 250 mg of oil and kept under magnetic stirring during 3 h at room temperature (RT) or at 90°C. Rapamycin concentration was determined by reverse-phase high-performance liquid chromatography (RP-HPLC) after 24 h settling at 4°C, using μBondapack C18 column (Waters Corporation, Milford, MA) with an ultraviolet detector at 278 nm. The mixture of 90% acetonitrile and 10% water (v/v) was used as a mobile phase, and delivered at a flow rate of 2.0 mL/min. The injection volume was 10 μL and the retention time was about 2.3 min.

For spectral analysis of the stability of rapamycin in Labrafac®, rapamycin was solubilized at 1 mg/mL in Labrafac® under magnetic stirring before being submitted to 3 to 6 short cycles of heating (70°C for <1 min) and cooling (RT) or incubated for 1 to 3 h at 70°C in Labrafac. Spectral analysis was then made by use of the CLARIOstar microplate reader (BMG Labtech, Champigny-sur-Marne, France).

Formulation and Physico-Chemical Characterization of Empty (LNCs) and Rapamycin-Loaded Lipid Nanocapsules (LNC-rapa)

LNCs were prepared according to a phase-inversion process adapted from Heurtault et al. (2002). This process involves the formation of an oil/water microemulsion containing an oily/fatty phase (triglycerides: Labrafac® WL 1349), a non-ionic hydrophilic surfactant (polyethylene glycol hydroxystearate: Solutol® HS15), and a lipophilic surfactant (lecithin: Lipoïd® S75-3). Briefly, 21 mg of Lipoïd® S75-3, 138 mg of Solutol® HS15, 345 mg of Labrafac®, 104 mg of NaCl and 898 mg of deionized water were mixed by magnetic stirring. 5 mg of rapamycin were added to other reagents for a final concentration of 1 mg/mL. Three cycles of progressive heating and cooling between 30 and 70°C were then carried out and followed by an irreversible shock, induced by addition of 3.6 mL of 0°C deionized water. Afterwards, slow magnetic stirring was applied to the suspension for 5 min. LNCs were filtered through a Minisart® 0.2 μm filter (Sartorius, Goettingen, Germany) and kept at 4°C. The average diameter and polydispersity index were determined using Malvern Zetasizer® Nano Serie DTS 1060 (Malvern instruments S.A., Worcestershire, UK).

Encapsulation of drug: For determination of drug encapsulation yield, three samples of filtrate were prepared by dissolution of an exact quantity of LNC dispersion in a 96/4 (v/v) methanol/tetrahydrofurane solution. Free rapamycin (non-soluble) was removed by the filtration performed through the Minisart® 0.2 μm filter and its concentration measured by spectrophotometry at 289 nm. Quantification was achieved by comparison between observed peak area ratios of rapamycin of the samples and a calibration curve performed using the same conditions. Samples were performed in triplicate and the loading capacity (LC) was calculated using the following equation:

$$\text{Drug content (wt\%)} = \frac{\text{mass of encapsulated drug}}{\text{mass of encapsulated drug} + \text{mass of LNC excipients}} \times 100 \quad (1)$$

The encapsulation efficiency (EE) of rapamycin was calculated using the Equation (2):

$$\text{Encapsulation efficiency (wt\%)} = \frac{\text{mass of encapsulated drug}}{\textit{mass of initial drug}} \times 100 \quad (2)$$

For electrical conductivity measurements, an electrical conductivity meter (Cond 330i/SET, WTW, Germany) was used in non-linear temperature compensation mode according to EN 27888. The conductivity variations were followed as a function of temperature to determine the emulsion inversion zone.

Cell Culture and Exposure to Hypoxia

Human malignant glioma cell lines U87MG were purchased from American Tissue Culture Collection (Rockville, MD). Tumor cells were cultured in Dulbecco's modified Eagle's medium 4.5 g/L glucose and L-glutamine (DMEM, Lonza, Verviers, Belgium) supplemented with 10% of heat-inactivated fetal bovine serum (FBS, Lonza) and 1% antibiotics suspension (10

units/mL of penicillin, 10 mg/mL streptomycin and 25 μg/mL amphotericin B, Sigma-Aldrich, Saint-Louis, MO, USA). Tumor cells were incubated at 37°C in 5% CO_2 and 21% (normoxia) or 0.4% O_2 (hypoxia). Hypoxia conditions were obtained by use of an InVivo$_2$ 400 SCI-tive hypoxia workstation (Ruskinn Technology, Ltd., Leeds, UK).

Irradiation Procedure

Irradiation was performed with the CP-160 cabinet x-ray system (Faxitron, Edimex, Le Plessis Grammoire, Angers, France) which delivers a dose of 1,5 grays by min. Irradiation was performed during 5.33 min in order to reach the dose of 8 grays. Irradiation was performed with cells covered. Depending on the condition considered, the cells were placed throughout the experiment in a conventional 21% O_2 incubator at 37°C/5% CO_2 (normoxia) or 0.4% O_2 (hypoxia) at 37°C/5% CO_2 in an InVivO2 400 SCI-tive hypoxia workstation (Ruskinn); they are only placed in an isolated flask for the duration of the irradiations.

Cytotoxicity Evaluation

Two assays were performed to determine the cytotoxicity effect of LNC-rapa on the glioblastoma cell line U87MG:MTS (3-(4,5-dimethylthiazol-2-yl)-5-(3-carboxymethoxyphenyl)-2-(4-sulfophenyl)-2H-tetrazolium) (Promega, Charbonnières, France) and clonogenic assay by crystal violet coloration (Sigma-Aldrich).

For the MTS assay, U87MG cells (5×10^4 cells/mL) harvested in the exponential growth phase were seeded in a 24-well plate in DMEM medium with 10% FBS, in humidified atmosphere (5% CO_2) at 37°C. Once the cells incubated in the exponential growth phase, serum-contained medium was removed and replaced by serum-deprived DMEM supplemented with 1% N1 supplement (Sigma-Aldrich). Free rapamycin dissolved in DMSO (1/10,000, non-toxic) was applied at various concentrations (0.04; 0.2; 1; 5; 10; 20; 100; 200 μM) for 4 h. 8Gy radiation was performed 6 h after the onset of initial treatment by Faxitron CP-160 (Faxitron X-rays, Lincolnshire, UK). Medium was changed every day. Forty-eight hours following the treatment, MTS reagent was diluted (1:5) in U87MG cell medium and incubated for 2 h at 37°C. The absorbance was measured at 492 nm using Multiskan® microplate spectrophotometer (Thermo Scientific).

For the clonogenic assay, U87MG cells (10^3 cells/mL) harvested in the exponential growth phase were seeded in a 6-well plate in DMEM medium with 10% FBS, in humidified atmosphere (5% CO_2) at 37°C. Once the cells incubated in the exponential growth phase, serum-contained medium was removed and replaced by serum-deprived DMEM supplemented with 1 % N1 supplement. Cells were treated for 4 h with rapamycin, LNC-rapa at 1 μM (IC50 LNC-rapa at 21% O_2 corresponding to a 1/1,000 dilution from initial suspension) and with empty LNCs at the same dilution than LNC-rapa. 8Gy radiation was performed 6 h after the treatment by Faxitron CP-160. Ten days after treatment, colonies were colorized by crystal violet and their number was evaluated with ImageJ Software version 1.43.

Depending on the condition considered, the cells were placed throughout the experiment in a conventional 21% O_2 incubator at 37°C/5% CO_2 (normoxia) or 0.4% O_2 (hypoxia) at 37°C/5% CO_2 in an InVivO2 400 SCI-tive hypoxia workstation (Ruskinn); they are only placed in isolated flasks for the duration of the irradiations.

Western Blotting

U87MG cells (2.4×10^5 cells/mL) harvested in the exponential growth phase were seeded in dishes in DMEM medium with 10% FBS, at 37°C in humidified atmosphere containing 5% CO_2 and 21 or 0.4% O_2. Once the cells incubated in the exponential growth phase, serum-contained medium was removed and replaced by serum-deprived DMEM supplemented with 1% N1 supplement. Cells were treated with rapamycin, LNC-rapa at 1 μM and with empty LNCs at the same dilution than LNC-rapa. 8Gy radiation was performed 6 h after the treatment by Faxitron CP-160 (cf. section Irradiation Procedure).

Sixteen hours after rapamycin initial treatment (untreated, rapamycin, LNC, LNC-rapa), soluble proteins for immunobloting were harvested from tumor cells lysed in 300 μL lysis buffer on ice. Cells were scrapped and lysed by sonication for 10 s.

Equal amounts of protein from each sample, estimated by the Bio-Rad Protein Assay (Richmond, CA), were separated by electrophoresis through a 4–20% SDS-polyacrylamide gel (Mini-protean® TGX™ Ge, BioRad), transferred to PVDF membranes (AmershamHybond, GE Healthcare, Buckinghamshire, UK) and blocked with 4% non-fat dry milk in 1X TBS plus 0.1% Tween 20 at RT for 1 h. The membranes were washed and incubated with a primary antibody diluted in 2% BSA in 1X TBS plus 0.1% Tween 20 overnight at 4°C. The membranes were then washed and incubated again for 1 h at RT with peroxidase-conjugated anti-rabbit or anti-mouse secondary antibody. The bound antibody was detected using the enhanced chemiluminescence reagent kit SuperSignal West Femto (Thermo Scientific, Waltham, MA, USA) and read with a bioluminescence detector Image Quant Las 4000 (GE Healthcare, USA).

Statistical Analysis

Three independent biological replicates were performed for all experiments described in this manuscript. Statistical analyses were performed with R software using two-way *analysis* of variance (ANOVA) test. Differences were considered significant if the p-value was ≤ 0.05.

RESULTS

Formulation and Physicochemical Characterization of Rapamycin-Loaded LNCs

As a lipophilic molecule with logP = 4.3, rapamycin can be encapsulated in the lipophilic core of lipid nanocapsules. The formulation of LNCs *via* a phase-inversion process described by Heurtault et al. (2002) involves three cycles of heating/cooling between 60 and 90°C. However, rapamycin degrades at higher temperatures as observed during the solubility assay. Three different oils were tested for the dissolution of rapamycin at room temperature (RT) and at 90°C: Captex® 8000, Miglyol® 812

TABLE 1 | Rapamycin solubility in different oils at RT and at 90°C.

Oil	Temperature	Initial rapamycin (mg/mL)	Dissolved rapamycin (mg/mL)	Dissolution rate (%)
Captex® 8000	RT	19.0	1.8	9.5
	90°C	16.8	0	0
Miglyol® 812	RT	19.2	1.4	7.3
	90°C	17.1	0	0
Labrafac®	RT	24.0	1.5	6.3
	90°C	21.1	0	0

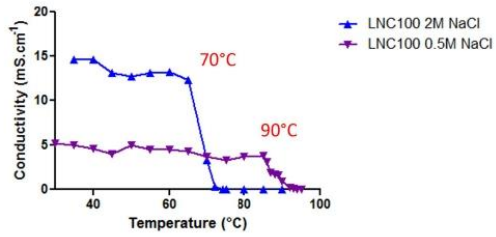


FIGURE 1 | Micro-emulsion conductivity. Micro-emulsion conductivity during cycles of heating/cooling for LNCs formulation performed with 2 M or 0.5 M NaCl aqueous solution.

and Labrafac®. Rapamycin concentration in the supernatant was determined by HPLC and the results are summarized in **Table 1**. At 90°C, rapamycin is completely degraded whatever the oil used. At RT, rapamycin has a comparable solubility in all three oils.

Finally, Labrafac®, pharmaceutically acceptable and in which the stability of rapamycin is confirmed during short cycles of heating and cooling at 70°C (**Supplementary Figure 1**), was used for the formulation of empty and rapamycin-loaded LNCs. Hence, a lower temperature (70°C) was employed in order to avoid rapamycin decomposition. To decrease the phase inversion temperature from 90 to 70°C, we increased the concentration of NaCl aqueous solution. Electrical conductivity of the micro-emulsion was measured as a function of temperature for the "classical formulation" with 0.5 M NaCl and for the formulation with 2 M NaCl (**Figure 1**). A steady state at a high conductivity value indicates that the continuous phase of the emulsion is water, whereas conductivity close to zero means that the continuous phase is oil. The region where the conductivity gradually changes with temperature represents the phase inversion from oil-in-water emulsion to water-in-oil emulsion. **Figure 1** shows that the phase inversion occurs at lower temperature (70°C) when 2 M NaCl aqueous solution is used as compared to 0.5 M NaCl solution (90°C). Thus, increasing NaCl concentration allows us to perform rapamycin encapsulation in non-degrading temperature range between 30 and 70°C.

Empty and rapamycin-loaded LNCs were characterized in terms of their average size and zeta potential. These values are presented in **Table 2**. LNC-rapa have an average size of 112.6 ± 8.4 nm with a polydispersity index (PDI) of 0.044 ± 0.011. The zeta potential is of −5.5 ± 0.4 mV. Rapamycin encapsulation efficiency and loading capacity were determined using the equations 1 and 2, these values are also reported in **Table 2**. The encapsulation efficiency is of 68.8 ± 7.1 wt% thus representing a loading capacity of the nanoparticle of 0.6 ± 0.1 wt%. This encapsulation efficiency rate was considered in the calculation of rapamycin concentration in biological assays. Insofar as low temperature-made LNC can exhibit fluctuations in their long-term stability with regard to preservation methods not yet fully elucidated, the LNCs used throughout of this work were prepared extemporaneously (**Supplementary Table 1**).

Effect of Rapamycin-Loaded LNCs (LNC-rapa) on mTOR Phosphorylation in U87MG Cells Depending on Oxic Condition and Exposure to Radiation Treatment

Rapamycin binds FKBP12 and the complex FKBP12/rapamycin inhibits mTOR phosphorylation that leads to 4E-BP1 dephosphorylation and inhibition of translation. To check if rapamycin encapsulated within LNCs keeps its biological proprieties, human U87MG glioblastoma cells, that are PTEN negative and thus overactivate Akt/mTOR signals, were treated with empty LNCs, LNC-rapa and free rapamycin dissolved in DMSO. The cells were cultured in serum-free medium in atmosphere containing either 21% O_2 or 0.4% O_2.

As cytotoxicity assay performed by MTS with free rapamycin demonstrated a toxic effect only at high concentrations, with more impact in normoxia than in hypoxia (IC50 of 20.54 μM at 21% pO_2 and 34.65 μM at 21% pO_2 and 0.4% pO_2, respectively, **Supplementary Figure 2**), the choice to use a relevant far much lower concentration while using the LNC nanocarrier was made. Hence a concentration of 1 μM (corresponding to the IC50 LNC-rapa at 21% O_2 and to a 1/1,000 dilution from the initial suspension while using LNC) was applied all throughout the work.

Western blot analysis was performed and relative phosphorylation was determined by volumetric ratio of p-mTOR/HSC70. The results presented in **Figure 2A** indicate that rapamycin-encapsulated within LNCs effectively inhibits mTOR phosphorylation (Ser2448) with modalities much more effective in hypoxia than in normoxia.

This observation is consistent with the one made by Brugarolas and coworkers who notably showed that hypoxia induced mTOR inhibition through TSC1/TSC2 tumor suppressor complex and the hypoxia-inducible gene REDD1/RTP801. They demonstrated that in contrast to energy depletion, mTOR inhibition by hypoxia does not require AMPK or LKB1 but depend on increased expression of the hypoxia inducible *REDD1* gene. They also showed that down-regulation of S6K, an mTOR target, phophorylation by Redd1 requires Tsc2 and Redd1 probably acts up-stream of the Tsc1/Tsc2 complex to down-regulate mTOR function in response to hypoxia (Brugarolas et al., 2004). Thus, at 0.4% oxygenation, mTOR is inhibited by rapamycin and hypoxia, with loaded-LNCs also exerting a higher effect in these conditions (**Figure 2A**).

TABLE 2 | Physicochemical parameters of LNC-rapa.

	Inversion phase (°C)	Size (nm)	PdI	Zeta-potential (mV)	Encapsulation efficiency (% w/w)	Loading capacity (%w/w)
LNC-rapa	70	112.6 ± 8.4	0.04 ± 0.01	−5.5 ± 0.5	68.8 ± 7,1	0.6 ± 0.1
LNC	90	92.3 ± 2.6	0.05 ± 0.02	−8.6 ± 0.6	0	0

Average particle size, PDI, zeta potential, encapsulation efficiency (EE) and loading capacity (LC) of empty and rapamycin-loaded LNCs.

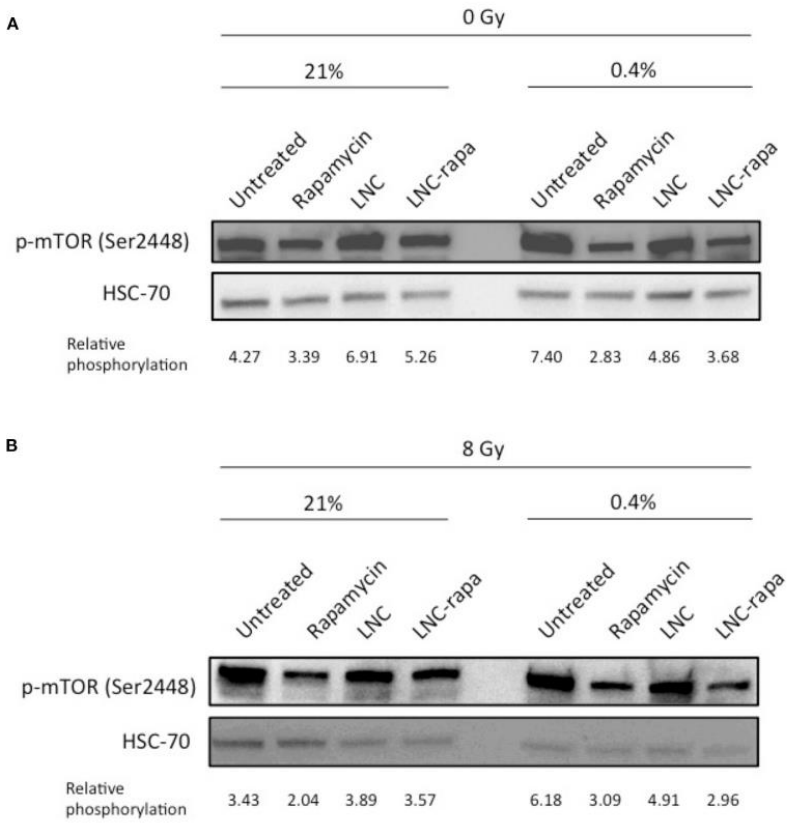


FIGURE 2 | Effects of LNC-rapa assessed on mTOR phosphorylation in U87MG cells depending on oxic condition and exposure to radiation treatment. U87MG cells were treated with rapamycin, empty LNCs (LNC) or rapamycin-loaded LNCs (LNC-rapa), and maintained at two oxygenation conditions: 21 and 0.4% O_2 before proceeding to western blot analysis. Relative phosphorylation of one representative experiment was determined by volumetric ratio of p-mTOR/HSC70. **(A)** 0Gy. **(B)** 8Gy irradiation.

As various synergies have been tested and since the conventional treatment of glioblastoma involves beam radiation, the impact of LNC-rapa on mTOR phosphorylation in U87MG cells was also tested after exposure to 8Gy irradiation. Similar results to the non-irradiated condition are obtained (**Figure 2B**).

Effect of LNC-rapa on U87MG Cell Growth Depending on Oxic Condition and Exposure to Radiation Treatment

To determine the effect of rapamycin encapsulated within LNCs on cancer cell survival and growth depending on the oxygen status and exposure to radiation treatment, a clonogenic assay

was performed. Hence, U87MG cells were grown under two oxygenation conditions (21 or 0.4% O_2) and treaded with either empty LNCs, LNC-rapa or free rapamycin at 1 μM before being exposed, 6 h later, to 0 or 8Gy irradiation. They were then maintained in culture for 10 days and colorized by crystal violet (**Figure 3A**). Under all the conditions tested, a very clear effect of the irradiations, in normoxia (21% pO_2) as in hypoxia (0.4% O_2), was observed (**Figures 3B,C**). Rapamycin, nanovectorized or as free, exerts only moderate effects, however significant at 0.4% O_2, demonstrating the similarity of action of encapsulated LNC-rapa vs. the free form (**Figure 3C**). Interestingly, rapamycin and LNC-rapa do not exert any synergistic effect related to radiation treatment and even slight but significant inhibitory effects impacted radiation efficacy at 0.4% O_2 (**Figure 3C**).

Activation of Alternative Signaling Pathways in Response to Exposure to LNC-rapa in U87MG

The observed duality of the effects of rapamycin and LNC-rapa associating a strong inhibition of mTOR phosphorylation to a moderated cytotoxic effect whatever the environmental conditions used (low/high oxygen or irradiating) led us to focus on the mechanisms that control the PI3K/Akt/ mTOR pathway. Since HIF exerts negative feedback on mTOR (Brugarolas et al., 2004) and mTORC2 complex also exerts feedback control while capable to phosphorylate Akt (Sarbassov et al., 2005; O'Reilly et al., 2006), HIF-1α protein expression and phosphorylation of Akt on Ser473 (Akt-p) were evaluated. Western Blot presented in **Figure 4A** shows that HIF-1α protein expression is reduced when cells are treated with free rapamycin and LNC-rapa whatever oxygenation condition considered. Inversely, these treatments enhance Akt-p protein level. **Figure 4B** shows that at 8Gy, Akt-p protein expression is reduced related to HSC70 in comparison with the 0Gy control condition. Again the down regulation of HIF-1α protein expression by free rapamycin and LNC-rapa is observed concomitantly with the induction of phosphorylation of Akt, thus emphasizing the possible double edge sword impact of LNC-rapa due to the multiplicity of signals downstream mTOR inhibition.

DISCUSSION

This work demonstrated that a new safe formulation of rapamycin encapsulated in lipid nanocapsules at low temperature and without the use of organic solvent, allows keeping its activity while specifically inhibiting mTOR phosphorylation. These observations also established that the mechanism of action of rapamycin-loaded LNCs, to some extent like free rapamycin, involve distinct modalities of responses at 0.4 vs. 21% oxygenation. Indeed, protein expression analysis shows that, if mTOR phosphorylation inhibition is higher at 0.4% O_2, the up-stream effector of PI3k/Akt/mTOR pathway, Akt phosphorylation, is higher too. Furthermore, free rapamycin and LNC-rapa inhibit HIF-1α expression at 21% O_2 and to a lesser extent at 0.4% O_2. This difference is linked to HIF-1α stabilization under hypoxia.

LNC-rapa as a New Safe Nanocarrier of Rapamycin

In the present study, we developed lipid nanocapsules capable to efficiently encapsulate rapamycin with yield close to 70%. The formulation was done between 30 and 70°C, a temperature range that protects rapamycin from thermal degradation. Capable to cope with poor water solubility of rapamycin and bioavailability due to their capability to effectively reached intracellular cell compartment (Paillard et al., 2010), rapamycin-loaded LNCs keep rapamycin biological proprieties with an effective inhibition of mTOR phosphorylation. Although this tool fulfills its role as a vector, it does not strengthen the activity of rapamycin or one of its selective aspects in our *in vitro* model tested as well as through multiple conditions (8Gy irradiation, 0.4% hypoxia, 21% normoxia).

In the plethora of new rapamycin nanovector formulations currently available, the loading capacities of each of them, their application methods and loco-regional bioavailability should make it possible to resolve the problem of efficiency and possibly synergy with conventional treatments. Thus a loading capacity of 0.6% for LNC-rapa remains low compared to other systems such as polysorbate 80-coated PLGA nanoparticles (Escalona-Rayo et al., 2019), lipid-polyaniline nanoparticles (Wang J. P. et al., 2016) or PEO/PDLLA electrospun nanofibers (Wang B. L. et al., 2016). Comparative studies in particular *in vivo* should make it possible to understand the rationale which makes one of these vectors an appropriate tool or not.

Forrest and coworkers have developed poly(ethylene glycol)-b-poly(ε-caprolactone) (PEG-PCL) micelles loaded with rapamycin and showed that this drug was efficiently loaded within PEG-PCL up to 10 wt% (more than 1 mg/mL) (Forrest et al., 2006). Other group also demonstrated that rapamycin encapsulation within poly(ethylene glycol)-Block-poly(2-methyl-2-benzoxycarbonyl-propylene carbonate) (PEG-b-PBC) micelles reduced its toxicity (Lu et al., 2011). Shi et al. (2013) developed elastin-based protein polymer nanoparticles loaded with rapamycin and decorated with its ligand FKBP. They showed that these objects slowed down the drug release as compared to non-decorated nanoparticles. Moreover, rapamycin elastin-like polypeptide nanoparticles decreased the gross toxicity and enhanced the anti-cancer activity on human breast cancer mice model (Dhandhukia et al., 2017a,b; Peddi et al., 2020). Finally, Tyler and coworkers incorporated rapamycin into biodegradable caprolactone-glycolide (35:65) polymer beads (Tyler et al., 2011). *In vitro*, rapamycin was cytotoxic toward 9L cells (rat glioma cells), causing growth inhibition at a concentration of 0.01 μg/mL. No *in vivo* toxicity was observed at 0.3, 3, and 30% loading doses implanted intracranially. Animals treated with the highest dose of rapamycin beads (30%) consistently demonstrated

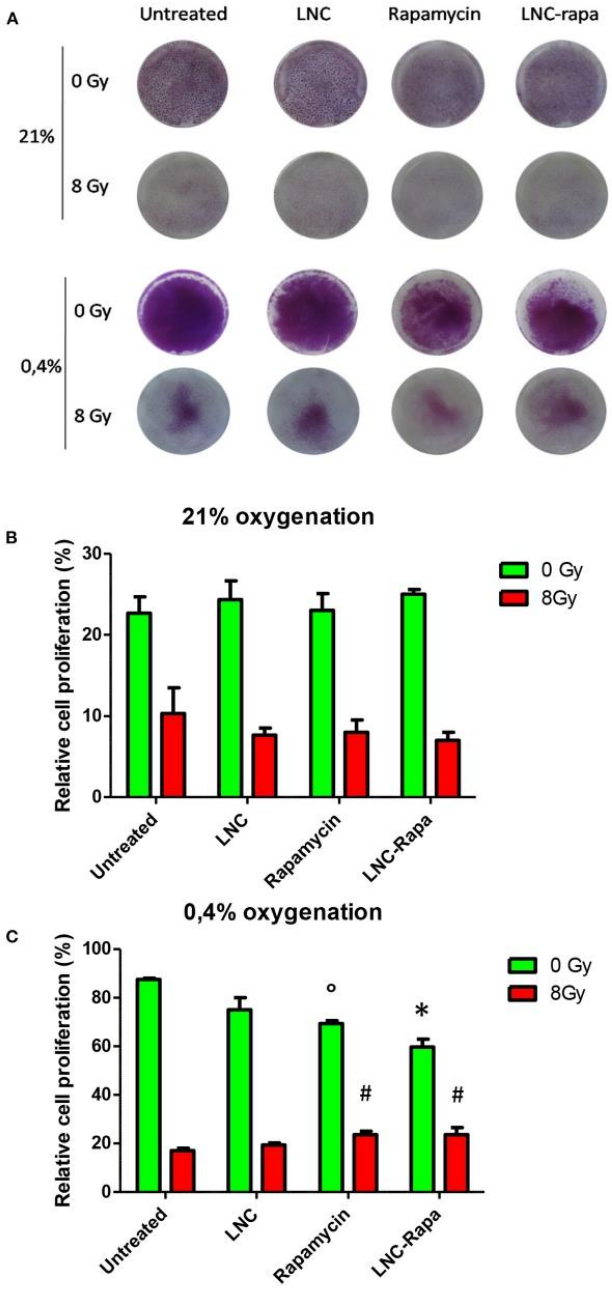


FIGURE 3 | Effects of LNC-rapa assessed by clonogenic assay on U87MG cell growth depending on oxic condition and exposure to radiation treatment. **(A)** Photography of 6-wells plates containing U87MG cells treated with LNCs, rapamycin or LNC-rapa, radiated at 0 Gy (top row) or 8Gy (bottom row) at 21 and 0.4% pO_2

(Continued)

FIGURE 3 | and stained with crystal violet. **(B,C)** Cell survival was determined by measuring crystal violet staining of wells exposed to 0 and 8Gy at 21% pO_2 **(B)** or 0.4% pO2 **(C)**. Data show the average values from a combination of three independent experiments and error bars display the standard deviation. Two-way ANOVA test was performed between LNC-rapa condition compared to LNC condition ($^{*}p \leq 0.05$) or between rapamycin treatment condition and untreated control condition ($^{\circ}p \leq 0.05$) or between rapamycin treatment condition and untreated condition ($^{\#}p \leq 0.05$).

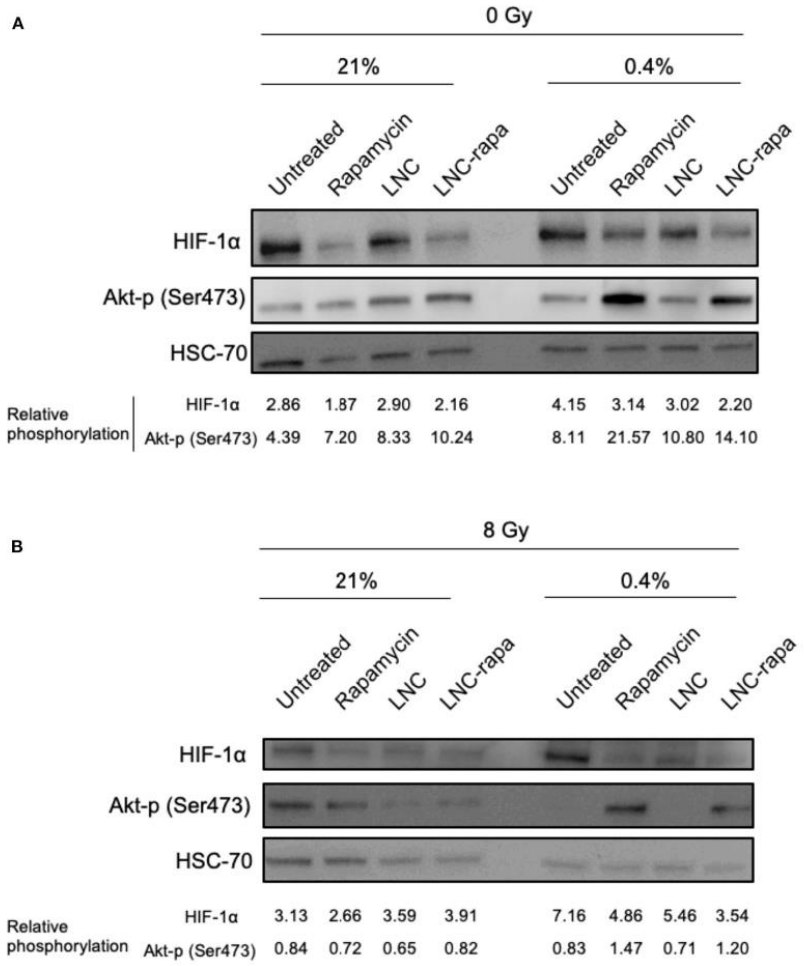


FIGURE 4 | Activation of alternative signaling pathways in response to exposure to LNC-rapa in U87MG. **(A,B)** U87MG cells were treated with free rapamycin, empty LNCs or LNC-rapa, radiated at 0 Gy **(A)** or 8Gy **(B)** and maintained at two oxygenation conditions: 21 and 0.4% before proceeding to western blot analysis. Relative phosphorylation of one representative experiment was measured by volumetry ratio of p-mTOR/HSC70.

significantly longer survival duration than the control and placebo groups. They also showed that radiation therapy in addition to the simultaneous treatment with 30% rapamycin beads led to significantly longer survival duration than each therapy alone.

Vectorized Rapamycin: A Double-Edge Sword "Interactor" in Cancer Cells

The result we obtained on mTOR phosphorylation by rapamycin and LNC-rapa associated with of HIF-1α down regulation and Akt phosphorylation can be linked to the observation made

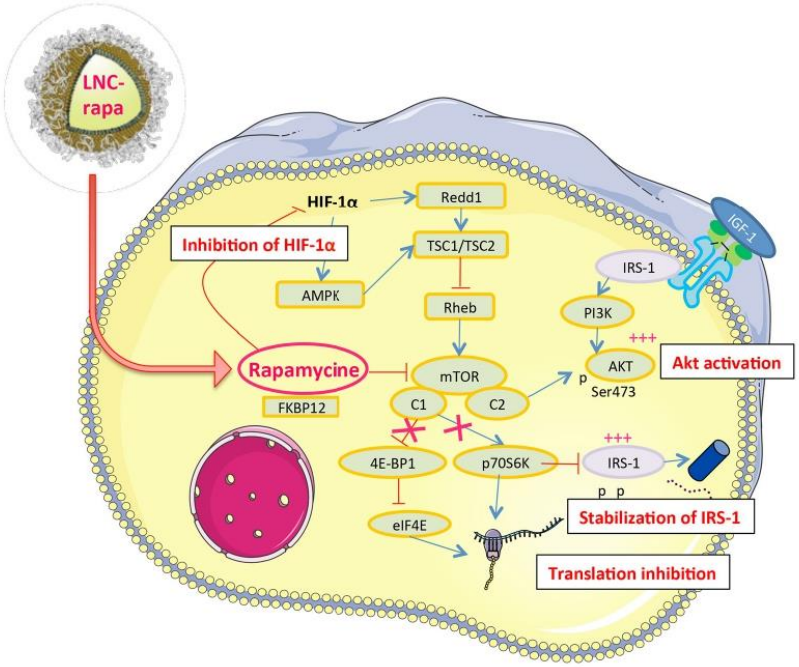


FIGURE 5 | Rapamycin a likely double-edge sword molecular interactor in U87MG glioblastoma cells. Nanovectorized rapamycin (LNC-rapa) or rapamycin as free, solubilized in DMSO, inhibits the stabilization and transcriptional activity of HIF1α which in turn inhibits the TSC1/TSC2 inhibitor and thus promotes the activation of mTOR. On the other hand, rapamycin inhibits mTORC1 but not mTORC2, which in turn induces Akt phosphrylation. Finally, by inhibiting mTORC1, rapamycin lifts the inhibition exerted by p70s6k on IRS-1, which stabilizes this protein and induces Akt phosphorylation *via* the IGF-1 receptor.

by Hudson et al. who reported that rapamycin inhibits both stabilization of HIF-1α and the transcriptional activity of HIF-1 in hypoxic cancer cells and mTOR dependent signals stimulate HIF-1α accumulation and HIF-1 mediated transcription in cells exposed to hypoxia or hypoxia-mimetic agent (Zhong et al., 2000). Rapamycin-sensitive functions of mTOR are not essential for the accumulation of HIF-1α but are needed for maximal expression of this protein, as well as for optimal HIF-1-dependent gene expression under hypoxic conditions. The notion that mTOR is a nutrient sensor may be particularly relevant to HIF-1 function, since decrease oxygen tensions are almost inevitable accompanied by limited supplies of glucose and amino-acids in mammalian tissues (Hudson et al., 2002). *In vivo*, rapamycin enhance thrombosis and also an increase in the hypoxic zone (Weppler et al., 2007). Hypoxia causes activation of the TSC1/2 complex, which functions to inhibit mTOR. This can occur both *via* induction of the HIF-dependent gene REDD1, and/or through activation of AMPK (Brugarolas et al., 2004; Liu et al., 2006). Rapamycin may be less effective in hypoxic regions of tumors since mTOR may already be at least partially inactivated by TSC. Thus the amount of hypoxia present at the start of treatment may play a part in determining sensitivity to rapamycin *in vivo* (Weppler et al., 2007) (**Figure 5**).

The higher Akt phosphorylation at 0.4% could also explain that cells are less sensitive to rapamycin than at 21%. Indeed, U87MG cell line is PTEN *null* that drives to a constitutive activation of the PI3K/Akt/mTOR pathway and could explains its radioresistance. Thus, mTOR inhibition could restore radiosensitivity but our results show that maximal cytotoxic effect was observed with 8Gy radiation and rapamycin or LNC-rapa were not sufficient to improve the cytotoxicity at the concentration of 1 μM. To well-understand this phenomenon, it is important to remind that mTOR exist in two complexes: mTORC1 and mTORC2. mTORC1 contains the mTOR, Raptor, mLST8/GβL, and PRAS40 proteins and controls cell size and protein translation *via* two major substrates, p70S6K and 4E-BP1. Activated S6 kinase causes feedback inhibition of insulin-like growth factor 1 (IGF-1)/insulin signaling by phosphorylating insulin receptor substrate 1 (IRS-1) and causing its degradation (Tremblay et al., 2007). mTORC2 has been shown to phosphorylate Akt at the serine 473 site, which enhances the catalytic activity of Akt already phosphorylated

on threonine 308 (Sarbassov et al., 2005). Rapamycin binds to FKBP-12 and this complex then binds to and causes the allosteric inhibition of mTORC1. Rapamycin effectively blocks S6K phosphorylation and also induces Akt S473 phosphorylation and Akt activity (O'Reilly et al., 2006). Physiologic activation of PI3k/Akt signaling is regulated by mTOR-dependent feedback inhibition of IRS expression and, consequently, IGF-1 receptor (IGF-1R)/insulin receptor signaling (Tremblay et al., 2007). Rapamycin relieves this feedback and induces Akt S473 phosphorylation in an mTORC2-dependent manner, leading to Akt activation, which may attenuate its therapeutic effects (O'Reilly et al., 2006). Furthermore, mTOR inhibitory drug rapamycin up-regulates IRS-1 protein levels and induces Akt phosphorylation that increase IGF—IR/IRS-1/PI3K signaling to Akt (O'Reilly et al., 2006) (**Figure 5**). In line with this, mTORC2, not inhibited by LNC-rapa, has recently been described as a downstream integrator of metabolic and epigenetic landscape leading to tumor cell survival and cancer durg resistance (Masui et al., 2019, 2020).

In response of those problems, Rodrik-Outmezguine et al. (2011) used a selective ATP-competitive mTOR kinase inhibitor AZD8055. This drug inhibits 4E-BP1 phosphorylation more effectively than rapamycin. It also inhibits mTORC2 and Akt S473 phosphorylation, which leads to Akt T308 dephosphorylation and suppression of Akt activity and downstream signaling. Unfortunately, even though mTORC2 inhibition is potent and persistent, inhibition of Akt T308 and Akt substrate phosphorylation is only transient. Authors demonstrated that this re-induction resulted from hyperactivation of PI3K. In cells in which mTOR kinase inhibitors relieve feedback inhibition of receptor tyrosine kinase, leading to activation of PI3K, the result is a new steady state in which mTORC1 is potently inhibited and Akt is phosphorylated on T308 but not on the S473. This Akt species is activated and able to phosphorylate key substrates in the cells. Induction of PI3K activation depends also from cell directory of activated tyrosine kinase receptors and from active ligands available (Rodrik-Outmezguine et al., 2011).

Alternatively, Kahn and coworkers showed *in vitro* that addition of AZD2014, another mTORC1/mTORC2 inhibitor, to culture media 1 h before irradiation enhanced the radiosensitivity of $CD133^+$ and $CD15^+$ glioblastoma stem-like cells (Kahn et al., 2014). The combination of AZD2014 and radiation delivered to mice bearing GSC-initiated orthotopic xenografts significantly prolonged survival of these animals as compared to individual treatments.

In parallel, dual PI3K/mTOR inhibitors were developed, notably the NVP-BEZ235. It demonstrated suppression of mTORC1 (S6K1, S6K, and 4E-BP1) and mTORC2 (AKT) downstream components resulting in cell cycle arrest and induced autophagy (Cerniglia et al., 2012). NVP-BEZ235 showed inhibited *in vivo* glioma proliferation and improved anti-tumor effects compared to rapamycin analogs. Mukherjee et al. (2012) showed that NVP-BEZ235 can inhibit DNA repair proteins ATM and DNA-PKC in GB that lead to a radiosensitizing effect. Nevertheless, because of the induction of autophagy that seems to be cytoprotective (Cerniglia et al., 2012), combination therapies with NVP-BEZ235 have been explored. One strategy utilized NVP-BEZ235 with autophagy inhibitor chloroquine to show a synergistic effect in *in vivo* tumor apoptosis (Fan et al., 2010). In line with this, Heinze et al., underlined that under hypoxia and nutrient-poor conditions, second generation mTORC1/C2 inhibitors displayed even stronder cytoprotective effect by reducing oxygen and glucose consumption (Heinzen et al., 2019).

However, those experiences were performed mainly *in vitro* and could yield different results *in vivo*. Indeed, some groups have reported that rapamycin sensitized U87MG xenografts to fractionated radiation therapy. Eshleman and coworkers also showed that there were no radiosensitizing effects of rapamycin on U87MG in the radiation clonogenic survival assays, nevertheless, they observed a great effect in the U87 xenograft and spheroids models (Eshleman et al., 2002). They proposed that other factors could also be important for the sensitizing effect of rapamycin. For example, rapamycin induces significant changes in glucose and nitrogen metabolism, and the starvation-like metabolic state induced by rapamycin could potentially decrease oxygen consumption in solid tumors and improve overall tumor oxygenation (Hardwick et al., 1999). Any decrease in the proportion of radioresistant hypoxic cells should significantly increase the efficacy of radiation. The authors also suggested that rapamycin could inhibit host-dependent processes that contribute to the profound sensitizing effect of rapamycin in xenograft model. Furthermore, rapamycin is a potent inhibitor of endothelial cell proliferation *in vitro*, therefore its systemic administration can inhibit angiogenesis. It reduces VEGF production by tumor cells and the inhibition of VEGF-induced proliferation in endothelial cells (Guba et al., 2002).

In the same way, Weppler et al. (2007) investigated the combination of rapamycin with short course of fractionated radiotherapy to minimize the anti-proliferative effect of rapamycin and thus evaluate its potential to contribute to the direct cytotoxic effect of radiation. They found that rapamycin did not significantly improve radiation response but increased variability in tumor response to radiotherapy, with several individual tumors showing large increases in growth delay. Thus, they underlined the importance to determine the biological factors that mediated this differential response in order to potentially identify patients that may benefit from combination treatment.

CONCLUSION

To conclude, rapamycin-loaded lipid nanocapsules for peripheral or loco-regional administration developed in this study represent a new safe nanocarrier of rapamycin capable to convey rapamycin and preserves its biological activity on cancer cells. We showed that activation of a negative feedback following mTOR phosphorylation inhibition is a serious brake on rapamycin cytotoxicity. The first solution could consist of changing rapamycin for dual PI3K/mTOR inhibitors like the NVP-BEZ235 which has demonstrated effectiveness *in vivo* (Cerniglia et al., 2012), or mTORC1/mTORC2 inhibitor is

AZD2014 which radiosensitizes glioma (Kahn et al., 2014). Nevertheless, rapamycin radiosensitizer effect have been proved *in vivo* or using fractionated radiation protocol (Eshleman et al., 2002). Moreover, if patients are biologically screened to select the most responsive ones, as underlined by Weppler et al., LNC-rapa can potentially be effective with an adapted radiation protocol.

DATA AVAILABILITY STATEMENT

All data generated or analyzed during this study are included in this published article (and its **Supplementary Information** files).

AUTHOR CONTRIBUTIONS

DS and EG wrote the manuscript. EG, FH, MC, FB, and FL contributed to the conception, design, and funding of the work. DS and SA contributed to the experiments. DS, NB, LR, AD, and EG contributed to manuscript revisions. All authors read and approved the submitted version.

FUNDING

This work was supported by the French National Research Agency (ANR) through the LabEx IRON (Innovative Radiopharmaceuticals in Oncology and Neurology) as part of the French government Investissements d'Avenir program (ANR-11-LABX-0018). It was also supported by the Institut National de la Santé et de la Recherche Médicale (INSERM) and by the University of Angers (Angers, France). This work was also supported by the NanoFar program (European doctorate in nanomedicine and pharmaceutical innovation) (Erasmus Mundus Joint Doctorate) funded by EACEA and by the NanoFar+ program (International strategy) funded by La Région Pays-de-la-Loire. The work was also related to: (i) the ANR under the frame of EuroNanoMed III (project GLIOSILK), (ii) the PL-BIO 2014–2020 INCa (Institut National du Cancer) consortium MARENGO (MicroRNA agonist and antagonist Nanomedicines for GliOblastoma treatment: from molecular programmation to preclinical validation), (iii) to the MuMoFRaT project (Multi-scale Modeling & simulation of the response to hypo-Fractionated Radiotherapy or repeated molecular radiation Therapies) supported by La Région Pays-de-la-Loire and by the Cancéropole Grand-Ouest (Vectorization, imaging, and radiotherapies network). DS and LR were PhD fellows funded by La Région Pays de la Loire and by the LabEx IRON-2/University of Angers, respectively. AD was a Ph.D. fellow from La Ligue Nationale contre le Cancer and was funded in this context by the Comité de Loire-Atlantique.

ACKNOWLEDGMENTS

The content of this manuscript has been published in part as part of the thesis of DS, Développement de nouvelles stratégies en nanomédecine pour le ciblage et la radiosensibilisation des cellules souches dans le glioblastome (Séhédic, 2014).

SUPPLEMENTARY MATERIAL

The Supplementary Material for this article can be found online at: https://www.frontiersin.org/articles/10.3389/fbioe.2020.602998/full#supplementary-material

Supplementary Figure 1 | Spectral analysis of rapamycin stability in Labrafac®. **(A)** Labrafac spectra at RT. **(B)** Labrafac spectra after 3 h heating at 70°C. **(C)** Rapamycin spectra after 3 h at RT in Labrafac. **(D)** Rapamycin spectra after six short cycles of heating and cooling (70°C to RT) in Labrafac. **(E)** Rapamycin spectra after 1 h heating at 70°C in Labrafac. **(F)** Rapamycin spectra after 3 h heating at 70°C in Labrafac. **(G)** Spectra of rapamycin, previously dissolved in methanol (MeOH), after three short cycles of heating and cooling (70°C to RT) in Labrafac. **(H)** Spectra of rapamycin, previously dissolved in methanol (MeOH), after 3 h heating at 70°C in Labrafac. Each curve represents one representative analysis of a triplicate.

Supplementary Figure 2 | Survival of U87MG cells in response of free-rapamycin treatment assessed by use of MTS assay. **(A)** U87MG cells were treated with free rapamycin at 21% (green curve) and 0.4% (red curve) oxygenation. **(B)** Calculated IC50 at 21 and 0.4% oxygenation following rapamycin treatment.

Supplementary Table 1 | Stability of 50 nm blank and rapamycin loaded LNC during storage at different temperatures. Note the modification of size and loss of polydispersity after 7 days storage (boxes highlighted in gray).

REFERENCES

Anandharaj, A., Cinghu, S., and Park, W. Y. (2011). Rapamycin-mediated mTOR inhibition attenuates survivin and sensitizes glioblastoma cells to radiation therapy. *Acta Biochim. Biophys. Sin.* 43, 292–300. doi: 10.1093/abbs/gmr012

Bai, R. Y., Staedtke, V., and Riggins, G. J. (2011). Molecular targeting of glioblastoma: drug discovery and therapies. *Trends Mol. Med.* 17, 301–312. doi: 10.1016/j.molmed.2011.01.011

Bjornsti, M. A., and Houghton, P. J. (2004). The TOR pathway: a target for cancer therapy. *Nat. Rev. Cancer* 4, 335–348. doi: 10.1038/nrc1362

Brugarolas, J., Lei, K., Hurley, R. L., Manning, B. D., Reiling, J. H., Hafen, E., et al. (2004). Regulation of mTOR function in response to hypoxia by REDD1 and the TSC1/TSC2 tumor suppressor complex. *Genes Dev.* 18, 2893–2904. doi: 10.1101/gad.1256804

Castellino, R. C., and Durden, D. L. (2007). Mechanisms of disease: the PI3K-Akt-PTEN signaling node - an intercept point for the control of angiogenesis in brain tumors. *Nat. Clin. Pract. Neurol.* 3, 682–693. doi: 10.1038/ncpneuro0661

Cerniglia, G. J., Karar, J., Tyagi, S., Christofidou-Solomidou, M., Rengan, R., Koumenis, C., et al. (2012). Inhibition of autophagy as a strategy to augment radiosensitization by the dual phosphatidylinositol 3-kinase/mammalian target of rapamycin inhibitor NVP-BEZ235. *Mol. Pharmacol.* 82, 1230–1240. doi: 10.1124/mol.112.080408

Chinnaiyan, P., Won, M., Wen, P. Y., Rojiani, A. M., Werner-Wasik, M., Shih, H. A., et al. (2018). A randomized phase II study of everolimus in combination with chemoradiation in newly diagnosed glioblastoma: results of NRG oncology RTOG 0913. *Neuro Oncol.* 20, 666–673. doi: 10.1093/neuonc/nox209

Courtney, K. D., Corcoran, R. B., and Engelman, J. A. (2010). The PI3K pathway as drug target in human cancer. *J. Clin. Oncol.* 28, 1075–1083. doi: 10.1200/JCO.2009.25.3641

Dhandhukia, J. P., Li, Z., Peddi, S., Kakan, S., Mehta, A., Tyrpak, D., et al. (2017a). Berunda polypeptides: multi-headed fusion proteins promote subcutaneous administration of rapamycin to breast cancer *in vivo*. *Theranostics* 7, 3856–3872. doi: 10.7150/thno.19981

Dhandhukia, J. P., Shi, P., Peddi, S., Li, Z., Aluri, S., Ju, Y. P., et al. (2017b). Bifunctional elastin-like polypeptide nanoparticles bind rapamycin and integrins and suppress tumor growth *in vivo*. *Bioconjug. Chem.* 28, 2715–2728. doi: 10.1021/acs.bioconjchem.7b00469

Engelman, J. A. (2009). Targeting PI3K signalling in cancer: opportunities, challenges and limitations. *Nat. Rev. Cancer* 9, 550–562. doi: 10.1038/nrc2664

Escalona-Rayo, O., Fuentes-Vazquez, P., Jardon-Xicotencatl, S., Garcia-Tovar, C. G., Mendoza-Elvira, S., and Quintanar-Guerrero, D. (2019). Rapamycin-loaded polysorbate 80-coated PLGA nanoparticles: optimization of formulation variables and *in vitro* anti-glioma assessment. *J. Drug Deliv. Sci. Technol.* 52, 488–499. doi: 10.1016/j.jddst.2019.05.026

Eshleman, J. S., Carlson, B. L., Mladek, A. C., Kastner, B. D., Shide, K. L., and Sarkaria, J. N. (2002). Inhibition of the mammalian target of rapamycin sensitizes U87 Xenografts to fractionated radiation therapy. *Cancer Res.* 62, 7291–7297.

Fan, Q. W., Cheng, C., Hackett, C., Feldman, M., Houseman, B. T., Nicolaides, T., et al. (2010). Akt and autophagy cooperate to promote survival of drug-resistant glioma. *Sci. Signal.* 3:ra18. doi: 10.1126/scisignal.2001017

Forrest, M. L., Won, C. Y., Malick, A. W., and Kwon, G. S. (2006). *In vitro* release of the mTOR inhibitor rapamycin from poly(ethylene glycol)-b-poly(epsilon-caprolactone) micelles. *J. Control. Release* 110, 370–377. doi: 10.1016/j.jconrel.2005.10.008

Guba, M., von Breitenbuch, P., Steinbauer, M., Koehl, G., Flegel, S., Hornung, M., et al. (2002). Rapamycin inhibits primary and metastatic tumor growth by antiangiogenesis: involvement of vascular endothelial growth factor. *Nat. Med.* 8, 128–135. doi: 10.1038/nm0202-128

Hardwick, J. S., Kuruvilla, F. G., Tong, J. K., Shamji, A. F., and Schreiber, S. L. (1999). Rapamycin-modulated transcription defines the subset of nutrient-sensitive signaling pathways directly controlled by the Tor proteins. *Proc. Natl. Acad. Sci. U.S.A.* 96, 14866–14870. doi: 10.1073/pnas.96.26.14866

Heimberger, A. B., Wang, E., McGary, E. C., Hess, K. R., Henry, V. K., Shono, T., et al. (2005). Mechanisms of action of rapamycin in gliomas. *Neuro Oncol.* 7, 1–11. doi: 10.1215/S1152851704000420

Heinzen, D., Dive, I., Lorenz, N. I., Luger, A. L., Steinbach, J. P., and Ronellenfitsch, M. W. (2019). Second generation mTOR inhibitors as a double-edged sword in malignant glioma treatment. *Int. J. Mol. Sci.* 20:4474. doi: 10.3390/ijms20184474

Heurtault, B., Saulnier, P., Pech, B., Proust, J. E., and Benoit, J. P. (2002). A novel phase inversion-based process for the preparation of lipid nanocarriers. *Pharm. Res.* 19, 875–880. doi: 10.1023/A:1016121319668

Hsu, S. P. C., Chen, Y.-C., Chiang, H.-C., Huang, Y.-C., Huang, C.-C., Wang, H.-E., et al. (2020). Rapamycin and hydroxychloroquine combination alters macrophage polarization and sensitizes glioblastoma to immune checkpoint inhibitors. *J. Neurooncol.* 146, 417–426. doi: 10.1007/s11060-019-03360-3

Hudson, C. C., Liu, M., Chiang, G. G., Otterness, D. M., Loomis, D. C., Kaper, F., et al. (2002). Regulation of hypoxia-inducible factor 1 alpha expression and function by the mammalian target of rapamycin. *Mol. Cell. Biol.* 22, 7004–7014. doi: 10.1128/MCB.22.20.7004-7014.2002

Jiang, B. H., and Liu, L. Z. (2009). PI3K/PTEN signaling in angiogenesis and tumorigenesis. *Adv. Cancer Res.* 102, 19–65. doi: 10.1016/S0065-230X(09)02002-8

Kahn, J., Hayman, T. J., Jamal, M., Rath, B. H., Kramp, T., Camphausen, K., et al. (2014). The mTORC1/mTORC2 inhibitor AZD2014 enhances the radiosensitivity of glioblastoma stem-like cells. *Neuro Oncol.* 16, 29–37. doi: 10.1093/neuonc/not139

Knobbe, C. B., Trampe-Kieslich, A., and Reifenberger, G. (2005). Genetic alteration and expression of the phosphoinositol-3-kinase/Akt pathway genes PIK3CA and PIKE in human glioblastomas. *Neuropathol. Appl. Neurobiol.* 31, 486–490. doi: 10.1111/j.1365-2990.2005.00660.x

Li, X., Wu, C., Chen, N., Gu, H., Yen, A., Cao, L., et al. (2016). PI3K/Akt/mTOR signaling pathway and targeted therapy for glioblastoma. *Oncotarget* 7, 33440–33450. doi: 10.18632/oncotarget.7961

Liu, L. P., Cash, T. P., Jones, R. G., Keith, B., Thompson, C. B., and Simon, M. C. (2006). Hypoxia-induced energy stress regulates mRNA translation and cell growth. *Mol. Cell* 21, 521–531. doi: 10.1016/j.molcel.2006.01.010

Lu, W. L., Li, F., and Mahato, R. I. (2011). Poly(ethylene glycol)-block-poly(2-methyl-2-benzoxycarbonyl-propylene carbonate) micelles for rapamycin delivery: *in vitro* characterization and biodistribution. *J. Pharm. Sci.* 100, 2418–2429. doi: 10.1002/jps.22467

Mao, H., LeBrun, D. G., Yang, J. X., Zhu, V. F., and Li, M. (2012). Deregulated signaling pathways in glioblastoma multiforme: molecular mechanisms and therapeutic targets. *Cancer Invest.* 30, 48–56. doi: 10.3109/07357907.2011.630050

Masui, K., Harachi, M., Cavenee, W. K., Mischel, P. S., and Shibata, N. (2020). mTOR complex 2 is an integrator of cancer metabolism and epigenetics. *Cancer Lett.* 478, 1–7. doi: 10.1016/j.canlet.2020.03.001

Masui, K., Harachi, M., Ikegami, S., Yang, H. J., Onizuka, H., Yong, W. H., et al. (2019). mTORC2 links growth factor signaling with epigenetic regulation of iron metabolism in glioblastoma. *J. Biol. Chem.* 294, 19740–19751. doi: 10.1074/jbc.RA119.011519

Mecca, C., Giambanco, I., Donato, R., and Arcuri, C. (2018). Targeting mTOR in glioblastoma: rationale and preclinical/clinical evidence. *Dis. Markers.* 2018:9230479. doi: 10.1155/2018/9230479

Mukherjee, B., Tomimatsu, N., Amancherla, K., Camacho, C. V., Pichamoorthy, N., and Burma, S. (2012). The dual PI3K/mTOR inhibitor NVP-BEZ235 is a potent inhibitor of ATM- and DNA-PKCs-mediated DNA damage responses. *Neoplasia* 14, 34–43. doi: 10.1593/neo.111512

Najberg, M., Haji Mansor, M., Boury, F., Alvarez-Lorenzo, C., and Garcion, E. (2019). Reversing the tumor target: establishment of a tumor trap. *Front. Pharmacol.* 10:887. doi: 10.3389/fphar.2019.00887

O'Reilly, K. E., Rojo, F., She, Q. B., Solit, D., Mills, G. B., Smith, D., et al. (2006). mTOR inhibition induces upstream receptor tyrosine kinase signaling and activates Akt. *Cancer Res.* 66, 1500–1508. doi: 10.1158/0008-5472.CAN-05-2925

Ostrom, Q. T., Gittleman, H., Liao, P., Vecchione-Koval, T., Wolinsky, Y., Kruchko, C., et al. (2017). CBTRUS statistical report: primary brain and other central nervous system tumors diagnosed in the united states in 2010–2014. *Neuro Oncol.* 19, v1–v88. doi: 10.1093/neuonc/nox158

Paillard, A., Hindre, F., Vignes-Colombeix, C., Benoit, J. P., and Garcion, E. (2010). The importance of endo-lysosomal escape with lipid nanocapsules for drug subcellular bioavailability. *Biomaterials* 31, 7542–7554. doi: 10.1016/j.biomaterials.2010.06.024

Peddi, S., Roberts, S. K., and MacKay, J. A. (2020). Nanotoxicology of an elastin-like polypeptide rapamycin formulation for breast cancer. *Biomacromolecules* 21, 1091–1102. doi: 10.1021/acs.biomac.9b01431

Raymond, E., Alexandre, J., Faivre, S., Vera, K., Materman, E., Boni, J., et al. (2004). Safety and pharmacokinetics of escalated doses of weekly intravenous infusion of CCI-779, a novel mTOR inhibitor, in patients with cancer. *J. Clin. Oncol.* 22, 2336–2347. doi: 10.1200/JCO.2004.08.116

Rodrik-Outmezguine, V. S., Chandarlapaty, S., Pagano, N. C., Poulikakos, P. I., Scaltriti, M., Moskatel, E., et al. (2011). mTOR kinase inhibition causes feedback-dependent biphasic regulation of AKT signaling. *Cancer Discov.* 1, 248–259. doi: 10.1158/2159-8290.CD-11-0085

Sarbassov, D. D., Guertin, D. A., Ali, S. M., and Sabatini, D. M. (2005). Phosphorylation and regulation of Akt/PKB by the rictor-mTOR complex. *Science* 307, 1098–1101. doi: 10.1126/science.1106148

Saxton, R. A., and Sabatini, D. M. (2017). mTOR signaling in growth, metabolism, and disease. *Cell* 168, 960–976. doi: 10.1016/j.cell.2017.02.004

Séhédic, D. (2014). *Development of new nano-medicine strategies for the targeting and the radiosensization of glioblastoma stem cells* (Université d'Angers). Available online at: https://www.theses.fr/2014ANGE0028

Shi, P., Aluri, S., Lin, Y. A., Shah, M., Edman, M., Dhandhukia, J., et al. (2013). Elastin-based protein polymer nanoparticles carrying drug at both corona and core suppress tumor growth *in vivo*. *J. Control. Release* 171, 330–338. doi: 10.1016/j.jconrel.2013.05.013

Shinohara, E. T., Cao, C., Niermann, K., Mu, Y., Zeng, F. H., Hallahan, D. E., et al. (2005). Enhanced radiation damage of tumor vasculature by mTOR inhibitors. *Oncogene* 24, 5414–5422. doi: 10.1038/sj.onc.1208715

Simamora, P., Alvarez, J. M., and Yalkowsky, S. H. (2001). Solubilization of rapamycin. *Int. J. Pharm.* 213, 25–29. doi: 10.1016/S0378-5173(00)00617-7

Sonoda, Y., Ozawa, T., Aldape, K. D., Deen, D. F., Berger, M. S., and Pieper, R. O. (2001). Akt pathway activation converts anaplastic astrocytoma to glioblastoma multiforme in a human astrocyte model of glioma. *Cancer Res.* 61, 6674–6678.

Stupp, R., Hegi, M. E., Mason, W. P., van den Bent, M. J., Taphoorn, M. J., Janzer, R. C., et al. (2009). Effects of radiotherapy with concomitant and adjuvant temozolomide vs. radiotherapy alone on survival in glioblastoma in

a randomised phase III study: 5-year analysis of the EORTC-NCIC trial. *Lancet Oncol.* 10, 459–466. doi: 10.1016/S1470-2045(09)70025-7

Stupp, R., Mason, W. P., van den Bent, M. J., Weller, M., Fisher, B., Taphoorn, M. J., et al. (2005). Radiotherapy plus concomitant and adjuvant temozolomide for glioblastoma. *N. Engl. J. Med.* 352, 987–996. doi: 10.1056/NEJMoa043330

Touat, M., Idbaih, A., Sanson, M., and Ligon, K. L. (2017). Glioblastoma targeted therapy: updated approaches from recent biological insights. *Ann. Oncol.* 28, 1457–1472. doi: 10.1093/annonc/mdx106

Tremblay, F., Brule, S., Um, S. H., Li, Y., Masuda, K., Roden, M., et al. (2007). Identification of IRS-1 Ser-1101 as a target of S6K1 in nutrient- and obesity-induced insulin resistance. *Proc. Natl. Acad. Sci. U.S.A.* 104, 14056–14061. doi: 10.1073/pnas.0706517104

Tyler, B., Wadsworth, S., Recinos, V., Mehta, V., Vellimana, A., Li, K., et al. (2011). Local delivery of rapamycin: a toxicity and efficacy study in an experimental malignant glioma model in rats. *Neuro Oncol.* 13, 700–709. doi: 10.1093/neuonc/nor050

Wang, B. L., Li, H. Y., Yao, Q. Y., Zhang, Y. L., Zhu, X. D., Xia, T. L., et al. (2016). Local *in vitro* delivery of rapamycin from electrospun PEO/PDLLA nanofibers for glioblastoma treatment. *Biomed. Pharmacother.* 83, 1345–1352. doi: 10.1016/j.biopha.2016.08.033

Wang, J. P., Guo, F., Yu, M., Liu, L., Tan, F. P., Yan, R., et al. (2016). Rapamycin/DiR loaded lipid-polyaniline nanoparticles for dual-modal imaging guided enhanced photothermal and antiangiogenic combination therapy. *J. Control. Release* 237, 23–34. doi: 10.1016/j.jconrel.2016.07.005

Wanigasooriya, K., Tyler, R., Barros-Silva, J. D., Sinha, Y., Ismail, T., and Beggs, A. D. (2020). Radiosensitising cancer using phosphatidylinositol-3-kinase (PI3K), protein kinase B (AKT) or mammalian target of rapamycin (mTOR) inhibitors. *Cancers* 12:1278. doi: 10.3390/cancers12051278

Weppler, S. A., Krause, M., Zyromska, A., Lambin, P., Baumann, M., and Wouters, B. G. (2007). Response of U87 glioma xenografts treated with concurrent rapamycin and fractionated radiotherapy: possible role for thrombosis. *Radiother. Oncol.* 82, 96–104. doi: 10.1016/j.radonc.2006.11.004

Wick, W., Weller, M., Weiler, M., Batchelor, T., Yung, A. W. K., and Platten, M. (2011). Pathway inhibition: emerging molecular targets for treating glioblastoma. *Neuro Oncol.* 13, 566–579. doi: 10.1093/neuonc/nor039

Yatscoff, R. W., Wang, P., Chan, K., Hicks, D., and Zimmerman, J. (1995). Rapamycin - distribution, pharmacokinetics, and therapeutic range investigations. *Ther. Drug Monit.* 17, 666–671. doi: 10.1097/00007691-199512000-00020

Zhong, H., Chiles, K., Feldser, D., Laughner, E., Hanrahan, C., Georgescu, M. M., et al. (2000). Modulation of hypoxia-inducible factor 1 alpha expression by the epidermal growth factor/phosphatidylinositol 3-kinase/PTEN/AKT/FRAP pathway in human prostate cancer cells: implications for tumor angiogenesis and therapeutics. *Cancer Res.* 60, 1541–1545.

Conflict of Interest: The authors declare that the research was conducted in the absence of any commercial or financial relationships that could be construed as a potential conflict of interest.

Copyright © 2021 Séhédic, Roncali, Djoudi, Buchtova, Avril, Chérel, Boury, Lacoeuille, Hindré and Garcion. This is an open-access article distributed under the terms of the Creative Commons Attribution License (CC BY). The use, distribution or reproduction in other forums is permitted, provided the original author(s) and the copyright owner(s) are credited and that the original publication in this journal is cited, in accordance with accepted academic practice. No use, distribution or reproduction is permitted which does not comply with these terms.

Communications

Poster et présentations orales lors de congrès

- Journée scientifique Jeunes & Chercheurs de la Ligue contre le Cancer, Paris, 20 Octobre 2020(Présentation poster)

- Nano Innovation Conference & Exhibition; Innovative approaches in UNMET clinical needs for maximum health care impact - Innovation in Academia, Rome, Italy 22 September 2021 (Présentation orale)

•Participation & scientific popularisation with GLIAD team, at "Fête de la Science d'Angers" October 9-10th 2021(vulgarisation scientifique)

•Oral presentation at C'Nano Toulouse 23-25 November 2021(presentation orale)

•Poster presentation at scientific days of Biology-Health Doctoral School December 9th-10th 2021 at Brest(presentation de poster)

•Participation through a talk to the SFR-ICAT Scientific Day on 9th June 2022(presentation orale)

•Oral presentation at the Erquy Workshop (Britany) on 5-8th October 2022 (Upcoming)

•Oral presentation at the Journée biomédicale d'Angers-Tours à Angers le 2 décembre 2022

Publications

- **Séhédic D, Roncali L, Djoudi A, Buchtova N, Avril S, Chérel M, et al. Rapamycin- Loaded Lipid Nanocapsules Induce Selective Inhibition of the mTORC1-Signaling Pathway in Glioblastoma Cells.** ***Front Bioeng Biotechnol*****. 2020;8:602998(Published)**

•Amel Djoudi*[1], Rodolfo Molina-Pena[1], Natalia Ferreira[1], Illaria Otonelli2, Giovanni Tosi2, Emmanuel Garcion[1], Frank Boury*[1]. Hyaluronic acid scaffolds for loco-regional therapy in nervous system related disorders. ***International Journal of Molecular Sciences*****.2022 (Published)**

•Amel Djoudi*[1], Rodolfo Molina-Pena[1], Natalia Ferreira[1], Sylvie Avril[1], Emmanuel Garcion[1], Frank Boury*[1] Development of BMP-4 loaded PLGA nanoparticles via a non-toxic phase separation process . *Pharmaceuticals.*2022 (Upcoming submission)

•Amel Djoudi[1], Rodolfo Molina-Peña[1], Natalia Ferreira[1], Sylvie Avril[1], Emmanuel Garcion[1], Frank Boury[1] Formulation of BMP-4 loaded nanocomposite hydrogel as a potential Glioblastoma treatment. *Gels.* 2022(Upcoming submission)

Rodolfo Molina-Pena[1], Clement Toullec[1], Amel Djoudi[1], Christine Jerôme, Emmanuel Garcion[1], Frank Boury*[1] Chitosan electrospun scaffolds as implantable Extra Cellular Matrix replacement and therapeutical systems for nervous system diseases. Materials 2022/2023 (Upcoming finalization)

Titre : DEVELOPPEMENT D'HYDROGELS NANOCOMPOSITES INNOVANTS POUR LE TRAITEMENT LOCOREGIONAL DU GLIOBLASTOME

Mots clés : Glioblastome, Libération prolongée de protéines,
Protéine morphogénique osseuse (BMP), Nanoparticules, Echafaudages nanocomposites

Résumé : Le glioblastome (GB) est la forme de cancer du cerveau la plus fréquente et la plus léthale. Il a une capacité de diffusion qui explique une impossibilité d'ablation complète de la tumeur par chirurgie. 90% des patients ont une récidive liée à la présence de de cellules GB résiduelles situées aux bords de la cavité de résection Un hydrogel nanocomposite pouvant libérer de manière prolongée la protéine BMP-4, qui se lie aux récepteurs BMPRII à la surface des cellules GB, peut être utile pour induire la différenciation des cellules GB résiduelles, permettre leur élimination sélective et donc réduire la récurrence de la tumeur. Dans ce projet, la BMP-4 a été initialement encapsulée dans des nanoparticules à base d'acide poly-lactique-co-glycolique (PLGA). Une efficacité d'encapsulation élevée a été obtenue via un procédé de séparation de phase utilisant des solvants non toxiques. Les nanoparticules chargées de BMP-4 ont ensuite été incorporées dans un hydrogel à base d'acide hyaluronique et de poloxamer 407 pour obtenir un système nanocomposite mimant la structure de la matrice extracellulaire du cerveau. Une étude de libération *in vitro* a révélé que l'hydrogel pouvait fournir une libération prolongée de BMP-4 jusqu'à 30 jours, utile pour établir un gradient de concentration de BMP-4 dans le cerveau et différencier les cellules GB. Une étude de biocompatibilité *in vivo* à 3 jours et à 7 jours visant à confirmer l'innocuité *in vivo* des implants avant de passer aux études d'efficacité dans un modèle de résection GB approprié est actuellement en cours.

Title : DEVELOPMENT OF INNOVATIVE NANOCOMPOSITE HYDROGELS FOR LOCOREGIONAL TREATMENT OF GLIOBLASTOMA

Keywords : Glioblastoma, Sustained protein release, Bone morphogenic protein (BMP), Nanoparticles, Nanocomposite scaffolds

Abstract: Glioblastoma (GB) is the most frequent and lethal form of brain cancer. It has a diffusive capacity which explains the impossibility of complete removal of the tumor by surgery. 90% of patients have a recurrence related to the presence of residual GB cells located at the edges of the resection cavity. A nanocomposite hydrogel capable of releasing in a prolonged manner the BMP-4 protein, which binds to the BMPRII receptors on the surface of GB cells, may be useful to induce the differentiation of the residual GB cells, allow their selective elimination, and thus reduce the tumor recurrence. In this project, BMP-4 was initially encapsulated in poly-lactic-co-glycolic acid (PLGA) nanoparticles. A high encapsulation efficiency was obtained via a phase separation process using non toxic solvents. The BMP-4 loaded nanoparticles were then incorporated into a hydrogel based on hyaluronic acid and poloxamer 407 to obtain a nanocomposite system mimicking the structure of the brain extracellular matrix. An *in vitro* release study revealed that the hydrogel could provide sustained release of BMP-4 for up to 30 days, useful for establishing a BMP-4 concentration gradient in the brain and differentiating GB cells. An *in vivo* biocompatibility study at 3 days and 7 days to confirm the *in vivo* safety of the implants prior to proceeding to efficacy studies in an appropriate GB resection model is currently underway.